The Anatomico-Functional Behaviour of Foveomacular Retinoschisis

Edward D. S. Bloch

Institute of Ophthalmology, University College London and the NIHR Biomedical Research Centre, Moorfields Eye Hospital NHS Foundation Trust

Supervisors: Professor Lyndon da Cruz
and Dr Christos Bergeles

Thesis submitted for the degree of Medicinae Doctor (Research), University College London

February 2023

SIGNED DECLARATION

I, Edward Bloch, confirm that the work presented in this thesis is my own. Where information has been derived from other sources, I confirm that this has been indicated in the thesis. Where information has been obtained with the help of others, this has been indicated below:

1. Chapter 6: Development of the deep learning segmentation algorithm was undertaken with the support of Mr. Theodoros Pissas, PhD student, School of Biomedical Engineering & Imaging Sciences, King's College London.

2. Chapter 6: The normative control group data were derived (with permission) from work by Dr. Jason Charng et al, Centre of Ophthalmology and Visual Science (incorporating Lions Eye Institute), The University of Western Australia, Perth, Australia.

Edward Bloch

1 February 2023

ABSTRACT

Foveomacular retinoschisis (FRS) describes a lamellar separation of the central neurosensory retina, as observed in acquired foveopathies, such as myopic foveoschisis (MFS), optic disc pit maculopathy (ODP-M) and idiopathic FRS (IFRS). The precise anatomico-functional behaviour and natural history of FRS remains largely unresolved and, while stability is exhibited in the majority of eyes, a subgroup is at risk of progression to foveal detachment (FD), with associated visual morbidity.

Since the abovementioned disorders demonstrate similar behaviour, regardless of the underlying pathophysiology or disease duration, it is hypothesised that anatomical and functional decline in FRS is related instead to the degree of biomechanical retinal deformation. This thesis explores the characteristics of FRS, through observational investigation, to clarify its behaviour and identify biomarkers with which to inform clinical practice.

A total of 201 eyes with FRS were identified. The overall incidence of progression to FD was 12% (17/140) in MFS, 58% (18/31) in ODP-M and 0% (0/30) in IFRS. OCT-derived metrics, including average retinal thickness and central retinal thickness, demonstrated association with development of FD in MFS and ODP-M respectively.

In those eyes that did not progress, visual acuity did not change significantly over a 4.5 years' follow-up. Cross-sectional comparison found non-significant differences in microperimetric sensitivity and fixation indices between eyes with FRS and age-matched controls. However, using a deep learning approach, it *was* possible to demonstrate correlation between the magnitude of the schisis cavity and worse retinal sensitivity, at a given locus, in eyes with FRS.

This thesis serves to introduce several novel concepts, to inform on the clinical characteristics of FRS. The results support the hypothesis that anatomico-functional behavior of FRS is associated with the pattern and magnitude of retinal deformation,

which in turn can be related to the distinct underlying pathomechanisms and their respective effects on the foveal ultrastructural arrangement.

IMPACT STATEMENT

This thesis explores the natural course and anatomico-functional correlates of a relatively poorly characterised retinal entity, foveomacular retinoschisis (FRS). Although cases of FRS represent a minority of the attendances in the outpatient clinic, the condition is far from uncommon and, in one form or another, is potentially as prevalent as 1-2% of the population. Fortunately, the majority of patients will be asymptomatic and retain long-term stability, but a subset will undergo progression to end-stage disease, often manifesting with profound and irretrievable visual loss. The challenge is in identifying those patients at risk and, where possible, intervening in a timely manner.

This dissertation addresses some of the shortcomings in our understanding of FRS and includes some of the largest natural history studies of various acquired forms of FRS, namely myopic foveoschisis (MFS), optic disc pit maculopathy (ODP-M) and idiopathic foveomacular retinoschisis (IFRS). Through studying the anatomical and functional characteristics of these eyes over a period of time, it has been possible to observe and measure associations between various qualitative and quantitative morphological biomarkers, and both visual function and the risk of progression to the pre-defined anatomical end-point.

From the perspective of a non-academic impact, the findings of this thesis can aid clinicians when differentiating causes of FRS, while also permitting the delivery of more accurate prognostic information and management options to patients. With this in mind, I have devised simple scoring systems which, following external validation, might be applied clinically to risk stratify patients, facilitate early identification of anatomical and visual decline, and optimise the timing of surgical intervention. The merit of such an individualised management approach is that progression may be detected earlier, or even pre-empted, through vigilant serial assessment and awareness of clinically relevant biomarkers. Moreover, risk-stratification serves to reduce the rate of clinical review in those with a low

possibility of progression, thereby minimising the burden on both the patient and healthcare service.

In terms of benefits inside academia, I have employed several novel methodological techniques in this dissertation, most notably having developed the first deep learning algorithm to quantify the dimensions of a schisis cavity. I have demonstrated the feasibility of this technique as a segmentation tool, as well as its usage in combination with psychovisual testing to measure anatomico-functional correlation. It is anticipated that artificial intelligence approaches will soon be introduced to assist in the management of retinal disease, affording a reduction in the clinical workload and providing patients with the convenience of community-based or semi-virtual review. As FRS becomes more prevalent, in particular in the context of high myopia, the proof-of-concept demonstrated herein may lay the groundwork for future automated decision-making tools.

The impact of this thesis continues to be realised through the dissemination of data in academic journals and presentation at international specialty meetings. I am therefore optimistic that the novel findings and concepts within this work will be influential in the future clinical management and research of FRS.

PUBLICATONS & PRESENTATIONS

Publications related to this thesis*

Published articles

- Bloch E, Georgiadis O, Lukic M, da Cruz L. Optic disc pit maculopathy: New perspectives on natural history. Am J Ophthalmol. 2019 Nov;207:159-169.
- Bloch E, Flores-Sánchez B, Georgiadis O, Sundaram V, Saihan Z, Mahroo OA, et al. An association between stellate nonhereditary idiopathic foveomacular retinoschisis, peripheral retinoschisis, and posterior hyaloid attachment. Retina. 2021 Nov;41(11):2361–9.

Submitted articles

- Bloch E, Flores-Sánchez B, Georgiadis O, Whiteman A, da Cruz L. Associations between optical coherence tomographic biomarkers and anatomico-functional changes in myopic foveoschisis. 2023

*UCL Research Paper Declaration forms can be found in APPENDIX

Presentations related to this thesis

Oral conference presentations

- Bloch E, Flores-Sánchez B, Pissas T, Charng J, Chen F, Bergeles C, da Cruz L. Modelling the anatomico-functional behaviour of foveomacular retinoschisis using a deep convolutional neural network. EURETINA congress (2022), Hamburg, Germany.

- Bloch E, Flores-Sánchez B, Georgiadis O, Sundaram V, Saihan Z, Webster A, da Cruz L. An association between nonhereditary idiopathic foveomacular retinoschisis, peripheral degenerative retinoschisis and vitreoretinal adhesion. EURETINA congress (2020), virtual meeting.
- Bloch E, Flores-Sánchez B, Whiteman A, Georgiadis O, da Cruz L. Factors associated with development of foveal detachment in myopic foveoschisis. EURETINA congress (2020), virtual meeting.
- Bloch E, Flores-Sánchez B, Whiteman A, Georgiadis O, da Cruz L. Factors associated with development of foveal detachment in myopic foveoschisis. BEAVRS conference, (2020), virtual meeting.

Poster conference presentations

- Bloch E, Flores-Sánchez B, Pissas T et al, Charng J, Chen F, Bergeles C, da Cruz L. Modelling the anatomico-functional behaviour of foveomacular retinoschisis using a deep convolution al neural network. BEAVRS meeting (2021), Manchester, UK.
- Bloch E, Flores-Sánchez B, Pissas T, Bergeles C, da Cruz L. The anatomico-functional behaviour of foveomacular retinoschisis. Royal College of Ophthalmologists Congress (2021), Liverpool, UK.
- Bloch E, Flores-Sánchez B, da Cruz L. Foveomacular retinoschisis associated with peripheral retinoschisis and anomalous posterior vitreous detachment in two siblings. EURETINA meeting (2020), virtual meeting.
- Bloch E, Georgiadis O, Lukic M, da Cruz L. Optic disc pit maculopathy: a retrospective study of the natural history of the disease. ARVO meeting (2018), Honolulu, USA.

ACKNOWLEDGEMENTS

There are so many people to whom I'm indebted, as I have journeyed through the past 5 years of research, without whose support and assistance, I would not have ever completed this dissertation.

In the first instance, I would like to acknowledge those people who contributed as subjects in my studies. Each one of these participants eagerly agreed to partake in tests to help better understand their condition; I attribute much of this goodwill to the high quality of care they had already received at Moorfields.

I am extremely lucky to have been part of several teams, between the NIHR Biomedical Research Centre at Moorfields, the Wellcome/EPSRC Centre for Interventional and Surgical Sciences at UCL, the Institute of Ophthalmology and the Robotics and Vision in Medicine lab at King's College London. As such I have met countless interesting and highly intelligent people, many of whom have become good friends.

To my principal supervisor, Lyndon da Cruz, I am truly grateful for the constant inspiration, guidance and mentorship throughout this period. It has been a privilege to work with Lyndon and I owe much of my recent achievements to his expert instruction, patience and good humour. Christos Bergeles, my subsidiary supervisor, has been a constant source of help and kindness over the past few years. I feel very honoured to have been a part of his exciting team and, in particular, would like to extend thanks to Theo, John, Ross, Claudio, Zizos and Sepehr for their expert assistance on complex engineering tasks.

My clinical colleagues and friends, especially Odysseas, Blanca and Conor, provided a sense of stability throughout my time in the Clinical Research Facility, offering me encouragement and a beer during the difficult periods and celebrating the good times in much the same manner. While all the staff members in the CRF contribute

to the amazing environment, special mention must go to Pany, Vince, Sash and Julie, without whom I would have been utterly lost.

I would also like to acknowledge my collaborators on various projects, including Pete, Vicki, Piotr, Yvonne, Jason, Fred, Mike, Marko and Omar, with whom it's been a pleasure to work.

Finally, I would like to thank my family, whose continued love and support sustains me in all my endeavours. I am truly grateful to my parents for their hard work and countless sacrifices to give me the opportunity to do something I find so enjoyable and fulfilling. But most of all, I am thankful to my long-suffering wife, Freya, and relatively short-suffering baby girl, Maja, who have kept me going, with coffee during long nights of writing and a welcome distraction the rest of the time. I owe it all to you.

LIST OF ABBREVIATIONS

AI – artificial intelligence

AL – axial length

AMD – age-related macular degeneration

ATN – atrophy, traction, neovascularisation,

ATS – average threshold sensitivity

AvRT – average retinal thickness

BCEA – bivariate contour ellipse area

CNVM – choroidal neovascular membrane

CPT – central point thickness

CRT – central retinal thickness

CSF – cerebrospinal fluid

CSH – central schisis height

CT – choroidal thickness

CMO – cystoid macular oedema

CNN – convolutional neural network

CRA – cilioretinal artery

cSLO – confocal scanning laser ophthalmoscopy

dB – decibel

DD – disc diameter

DL – deep learning

DSC – dice similarity coefficient

ERP – epiretinal proliferation

EPR – electronic patient record

ERM – epiretinal membrane

ESCS – enhanced S-cone syndrome

ETDRS – Early Treatment of Diabetic Retinopathy Study

EZ – ellipsoid zone

FAZ – foveal avascular zone

FCNN – fully convolutional neural network

FD – foveal detachment

FFA – fundus fluorescein angiography

FFR – familial foveal retinoschisis

FRS – foveomauclar retinoschisis

FTMH – full thickness macular hole

GC – ganglion cell

GFAP – glial fibrilliary acidic protein

GFS – Goldmann-Favre syndrome

HFL – Henle's fibre layer

IFRS – idiopathic foveomacular retinoschisis

ILH – inner lamellar hole

ILL – internal limiting lamina

ILM – internal limiting membrane

ILR – inner layer retinoschisis

INL – inner nuclear layer

IOP – intraocular pressure

IoU – intersection over union

IPL – inner plexiform layer

IQR – interquartile range

IRF – intraretinal fluid

IS - inner segment

IZ – interdigitation zone

JPL – juxtapapillary laser

LHEP – lamellar hole-associated epiretinal proliferation

LogMAR – logarithm of the minimal angle of resolution

MC – Müller cell

MCC – Müller cell cone

mfERG – multifocal electroretinogram

MFS – myopic foveoschisis

MGS – morning glory syndrome

MHRD – macular hole retinal detachment

MIP – minimal intensity projection

ML – machine learning

MLP –multi-layer perceptron

MLR – multi-layer retinoschisis

MP - microperimetry

MPH – macular pseudohole

MTM – myopic traction maculopathy

NFL – nerve fibre layer

NIR – near-infrared

NN – neural network

OCT – optical coherence tomography

ODP(-M) – optic disc pit (maculopathy)

OLH – outer lamellar hole

OLR – outer layer retinoschisis

ONL – outer nuclear layer

OPL – outer plexiform layer

OS – outer segment

PPV – pars plana vitrectomy

PPVP – posterior pre-cortical vitreous pocket

PRL – preferred retinal locus

PRS – peripheral retinoschisis

PS – posterior staphyloma

PTMH – partial thickness macular hole

PVC – posterior vitreous cortex

PVD – posterior vitreous detachment

ReLu – rectified linear unit

RNFL – retinal nerve fibre layer

RPE – retinal pigment epithelium

SA – schisis area

SAS – subarachnoid space

sd – spectral domain

SD - standard deviation

SE – spherical equivalent

SNIFR – stellate nonhereditary idiopathic foveomacular retinoschisis

SPLIFR – stellate progressive liquefaction-induced Foveomacular retinoschisis

SRF – subretinal fluid

SRS – subretinal space

TEM – transmission election microscopy

TLMH – tractional lamellar macular hole

VA – visual acuity

VEGF – vascular endothelial growth factor

VF – visual field

VMA – vitreomacular adhesion

VMI – vitreomacular interface

VMT – vitreomacular traction

VMTS – vitreomacular traction study

VRI – vitreoretinal interface

XLRS – x-linked retinoschisis

zMC – z-shaped Müller cell

TABLE OF CONTENTS

LIST OF TABLES

LIST OF FIGURES

formation in susceptible eyes. The natural history is one of spontaneous improvement, even in the absence of clear evidence of complete PVD. 285

For all patients with foveomacular retinoschisis

(1 in 100)…

…and for my wife Freya

(1 in 8 billion)

CHAPTER 1

FOVEOMACULAR RETINOSCHISIS: INTRODUCTION AND OVERVIEW

"*If one is to understand the great mystery, one must study all its aspects*"

– Senator Palpatine

1.1 Introduction

Derived from the Latin words *rēte* and *tunica*, meaning 'net-like layer' and the Greek word *σχἵσἵς*, meaning 'division', the term 'retinoschisis' was coined by Wilczek in 1935, to describe a case of peripheral temporal 'retinal cleavage'. We now recognise this common condition as senile or acquired retinoschisis, which is characterised by its association with absolute scotomata (1,2). However, retinoschisis has since become a descriptive term for a wide variety of types of retinal separation, regardless of the underlying aetiology or functional characteristics. This includes inherited disorders, such as X-linked retinoschisis, the macular retinoschisis associated with tractional disorders like vitreomacular traction, epiretinal membrane or myopic traction maculopathy, as well as fluid accumulation in conditions such as optic disc pit maculopathy. The capacity for various conditions, with distinct pathophysiological mechanisms, to present with such similar morphological changes remains a relatively poorly explored phenomenon.

The introduction of optical coherence tomography (OCT), now ubiquitous in ophthalmic practice worldwide, has transformed our understanding of posterior segment structure and pathology, permitting important insights into the anatomico-functional behaviour of the retina *in vivo*. Based on OCT findings, further terminology has emerged, such as 'maculoschisis', 'foveoschisis' and 'foveomacular retinoschisis', which are frequently used interchangeably to refer specifically to lamellar cleavage affecting the posterior retina. Opinion has historically been divided, as to whether it is semantically correct to describe retinal splitting without absolute scotoma as 'schisis', but it is now widely accepted as anatomical terminology devoid of any implication regarding visual function (3,4). To avoid confusion, I will use 'foveomacular retinoschisis' and related terms as structural descriptors only, in cases of lamellar separation of the neurosensory retina.

The observation of foveomacular retinoschisis (FRS) as a feature of various retinal disorders raises the question as to whether it is indicative of a particular underlying pathological process that is common to these different conditions or whether it

simply represents compensatory deformation of the retinal ultrastructure in the face of external stress, and is therefore a potential manifestation of any mechanical foveopathy. Regardless, we might predict that, given the common morphology, these conditions would exhibit comparable functional behaviour. In order to answer this, we would need to explore the clinical characteristics of FRS, as well as its natural history and anatomico-functional interaction, across a range of different pathologies.

In this chapter, I first provide an overview of the pertinent vitreoretinal anatomy, in both health and disease, followed by a review of the current understanding of diseases that manifest in foveomacular retinoschisis and, finally, a summary of the central thesis to this dissertation.

1.2 Vitreoretinal anatomy

In order to understand the anatomical changes seen in the context of retinoschisis, we must first be familiar with the basic ultrastructure of the vitreous and retina, with particular attention to the corresponding features on OCT. We owe much of our historical understanding of vitreoretinal anatomy to histological studies, but modern OCT has afforded us the ability to visualise these structures at ultra-high resolution *in vivo*. Although the correspondence between the modalities is accurate, it is not absolute and the origin of some observed tissue optical properties on OCT remains subject to debate.

1.2.1 The retina

The retina is a multilayered structure that is embryologically derived from the neural tube and can be subdivided into a sensory and a neural component (5). The sensory outer retina is comprised of rod and cone photoreceptors and is naturally stimulated by light, the phototransduction of which is the initial step on the visual pathway. The

neural inner retina is the site of complex synaptic processing of interneurons and projection neurons, concerned with the early steps of visual processing (6).

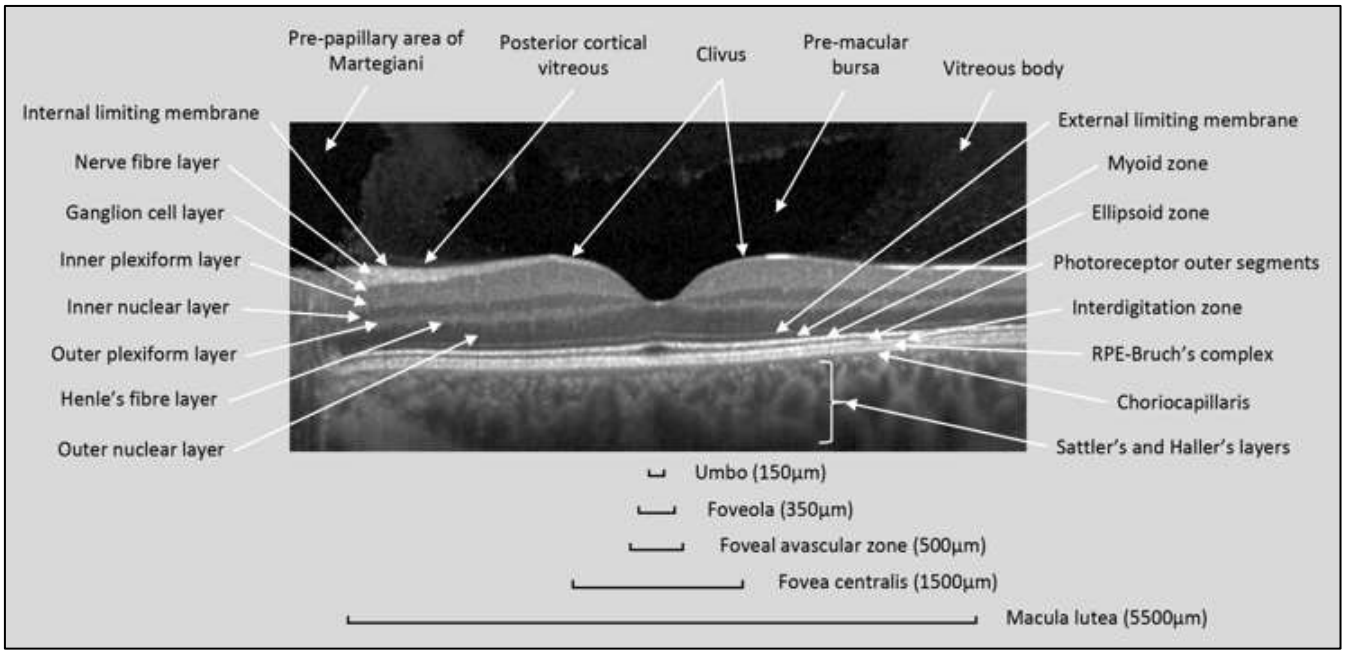

Figure 1-1: OCT-based anatomical landmarks of the vitreous, retina and choroid

On OCT (Figure 1-1) the innermost element of the retina is the internal limiting membrane (ILM), a very thin layer that contributes to the vitreoretinal junction and, in the absence of posterior vitreous detachment, is indistinguishable from the vitreous cortex. Immediately beneath the ILM is the hyperreflective retinal nerve fibre layer (NFL), followed by a relatively hyporeflective ganglion cell layer. Posterior to this are two lighter bands, the inner plexiform layer (IPL) and outer plexiform layer (OPL), containing neuronal axons and synapses, which straddle a darker inner nuclear layer (INL), containing the bipolar, amacrine, horizontal cell somata (7,8). Finally, the central inner retina is separated from the outer retina at the level of Henle's fibre layer, containing horizontally arranged photoreceptor and Müller cell processes, in a ratio of up to 1:1 (9,10). OCT visualisation of HFL is inconsistent, due to the optical properties of form birefringence. It is often best visualised with a laterally or vertically tilted incident beam or in the presence of outer retinal pathology, due to backscattering of light, or in the presence of Müller cell gliosis (e.g. drusen or photic retinopathy respectively) (Figure 1-2) (11–13).

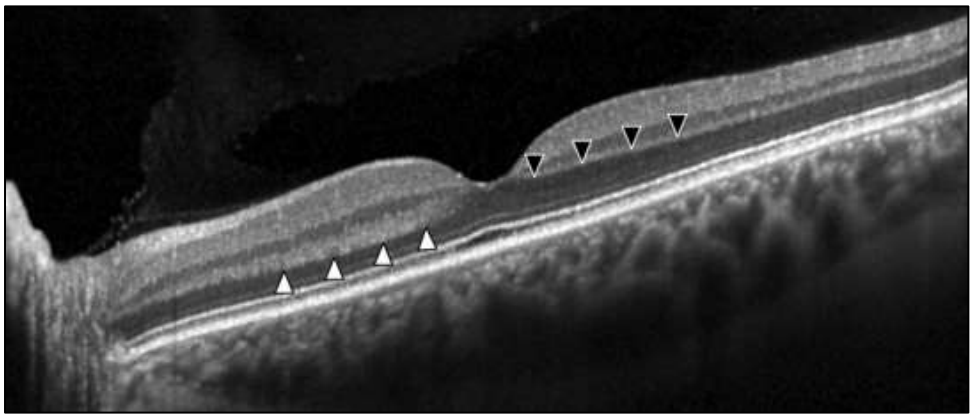

Figure 1-2: Visualisation of Henle's fibre layer with a tilted incident beam demonstrates the form birefringence; nasally HFL appears brighter (white arrowheads) and temporally it appears darker (black arrowheads)

The outer retina is defined by distinct bands of alternating relative hyper- and hyporeflectivity. The innermost thin, hyperreflective line is the external limiting membrane (ELM), which divides the overlying photoreceptor cell somata, contained within the ONL, from the myoid zone of the photoreceptor inner segments (IS). Subjacent to this is a hyperreflective band that has been suggested to represent the photoreceptor inner segment (IS) ellipsoid zone (EZ), though is often alternatively ascribed to the IS/OS junction (14,15). Posterior to this is a relatively hyporeflective region, composed of the both the photoreceptor outer segments (OS) and the interdigitation zone (IZ), wherein photoreceptor OS are ensheathed in retinal pigment epithelium (RPE) apical processes, in a structure known as the contact cylinder (8,15). Outermost is the hyperreflective RPE-Bruchs-choriocapillaris complex, the constituent layers of which are often difficult to resolve on OCT (16,17).

1.2.2 The fovea

The segmentation of retinal layers observable on OCT occurs due to the variable optical properties of the tissues, causing scattering of light along its path to the photoreceptor. The inverted morphology of the retina, with photoreceptors being outermost, is essential to provide support for the photoreceptor cells from the RPE

and choroid. As such, further retinal specialisation is necessary to minimise light scatter and increase visual acuity, including the displacement of retinal tissue at the fovea. The fovea centralis is defined as a circle, of 1.5mm diameter, which lies about 2 disc diameters temporal and 1/3rd disc diameter inferior to the centre of the optic nerve. It corresponds approximately to the central 5.5˚ of visual field and can be subdivided into concentric zones. The foveal avascular zone (FAZ) is around 500µm diameter, wherein the absence of blood vessels prevents 'light screening'; the central 350µm of the FAZ comprises the foveola, representing around 1˚ of visual field, and is devoid of all retinal neurons and microglia, with the exception of tightly-packed cone photoreceptors and Müller cell processes (the photoreceptor cell somata are stacked here, giving rise to a thickened ONL); the very central 150µm of the fovea is termed the umbo and is the source of the foveal light reflex (Figure 1-1 and Figure 1-3) (18–23). Histologically, ganglion cells (GCs), which are absent in the foveola, are first observed 300µm eccentrically to the fovea and peak in density at about 650µm. The peak ratio of GC to cone photoreceptor is around 2-3:1, and dense packing of so-called 'midget' photoreceptor, bipolar and GCs in the foveal walls is critical for high acuity vision (21,24–26). The surrounding macula lutea area is defined as a 5.5mm diamater circle centred on the fovea and characterised histologically by a thickness of two or more GCs. The macula is further subdivided into an outer perifoveal zone, a 1.5mm wide annulus located 500µm from the foveal edge, and the inner parafovea, a 500µm belt between the perifovea and fovea (21,27). These regions encircle the central 18˚ and 8˚ of visual field respectively. The retina is thickest at the foveal wall, from which point the downward sloping clivus forms the foveal pit. On OCT, the foveal pit is characterised by a lack of inner retinal layers and a thick ONL (9,28,29).

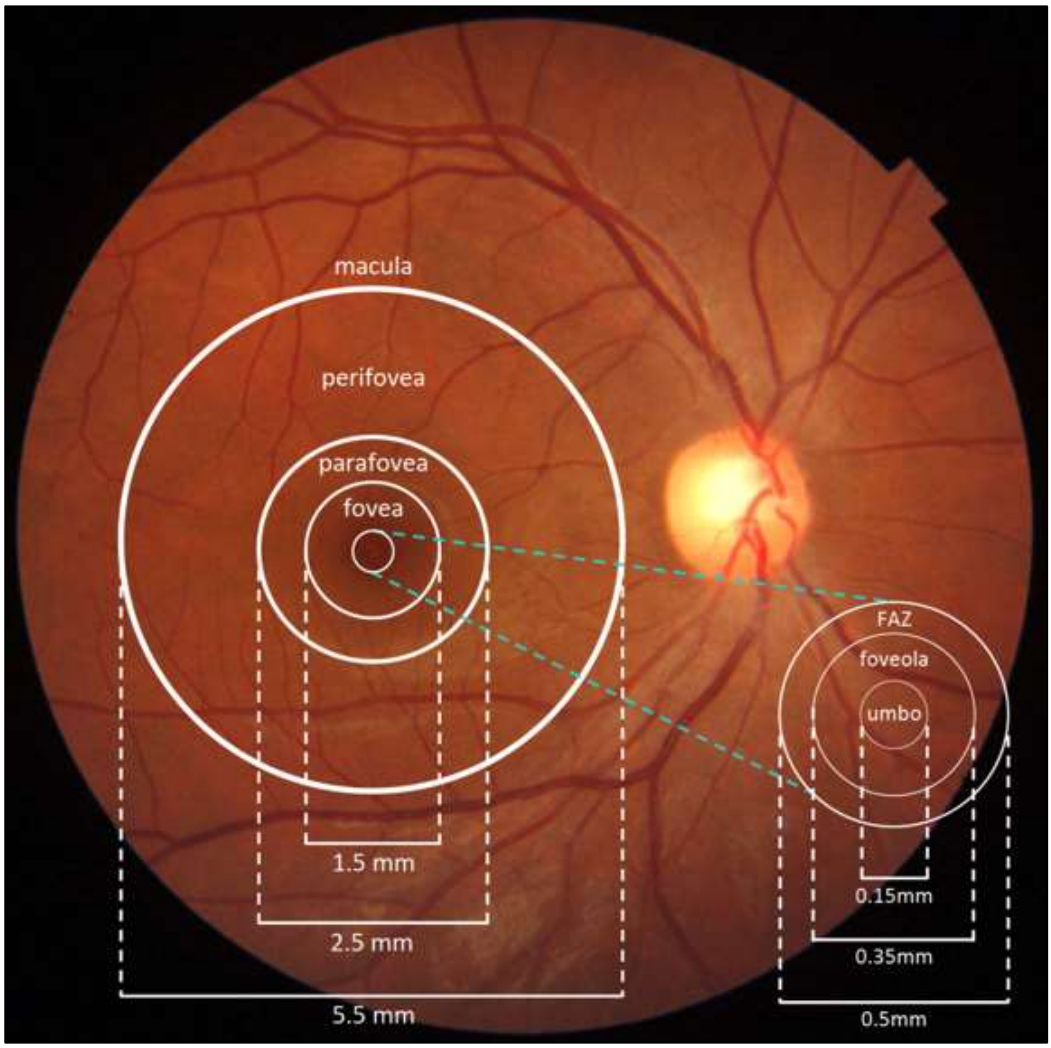

Figure 1-3: Fundus photograph of the macula demonstrating anatomical landmarks

1.2.3 The vitreous

The vitreous body is a clear gel-like structure, 98% of which is composed of water and the remaining 2% is made up of structural proteins, such as fibrillin, opticin, types II and IX collagen, and other extracellular matrix components, including hyaluronan and veriscan (chondroitin sulfate proteoglycan) (30–36). Microscopically, the vitreous comprises a membranous, continuous posterior vitreous cortex (PVC), extending from the ora serrata to the posterior pole, enclosing the vitreous body (Figure 1-4A). A series of anteroposterior parallel 'membranelles' arise from the

anterior vitreous base and insert throughout the posterior pole at the vitreoretinal interface (VRI) (Figure 1-4B) (36–38). The PVC is thin over the macula and absent over the optic disc (36). Within the vitreous body are cisternal spaces, extending from Berger's space (the retrolental space of Erggelet) through Cloquet's canal, opening into the pre-papillary area of Martegiani (39,40). Overlying the macula is the premacular bursa or 'posterior precortical vitreous pocket' (PPVP), which is continuous with a larger equatorial cistern anteriorly and separated from Cloquet's canal by the septum interpapillomaculare (40–43).

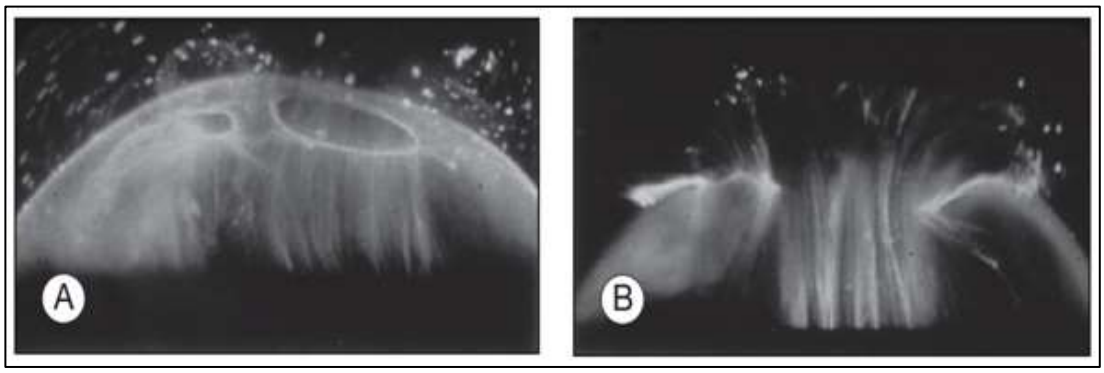

Figure 1-4: Human vitreous morphology visualised by dark-field slit illumination; (A): Vitreous body is enclosed by the vitreous cortex, with a hole in the prepapillary cortex (left) and a larger posterior precortical vitreous pocket (right); (B): A bundle of prominent membranelles is seen coursing anteroposteriorly and entering the retrocortical space via the premacular cortex. Credit: Sebag and Green (2018) (36) [images reproduced with permission of the rights holder, Elsevier]

The VRI consists of the PVC anteriorly and the ILM posteriorly (37). The PVC is 100-110µm thick and arranged in densely packed, lamellar collagen fibres, the posterior portion of which contains fibroblasts and hyalocytes. Hyalocytes are mononuclear cells that synthesise glycoproteins and collagen, may demonstrate phagocytotic properties and, under certain conditions, produce cytokines and growth factors (37,44–47). The PVC is separated from the neurosensory retina by the internal limiting lamina (ILL). The ILL is a multi-lamellar structure, made up of a lamina rara externa, a lamina densa and a lamina rara interna; it serves as a basement membrane for the Müller cell endplates, in combination with which it forms the ILM

(Figure 1-5) (36,42). This basal lamina structure is a thin sheet of extracellular matrix, containing a highly cross-linked framework of collagen type IV to help maintain stability of the ILL and non-covalently-bound chondroitin sulfate proteoglycans, along with fibronectin and laminin constituents, which provide fascial (as opposed to focal) vitreoretinal adhesion (48–50). The ILL is topographically varied; it becomes progressively thicker from the equator (~300nm) to the posterior pole (>1.8µm) (36,51,52). Moreover, the orientation of vitreous fibrillar attachment in the basal lamina varies between the foveola and foveal walls. The parafoveal ILL is thicker (900nm-1µm), revealing numerous horizontally aligned fibres and an electron dense vitreal surface, projecting many dark knob-like insertions, on histological sections. The foveolar ILM, by comparison, is thinner and electron-lucent with scattered integration of single electron dense knobs (9,22). These knobs are thought to represent remnants of vitreous collagen fibrils that are normally adhered to the basal lamina; the variance in their distribution may underlie the morphology in disorders of the VRI (23,46,53,51,22,54). Thinning of the ILM and vitreous incarceration (vitreoretino-vascular bands) in the vicinity of major retinal vessels render these points vulnerable to preretinal gliosis and perivascular rarefaction (55,56).

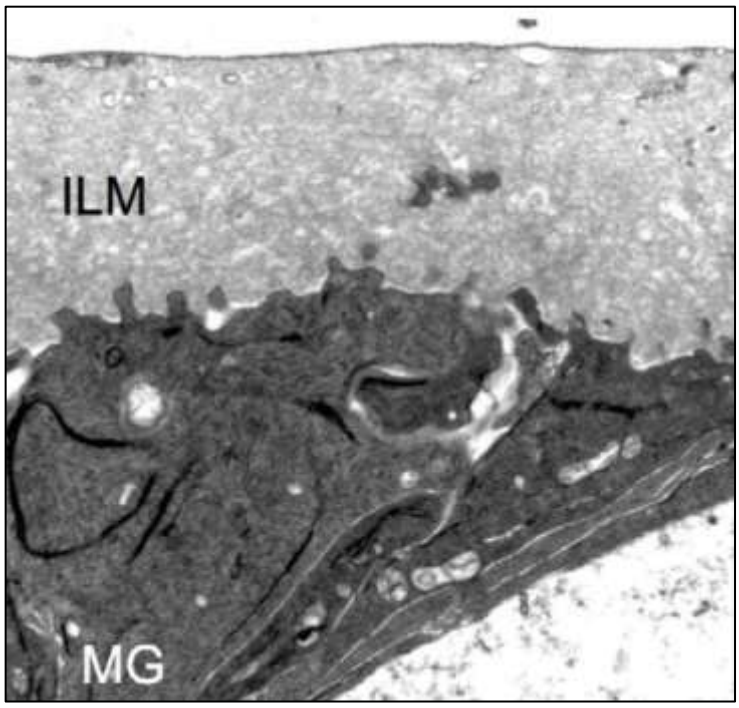

Figure 1-5: Transmission electron microscopy demonstrating the Müller glia (MG) projecting insertions into the ILL to form the ILM. Credit: Almeida et al (2015) (57) [image Creative Commons licensed]

.

1.2.4 The Müller cell

First discovered by Heinrich Müller in 1851, the Müller cell (MC) is a type of radial glial cell that is physiologically and structurally adapted to the local microenvironment of the retina. The cell soma of the MC is located within the INL and bidirectional processes extend apically to form the ILM and basally to project microvilli into the subretinal space. They are the only retinal cell to extend across the full thickness of the retina and also have side branches, which contact and ensheath virtually every neuronal and vascular component of the retina, giving rise to so-called 'neuro-glial-vascular units' (Figure 1-6) (9,50,58).

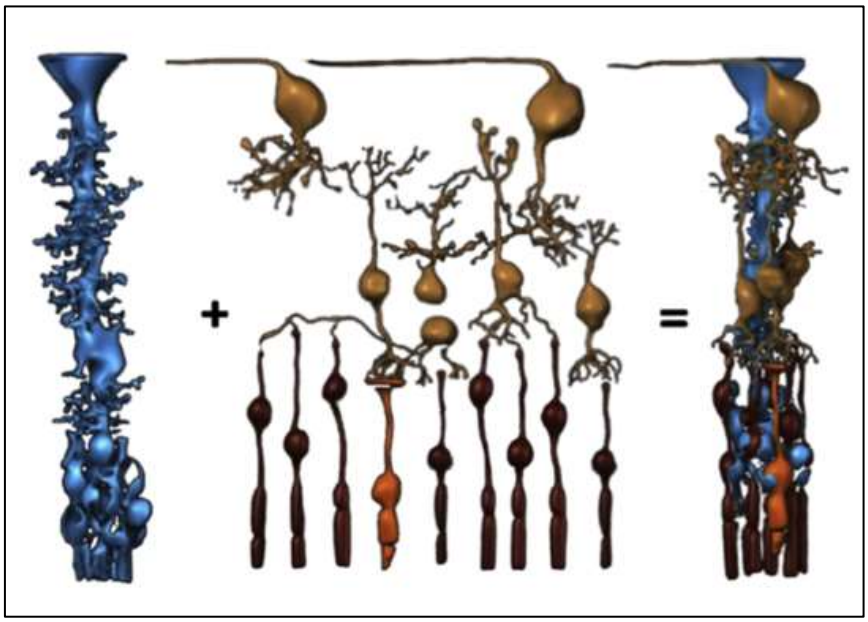

Figure 1-6: A diagrammatic illustration of the structure of the primate Müller cell (blue) and its anatomical relationship with the retinal neurons (light brown) and photoreceptor cells (dark brown). Adapted from Bringmann et al (2018) (9) [images reproduced with permission of the rights holder, Elsevier]

1.2.4.1 Müller cell ultrastructure and function

The ultrastructure of the MC reflects its extensive and varied anatomical and functional role in the retina. For example, the endfoot of the inner process contains an abundance of intermediate filaments and smooth endoplasmic reticulum, as well as membrane channel proteins, such as aquaporin-4 (AQP4) (22,59–62). This implies a role in molecule exchange between the MCs and the basal lamina and vitreous (50). By contrast, the outer processes contain stacks of Golgi bodies close to the somata, suggesting a secretory function (e.g. of growth factors, chemokines and lipoproteins) and intra- and transcellular transport (e.g. of retinoschisin) (61,63,64). Additionally, MCs processes contain ample mitochondria, indicating a key role in supporting photoreceptor metabolic demand. Distally, the outer processes of the MCs have a continuous subplasmalemmal layer of filamentous actin, surrounding the photoreceptors and forming zonulae adherentes, which make up the ELM, providing a diffusion barrier from the subretinal space, into which MCs project microvilli (61,65–67). MCs play additional critical roles in synaptic signaling and neuronal processing within the sensory retina. This includes uptake and exchange of excitatory and inhibitory neurotransmitters (e.g. glutamate and γ-aminobutyric acid (GABA)), cation (particularly potassium ion) homeostasis and neuromodulation through the regulation of various extracellular neuroactive elements via channel- and transporter-mediated mechanisms (50,68–73). As such, MCs also regulate retinal volume changes by controlling the transcellular osmotic gradient and permitting water flux to optimise neuronal excitability (68). A large proportion of this homeostatic activity takes place in the lateral processes of the MC, located mostly in the plexiform layers. Herein, groups of polyribosomes synthesise proteins, such as those contributing to molecule uptake carriers or ion and water channels, in response to changes in the extracellular milieu during neuronal activity (50,74). Finally, MCs may also function as ‘living optical fibres’, focusing incident photons onto their ‘private’ photoreceptors in a pixel-like manner, thus minimising the light-scattering effects of the inner retina (75,76).

In summary, the MC has an intimate ontogenetic, anatomical and functional relationship with the retinal neuron (Figure 1-7). Their common phylogenetic origin results in a complex structural and physiological symbiosis, which allows elaborate processing of visual information and retinal homeostasis. It is clear from the intricate balance required for normal functioning of the healthy retina, that any disturbance of the MC ultrastructure in disease may have profound and deleterious consequences.

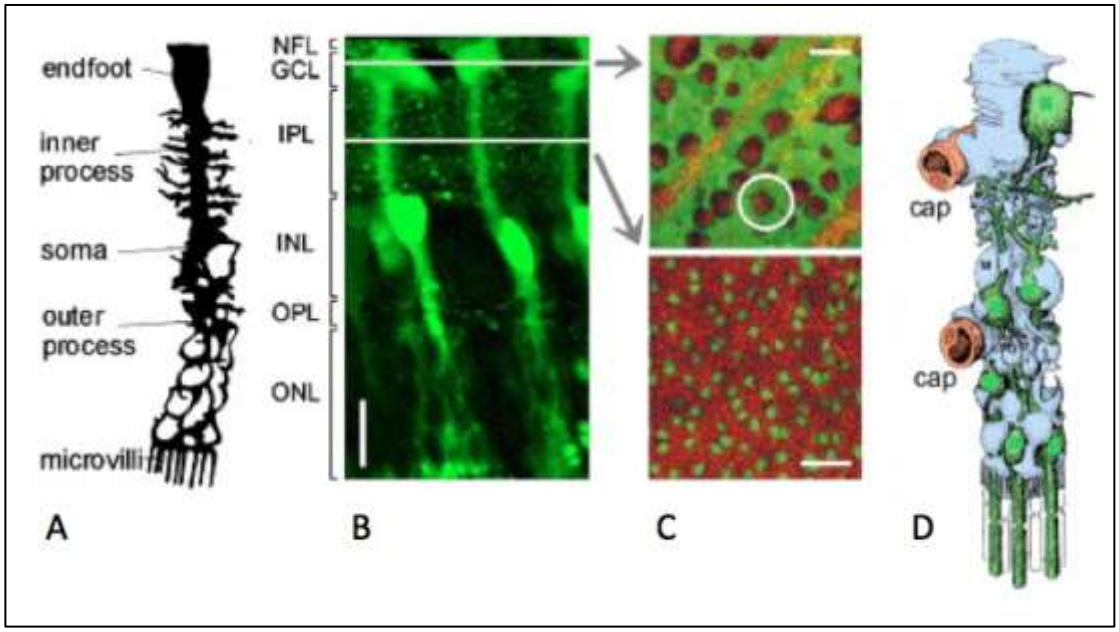

Figure 1-7: Morphology of the Müller cell: (A) Diagrammatic representation of Golgi-labelled rabbit MC; living guinea pig MCs in a slice (B) and flat-mount (C); (D) illustration of relationship between MC (blue) and retinal vessels (red) and neurons (green). Credit: Bringmann et al (2006) (77) [images reproduced with permission of the rights holder, Elsevier]

1.2.4.2 Müller cell reactive gliosis

Almost every known retinal pathology can be associated with MC reactive gliosis, manifesting as variety of specific and non-specific morphological and biochemical changes. Non-specific MC gliosis is characterised by cellular hypertrophy,

proliferation and the upregulation of intermediate filaments, such as nestin, vimentin, glial fibrillary acidic protein (GFAP) and ERK1/2 (50,72,78–81). Specific responses depend on the stimulus, whether it be mechanical or photic damage to photoreceptors, biochemical toxicity (e.g. hepatic and methanol-induced retinopathy) or ischaemic injury, and are characterised by release of particular growth factors, cytokines and antioxidant proteins (50,82–84). The primary purpose of gliosis is to provide neuroprotection and limit early tissue damage, following which, dedifferentiation of MCs into retinal progenitor cells, with the capacity for axonal regeneration and synaptic remodelling, is observed (85–87). However, this rapid change in physiology is not without detrimental effects; MC gliosis can have direct cytotoxic effects through release of pro-inflammatory cytokines, chemoattractant proteins and nitrogen free radicals, while secondary consequences of scar formation, with excessive cell proliferation and aberrant remodelling, combined with changes in extracellular homeostasis can exacerbate downstream disease progression (50,88–93).

The process of MC reactive gliosis may underpin the structural alterations seen in retinoschisis, while also being responsible for remarkable retention of function and anatomical recovery (e.g. in foveoschisis and macular hole closure respectively). The capacity of MCs to re-enter the cell cycle and trandifferentiate into various neuronal and immune cell types is an incompletely understood phenomenon, but it represents an exciting potential target for therapeutic approaches (50).

1.2.4.3 Müller cell subtypes

In 1907, Rouchon-Duvignead published his findings of a small island of approximately 2000 thin cone photoreceptors cells in the fovea of primates and humans, which he termed the ‘bouquet of central cones’ (94). It was not until 1969, when Yamada first identified the presence of MCs overlying the photoreceptors in the central fovea, which Gass subsequently termed the “Müller cell cone” (MCC) in 1999 (23,95). This concept has since been supported by histological studies that have

characterised a population of 25-35 specialised MCs, whose processes do not leave the foveola (Figure 1-8 & Figure 1-9A) (22,96,97). Instead, these specialised MCs serve to mechanically stabilise foveal architecture, through vertical attachment between the photoreceptors of the cone bouquet and the floor of the foveal pit, via a central 'stalk' around 20-50µm thick. Additional foveal stability is afforded by an elaborate 'plait' of MC processes running horizontally beneath the basal lamina of the ILM, which provide mechanical support, as well as providing a smooth, thin VRI to prevent light scatter (22,97–100). With the exception of the apex of the cone, which attaches to photoreceptor processes in the central 40µm at the ELM, the MCs of the MCC are free of neuronal axons and do not provide the equivalent functional support of a 'typical' MC (9,95,101–104). The MCs in the MCC have a low-density, lucent cytoplasm, containing high levels of macular pigment, which helps reduce chromatic aberration and absorb short-wavelength light, protecting and supporting the optical function of the fovea (22,105–107).

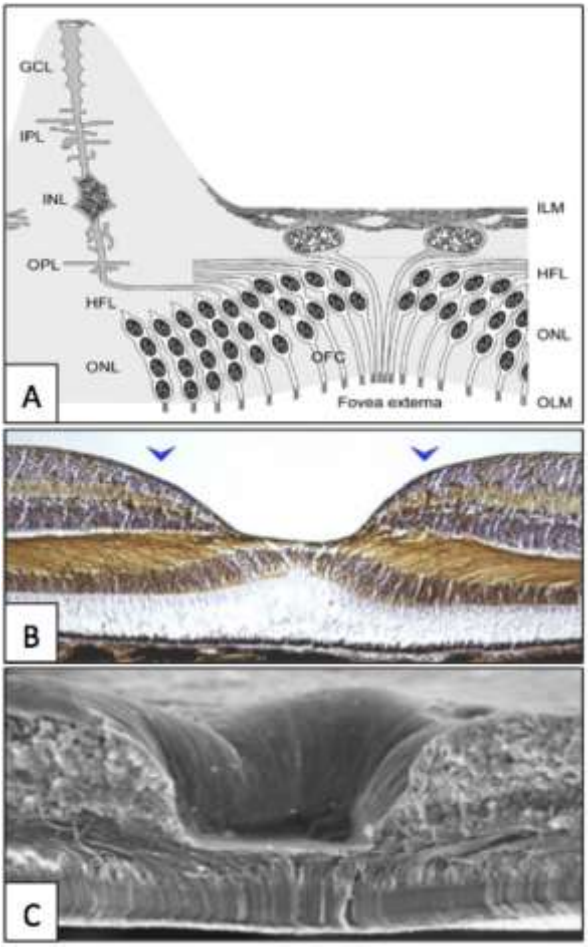

Figure 1-8: The primate Müller cell distribution; (A): Diagrammatic representation of the foveal MCs (Syrbe et al, 2018) [images reproduced with permission of the rights holders, Science Direct] (22); (B): Cross-section of primate fovea with vimentin immunohistochemical staining (in brown) of MCs and (C): scanning electron micrograph of a primate fovea, demonstrating the oblique arrangement of zMCs in HFL (Bringmann et al, 2018) (9) [images reproduced with permission of the rights holders Elsevier]

Unlike the MCs of the MCC, the MCs outside the foveola demonstrate a 'z-shaped' anatomical configuration (zMCs) (Figure 1-8 & Figure 1-9B) (108). These 'parafoveolar' zMCs are orientated vertically in the outer retina, where they enclose the photoreceptors, proximally to the cell somata, forming the ELM. The outer processes are then displaced laterally, running obliquely through Henle's fibre layer in the foveal walls and parafovea, surrounding the unmyelinated photoreceptor cell processes and somata, until they synapse in the OPL. The outer processes of zMCs

are elongated to span this lateral displacement of 50-350µm in the foveal walls and parafoveal region (109–111). It is here that the density of MCs is greatest, in excess of 30,000/mm^2 (19). The MC outer processes then continue more-or-less vertically (<50µm displacement) from the level of the OPL to the cell somata in the INL, from where the inner process projects upward towards the ILM (9,110). However, the laterally displaced zMC endplates do not contribute to the ILM to the same extent as those in the MCC, but rather a coexistent, atypical subtype of MC with soma located in the inner retinal surface project irregular, horizontal fibres to form the ILM (9,22,50,99,111).

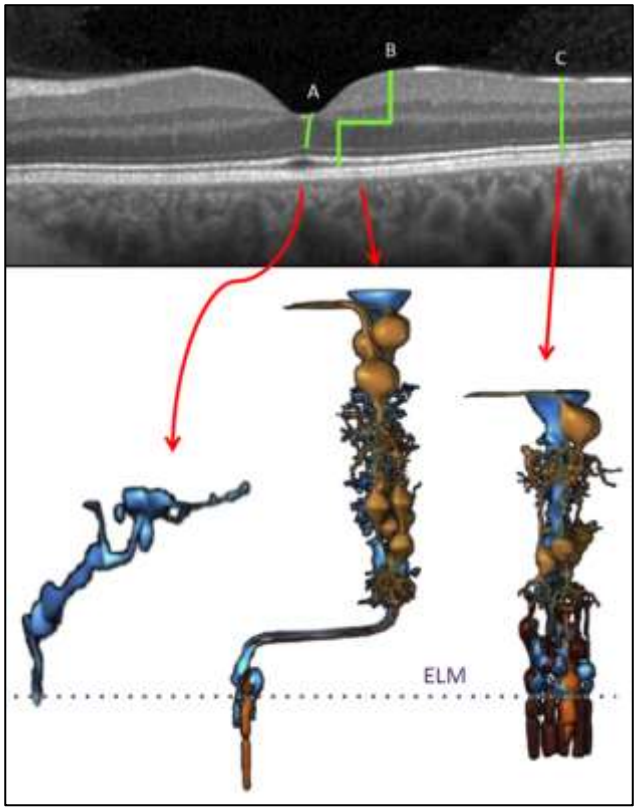

Figure 1-9: Different Müller cell subtypes: (A): MC of the MCC; (B): z-shaped MC; (C): straight (peripheral) MC; Dashed line denotes relationship with ELM. Adapted from Bringmann et al (2018) (9) [images reproduced with permission of the rights holder, Elsevier]

The lateral displacement of processes in HFL is maximal at about 400µm eccentricity, declining sharply at 2.5-3mm from the foveal centre (111,112). In the peripheral

retina, MCs are typically orientated vertically in the retina and so HFL is absent here, although MC density remains stable at around 6,000/mm^2 (Figure 1-9C) (9,19,112).

1.2.4.4 Role of Müller cells in foveal structure and development

Müller cell subtype heterogeneity plays an important role in the normal development and structure of the fovea. Histologically, the adult human fovea consists of a bowl-like pit, characterised by densely packed cone photoreceptors, but devoid of rod photoreceptors and inner retinal layers. The central photoreceptor axons are displaced laterally, running alongside the zMCs in HFL, until the presynaptic pedicle meets with secondary bipolar neurons in the parafoveal OPL. The embryogenesis of the fovea is a complex process of domain-specific gene expression, directing localised inhibition of cell differentiation and signaling directional GCL axonal growth. The earliest signs of foveation occur around gestational weeks 25-28, as medial displacement of central photoreceptors causes the density to treble to 36,000/mm^2, while horizontal orientation of HFL can be appreciated by 35-37 weeks gestation (113–117). At birth, the foveal pit contains residual GCL and IPL layers, and cone photoreceptors are seen to begin to angle out with the foveal slope into HFL. Further post-natal medial displacement of the central photoreceptors results in a 4-fold increase in the foveolar cone density and, by 15 months, a definitive foveal structure is visible. The lower range of adult cone density (98,000-324,000/mm^2) is achieved by 4-6 years and complete development is observed by around 13 years (18,114–116,118). The late formation of the fovea, after cellular proliferation and differentiation, indicates that there may be a process of mechanical re-shaping at play. Bi-directional displacement of the inner retina that occurs ante-natally, at about 28 weeks, is thought to be mediated by the withdrawal of astrocytes from the foveal pit (possibly due to horizontal contraction of stellate and bipolar astrocytes in the GCL and NFL) (113,119–121). In contrast, the central contraction of the outer retina, causing this subpopulation to become thinned and densely packed, begins around the same time and continues for several years post-natally. Bringmann et al have proposed a ‘sliding zone’ at the level of HFL, wherein

vertical contraction of the foveolar MCC, combined with horizontal contraction of the zMC side processes in the OPL, leads to elongation the central photoreceptors and erection of the foveal walls (9,50). As such, arrest of foveal maturation, as seen in cases of foveal hypoplasia, is characterised by a lack of inner retinal displacement. Depending on the stage of arrest, there is a variable degree of foveal cone packing, which gives rise to ONL and HFL thickening centrally and thinning in the parafoveal region, relative to normal subjects (Figure 1-10) (122–124).

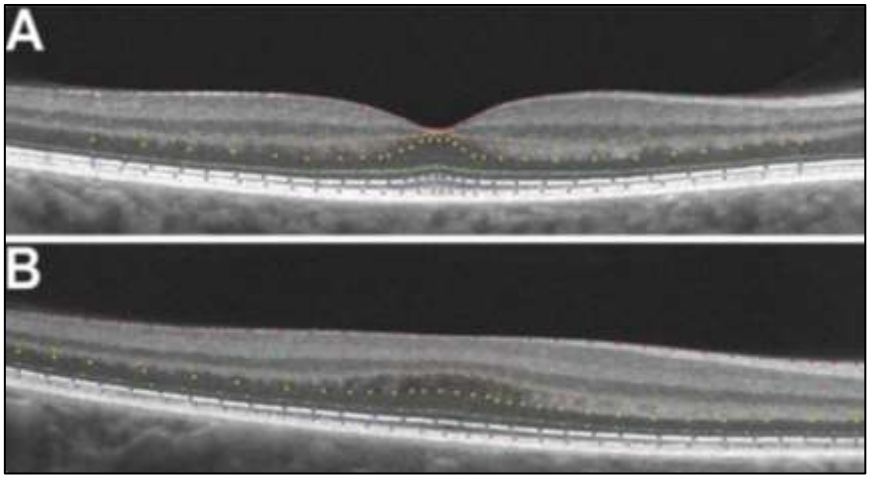

Figure 1-10: Comparison of retinal layer segmentation on OCT between a normal subject (A) and a subject with albinism and foveal hypoplasia (B). HFL (denoted between the orange and yellow lines) is thicker centrally, but thinner paracentrally, in the subject with albinism. Credit: Lee et al (2018) [image Creative Commons licensed] (123)

Structural stability of the foveal contour is maintained through life by the distinct biomechanical behaviours of the MC subtypes. Under normal conditions, GFAP and vimentin expression from MCs is downregulated, to limit unnecessary cell hypertrophy or stiffness (9). However it has been shown that the MCs in the fovea, particularly along the outer processes as they draw through HFL, express higher levels of GFAP throughout life (9,21,119,121). This suggests that these components are under continuous mechanical stress, requiring low levels of gliosis and upregulation of intermediate filaments to maintain foveal structural stability. Beyond about 300-600µm eccentricity, GFAP expression disappears (22). This

indicates that the preservation of foveal architecture is a perpetual, delicate balancing act of opposing glia-mediated tensile forces and is thereby rendered particularly vulnerable to any external tractional forces that threaten to disturb this equilibrium (Figure 1-11).

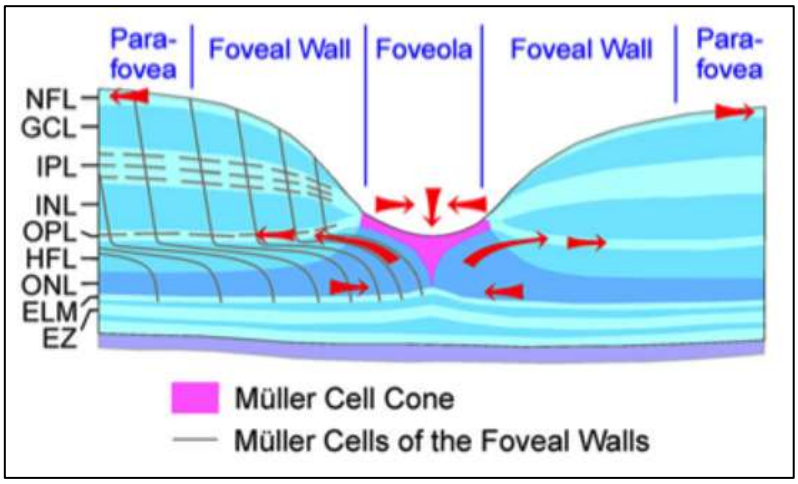

Figure 1-11*: *The tangential force vectors (red arrows) exterted by the MCC (pink) and zMCs (black) to maintain foveal architecture. Credit: Bringmann et al (2020) (99) [images reproduced with permission of the rights holder, Springer Nature]

1.2.4.5 Gross mechanical deformation of Müller cells

Due to its lack of vertically orientated fibres, HFL is a structurally weak point in the fovea and many disorders characterised by traction or macular oedema will manifest as schisis or fluid accumulation in this layer. However, this anatomical configuration also affords the retina with a degree of flexibility, through which extrinsic forces can be compensated for, through verticalisation and elongation of the outer processes within HFL, providing a dampening effect and maintaining function. In the case of tractional foveoschisis, this compensatory mechanism gives rise to a characteristic feature of intraretinal 'bridges', assumed to comprise bundles of stretched and bevelled zMCs and photoreceptor axons, spanning empty, intraretinal spaces (100).

The extent of stretching that a MC can withstand depends on both its morphology in its resting state (i.e. its subtype – see Figure 1-9) and its elastic (Young's) modulus. The elastic modulus describes the measure of an object's resistance to non-permanent deformation and is defined as the ratio of tensile stress (i.e. applied force per unit area) and tensile strain (i.e. deformation/elongation as a result of stress). According to Hooke's law, a solid material will undergo elastic deformation in a linear manner, within the limits of its elastic modulus. Beyond this, the tensile capacity is overcome, resulting in permanent deformation or fracture. It is challenging to estimate the elastic modulus of the MC as it is mechanosensitive to both intrinsic stretch and surrounding physiological changes (125–128). It has been shown that MCs undergo morphological, cytoskeletal and gene regulatory changes in response to change in the extracellular substrate (126–128). For example, in the case of epiretinal membrane (ERM) (discussed in 1.3.1.2), TGF-β-induced α-smooth muscle expression and myofibroblastic transdifferentiation, results in an intrinsic increase in MC stiffness and contractility (128). As such, *in vitro* measures of MC stretch translate poorly into *in vivo* studies of disease. Histological study of Henle fibre length, gives a broad estimate of between 406-675µm (109), while OCT offers the capacity to evaluate MC stiffness and stretch as a function of HFL deformation *in vivo*.

Govetto et al have investigated the properties of MCs using OCT to model zMCs as 3 rigid bodies (R_1, R_2 and R_3) of 3 lengths (L_1, L_2 and L_3), which are attached at two hinge points, around which the angle (Θ) can vary, with respect to the fixed vertical positions of R_1 and R_3 (Figure 1-12) (100). In its resting state in the normal fovea, a zMC was assumed to have an angle Θ of 90˚, which could decrease to 0˚ in association with elongation of L_2, in response to mechanical retinal deformation. By modeling the entire MC complex as an elastic spring, the variable MC stiffness could be measured as a function of the angle Θ, proportional to the inverse square of L_2.

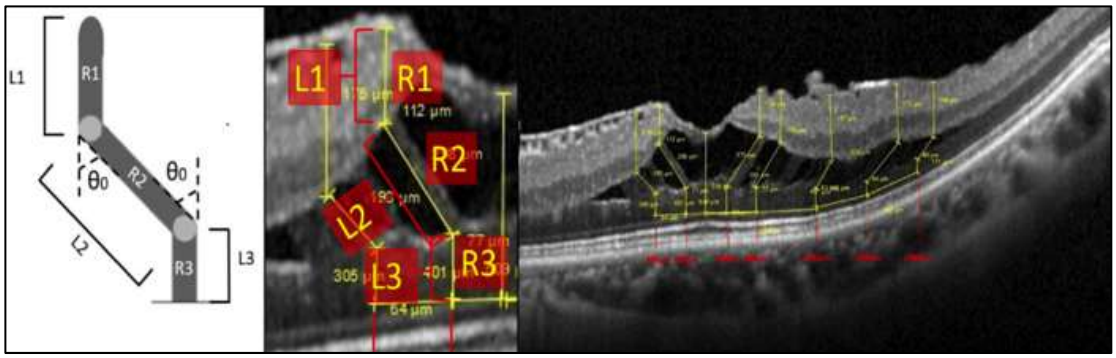

Figure 1-12: Modelling of zMC as 3 rigid bodies (R1-3), with lengths L1-3 and angle Θ. The R2 segment corresponds to the intra-schitic bridge of the zMC and is measured at various locations up to 3000µm from the fovea. Credit: Govetto et al (2019) (100) [images reproduced with permission of the rights holder, BMJ]

By measuring the values Θ and L_2 in various points around the fovea in eyes with ERM foveoschisis and myopic traction maculopathy (MTM), Govetto et al predicted that MC stiffness increases rapidly with lower values of Θ (particularly below 20˚), at which point significant mechanical stress is transmitted to the photoreceptors (Figure 1-13). Moreover, they determined that variations in angle Θ were functionally relevant, with smaller angles 200µm nasal and temporal to the fovea being significantly associated with worse visual acuity. In absolute terms, the length, L_2, was maximally 471µm in MTM and 300µm in ERM, when measured 500µm from the foveal centre.

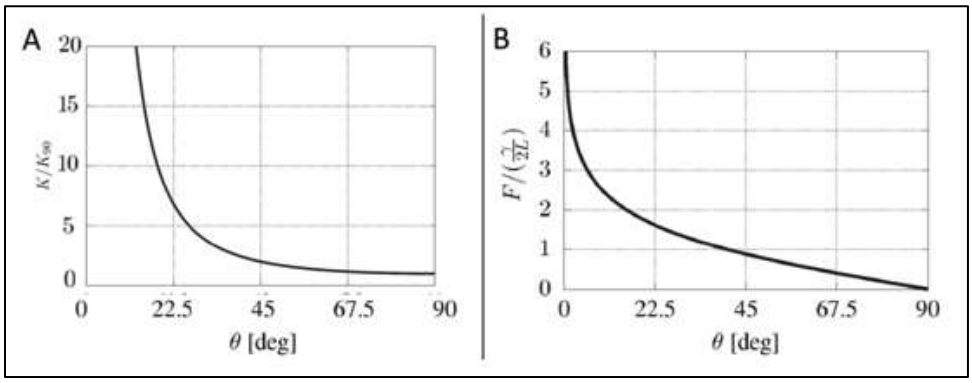

Figure 1-13: Muller cell stiffness variation according to Θ: (A): cell stiffness K(Θ) versus angle Θ (normalised to K90, for Θ=90˚, i.e. relaxed position); (B): Force (F) as

a function of the angle Θ. Credit Govetto et al (2019) (100) [images reproduced with permission of the rights holder, BMJ]

In summary, MC behaviour is critical for the formation and maintenance of the foveal contour in health and also the morphological changes observed in tractional foveomacular disease. In the following subsections I will explore how the anatomico-functional manifestations of various vitreoretinal pathologies can be related back to the ultrastructure of the retina and, in particular, that of the Müller cell.

1.2.5 Modelling forces in the retina

In the healthy eye, there is a multitude of forces, besides those exerted by MCs (Figure 1-14A), which serve to maintain the foveomacular architecture. These forces include external forces, such as hydrostatic and oncotic pressure gradients, maintained by the blood retina barrier, the RPE pump, the intraocular pressure (IOP) and the choroidal extracellular matrix; other physical external forces, such as vitreous support and both scleral and optic nerve rigidity; intrinsic retinal forces, such as the intrinsic elastic properties of other neuroglial cells and intercellular electrostatic interactions, photoreceptor interdigitation and the interphotoreceptor proteoglycan matrix. (129–137). In the context of disease, disequilibrium of these forces can lead to morphological disturbances and the accumulation of intra- or sub-retinal fluid. Not only can these existing forces modify, but also novel forces may be introduced. Such forces may be external or internal; they may be tangential, with a net centrifugal or centripetal vector, or purely perpendicular, with an anteroposterior vector (Figure 1-14B) (98,99,138–141).

For the purposes of this thesis, I will refer to the tangential forces (such as those exerted by ERMs or those intrinsic to the MCC and zMCs) as having medially- or laterally-directed vectors, with respect to the fovea. This differentiates them from the broad macular forces generated at the inner retina (e.g. through ILM fibrosis), which will be termed centripetal vectors, and those of the sclera (e.g. in posterior staphyloma), which will be termed centrifugal vectors. Finally, those force vectors

which are generated perpendicular to the retina, e.g. by vitreomacular traction (VMT) or intraretinal expansion (as in optic disc pit maculopathy (ODP-M)) will be referred to as anteroposterior vectors. Figure 1-14C-H demonstrates examples of force vectors in various vitreomacular foveopathies, including ERM (C&D), VMT (E), ODP-M (F) and myopic foveoschisis (G&H).

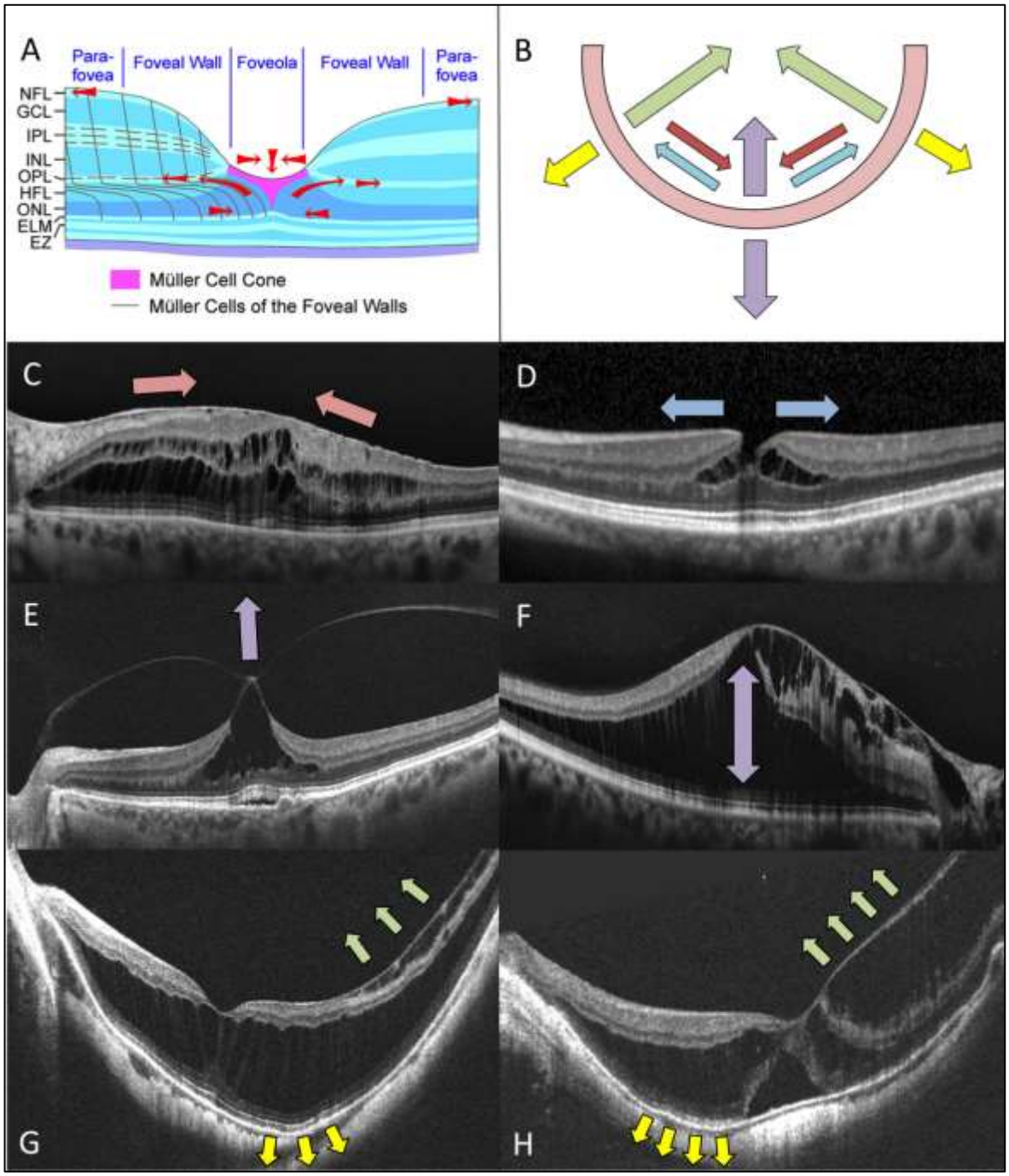

Figure 1-14: "May the forces be with you" - force vectors acting on the retina: A: Effective traction vectors in the normal fovea (red arrows). Credit: Bringmann et al

(2020) (99); B: Effective traction vectors in the diseased retina: centripetal (green arrows) and centrifugal (yellow arrows) vectors; tangential vectors, comprising medial (red arrows) and lateral (blue arrows) vectors with respect to the fovea; anteroposterior vectors (purple arrows); C-H: Examples of traction vectors in various vitreomacular pathologies [image reproduced with permission of the rights holder, Springer Nature]

In reality, mechanical foveomacular retinoschisis is the net result of various combinations of force vectors. As such, dissimilar pathologies can present with comparable structural changes (see Figure 1-15). In this thesis, I will explore the possible mechanisms through which different conditions manifest in similar morphologies and how the underlying diagnosis may be differentiated and the clinical course predicted. In the remainder of this chapter, I provide a brief overview of both acquired and congenital foveopathies that are typified by FRS, as well as pertinent differential diagnoses.

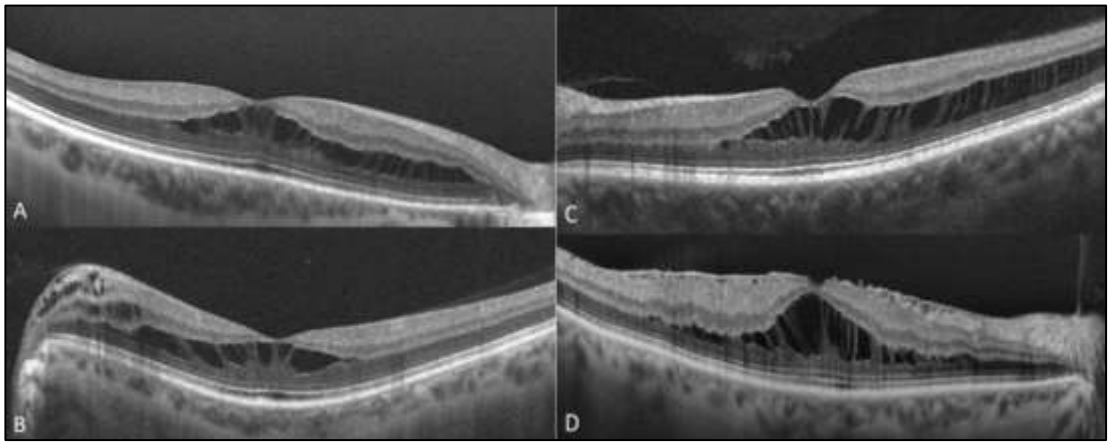

Figure 1-15: OCT scans demonstrating similar schitic morphologies resulting from different underlying pathologies: (A): myopic foveoschisis; (B): optic disc pit maculopathy; (C): idiopathic foveomacular retinoschisis; (D): ERM foveoschisis

1.3 Acquired foveomacular retinoschisis

Equipped with an understanding of the foveomacular ultrastructure in health, it is possible to model the anatomico-functional behaviour of FRS. By far the commonest acquired causes of FRS are vitreomacular interface (VMI) disorders, which comprise conditions such as vitreomacular traction, epiretinal membrane and lamellar or full thickness macular hole. While an exhaustive review of the literature concerning VMI disorders is beyond the scope of this thesis, I have used these conditions to demonstrate how different force vectors manifest in particular structural changes, as a result of the variable effects on MC morphology.

As discussed in 1.2.3, the outer portion of the ILM is comprised of MC endplates and the inner portion contains the anchoring fibrils of the vitreous body. With age, changes in the biochemical composition and rheological properties of the vitreal gel result in progressive liquefaction (synchysis) and collapse (syneresis) of the vitreous (31,142,143). This process culminates in the development of a posterior vitreous detachment (PVD), wherein the vitreous gel separates completely from the retina between the ILL and the PVC. During the process of PVD development, vitreous liquefaction may outpace the weakening of vitreoretinal adhesions, causing incomplete delamination of the PVC from the ILM overlying the macula, which is known as 'anomalous PVD' (144). Anomalous PVD can manifest as either a full thickness adherence of the vitreous at the fovea or a partial thickness adherence, due to splitting within the PVC (vitreoschisis), leaving remnants of cortical vitreous on the retinal surface (138,144–146). In the case of the former, this may cause direct distortion of the retina, as a result of focused vitreal forces, while the latter may provide a scaffold for uncontrolled cellular proliferation, followed by transdifferentiation and contraction. In both circumstances, mechanical disruption of the normal foveomacular architecture may be observed (98,99,141,147).

1.3.1.1 Vitreomacular traction syndrome

Vitreomacular traction syndrome (VMTS) describes a group of conditions arising due to mechanical forces, which are exerted on the macula by the presence of residual vitreal attachment, following anomalous PVD (147–152). Based on OCT imaging, the International Vitreomacular Traction Study group classified VMTS as vitreomacular adhesion (VMA) when there is “perifoveal vitreous separation with remaining vitreomacular attachment and unperturbed foveal morphologic features”, and vitreomacular traction (VMT) as ”anomalous posterior vitreous detachment accompanied by anatomical distortion of the fovea” (152). VMA and VMT can be further subdivided into broad (>1500µm) and focal (≤1500) attachment (145,152–154).

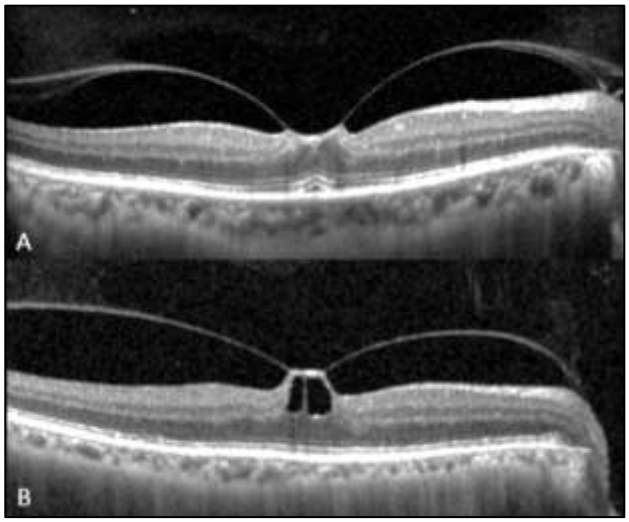

Figure 1-16: Features of focal VMT on OCT; (A): Anteroposterior traction delineating the MCC. (B): Traction causing elongation of the vertical stalk of the MCC and development of a pseudocyst

In its early stages, VMT is frequently typified by loss of the foveal depression, which Spaide et al noted tends to form when the extent of posterior vitreous attachment is ≤840µm (153). As the focus of vitreous attachment decreases to approximately 280µm (corresponding roughly to the diameter of the foveola and, therefore, the MCC (Figure 1-16A)), further distortion may result in the formation of a foveal ‘pseudocyst’ (98,148,152,153,155). On OCT, the pseudocyst is often associated with

detachment of the MCC from HFL/ONL of the foveal walls and elongation of the vertical MCC stalk (Figure 1-16B & Figure 1-17A) (98). Progressive traction may cause elevation of the inner retinal layers of the foveal wall, characterised by the formation of a schisis cavity between the parafoveal HFL and OPL, through which the z-shaped MCs can be seen as bundles, obliquely traversing the schitic cavity. Sustained, unopposed traction of the zMCs may result in the development of an outer lamellar hole (OLH) or foveal detachment (FD) (Figure 1-17B&C) (98). Finally, complete operculation of the MCC can lead to the formation of an inner lamellar hole (ILH) or full thickness macular hole (FTMH) (Figure 1-17D) (141,148–150,152,156). The extent of stretch that the MCC can withstand before rupture of the central stalk appears to be variable and dependent on several factors, such as the breadth of VMT, vitreo-foveal angle and also choroidal thickness (157–160). MCC tensile capacity is likely to be significantly less than that of the zMC, given that the vertical orientation at rest affords less redundancy. Although not quantified, MCC stretch can be estimated by looking at OCT studies of VMT progression. For example, Uzel et al reported that a central foveal thickness of >471µm was associated with worse visual outcomes (i.e. approximately 250µm from normal baseline), while Petrou et al also found that greater CMT was associated with higher progression to FTMH (159–162). Figure 1-18 demonstrates proposed tractional effects of VMT with respect to the MC subpopulations.

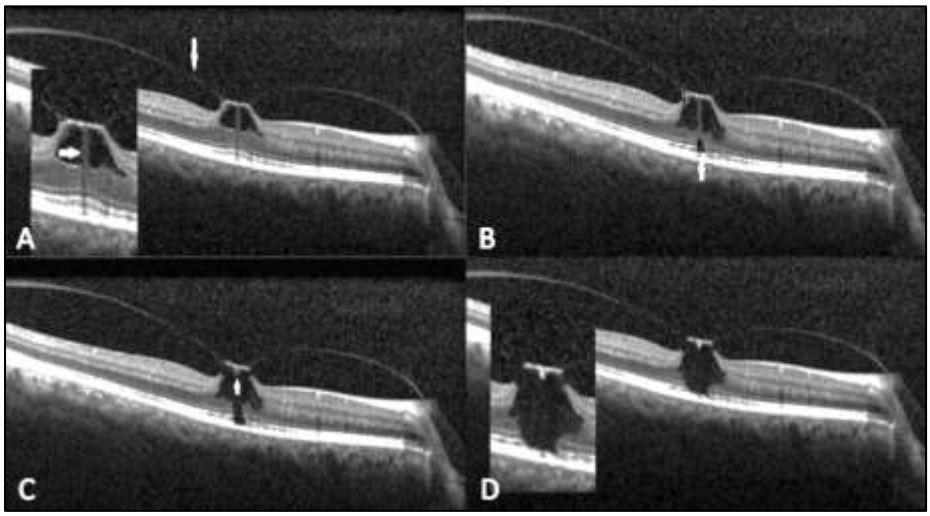

Figure 1-17: OCT scans demonstrating the development of FTMH via VMT: (A): pseudocyst formation, followed by (B) OLH formation, (C) MCC rupture and (D) operculation. Adapted from: Theodossiadis et al (2014) (157) [images reproduced with permission of the rights holders, Springer Nature]

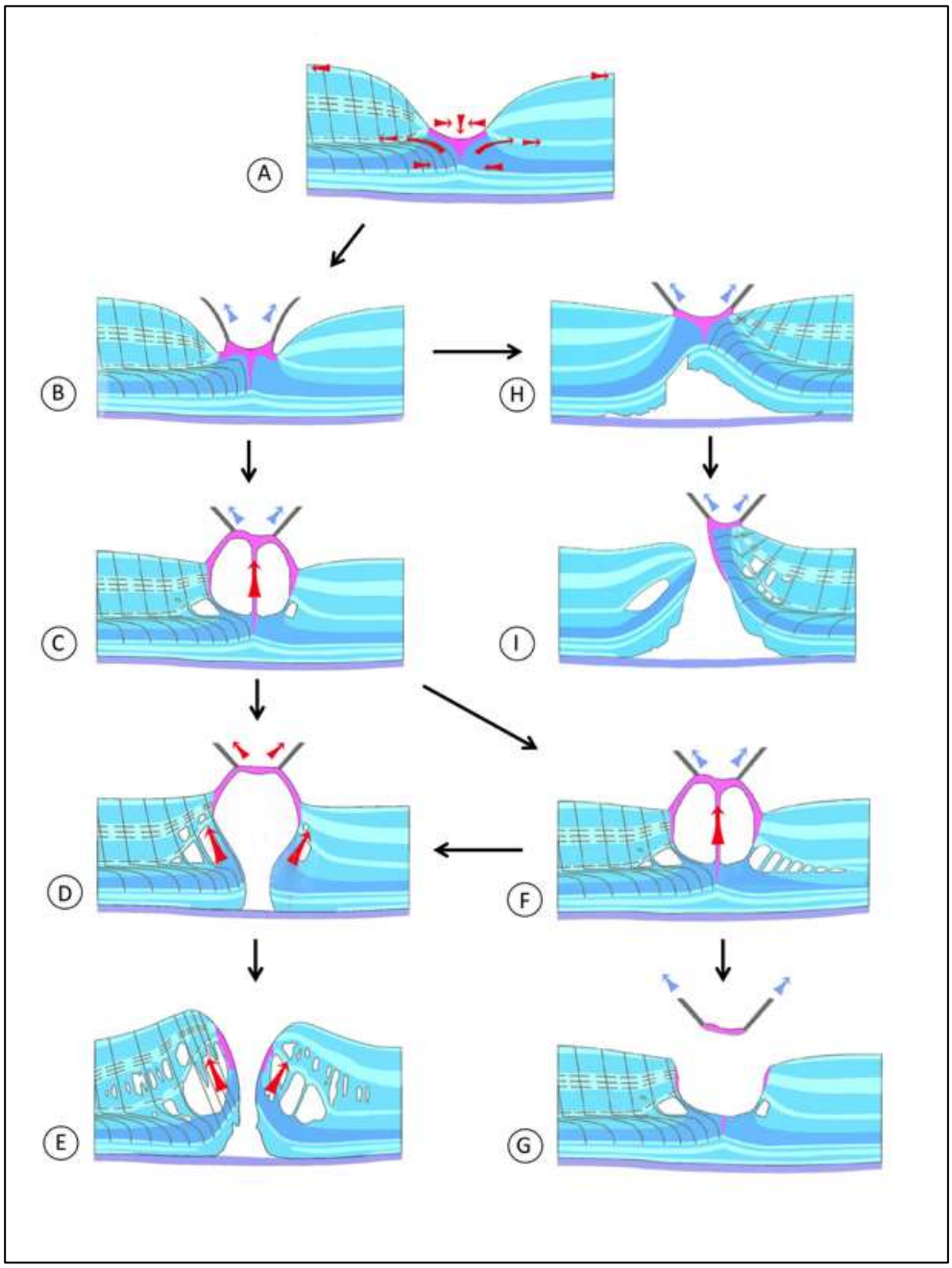

Figure 1-18: Diagrammatic illustration of the tractional forces in VMT, with respect the foveal MC subtypes; (A): Under normal circumstances, the medial forces exerted within the MCC (pink) are balanced with the lateral forces of the zMCs (black lines); (B): anteroposterior traction over the MCC due to focal VMT; (C): Progressive elongation of the MCC vertical stalk with early pseudocyst formation; (D): Rupture of the vertical MCC component, with unopposed lateral zMC forces, leading to formation of OLH; (E): Operculation of the MCC resulting in FTMH; (F): sustained traction without MCC rupture may lead to the formation of a schisis

cavity within HFL; (G): operculation of the inner portion of the MCC without rupture of the vertical stalk may result in the formation of an ILH; (H): an alternative pathway if traction is sufficiently concentrated, is the development of a primary FD; (I): sustained traction in this situation may result in the formation of an ILH and/or FTMH. Adapted from Bringman et al (2020a/b, 2021) [images either Creative Commons licensed or reproduced with permission of the rights holders, Springer Nature and BMJ] (98,99,141)

1.3.1.2 Epiretinal membrane

Epiretinal membrane is another common VMI disorder that can cause disruption of the normal foveomacular architecture (163–169). Comprising an avascular fibrocellular membrane superjacent to the inner retinal surface, the term ERM encompasses a range of morphologies, from an asymptomatic 'cellophane' macular reflex to a premacular fibrotic membrane, as originally described histologically by Foos et al and staged clinically by Gass (170,171).

ERM is usually 'idiopathic' or 'primary', but may also occur following ocular surgery or secondary to intraocular inflammation, retinal vascular disease or retinal detachment (172). In the case of primary ERM, it is thought that anomalous PVD and subsequent residual epimacular cortical vitreous remnants contribute to fibroglial proliferation onto the macular surface (144,170,173–179).

Histologicially, ERMs can be defined as 'simple' or 'complex' (170). The simple ERM contains a monolayer of type IV collagen-producing glial cells, which are known as laminocytes and stain positively for glia-specific proteins, such as GFAP and cytokeratin markers (177,180–182). Proliferation and migration of these accessory glial cells over the ILM cause development of a non-contractile cellophane maculopathy that is rarely visually symptomatic (Figure 1-19A). By contrast, the complex ERM is separated from the ILM by a layer of type II collagen-containing PVC, which provides a scaffold for cellular proliferation and migration of glial cells and

hyalocytes (183,184). There is a polymorphous cell population in a complex ERM, including myofibrocytes, macrophages and epithelial cells, due to the capacity of MCs and hyalocytes to undergo transdifferentiation during the pathogenesis (176,185–187). Consequent formation of an extracellular matrix, containing proteins such as fibronectin, vitronectin, laminin, tenascin, thrombospondin and collagen, results in the formation of an irregular network of fibrils on the retinal surface (177,183,184,188–190). Following this, MC transdifferentiation into myofibroblasts is associated with a reduction in glial-specific proteins and an increase in the expression of α-smooth muscle actin, resulting in contractility of the ERM (188,191–193). Focal connections between the ERM and MC fibres mean that this contraction generates a continuous cycle of MC reactivity and gliosis, manifesting as hypertrophy and alterations in plasma membrane properties, supporting yet further release of growth factors and cellular proliferation.

The distribution of ERM tends to be broader than that of VMT, such that the tractional forces primarily follow a tangential, as opposed to anteroposterior, orientation. The manifestations of such irregular force vectors are protean, including macular wrinkling, dragging of retinal vessels and macular hole formation. For example, if the overall vector of the tangential forces is medially-directed, we might expect that an ERM leads to formation of a macular pseudohole (MPH), macular thickening or macular pucker (Figure 1-19C), while laterally-directed force vectors could result in pseudocyst formation, foveoschisis and lamellar or full thickness holes (Figure 1-19B) (97,194). Considering the orientation of MC processes in the MCC and inner foveal wall, laterally-directed forces are more likely to manifest in separation of the MCC from the inner foveal walls and focal schisis between the parafoveal HFL and OPL (138,188,195,196). Medially-directed forces, on the other hand, do not tend to cause disruption to the MCC. However, disruption of the foveal architecture through the development of ‘ectopic inner foveal layers’ (EIFL) may be associated with significant visual morbidity (194,197). Although less commonly observed in latter cases, schisis cavities have been described in the inner retina, e.g. within the NFL, in relation to ILM dehiscence (198).

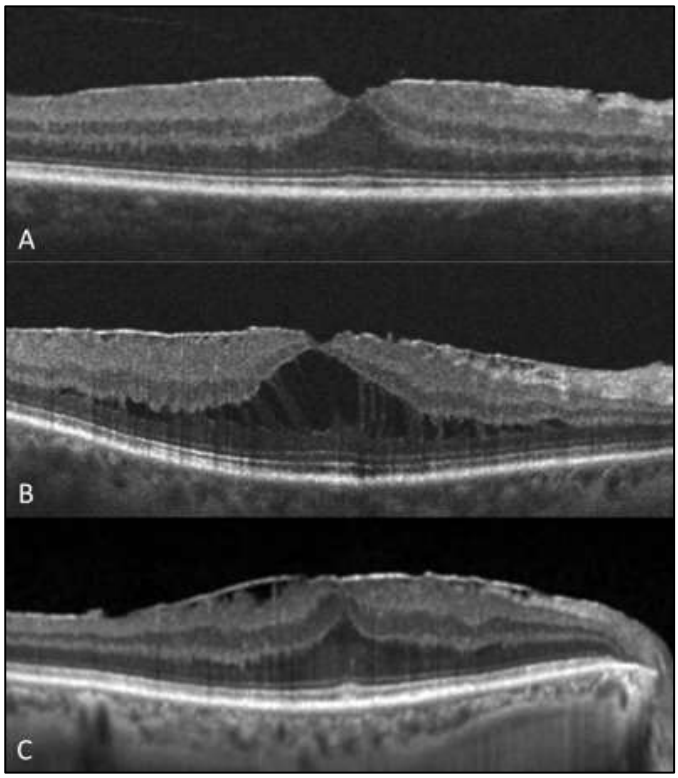

Figure 1-19: Various morphologies in ERM on OCT; (A): simple ERM (cellophane maculopathy); (B): complex ERM with foveoschisis; (C): complex ERM causing macular pucker with EIFL: Credit: (A): (Luu et al (2019); (C): Doguizi et al (2018) (199,200) [images reproduced with permission of the rights holders, Springer Nature]

The features of ERM traction are demonstrated in Figure 1-20. In reality, VMT and ERM are frequently observed concurrently, giving rise to a varied combination of features, including the development of OLH, FD and FTMH (Figure 1-18) (201,202).

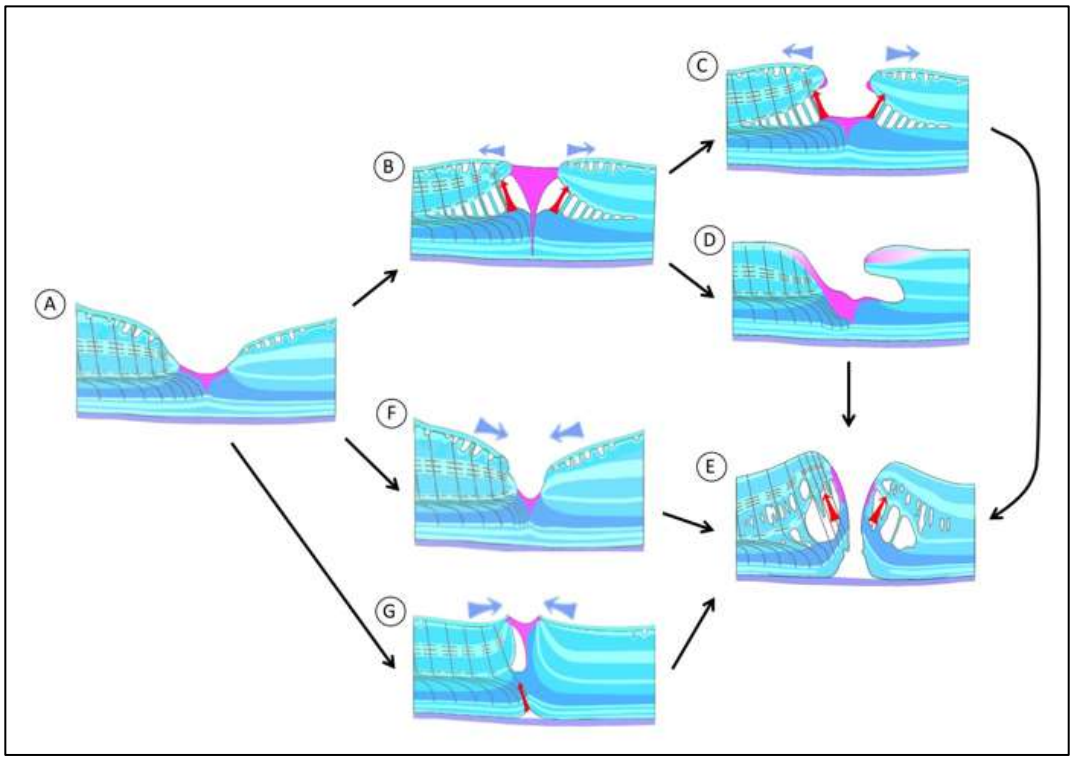

Figure 1-20: Diagrammatic illustration of the tractional forces in ERM, with respect the foveal MC subtypes; (A): early ERM formation; (B): sustained laterally-directed traction (blue arrows) from complex ERM, resulting in elongation of MCC (pink) and development of foveoschisis cavity in HFL; (C): rupture of the foveal wall component of the MCC, with formation of tractional lamellar macular hole; (D): foveal tissue loss with formation of degenerative lamellar macular hole; (F): sustained medial forces (blue arrows) from complex ERM, resulting in formation of a pseudohole; (G): formation of macular pucker with ectopia of inner retinal layers and, if sustained contraction, the formation of a FD. Progression to a FTMH (E) may be observed in all cases. Adapted from: Bringmann et al (2020a/b, 2021) [images either Creative Commons licensed or reproduced with permission of the rights holder, Springer Nature and BMJ] (98,99,141)

1.3.1.3 Inner lamellar hole

First described by Gass in 1976, the term 'lamellar' macular hole (LMH) referred to an oval, reddish macular lesion with associated cystoid macular oedema,

demonstrating histological evidence of tissue loss (203). Following the advent of OCT, this definition was gradually refined to describe a morphology including various features, such as an irregular foveal contour, a break in the inner fovea, intraretinal splitting and intact photoreceptors (204–208). Gaudric et al argued that a 'true' LMH depends on the presence of foveal tissue loss, and should not be confused with MPH, which may present with 'straight' or 'stretched' edges, depending on the predominant vector of ERM contraction (Figure 1-21) (207). The precise mechanism and diagnostic criteria for LMH remain contentious (205–207,209,210).

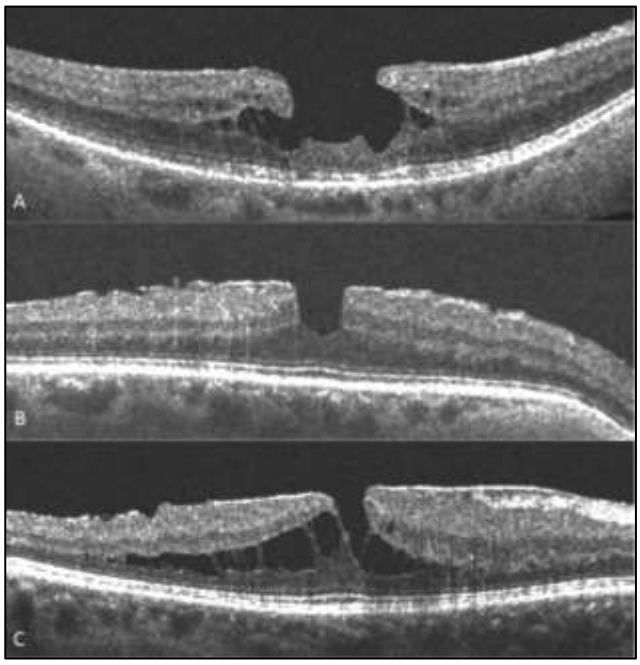

Figure 1-21: Degenerative and tractional ERM morphologies; (A): 'true' lamellar hole with foveal tissue loss; (B): macular pseudohole with 'straight' edges; (C): macular pseudohole with 'stretched' edges. Credit: Gaudric et al (2013) (207) [images reproduced with permission of the rights holder, Elsevier]

In 2016, Govetto et al further characterised LMHs into two distinct subtypes, based on morphological features: 'tractional' LMH and 'degenerative' LMH, with occasional overlap between the two (195). Degenerative lamellar macular holes (DLMHs) were characterised by the presence of a foveal 'bump', a non-specific plane of retinal cleavage, the presence of lamellar hole-associated epiretinal proliferation (LHEP) and, frequently, EZ disruption. In addition, the inner/outer defect diameter ratio

tends to be >1:2 and the edges of the cavitation are generally rounded, without bridging MC processes. These features led the authors to refer to DLMHs as having a 'top hat' morphology (Figure 1-22). It is also noted that DLMHs appear to have relatively reduced retinal thickness and worse best-corrected visual acuity than their tractional counterparts (195,211,212).

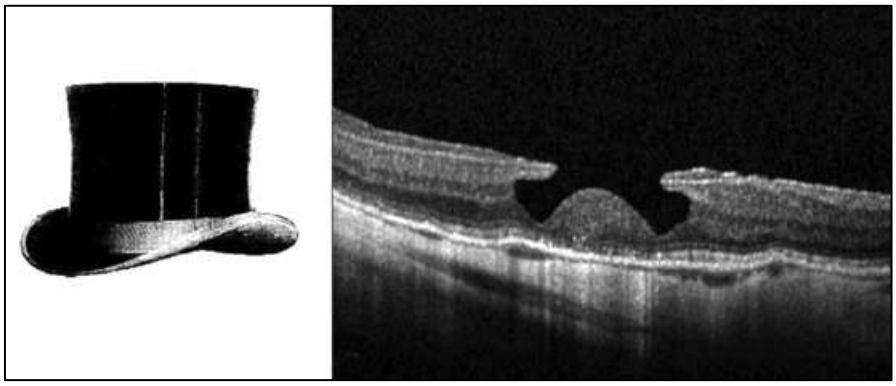

Figure 1-22: 'Degenerative' lamellar macular hole, with 'top hat' morphology and epiretinal proliferation. Credit: Govetto et al (2016) (195) [image reproduced with permission of the rights holder, Elsevier]

LHEP comprises a homogenous, isoreflective material that forms on the surface of the ILM and, unlike ERM, is indistinct from the underlying retinal surface on OCT (211,213,214). First termed by Pang et al, it was initially thought to be a feature specific to LMHs, but has since been noted in cases of FTMH and macular pucker, and may be better termed 'EP' (141,213). Histologically it shows features of cellular proliferation (positive immunoreactivity for GFAP and anti-glutamine synthetase), but not contractile proteins, such as α-smooth muscle actin or myofibroblasts, as in ERM (215). It has therefore been suggested that EP is likely to originate from migration of Müller cells from inner retina following LMH formation (98,213,216,217). Morphologically, DLMHs may be initiated by paracentral traction as seen in other VMI disorders, but the subsequent development of EP and focal cavitation with undermining of the parafoveal tissue is driven by a chronic degenerative process that follows separation of the MCC from the inner foveal walls (98). As such, DLMH may be considered to have a distinct pathoanatomical pattern from other VMI disorders (98,208).

By contrast, so-called 'tractional' lamellar macular hole (TLMH) develops following the disruption of the junction between the MCC and the inner foveal wall (98,195,206,207). This process often manifests with formation of a parafoveal schisis cavity between HFL and OPL, and disruption of the inner foveal wall at the level of the ONL. This morphology is typical in cases of laterally-directed tangential forces, such as those frequently exerted by an ERM (195,207). However, it has been demonstrated that complete operculation of the MCC in VMT may also result in TLMH, due to the unopposed intrinsic lateral force vectors of zMCs in the foveal walls, even in the absence of a pre-macular structure (98). Govetto et al termed this type of LMH as having a 'moustache' appearance on OCT, as characterised by the schitic separation at the level of HFL and the dehiscence of the MCC (Figure 1-23). Morphologically, TLMH tends to have an inner/outer defect diameter ratio of <1:2, an intact EZ and a 'sharp-edged' schisis contour (195). The anatomical and functional features of TLMHs appear to remain stable over time. Using the mathematical model described in 1.2.4.5, Govetto et al investigated the relative MC deformation in TLMH, demonstrating that the angle θ is low (i.e. the MC is verticalised) at the fovea, but progressively increases away from the centre, while the R2 length (L_2) progressively increases towards the centre (100). This suggests that the mechanical stress in TLMH is concentrated over the fovea, in the vicinity of the MCC, and decreases significantly in the parafovea, where partial stretch of the zMCs is able to provide an adequate dampening effect, thus maintaining function and preventing anatomical progression (100).

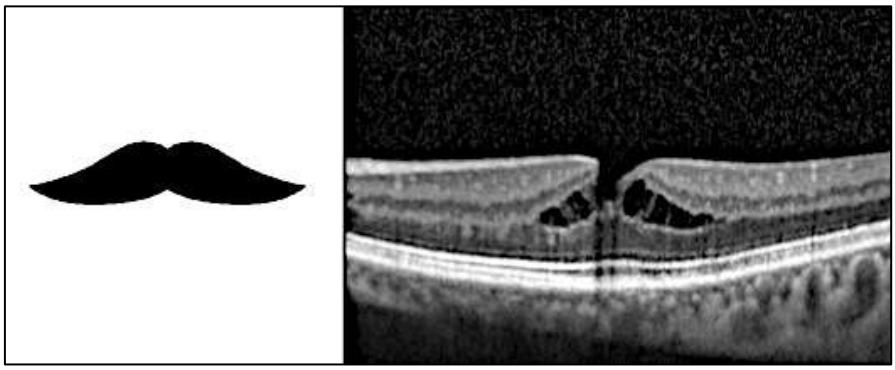

Figure 1-23: 'Tractional' lamellar macular hole, with 'moustache' morphology and foveoschisis. Credit: Govetto et al (2016) (195) [image reproduced with permission of the rights holder, Elsevier]

Most recently, in 2020, Hubschman et al have proposed a comprehensive consensus on OCT-based definitions for LMH (208). They suggest that the term LMH is reserved solely for the degenerative subtype, and that a new term, 'ERM foveoschisis' be used to all forms of tangential tractional disorders in the non-myopic eye. The offered criteria for ERM foveoschisis include: mandatory criteria of (a) contractile ERM; and (b) foveoschisis; and optional criteria of (c) microcystoid spaces in the INL; (d) retinal thickening; and (e) retinal wrinkling. It is suggested, therefore, that the entity known previously as either 'MPH with stretched edges' or 'tractional LMH' is reclassified as 'ERM foveoschisis', in accordance with its likely pathogenesis. Finally, it is suggested that the term macular pseudohole is reserved for those cases with fovea-sparing ERM, a steepened foveal profile and associated retinal thickening (208). In practice, the vectors of complex ERMs are inherently random, such that substantial overlap between the different morphologies may be observed (Figure 1-24).

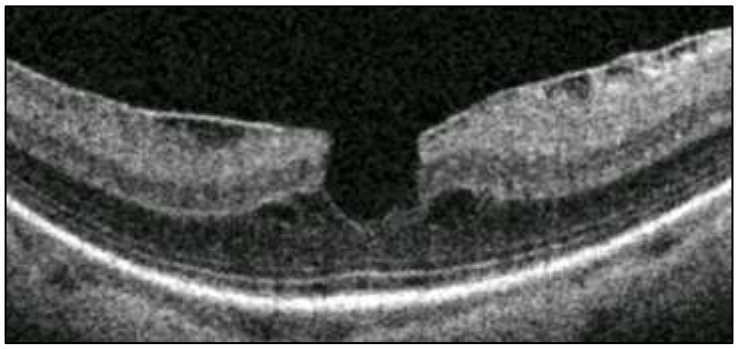

Figure 1-24: OCT demonstrating macular pseudohole with ERM foveoschisis, as a result of mixed tractional vectors

1.3.1.4 Outer lamellar and full thickness macular hole

While inner LMHs are characterised by disruption of the MCC and preservation of the foveal ELM and ONL, outer lamellar holes comprise the opposite. This is presumed to follow elongation and disruption of the MCC vertical stalk (i.e. during pseudocyst formation or ERM foveoschisis), wherein oblique straightening of the zMCs in the foveal wall transmits unopposed tension to the outer retina (141). This force is concentrated at the fovea, wherein MC-photoreceptor density is greatest, causing eventual dehiscence of the ONL, with associated defects in the photoreceptors EZ and IZ lines, as well as variable disruption to the ELM. If the inner retina remains intact, an OLH forms. OLH may, in turn, be associated with formation of foveal detachment; if there is also tractional disruption of the MCC at the foveal walls, a FTMH can develop (Figure 1-25).

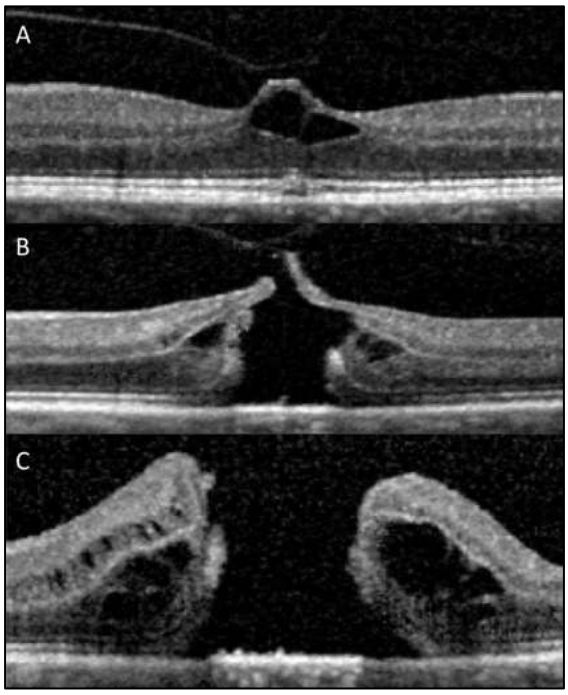

Figure 1-25: OCT demonstrating progression of VMT with pseudocyst (A), OLH and inner retinal operculation (B) and formation of FTMH. Credit: Bringmann et al (2021) (141) [images reproduced with permission of the rights holder, Science Direct]

In summary, study of the pathomechanical behaviour in VMI disorders serves to demonstrate the intrinsic forces within the retina and the vectors along which these act, with respect the different MC subpopulations. Retinoschisis appears to arise in the presence of both laterally-directed tangential traction (as in ERM) and anteropostrior traction (as in VMT). In the case of the former, this appears to manifest as a more stable foveoschitic morphology, due to the dampening capacity of zMC stretch. Direct disruption of the MCC in VMT, however, conveys a higher rate of progression to OLH and FTMH, as a result of unopposed centrifugal forces, acting along the path of the zMC to the outer retina. In some cases, sustained traction on the retina (particularly in the context of retinal thickening, stretch or broad premacular traction) can also result in the formation of a FD. Although not necessarily schitic conditions *per ses*, OLH, FD and FTMH can represent the anatomical end-point of a spectrum of disorders, which are characterised by schisis during their development. In this thesis, I will explore how the same

pathoanatomical mechanisms might be applicable to other, less common forms of acquired FRS.

1.4 Congenital foveomacular retinoschisis

1.4.1 X-linked retinoschisis

X-linked retinoschisis (XLRS) (OMIM 312700), also known as juvenile or congenital retinoschisis, is an inherited disorder of the retina, caused by a mutation in the retinoschisin 1 (*RS1*) gene on the X chromosome (Xp22.1-p22.3). Haas described the features of the disease in 1898, which was first referred to as XLRS by Jager in 1953 (218,219). It is the most common form of juvenile-onset retinal degeneration and is thought to affect between 1 in 5,000-30,000 males (depending on the population demographic), while female carriers are generally asymptomatic (220,221).

It was initially thought that the XLRS phenotype could be related to inherited defects in MCs, based on electrophysiological and histopathological findings (95,222–225). However, following formal identification of the putative gene by Sauer et al in 1997, genetic and biochemical studies have revealed a more complex underlying molecular pathophysiology (226–230). The human *RS1* gene encodes retinoschisin, a 24kDa, 224-amino acid secretory protein, specific to the retina and the pineal gland (230–233). In the adult retina, it is expressed predominantly by photoreceptor and bipolar cells and contributes to cellular adhesion, migration, organisation, signalling and interaction (227,229,230,232,234–238). For example, retinoschisin binds to cell membrane phospholipids and contributes to structural cell membrane microdomain stability and preservation of cytoskeletal architecture (239,240). The apparent presence of retinoschisin proteins throughout the neuroretina suggests that it may also contribute to the general retinal extracellular matrix, establishing a multimolecular scaffold to stabilise synapses and preserve overall retinal tissue integrity (240). This may underlie the clinical observation that, in XLRS, disruption of retinal architecture is widespread and not isolated to the outer layers, as in FRS.

Additionally, retinoschisin may regulate cellular volumes and transmembrane ionic concentrations, through its relationship with membrane proteins (241–246). These complex intra- and extracellular roles of the retinoschisin protein can explain the appearance of extracellular fluid accumulation, forming cystic cavitations (that do not leak on fluorescein angiography), as well as the progressive neuronal dysfunction and photoreceptor degeneration that is observed in XLRS.

Clinically, XLRS is characterised by bilateral foveoschisis and, in around half of patients, peripheral retinoschisis (247–250). While early OCT and histopathology studies suggested that there was a single cleavage plane in XLRS (223,251–253), subsequent evidence has shown that macular schisis can affect all retinal layers (254–257). 3 discrete locations for schisis cavity formation throughout the macula have commonly been described: the NFL, INL and the ONL/OPL junction (HFL), while isolated cysts have also been reported in the GCL. Schisis involving the fovea appeared to primarily involve the INL and, to a lesser extent, the OPL, while multiple layers are involved in the para-/extrafoveal regions (Figure 1-26) (255–260).

The genetic penetrance of XLRS is almost complete, yet there is a high degree of variability in phenotypic expression (250,261–263). As such, the natural course is largely unpredictable, but characteristically involves the deterioration of visual acuity over the first two decades of life, with ensuing stability until the fifth decade, at which point macular atrophy with coalescence of cysts to form a large schisis cavity are the primary drivers of vision loss (Figure 1-27) (247–250,264–266). Although vitreous or intra-schisis haemorrhage and retinal detachment may complicate the clinical course in around 10% of cases, the prognosis for vision during the first decades of life is initially good in over 80% of cases (247,248,267–270). Foveoschisis on OCT and inversion of the b:a waveforms (electronegativity) on ERG will often arouse initial suspicion of XLRS, although formal diagnosis relies on genetic testing (271,272).

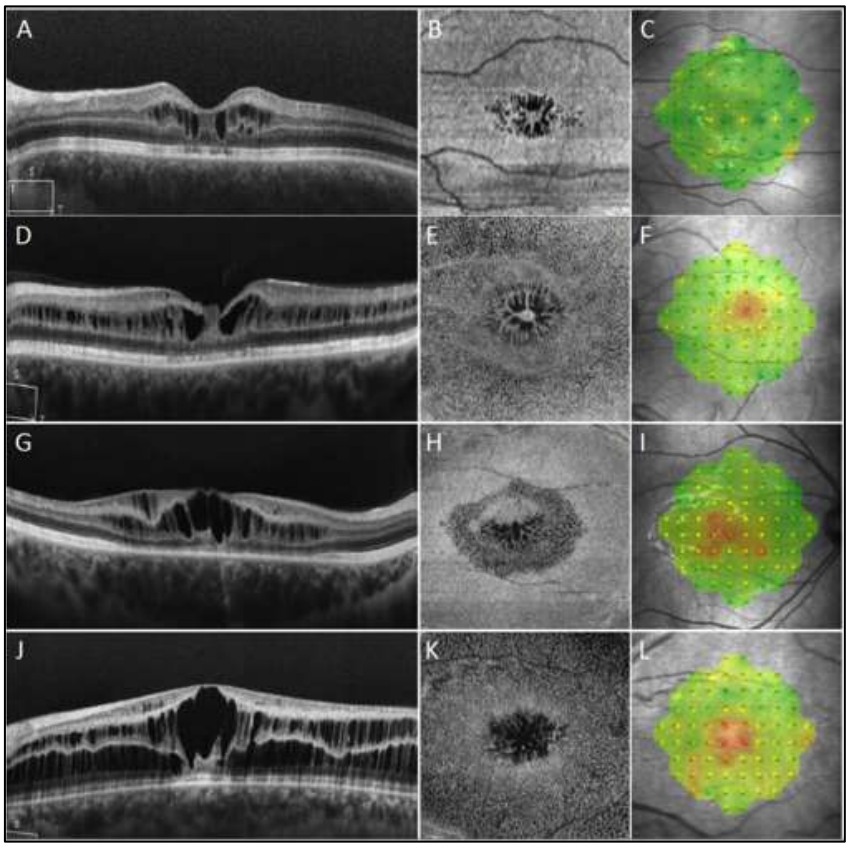

Figure 1-26: (A, D, G, J): OCT; (B, E, H, K): en face minimal intensity projection; (C, F, I and L): microperimetry, demonstrating the variable morphology and function of XLRS in different subjects. (A-C) 18-year-old with VA of 0.30 logMAR; (D-F) 30-year-old with of VA 0.48 logMAR; (G-I) 22-year-old with VA of 0.48 logMAR; (J-L) 16-year-old with VA of 0.48 logMAR

Many factors are thought to contribute to the broad spectrum of morphologies seen in XLRS, including age, environmental factors and genetic modifiers (250,261,264,265,273,274). Presentation and progression appears to be patient-specific, rather than mutation-specific, with comparable findings in each eye (266).

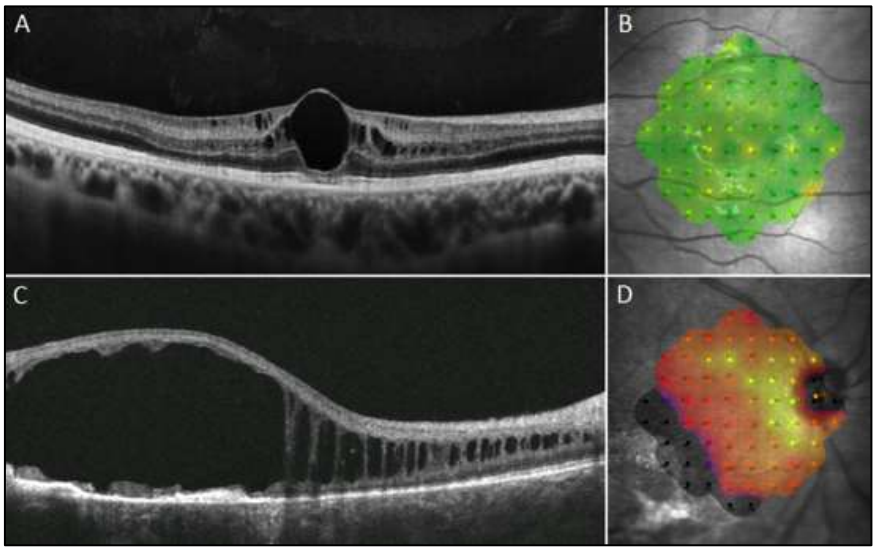

Figure 1-27: Morphological and function differences with time: (A&B) 21-year-old with VA of 0.18 logMAR; (C&D) 48-year-old with VA of 0.78 logMAR

It is notable that the anatomical distribution and natural history of retinoschisis in XLRS differs from that of the mechanical foveopathies. This distinction is most apparent on OCT, where perifoveal intra-schitic bridges can be observed within the INL (i.e. affecting the vertical inner process of the MCs, distal to its horizontal component), rather than HFL. XLRS does not manifest in leakage on FFA, indicating that these cystoid spaces are not a result of capillary hyperpermeability or fluid flowing down an oncotic pressure gradient. It seems more plausible that cytopathological disruption results in interruption of the normal transretinal hydrostatic pressure gradients, leading to multilayer fluid accumulation (275,276). Its association with outer retinal disruption, as well as the demographic and ancillary investigative particularities, mean that XLRS can usually be easily distinguished from acquired FRS. These morphological differences reflect the fact that XLRS is not a tractional foveopathy causing distortion of the MC architecture, but an inherited retinal dystrophy, underpinned by a series of complex cyto-biochemical disturbances. As such, in XLRS, it is impossible to characterise the anatomico-functional behaviour of the schisis in isolation. I will only include XLRS further in this thesis, as a negative control, in order to illustrate the differing anatomico-functional behaviour of a non-biomechanical, congenital foveopathy.

1.4.2 Other forms of congenital foveomacular retinoschisis

There are several other heritable disorders that present with lamellar foveal separation and ought to be considered as differential diagnoses for XLRS. Several groups have described an apparent autosomal recessively-inherited 'familial foveal retinoschisis' (FFR), predominantly affecting females, but morphologically indistinguishable from XLRS (277–279). Recently, mutations in the *CRB1* gene have been identified in some cases of FFR (Figure 1-28) (280–286). *CRB1* (OMIM: 604210) encodes the human orthologue of the *Drosphilia melanogaster* protein Crumbs and has been associated with several retinal phenotypes, including retinitis pigmentosa and Leber congenital amaurosis (280,281,286–288). The Crb1 transmembrane protein is thought to localise in the sub-apical region of MCs, above the zonulae adherentes, and to the vesicles in the vicinity of the myoid region of the inner segments of photoreceptors. Herein, it plays a critical role in the development of MC microvilli, as well as photoreceptor morphogenesis, polarity and function (289–294). Other cases of presumed sporadic and even autosomal dominant patterns of inheritance of FFR have been described, but the putative genes in these cases remain elusive (295–298).

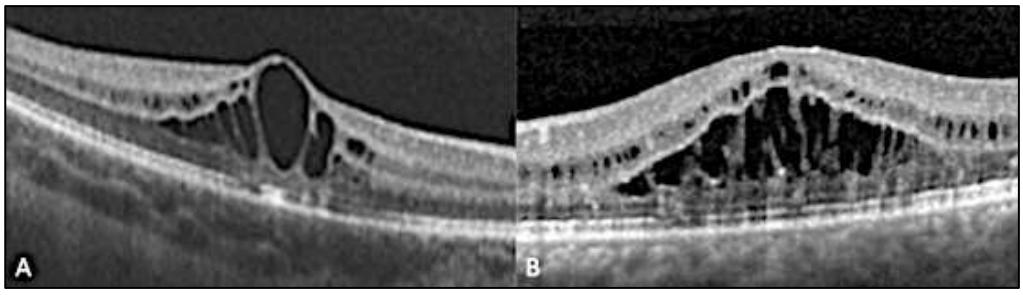

Figure 1-28: (A&B): Examples of foveoschisis and associated outer retinal changes in individuals with mutations in the CRB1 gene. Credit: (A): Khan et al (2018); (B): Oh et al (2020) (285,288) [images Creative Commons licensed or reproduced with permission of the rights holder, Sage]

Pathogenic mutations have also been identified in the nuclear receptor (*NR2E3*) gene on chromosome 15q23, producing various vitreoretinal degenerative phenotypes, including enhanced S-cone syndrome (ESCS) and Goldmann Favre syndrome (GFS) (299–303). NR2E3 (OMIM: 604485) encodes a ligand-dependent transcription factor that regulates the differentiation of photoreceptor cells; mutations in this locus manifest as an absence of rod photoreceptors, the progenitors of which adopt an S-cone fate instead (302,304). In GFS, the more severe phenotype, it is suggested that a lack of outer retinal tight junction formation can result in variable IRF accumulation, without angiographic leakage, manifesting as both central and peripheral schitic changes (Figure 1-29) (304–311).

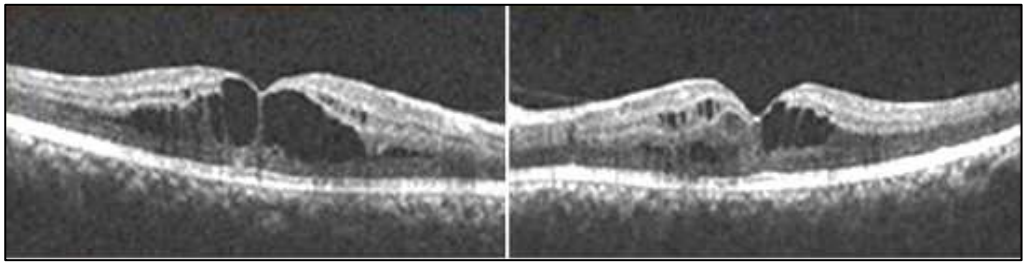

Figure 1-29: OCT in GFS: Cystoid appearance involving the OPL, INL, with EZ disruption. Credit: Chawla et al (2019) (311) [images reproduced with permission of the rights holder, BMJ]

Other rarer inherited disorders have also been associated with a foveoschisis-like phenotype, including Müller cell sheen dystrophy, Kearn-Sayres syndrome and 'MFRP-related nanophthalmos-retinitis pigmentosa-foveoschisis-optic disc drusen' syndrome, as well as some retinitis pigmentosa phenotypes (312–321). As with XLRS, these inherited retinal dystrophies can usually be distinguished from mechanical foveopathies based on history and examination alone, with earlier age-of-onset, bilaterality, family history and poor visual function being strongly indicative of a hereditary disorder. However, where diagnostic confusion arises, OCT can provide additional insight, with the lack of vitreoretinal traction and optic disc anomaly, or the presence of photoreceptor degeneration, essentially ruling out a diagnosis of acquired FRS.

1.5 Differentiating FRS from other foveomacular disorders

1.5.1 Cystoid macular oedema

The most similar, and thus important, acquired condition to distinguish from FRS, is cystoid macular oedema (CMO). This can be particularly challenging, considering they can frequently co-exist, such as in cases of intermediate uveitis or diabetic macular oedema (DMO), in which the confounding presence of a disorder of the VMI (e.g. ERM) can lead to diagnostic uncertainty.

CMO is a characterised by an abnormal increase in extra- and intracellular fluid volume, due to imbalance in retinal fluid homeostasis, typically manifesting as cyst-like accumulations (Figure 1-30). Under physiological conditions, the retina is maintained in a relatively dehydrated state, due to the action of the inner and outer blood-retinal barrier (comprising the retinal vascular endothelial cells and the retinal pigment epithelium respectively), as well as the action of specialised mural cells (e.g. pericytes) and glial cells (e.g. astrocytes and MCs) (276,322,323). MCs, in particular, play a key role in potassium spatial buffering (via Kir channels) and induced transport of water molecules (through AQP4 channels) (324–326). These channels are most densely packed at the MC footplates and around the superficial and deep retinal capillary plexi, such that water and potassium can be readily shuttled into the vitreous and blood to maintain interstitial homeostasis (322).

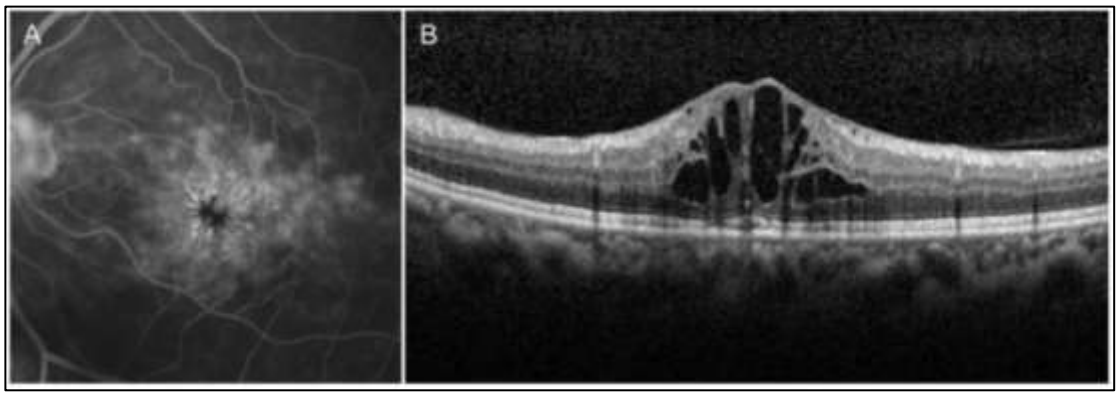

Figure 1-30: CMO; (A): Fluorescein angiography, revealing petalloid leakage at the fovea; (B): OCT, demonstrating cystoid fluid accumulation in the OPL and INL.

Credit: Chung et al (2019) (327) [images reproduced with permission of the rights holder, Press of the International Journal of Ophthalmology]

Breakdown of the blood-retinal barrier and subsequent glial cell activation results in downstream release of inflammatory mediators and increased capillary permeability. According to the rules of the Starling equation, fluid exudation will occur down the osmotic and hydrostatic pressure gradients, typically accumulating in the INL and OPL, between the intermediate and deep capillary plexi respectively (Figure 1-31A&B) (276,322,328,329). The predilection of IRF for the perifovea is thought to be a consequence of accumulation of neuro-glial junctional proteins along the distribution of the z-shaped Müller cells, creating an oncotic pressure gradient, as well as reduction in AQP4 expression in MCs, causing a reduction in the hydrostatic pressure gradient along the so-called 'glymphatic' trans-glial drainage pathway (Figure 1-31C&D) (275,276). Prolonged presence of fluid and disruption to the delicate extracellular milieu will eventually lead to irreversible neuronal toxicity and degeneration. Clinically, CMO is typified by fluid accumulation in the INL and OPL on OCT, and characteristically reveals a petalloid pattern of leakage on fundus fluorescein angiography (FFA) (276,322,329,330). The success of therapies targeted at vascular endothelial growth factor (VEGF) and inflammatory mediators reflects the role of blood-retina breakdown and glial-mediated inflammation in the pathogenesis of CMO (323,331–334).

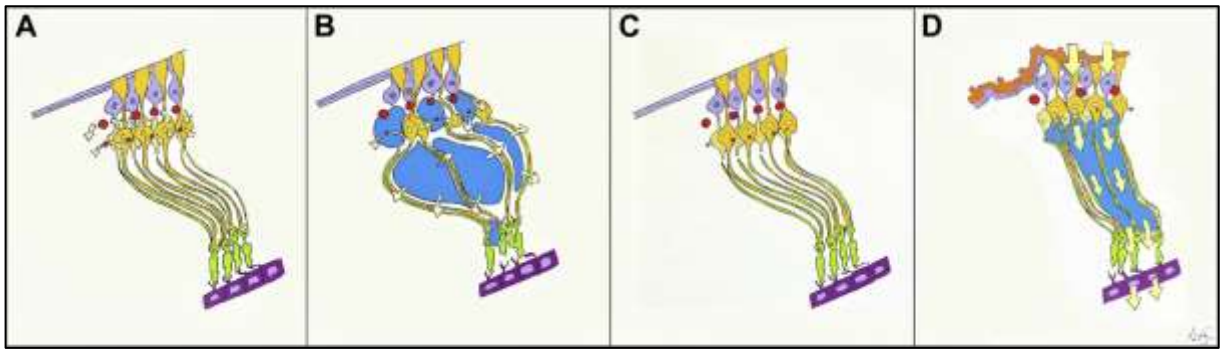

Figure 1-31: Pathophysiological differences between exudative and mechanical intraretinal cystoid spaces; (A): Vascular disruption with capillary permeability and fluid exudation (according to the Starling equation), denoted by arrows, causes

fluid accumulation down an oncotic pressure gradient between the superficial and deep capillary plexi. This results in fluid accumulation in the INL and ONL (B). (C): In mechanical disorders there is no vascular disruption, but traction causes cell displacement (D), which is filled with fluid flowing physiologically down the paracellular (glymphatic) hydrostatic pressure gradient (and is thus not subject to the Starling equation). Credit: Govetto et al (2020) (335) [images reproduced with permission of the rights holder, Elsevier]

While mechanical disorders of the retina may also present with perifoveal intraretinal spaces, the basic differences in pathophysiology to that of CMO are reflected in both its functional and anatomical behaviour. Although angiographic leakage has been reported in cases of tractional foveoschisis, it does not form petalloid pattern, nor is it directly associated with foci of traction, indicating that it is due to low-level inflammation or a consequence of homeostatic disruption due to the underlying 'Mülleropathy' (336). This suggests that, unlike CMO, the intraretinal cysts observed in mechanical foveopathies are not a consequence of exudation according to the Starling equation (335,337). In fact, in contrast to the variably-sized cystoid collections in CMO, the regular intraretinal fluid spaces in tractional FRS are thought to result from the retention of the physiological osmotic pressure gradient (from vitreous to choroid), following the trans-glial glymphatic pathway of the z-shaped MCs (Figure 1-31) (276). Functionally, visual acuity is significantly better in tractional disorders compared to CMO, even in the context of chronicity, suggesting that there is not as marked a disruption to the normal neuro-glial physiology (195,335). Finally, a lack of response of tractional FRS to anti-VEGF and corticosteroid therapy, compared to the success of surgery to remove mechanical traction or prevent ingress of vitreous (and vice versa), strongly indicates a fundamental dissimilarity between these two pathologies (335,337). Therefore, the difference between tractional and exudative cystoid spaces is not only of anatomico-functional interest, but also clinically relevant, and therefore important to distinguish. Govetto et al have demonstrated how multimodal imaging can be applied to reliably differentiate CMO from tractional disorders (Figure 1-32) (335).

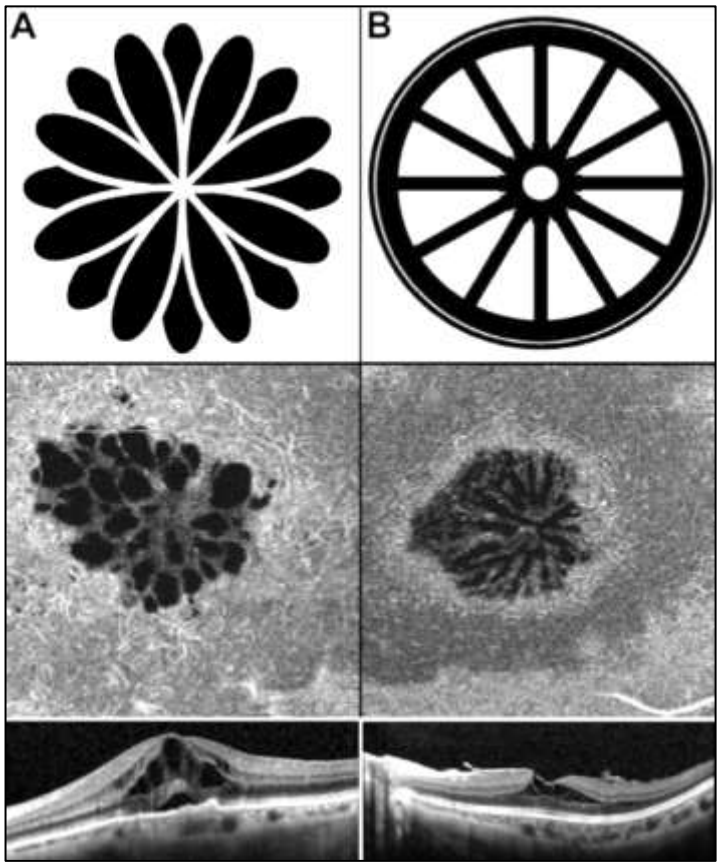

Figure 1-32: (A): CMO: petalloid pattern (top), as seen on en face imaging (middle), due to intraretinal cystoid spaces (bottom); (B) Tractional ERM foveoschisis: spoke-wheel like pattern (top), as seen on en face imaging (middle), due to schisis in HFL (bottom). Credit: Govetto et al (2019) (335) [images reproduced with permission of the rights holder, Elsevier]

FRS has also been infrequently reported in the context of other acquired disorders, such as macular telangiectasia type 2 and age-related macular degeneration (AMD) (338,339). The paucity of reports of such clinical cases suggests that these are more likely to represent dual pathologies, rather than clinical associations (340). In fact, Bringmann et al used macular telangiectasia type 2 as an example of cystic degeneration of the ONL due to loss of PR cells, to demonstrate that, unlike tractional foveopathies, this condition did not result in disruption of the foveal architecture, due to the preserved action of the MCC (99).

As such, for the purpose of this thesis, I will not investigate disorders that are characterised by either exudation or primary degeneration of the neural retina, and

thus an absence of lamellar (schitic) splitting of the retina, as in true FRS. These include various forms retinopathy, such as Coats' disease, chronic central serous chorioretinopathy, choroidal neovascularisation and treated ocular tumours, which are also occasionally mislabelled as schitic disorders.

1.6 Hypothesis and aims of the thesis

Based on the evidence in the literature and the concepts that I have outlined to this point, it appears that acquired FRS manifests through progressive deformation of normal MC architecture at the fovea, under the influence of various internal and external force vectors. While FRS is most commonly seen in the context of VMI disorders, it is also observed in cases of myopic foveoschisis, optic disc pit maculopathy and idiopathic foveomacular retinoschisis (Figure 1-15). Considering the common morphological characteristics of these disorders, we might expect them to demonstrate similar functional behaviour, regardless of the underlying causative condition, or duration of disease.

Therefore, I hypothesise that, regardless of aetiology or chronicity, visual function in cases of acquired FRS is not related to the presence of schisis *per se*, but rather to the degree of retinal deformation. In turn, the extent of retinal distortion and likelihood of progression to a common anatomical end-point (i.e. foveal detachment or macular hole formation) can be understood as a function of the biomechanical properties of the MC populations within the fovea. If this anatomico-functional relationship can be modelled and measured, it may ultimately inform on prognosis and guide treatment of these disorders.

In order to investigate this, I aim to:

1. Explore the natural history of acquired forms of FRS, namely myopic foveoschisis, optic disc pit maculopathy and idiopathic foveomacular retinoschisis.

2. Study the anatomical characteristics in each condition through observational study, to establish and, where possible, quantify any relationship with visual function and disease progression.

1.7 Overview of the thesis

Following this review of the literature, chapter 2 provides an overview of the subjects and methodology used throughout the thesis. In chapters 3, 4 and 5, I explore the natural history and anatomico-functional associations in MFS, ODP-M and idiopathic FRS respectively, using a series of retrospective and cross-sectional, observational study designs. Chapter 6 comprises a cross-sectional study of a cohort of subjects with FRS, in which I employ a machine-learning approach and psychovisual testing to further explore anatomico-functional associations. Finally, in chapter 7, I draw comparisons between the various pathologies and the findings of the thesis are brought together in the conclusion.

CHAPTER 2

METHODOLOGY

"Everything that has transpired has done so according to my design"

– Emperor Palpatine

2.1 Study design

This thesis reports on the observed anatomico-functional behaviour of foveomacular retinoschisis (FRS) in the context of various pathologies, most of which are relatively uncommon. Furthermore, in these conditions the incidence of outcomes of interest, such as foveal detachment, is small. As such, large sample populations with long follow-up duration are needed in order to measure associations with any precision.

Moorfields Eye Hospital NHS Foundation Trust comprises over 30 sites in London and the South East of England and recorded over 780,000 patient attendances in 2018/19 (341). This affords a wealth of clinical data, both historically and contemporaneously, from which to derive further understanding of the long-term natural history and clinical outcomes of ophthalmic disease, with high external validity.

The best way of exploiting the volume of this clinical resource and that allows assessment of the effects of various factors on anatomico-functional outcomes, is the analysis of retrospective and cross-sectional data collection. However, it must be acknowledged that an observational approach is limited due to its use of secondary data. Specifically, that the data may suffer from inconsistencies or incomplete documentation of variables (information bias) and the effect of residual confounding variables on the interpretation of observed associations (low internal validity). While the trust comprises both large tertiary units, as well as smaller local departments, there is liable to be a degree of selection bias introduced, when a study sample is taken from a specialist centre, which may lead to overestimation of the population-wide prevalence of rare or advanced diseases.

In order to ensure that the research in this thesis has been reported as completely as possible, I have cross-checked against the 'Strengthening of the Reporting of Observational Studies in Epidemiology (STROBE)' checklist for cohort studies (see APPENDIX) (342).

In the following sections, I will outline the general methodology used for patient selection, data acquisition and analysis, with further specifics provided in each respective chapter.

2.2 Subjects

The method of identification of suitable patients varied according to the study design employed in each chapter. In chapters 3, 4 and 5, for example, where I have performed a retrospective, observational cohort study, patients were identified using an electronic patient record (OpenEyes^{TM}, Apperta Foundation CIC), using pre-specified search terms. Following which, inclusion and exclusion criteria were applied, as detailed in each respective chapter. Data that were collected from patient records comprised information that was gathered as part of the normal standard of care. Detailed patient selection, inclusion and exclusion criteria are provided in each chapter.

Chapter 6 was performed as a cross-sectional, observational study, in which patients, who were identified through either their medical record or during attendance in a clinic, with a condition of interest, were invited to partake in further non-invasive investigative tests on the same day, as part of this research study. No additional visits or experimental interventions were required in any of the above studies.

2.3 Data acquisition

2.3.1 Demographic data

Moorfields Eye Hospital electronic patient record (EPR) is linked to the Profile Information Management System, which is an NHS Digital controlled system containing patient-specific details. Using these systems, non-identifiable

demographic information, such as age, sex, ethnicity, as well as clinic visit dates, was extracted.

2.3.2 Clinical data

Historical clinical data are stored both in paper and electronic records, with clinical letters retrospectively uploaded as far back as 2003. In some settings, paper notes were used alongside the EPR as recently as 2020. In cases where insufficient clinical information was available on EPR, paper notes were also examined.

Where relevant, data collected included past medical and ophthalmic history, medication and family history, laterality of affected eye, spherical equivalent (SE), axial length (AL) and visual acuity (VA). VA is routinely measured using a Snellen chart at 6 metres and recorded as a fraction, but also occasionally measured as a logarithm of the mean angle of resolution (logMAR) or in Early Treatment of Diabetic Retinopathy (ETDRS) letters, using a Bailey-Lovie or standardised ETDRS chart (343–345). For the purpose of consistency and ease of analysis, all VA data were converted to logMAR and reported as such throughout this thesis. In the event that the patient had 'counting fingers' or 'hand movements' at 1 metre, this was reported in estimated logMAR equivalent, as 1.85 and 2.30 logMAR respectively, as previously described (346).

In clinical settings, patients are asked to perform the VA test with refractive best correction (glasses or contact lenses) or unaided, followed by further pinhole assessment if 6/6 is not achieved. For the purpose of this study, 'best-measured' VA was recorded, meaning that if the patient did not have refractive correction available, the best result of uncorrected or pinhole VA was used (347).

2.3.3 Microperimetry

Macular analyzer integrity assessment (MAIA) microperimetry (MP) (Centervue, Padova, Italy) uses a combination of confocal scanning laser ophthalmoscope (cSLO) retinal imaging and static perimetry. It allows for the co-localisation of retinal sensitivity and fundus morphology, as well as live fixation-tracking. It has been validated as a reliable tool for assessment of macular sensitivity and is increasingly being used as a clinical and research tool (348–350)

Light stimuli are presented to the retina using white light-emitting diodes, with a Goldmann III stimulus size (0.43˚ diameter and 4.0mm^2 area) and 200ms duration. The maximum illumination level is 1000 apostilbs (asb), corresponding to 318.47cd/m^2; the background illumination is 4asb and the dynamic stimulus range is 0 to 36 decibels (dB). The dB range represents a relative, inverted logarithmic scale, whereby 0dB is the brightest possible stimulus (1000 asb) and 36dB is the dimmest stimulus (0.25 asb). The projection strategy used is a 4-2 full threshold, with initial 4dB bracketing, followed by 2dB steps until failure. The normative data included in the MAIA user manual indicates that normal sensitivity ranges from approximately 25-35dB, with an average of 30dB (Figure 2-1).

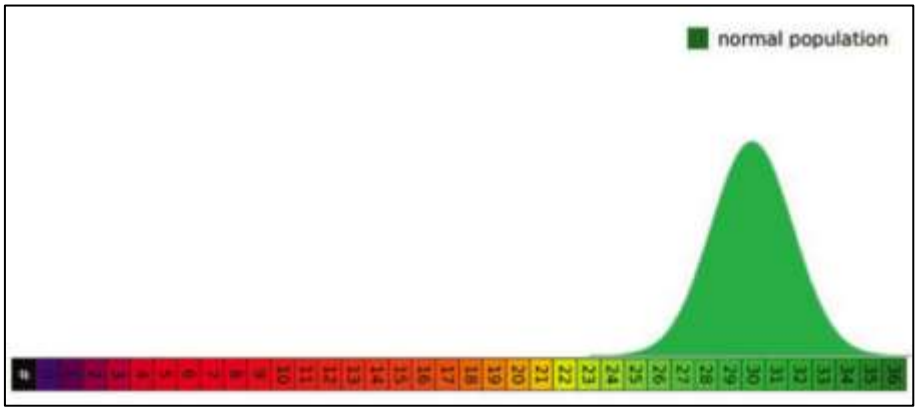

Figure 2-1: Normative chart provided by MAIA

Analysis of fixation is performed by tracking eye movement during testing at a rate of 25 times/second. The resulting distribution is plotted over the SLO image in a point wise fashion, creating a ‘cloud’ of points, which represents the subject’s

preferred retinal locus (PRL) (Figure 2-2A). The PRL_initial (P1) is calculated during the first 10 seconds of testing, while subjects commit the highest effort to hold fixation and the stimulation grid is focused about this point. The PRL_final (P2) is calculated according to the average fixation points during the remainder of the test; extent of deviation between the loci of P1 and P2 represents the stability of the subject's fixation.

Fixation stability is quantified in MAIA, according to the percentage of fixation points that are located within a defined area. Fixation is considered "stable" if ≥75% of points are located within 1˚ of P1, "relatively unstable" if <75% are within 1˚ of P1, but ≥75% are within 2˚ of P2 and "unstable" if <75% are located within 2˚ of P2 (Figure 2-2B).

Furthermore, fixation stability can also be calculated according to ellipses around the cloud of points, which are automatically created to demonstrate the horizontal and vertical distribution of points around the mean ±1 standard deviation (63% of points) and ±2 standard deviations (95% of points). Both the bivariate contour ellipse areas (BCEA) for 63% and 95% and the orthogonal diameters of the ellipse can be used to measure and compare fixation stability (Figure 2-2D).

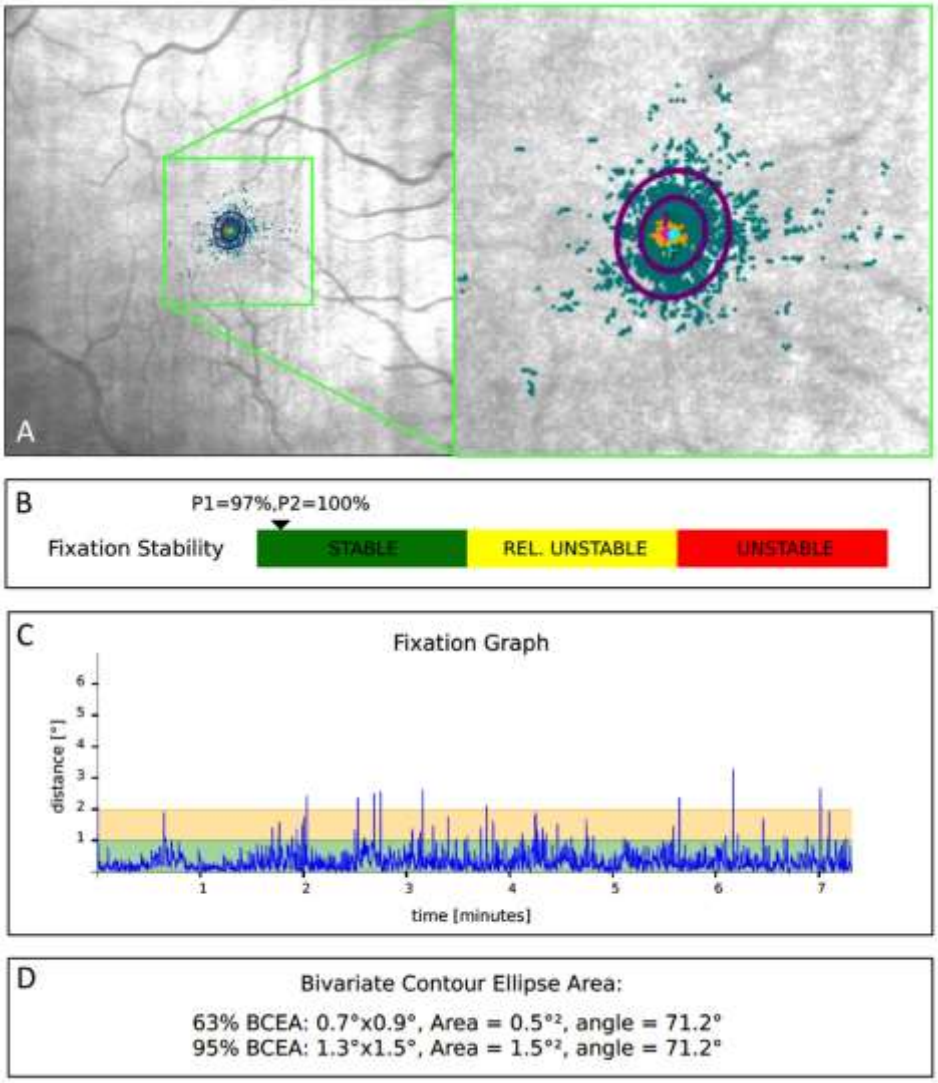

Figure 2-2: Fixation parameter outputs of MAIA microperimetry: (A): Fixation clouds (orange/blue) with initial (pink) and final (turquoise) PRLs, and bivariate contour ellipse areas (BCEA) (purple ellipses); (B): fixation stability indices (P1 and P2); (C): graph of deviation from initial fixation; (D): 63% and 95% BCEA metrics.

Throughout this thesis, I use a 68-point "expert" test, consisting of a 10-2 pattern of loci, distributed between 1.4˚ and 9.1˚ from the horizontal and vertical meridians (Figure 2-3). The fixation target is a 1˚ diameter red circle, broken into 4 segments. Testing was performed following 20 minutes dark adaptation under mesopic conditions. Tests were performed following pupil dilation, which has been shown not to significantly affect performance (351).

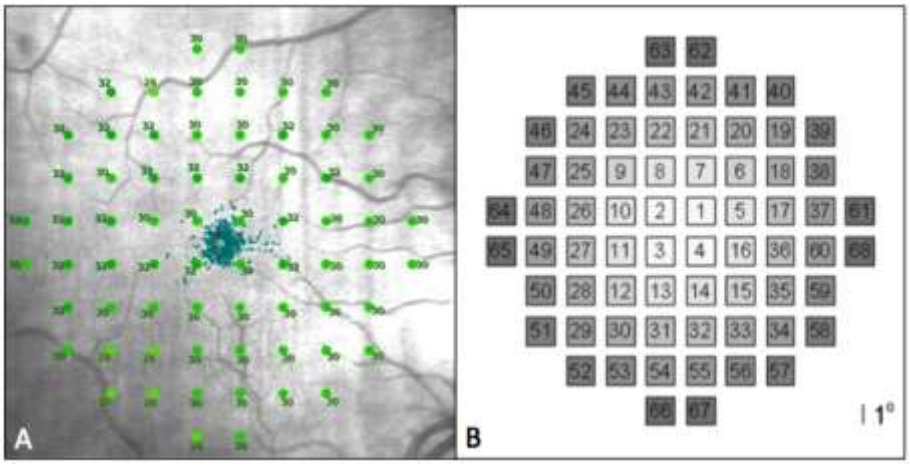

Figure 2-3: 68-point test; (A): microperimetry grid with local stimuli thresholds; (B): Grid demonstrating increasing loci eccentricities of 1.4˚, 3.2˚, 4.2˚, 5.1˚, 5.8˚, 7.1˚, 7.8˚, 8.6˚ and 9.1˚. Credit: Charng et al (2020) (352) [images Creative Commons licensed]

Molina-Martin et al have attempted to define normative values for average threshold sensitivity (ATS) and fixation patterns in microperimetry in a sample of 237 eyes of healthy subjects, using a 37-loci grid of 3 concentric circles (353). The median retinal sensitivity across all subjects was 32.90dB (interquartile range 1.80), while the median P1 and P2 values were 98.0% (IQR 6.0) and 100.0% (IQR 1.0) respectively. There was a significant association with age and worsening sensitivity and fixation noted; those ≤40-years-old scored a median of 33.1dB (IQR 1.7), 98.2% (IQR 4.0) and 100.0% (IQR 0.6) for ATS, P1 and P2 respectively, while >40-year-olds achieved a median of 32.2dB (IQR 2.1), 96.2% (IQR 9.0) and 99.8% (IQR 1.5) for the same parameters. These findings suggest that, under normal circumstances, subjects of all ages should obtain parameters within the abovementioned 'normative' parameters outlined by the MAIA system (ATS ≥25dB, P1 ≥75%). However, work by Charng et al using the larger, 68-loci grid, has demonstrated that there is both an age- and loci-specific variability in sensitivity, with up to 10% of points falling below the 25dB cut-off. They suggested that there is a 0.6dB/decade age-related decline in loci-specific ATS and found that better accuracy could be achieved by performing an interquartile regression to derive a relationship between pointwise sensitivity and age at the 2.5th and 97.5th percentiles, at each locus eccentricity (352). Considering this possible

source of confounding, I collaborated with Charng et al, to allow me to use their data to provide me with an age- and loci-matched normative group, against which I have compared the microperimetric data for those subjects in chapter 6.

In spite of the above finding, a cut-off for normal ATS of ≥25dB still appears to be appropriate, considering Charng et al's mean (±standard deviation (SD)) of 27.4 (±1.4) when using the 68-loci grid.

2.3.4 Optical coherence tomography (OCT)

Three different spectral domain (sd) OCT acquisition devices are used interchangeably at Moorfields Eye Hospital: The Topcon 3D OCT-1000 (Topcon Medical Systems Inc., Paramus, NJ), the Heidelberg Spectralis (Heidelberg Engineering Inc, Heidelberg, Germany) and, to a lesser extent, the Zeiss Cirrus 5000 (Carl Zeiss Meditec Inc., Dublin, CA). Variation of the software used for segmentation and automatic retinal thickness analysis algorithms suggest that thickness parameter quantification will differ between devices. Measurements from the Spectralis and Cirrus devices have been shown to be highly correlated (>0.85), while Topcon measurements may be significantly lower and thus poorly correlated (0.40). Approaches to address this discrepancy are discussed further in 2.3.6.1.

Throughout the thesis, qualitative OCT data are gathered using scans from all the different acquisition devices. In Chapter 3, three clinician graders contributed to the image analysis. In order to ensure inter-observer consistency, a standard operating procedure was compiled for characterisation of OCT features in myopic foveoschisis; this has been included in the APPENDIX.

2.3.4.1 Topcon 3D OCT-1000

The 3D OCT-1000 combines sd-OCT technology with superluminescent diode light at 830nm and acquisition rate of 18,000 A-scans/second, co-registered to full colour high-resolution fundus photography. Standard 6x6 horizontal macular grids (512 A-scans x 128 B-scans) were acquired (Figure 2-4A) and the Topcon proprietary software automatically segments the internal limiting membrane (ILM) and retinal pigment epithelium (RPE) layers to calculate the ETDRS plot, with 3 circles of 1, 3 and 6mm, subdivided by superior, nasal, temporal and inferior regions, into 9 subfields. This system provides automated outputs for both centre point thickness (CPT) and average retinal thickness (AvRT) in the ETDRS plot area.

2.3.4.2 Heidelberg Spectralis OCT

The Heidelberg Spectralis sd-OCT emits superluminescent diode light with a centre wavelength of 870nm and simultaneous infrared *en face* imaging. Coupled cSLO allows adjustment for eye movements, using proprietary 'TruTrack®' technology, while an acquisition rate of 40,000Hz permits axial resolution of up to 3.9µm. The most commonly used protocol is "fast macular volume" preset, comprising a 49-line horizontal raster covering 20˚x20˚ (512 A-scans/B scan), centred on the fovea (Figure 2-4B).

2.3.4.3 Zeiss Cirrus 5000 OCT

The Cirrus 5000 sd-OCT emits superluminscent diode light at 840nm and has a scan speed of 27,000 A-scans/second, giving axial and transverse resolutions of up to 5µm and 15µm respectively. The 6x6mm macular cube (512x128) scan was used (Figure 2-4C), which allows visualisation of segmental *en face* projections, including near-infrared reflectance (NIR) (Figure 2-5A) and ILM to RPE minimum intensity projection

(MIP) (i.e. projection of the darkest region within the retina) (Figure 2-5B). Cirrus single-line HD scans were used for the creation of composite widefield OCT images.

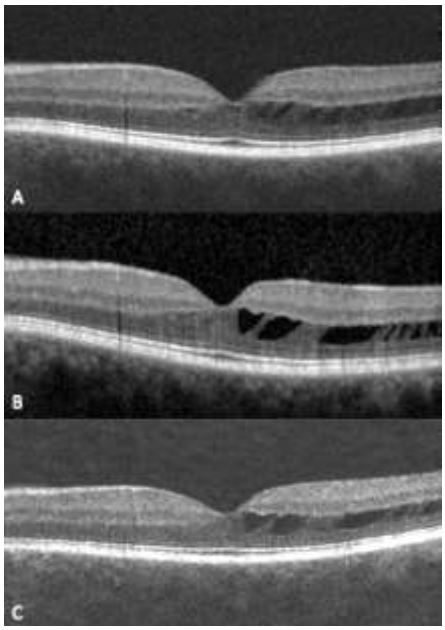

Figure 2-4: OCT scans of an eye with idiopathic FRS taken at different time points with (A): Topcon OCT-1000; (B): Heidelberg Spectralis; (C) Zeiss Cirrus 5000

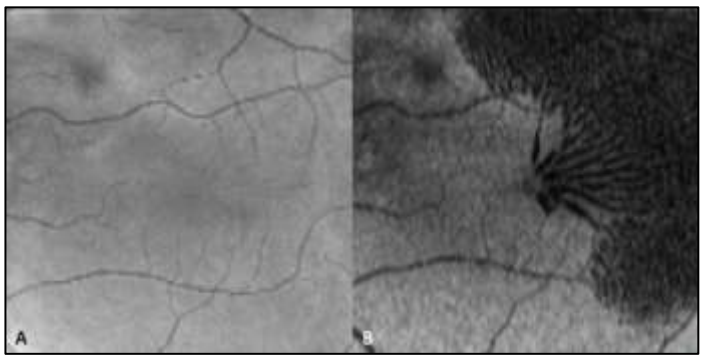

Figure 2-5: En face imaging in an eye with idiopathic FRS; (A): near-infrared reflectance; (B): minimal-intensity projection

2.3.5 Retinal photography

Colour fundus photography was taken using the Topcon 3D OCT-1000 and pseudocolour images were generated using the Optos ultra-widefield SLO (Optos, Marlborough, MA).

2.3.6 Image analysis and editing

Image manipulation, processing and analysis were undertaken using FIJI™ (Fiji is just ImageJ, US National Institute of Health, Bethesda, MA), an open-source version of ImageJ software focused on biological image analysis (354,355). For the purpose of creating diagrams, composite clinical images and editing or adapting figures in this thesis, GNU Image Manipulation Program was used (The GIMP Development team. GIMP [Internet]. 2019. Available from: https://gimp.org). GIMP is a free, open source, raster graphics editor.

2.3.6.1 Quantitative OCT parameters

In order to quantifiably measure associations between macular morphology and VA in Chapters 3 to 5, OCT parameters were acquired using the proprietary linear measuring software in the Topcon 3D OCT-1000 ImageNet programme. All measurements were taken vertically to avoid errors due to rescaling.

Quantitative OCT parameters collected included central retinal thickness (CRT), average retinal thickness (AvRT), central schisis height (CSH) and choroidal thickness (CT). Measurement area for AvRT was defined by the limits of 6mm ETDRS circle (Figure 2-6). In the event of ILM or RPE segmentation errors, the boundaries were manually redrawn.

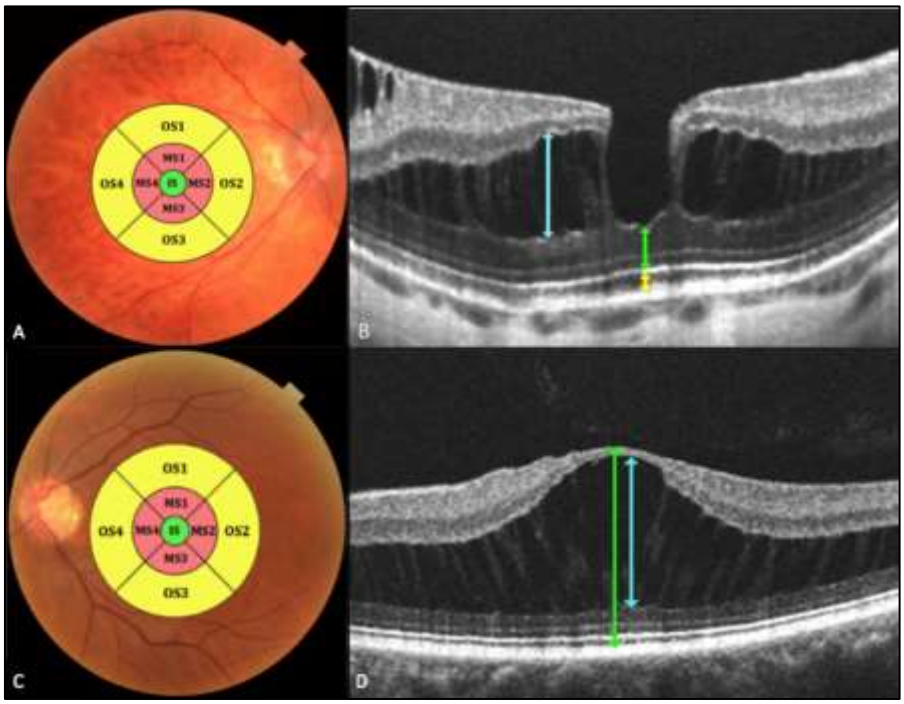

Figure 2-6: Measurement methods for OCT quantitative parameters in a case of MFS (A&B) and ODP-M (C&D): (A&C) ETDRS grid defined the area used to estimate the AvRT, incorporating the automated measurements from the outer, middle and inner segments (OS, MS, IS); (B&D) CRT was taken from the centre of the fovea (green arrow); maximum CSH was taken at the largest point of schisis within 0.5mm of the foveal centre (blue arrow); CT was measured directly beneath the fovea (yellow arrow)

2.3.6.2 Schisis area calculation

In chapters 3-5, schisis area (SA) was estimated using 6x6mm colour thickness maps, extracted from the Topcon OCT. A sample of normal eyes revealed an AvRT of 266 (± 24) µm. Therefore a cut-off for normal was made at 2 standard deviations above average (approximately 325µm). A colour thresholding algorithm was devised to segment out regions of >325µm thickness, using the colour scale provided. This comprised altering the 8-bit (256-value) RGB image as follows: hue threshold to 50-200, the saturation to 100-255 and brightness to 0-255. Figure 2-7 demonstrates this threshold applied to the scale bar. The thresholded area was subsequently binarised

to create a mask, from which the area affected could be calculated, as a proportion of the total area of the 6x6mm ETDRS circle (i.e. 27.3mm^2).

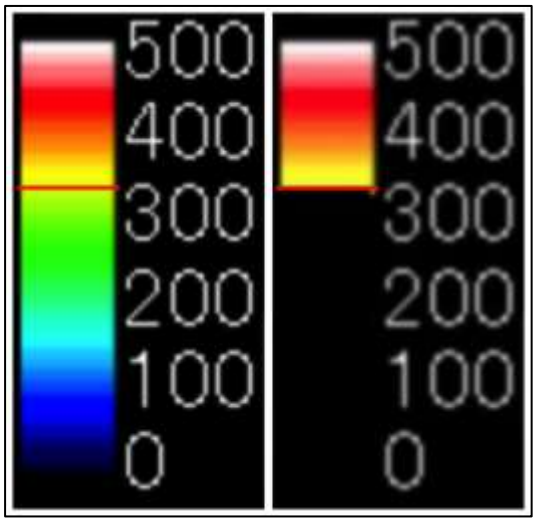

Figure 2-7: Left: colour thickness reference map (Topcon 3D OCT-1000) with red line denoting limit of normal (mean + 2 SD); right: colour map with thresholding algorithm applied

While this technique is limited in its value of picking up areas of small schisis (particularly in the region of the fovea, where the thickness is likely to be less than the average retinal thickness), it is a quick and repeatable method of quantifiably mapping out the area of large schisis cavities. Figure 2-8 demonstrates its application in cases of FRS.

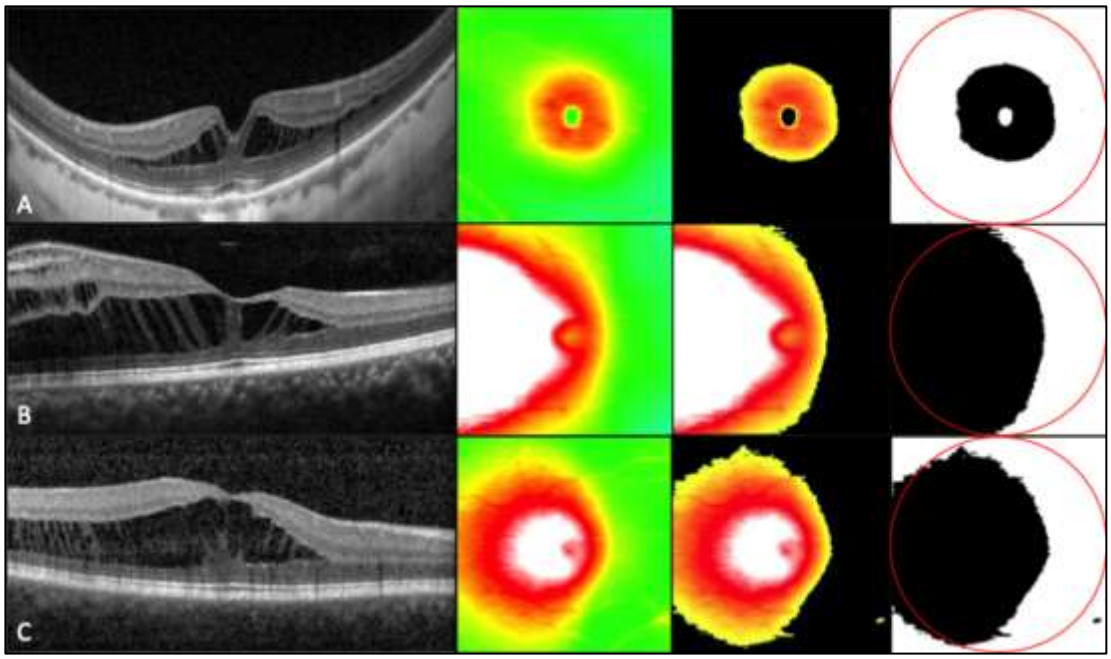

Figure 2-8: Examples of application of colour thresholding algorithm in cases of (A) MFS; (B) ODP-M and (C) IFRS. Colour map is thresholded and then binarised before the region-of-interest (6mm ETDRS grid) is overlain to calculate SA

2.4 Statistical analysis

Statistical analyses were performed using the following software packages: Stata (v15-17, StataCorp, College Station, TX) and SPSS (v25, IBM, Armonk, NY). Normality testing (Shapiro-Wilk) was used to determine the probability of a given dataset following a Gaussian distribution, accepting an alpha level of ≥0.05 as confirmatory. In cases where normality could not be assumed, histograms were analysed for skewness or kurtosis and, where appropriate, data transformation was performed. For example, while VA is reported in logMAR throughout the thesis, it was transformed to decimal for the purpose of linear regression anaylsis, if the sample data followed a non-normal distribution. Parametric or non-parametric tests were used for within- and between-group comparisons, while univariate and multivariate linear and logistic regression models were used to measure associations. In chapter

6, a mixed effect multilevel model was used to account for clustering effects of data at subject level.

Boxplots and histograms are used to display data graphically throughout the thesis. For histograms, error bars represent the 95% confidence interval. In the case of boxplots, as per convention, the box represents the first and third quartile, with the central line and cross indicating the median and mean respectively; whiskers denote the minimum and maximum values, while any outliers were defined as a value that lay outside of the IQR x 1.5, herein represented with a round marker.

2.5 Ethics

All identifiable data were removed and patients were anonymised, prior to data analysis. For the purpose of using retrospective data, specific consent was not sought, but data were not included if patients had previously indicated that they did not want their information used for the purposes of research.

Study approval was sought and acquired from the local Research Ethics Committee, the Health Research Authority and Health and Care Research Wales (see APPENDIX). All research adhered to the tenets of the Declaration of Helsinki.

CHAPTER 3

A RETROSPECTIVE OBSERVATIONAL STUDY OF THE ANATOMICO-FUNCTIONAL BEHAVIOUR OF MYOPIC FOVEOSCHISIS

"Many of the truths we cling to depend greatly on own our point of view"

– Obi-Wan Kenobi

3.1 Introduction

Myopic foveoschisis (MFS) describes the manifestation of foveomacular retinsoschisis (FRS) occurring in the context of high myopia. Worldwide, myopia was estimated to affect 2.5 billion people in 2020, comprising approximately one third of the population (356). High myopia, defined either as an axial length greater than 26.5mm or a dioptric correction of less than -6.00D, has a reported global prevalence of up to 6.5% and is projected to increase to around 10% by 2050 (356–362). The term pathological myopia is often used to describe the degenerative changes that accompany axial elongation, and, in some instances, specifically the myopic maculopathy associated with a refractive error ≤-8.00D (363). In particular, axial length ≥30mm carries a high risk of anatomical failure of the macula, with a cumulative incidence of visual impairment of 90% (compared to 3.8% in those with axial length 24-26mm) (364).

A principal feature of pathological myopia is the formation of scleral ectasia, known as posterior staphyloma (PS) (365,366). PS arises due to abnormal properties of scleral collagen, which predisposes to progressive globe thinning and elongation, and can even occur in those with 'normal' axial length (367,368). The resulting out-pouching of the uveal tissue, usually observed in the posterior retina, is thought to be present in anywhere between 23-90% of individuals with high myopia (367,369–372). PS is associated with macular pathology, such as FRS, macular hole, retinal detachment, choroidal neovascularization (CNVM) and chorioretinal atrophy, in around 78-88% cases (367,369,370,373–379). Curtin was the first to provide a detailed categorisation of PS, according to both configuration (types I to X) and axial depth (grades 1 to 4) (Figure 3-1) (376). Further characterisation by Hsiang et al, in 2008, reported macular staphylomas (i.e. types II, I and IX) to be the most commonly associated with macular retinoschisis (367). The presence of dome-shaped maculopathy, a natural phenomenon characterised by localised thickening of sclera, causing inward bulging at the macula, appears to be protective against MFS and is observed in around 10% of high myopes (Figure 3-2) (380,381).

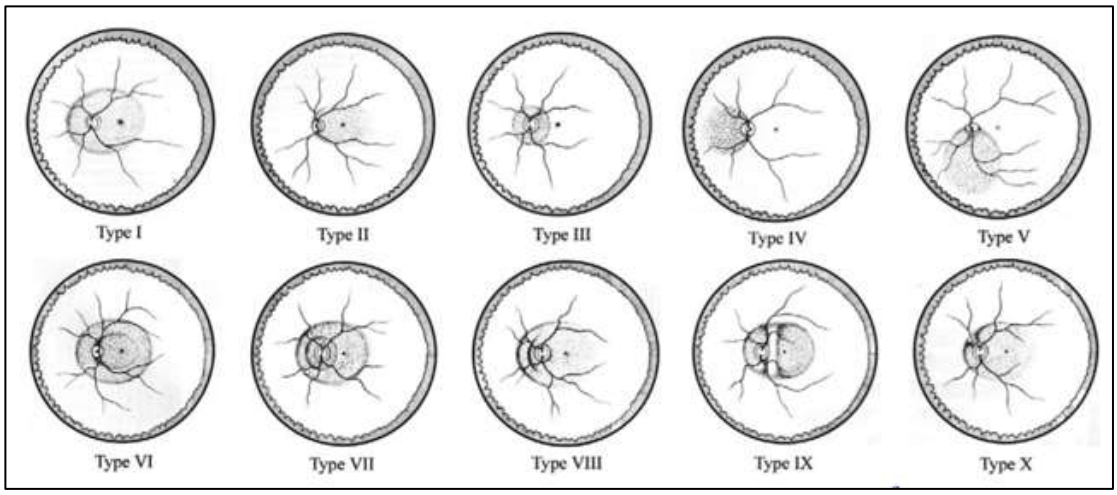

Figure 3-1: Curtin's classification of the different configurations of posterior staphyloma. Types I, II and IX are associated with MFS (Hsiang et al 2008). Credit: Curtin (1977) (376) [image reproduced with permission of the rights holder, AOS]

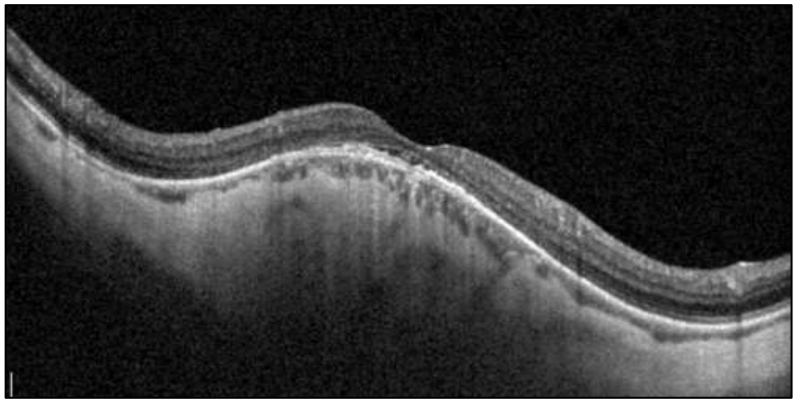

***Figure 3-2*: OCT demonstrating localised scleral thickening in 'dome-shaped maculopathy'**

While it has long been recognised that macular detachment can occur in the context of high myopia and PS, despite the absence of a macular hole (382), it was not until 1999, that Takano and Kishi coined the term MFS to describe the retinoschisis identified on OCT in myopic eyes with PS (Figure 3-3) (382,383). The natural course of MFS appears to be largely favourable; the rate of stability, as documented in natural history studies, ranges from 71-87% (377,384–387). Progression is rare, but may manifest as the development of partial thickness macular hole (PTMH), FMTH,

FD or macular hole retinal detachment (MHRD). In 2004, Panozzo and Mercanti introduced the term 'myopic traction maculopathy' (MTM), to incorporate both foveoschisis and these associated pathologies, as reference to their likely tractional aetiology, which constitutes a separate entity to the tractional VRI disorders observed in non-myopes (377). The overall prevalence of MTM in highly myopic eyes is estimated to range from 4.7-34% (372,378,379,388–391).

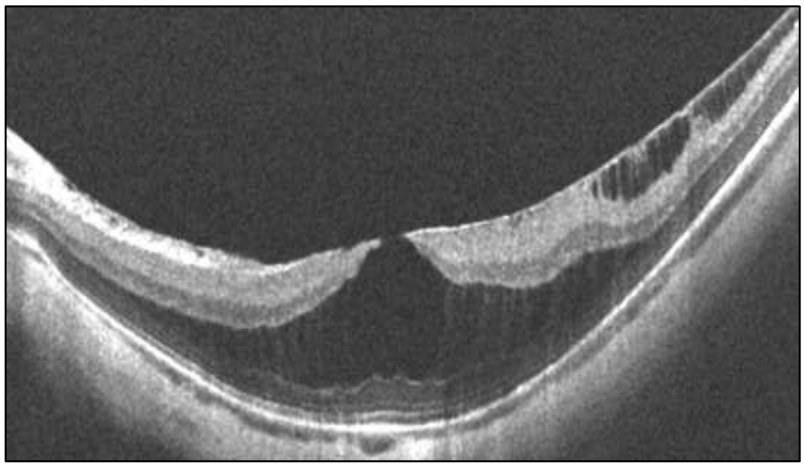

Figure 3-3: OCT demonstrating MFS associated with PS

The average age of presentation with MFS has been reported between 51-66 years (385,387,390,392–394), and association has been demonstrated with increasing age (378,379,385). Mean refractive error is between -13.0 and -16.9D, and axial length 29.2-30.3mm (266,385,390,392–394). While axial length is generally thought to stabilise after the first two to three decades of life, there is evidence that PS can continue to worsen, even beyond the 6th decade (365,367,395,396). Moreover, the average age at which high myopes undergo spontaneous vitreous liquefaction and detachment is thought to be around 10 years prior to that of their emmetropic counterparts (397–400). It follows, therefore, that changes at the vitreomacular interface in the early 6th decade, in the context of PS progression, could culminate in the development of MFS over the following decade of life. Several studies reporting the natural course of MFS have found a preponderance of females amongst those affected with high myopia (63%-85%) (377,385–387). This may reflect a sex-linked

inheritance pattern, while a possible role of oestrogen receptor expression in the pathogenesis of myopic maculopathy has also been suggested (401–403).

3.1.1 Pathogenesis

The pathogenesis of MFS appears to be multifactorial, involving both posterior elongation of the globe and pre-retinal tangential and anteroposterior traction, occurring on a background of atrophic weakening of the retinal ultrastructure. Other factors, such as RPE functional failure and alterations in cell adhesion properties, may play a part, but the contribution is thought to be small (390,404). Although RPE dysfunction does have a reported role in the context of myopic macular atrophy, considering that subretinal fluid is a late manifestation of MTM, which often undergoes complete resolution following surgical relief of anterior traction, it seem unlikely that this represents a primary driver of the pathomorphology in MFS (404,405).

Early histological evidence was limited in its capacity to detect changes in the VRI, but identified axial elongation and its correlation with PS, which in turn is associated with other myopic changes, such as chorioretinal atrophy and lacquer cracks (94,375,376,405). This led to observers attaching primary significance to the presence of PS in the development of myopic maculopathy. However, development of OCT over the last 20 years has enabled a greater understanding of the pathoanatomical features of MFS; Takano and Kishi demonstrated a higher rate of retinoschisis *in vivo* (34%), than previously observed using biomicroscopy alone (383). They postulated that the observed schisis could be a degenerative process within the PS and that tangential contraction of the vitreous may play a role in the subsequent formation of FD or FTMH. This theory was supported by further OCT studies, which found significant relationships between the presence and location of PS and foveoschisis (372,379,392).

In their OCT analysis of 125 eyes with high myopia, Panozzo and Mercanti reported the presence of epiretinal traction in almost half of cases; 25% had tangential

epiretinal membrane (ERM) traction, while a further 13% had anteroposterior vitreomacular traction (VMT) combined with tangential ERM traction. The remaining 9% had VMT alone (375). Of 25 patients with MFS, 23 had evidence of epiretinal traction, while the remaining 2 cases had concurrent posterior staphyloma without traction. Interestingly, only 10 of these patients (40%) were reported as being symptomatic. Subsequent imaging and histological studies have supported the idea of traction forming part of the aetiological mechanism for MFS, even in the absence of PS (372,385,390,406–408). Wu et al performed a cross-sectional study in 2009 and found that the variables associated with the presence of MFS on multivariate analysis were axial length >31mm, chorioretinal atrophy and VMI factors (390).

The exact mechanism by which traction arises in MFS remains somewhat controversial. Worst described a vitreous lacuna anterior to the macula in adult eyes, which he termed the bursa premacularis, which is equivalent to the posterior precortical vitreous pocket (PPVP) described by Kishi and Shimizu. This represents a liquefied space, with a posterior wall made up of vitreous cortex that attaches to the retina (see Figure 1-1 and Figure 1-4A) (41,43,409,410). PVD occurs when liquefied vitreous breaches the posterior cortex, passing into the retrohyaloid space. Although it has been shown that vitreous liquefaction and PVD occurs earlier in myopes than non-myopes (397,398,410,411), this premacular cortical vitreous, already separated from the vitreous gel by the PPVP, can persist over the macula, even in the presence of apparent complete PVD with Weiss ring, in as many as 44% of all eyes at autopsy (145). This layer of cortex is impossible to visualise directly on fundal examination and only recent high-resolution OCT has allowed for detailed *in vivo* characterisation. Itakura et al reported a preponderance of residual vitreous cortex in high myopes (40.5%) compared to normals (8.7%), which is supported by transmission electron microscopy (TEM) findings from ERMs removed from myopic eyes (412–414).

Vitreoretinal traction often behaves differently in myopes than non-myopes. The cause of this discrepancy is not well understood, but a clue to this phenomenon may be found in the morphology of the liquefied PPVP, which is larger in high myopes and significantly correlated with refractive error (410,412). This may result in earlier,

incomplete PVD in myopes, with larger areas of remnant pre-macular cortical vitreous attachment. This variation, when combined with a greater axial length and PS, could, in part, explain the structural configurations often seen in MFS.

Studies have also supported a role for ILM fibrosis and retinal vessels sclerosis in the development of MFS. Ikuno et al first noted an increase in the formation of retinal microfolds, which coincided with the retinal arterioles, following ILM peeling. They suggested that the retinal redundancy afforded through ILM peeling disclosed the centrifugal force vectors of sclerotic arterioles that were not sufficiently flexible to stretch with axial elongation of the eye (415). Further studies support this hypothesis, with Shimada et al reporting the presence of paravascular cysts, microfolds and holes in high myopia as 49.5%, 44.6% and in 26.8% of cases respectively (388,404,416–420). These paravascular abnormalities have also been implicated as risk factors for the formation of retinoschisis at vascular arcades (421). The role of the retinal microvasculature in the pathogenesis of MFS is unresolved. It might be postulated that sclerosis and non-compliance of the macular vascular network may contribute to the formation of foveoschisis through creation of an inward 'trampoline-like' effect. However, the absence of a smooth muscle-containing tunica media in retinal capillaries, alongside the observation that parafoveal vascular density is relatively decreased on OCT-angiography in highly myopic eyes, suggests that these plexi do not contribute significantly to the observed pathomorphology (422–424). The contribution of pericytes to fibrosis has been reported in diabetes and AMD, but their behaviour in myopic maculopathy remains unclear (425,426).

Evidence from TEM of excised ILM from patients with MFS have shown cellular proliferation and abnormal collagen production, as well as migration of glial and RPE-like cells, which may cause adherence of the non-compliant ILM to both the PVC and the underlying retina (427–429). Bando et al reported the presence of both collagen fibre and cellular debris on the inner ILM surface in 70% of MFS histological samples, compared to none with idiopathic FTMH (427). In addition, it has been demonstrated that ILM from patients with MFS was significantly thicker than that in

idiopathic FTMH, with immunofluorescence and biochemical evidence of excessive MC gliosis and astrogliosis (430,431). While this is likely to be a protective response to tissue deformation, it increases the intrinsic biomechanical stiffness of the ILM and predisposes patients to MFS formation.

The pattern of MFS on OCT has commonly been described as a separation of the retina, at the level of HFL, into a thinner outer layer and a thicker inner layer (383,392–394). In 2009, Fang et al noted that, although the abovementioned outer schisis cavity was ubiquitously present, 44% of their patients had an additional inner schisis (Figure 3-4) (428). This was supported on sd-OCT studies which found that all cases of MFS have an outer schisis, but that a proportion, between 14-50% have an inner schisis in addition to this. (372,384,394,432). This inner schisis has primarily been observed between the IPL and ILM (372,384,394). As in other forms of tractional foveopathy, the presence of bridging fibres, assumed to be MC processes, across schisis cavities are visualised on OCT (392–394,428). Shinohara et al have described an anatomical relationship between the distribution of PS and that of schitic retina (372). Although PS was not found to be a pre-requisite for MFS formation, they concluded that the outer schisis was primarily caused by its development. Inner schisis, on the other hand, was significantly associated with the presence of traction at the VRI, including separation of the stiff ILM, spanning from the parafovea to the retinal arterioles (Figure 3-4); Sayanagi termed this appearance an 'ILM detachment' (433). At the point that the ILM is tethered at the vascular arcade, the schisis cavity often becomes multilayered, due to the insertion of vitreoretino-vascular bands, resulting in strong focal adhesions. These OCT findings are consistent with the aforementioned evidence that proposes that ILM fibrosis and paravascular adhesions are related to the development of MFS (415,416,421,430,433).

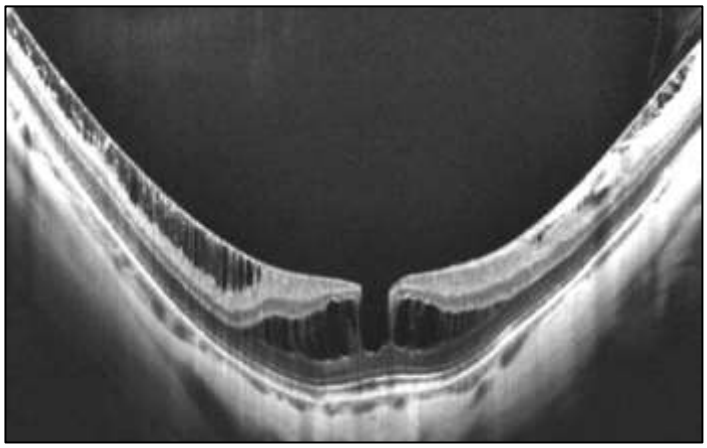

Figure 3-4: OCT in MFS, demonstrating central outer schisis cavity (in HFL) and extrafoveal inner retinal schisis cavity with 'ILM detachment'

There is no single unifying pathoanatomical mechanism for MFS, and it likely represents the complex interplay of both scleral ectasia and VMI disorders in the myopic eye (404,419). The apparent tautness of the inner retina over a posterior staphyloma seems to prevent it from conforming to the concavity of the globe, leading to progressive stretching and separation. The potential causes of traction on the inner retina are diverse and Johnson has proposed they could fall into any one, or combination, of the following: VMT, remnant cortical vitreous layer, ERM, intrinsic ILM non-compliance or retinal arteriolar stiffness (Figure 3-5) (419). Given this complex pathophysiology, a tailored approach may be preferable, to identify the pathological idiosyncrasies in individual cases, thereby avoid unnecessary surgical steps, which could increase the risk of iatrogenic damage (404,419,434).

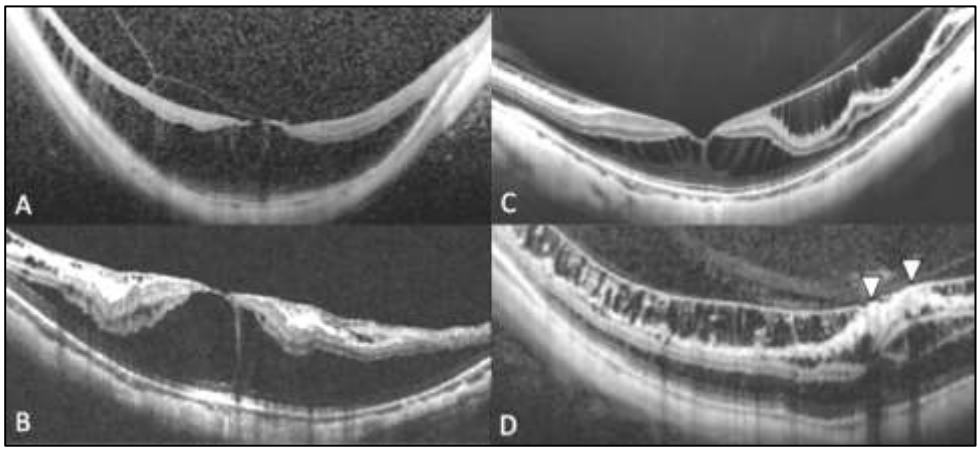

Figure 3-5: Various features of the VMI disorders observed MFS; (A): VMT, (B): ERM; (C): ILM detachment/non-compliance; (D): arteriolar stiffness with perivascular abnormalities (arrowheads denote location of retinal vessels)

3.1.2 Natural history

Progression of MFS to FD, PTMH and FTMH can be readily identified using OCT (377,383,392,393,409,435). In 2008, Shimada et al categorised the formation of a foveal detachment from MFS into 4 distinct stages, according to OCT characteristics (Figure 3-6). The initial stage involves an irregularity in the thickness of the outer retinal layer, which is followed by the development of an OLH. This OLH elongates vertically in the third stage, with formation of a FD. Finally the upper edge of the OLH becomes continuous with the inner retinoschisis layer, resulting in a partial resolution of the schisis and enlargement of the detachment. Although only reported in 5 eyes, Shimada et al described a relatively rapid progression through stages 1 to 3, averaging 4.5 months, with a small mean visual decline. Progression to stage 4, however, with or without development of a FTMH, is associated with significant deterioration in vision (436). By contrast, the development of isolated ILH in MFS appears not to be as visually significant and only rarely progresses to FTMH, presumably through a similar mechanism to VMT, as described in section 1.3.1.1 (437,438).

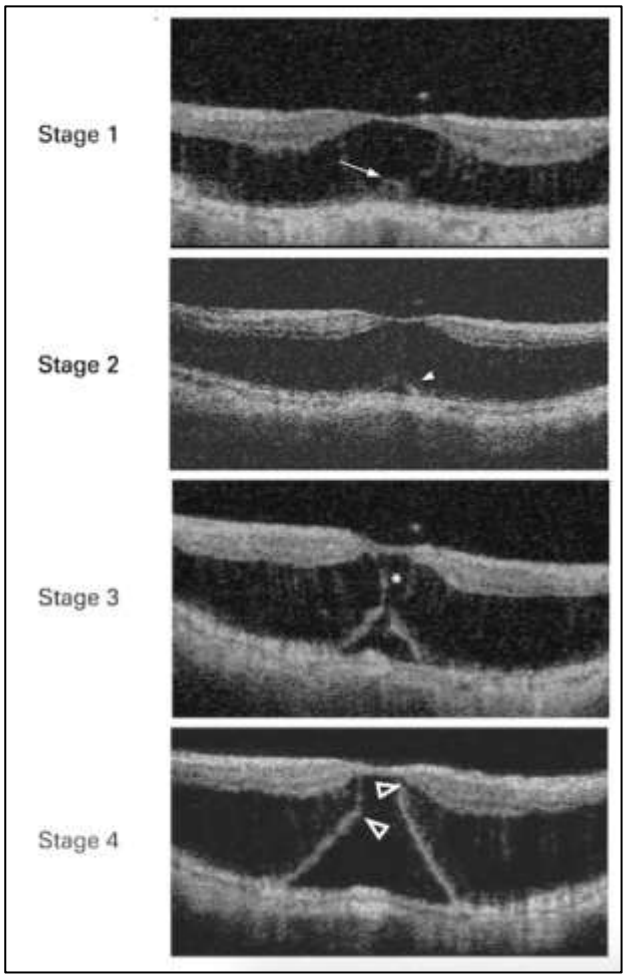

Figure 3-6: Stages of progression from MFS to FD: Stage 1: focal thickening of the outer retina is seen (arrow); stage 2: an OLH develops (arrowhead); stage 3: horizontal widening of the schisis cavity anterior to the OLH (asterisk) as FD develops; stage 4: upper edge of the FD becomes continuous with schisis cavity (open arrowhead). The schisis cavity narrows centrally as the FD enlarges. Credit: Shimada et al (2008) (436) [images reproduced with permission of the rights holder, BMJ]

This description of progression from MFS to FD is in keeping with our current understanding of foveal MC morphology. In their mathematical modelling of the stiffness of MCs, as a function of the angle θ between segments (see 1.2.4.5), Govetto et al demonstrated that, in MFS, the R2 segment length (L_2) was uniformly elongated, with a θ value close to 0˚ in all measured locations (196). This indicates

that the mechanical forces in MFS are stronger and more uniformly distributed across the whole macula, than in ERM foveoschisis (Figure 3-7).

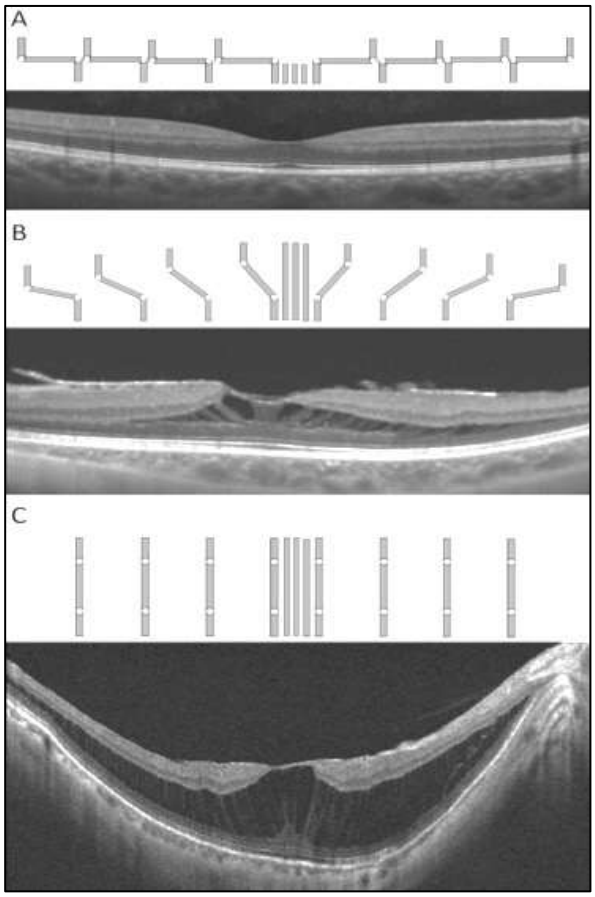

Figure 3-7: Variations in the morphology of MCs in (A): the normal fovea, (B): ERM foveoschisis and (C): MFS. Credit: Govetto et al (2019) (100) [images reproduced with permission of the rights holder, BMJ]

In the absence of a definitive pathomechanism, the provision of accurate prognostication and management for individual cases of MFS remains challenging (404). While MFS generally follows a favourable clinical course, with low rates of anatomical progression or development of visual symptoms, due to the apparent capacity of the retina to maintain function despite marked laminar separation, a minority of eyes do progress to end-stage disease (i.e. FD and/or FTMH), which carries a poor functional prognosis. (377,378,385,388–390,392,408,439,440).

Several staging systems have been devised to standardise the classification and staging of MTM. In 2013, Shimada et al retrospectively investigated the influence of the extent of schisis on rate of progression of MFS in 207 eyes (385). Schisis extent was defined as follows: S0 (schisis absent), S1 (extrafoveal schisis), S2 (foveal only schisis), S3 (foveal with partial extrafoveal schisis) or S4 (schisis involving entire macula) (Figure 3-8). Progression was defined as an increase in the height or extent of MFS, as well as development of PTMH, FTMH or FD. Over a mean follow-up period of 36 months, they found that the rate of spontaneous improvement was low (4%), while 24 eyes (12%) demonstrated progression. Eyes with S4 myopic traction maculopathy were at significantly higher risk (43%) of progressing than the other groups (8%), with associated worsening of vision from baseline. Overall, they concluded that MFS is generally a stable condition, and surgery is often best reserved for those demonstrating early signs of progression and decline in visual acuity (385). Using the same grading tool, Cheng et al prospectively reported on 50 eyes of 38 patients with MFS and found that 52% had total macular involvement (S4) at baseline (386). Over a mean period of 32 months, VA remained stable in 36 (72%) cases, while the remaining 15 eyes (28%) showed VA deterioration of ≥2 lines. Eyes with S4 macular involvement were found to have a higher rate of microstructural abnormalities and propensity to progress.

It has been suggested that the height of the schisis cavity is a poor correlate for visual function and thus of weak predictive prognostic value (393,392,441). This may be due to the fact that once a FD forms, the retinal forces are somewhat relieved and schisis height decreases (394,436). Gaucher et al noted a decrease in VA and increase in metamorphopsia in patients who had an observed thickening of schisis during follow-up, however they also described eyes with marked macular thickening that retained good visual function (389). They concluded that the factors indicative of poor visual prognosis were independent of the macular thickness *per se*, instead relating to the presence of a pre-macular structure (PMS) (e.g. condensed posterior hyaloid, fibrous proliferation or ERM) or the formation of a FD. Absence of these, along with absence of PVD, was suggestive of stability. 20 cases (69%) with pre-macular tractional structures demonstrated gradual visual decline over a mean

period of 31 months. In a retrospective study of 56 eyes with MFS, Rey et al have also demonstrated that, after a mean follow-up of 15.7 months, 71.4% remained stable. Of those who progressed and required surgery, 81.2% had evidence of a pre-macular structure (387).

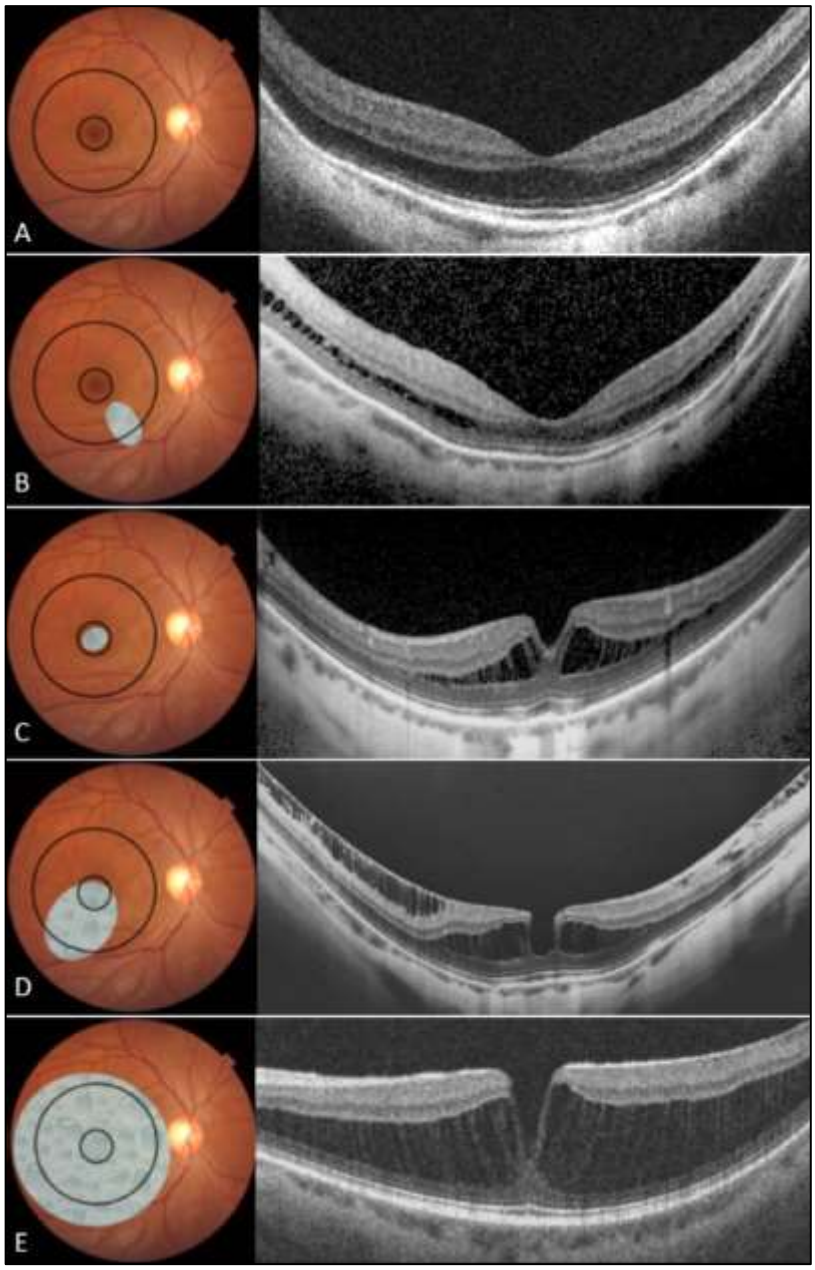

Figure 3-8: Schisis extent according to S0-S4 classification (385); (A): S0, no macular schisis; (B): S1, extra-foveal schisis; (C): S2, fovea-only schisis; (D): S3, fovea and partial macula-involving schisis; (E): S4, total macular schisis

Given the somewhat unpredictable nature of MFS progression, further attempts have been made to stratify risk according to OCT characteristics. Although Shimada et al's S0-4 schisis extent classification seems to yield associations with function and rate of progression, it does not account for the vertical distribution of the schisis, or other factors such as pre-macular structure or staphyloma (385). Ruiz-Medrano et al devised the 'ATN' classification system for myopic maculopathy (referring to atrophic, tractional and neovascular components). The tractional grading component of this system comprises from T0 (no macular schisis), T1 (inner or outer schisis), T2 (inner and outer schisis), T3 (foveal detachment), T4 (FTMH) and T5 (MHRD) (Figure 3-9) (442,443). This has since been refined by Li et al, in 2021, to categorise those with inner schisis only as T1 and those with outer schisis ± inner schisis as T2 (444). Although the inter-observer agreement has been shown to be good for this as a unifying classification system, the clinical relevance of each grade remains unclear (443,445). Finally, Parolini et al have developed the MTM grading system, which includes a stepwise classification of MFS, according to the influence of both 'tangential' and 'perpendicular' forces (140). Herein, they give values for predicted VA, rate of progression and suggested surgical approach. Whilst it remains the closest system to one incorporating all the pathoanatomical features of MTM, it does not attribute weight to certain significant factors, such as ILM detachment. Its validity is also limited by small numbers in some of the described stages and the authors do not provide information on the actual observed rates of progression in each group.

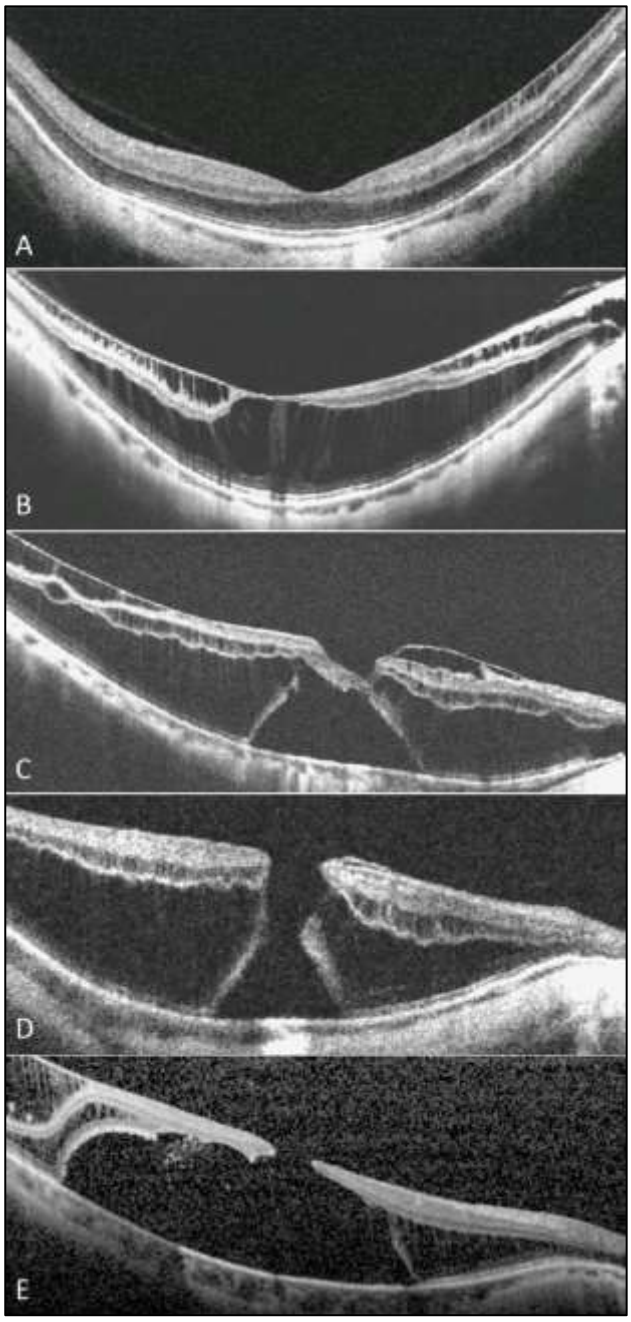

Figure 3-9: Morphology according to modified ATN grading system (442): (A): inner schisis only; (B): outer +/- inner schisis; (C): foveal detachment; (D): full thickness macular hole; (E): evolving macular hole retinal detachment.

3.1.3 Therapeutic approaches

Various surgical approaches continue to be evaluated for the management of MTM. Whilst the perfect technique and timing of intervention remains elusive, due to a lack of large-scale prospective data, there are some trends that could shed light on the underlying pathophysiology. For many years, scleral reinforcement techniques were deemed superior to pars plana vitrectomy (PPV) in cases of MHRD (446,447). In 2003, Kuhn postulated a role for ILM peeling and reported a case where this technique resulted in resolution of a focal detachment overlying a PS (448). Since then, advances in imaging and surgical systems has led to a trend for PPV and ILM peeling, with or without gas tamponade and, despite the recognised risk of creating an iatrogenic FTMH (up to 21%), the visual outcomes are generally favourable. (388,409,449–458). Kwok et al have also shown promising outcomes with PPV and gas tamponade without ILM peeling (459), although this approach remains largely unpopular. Recent reports suggest that fovea-sparing ILM peeling could offer a practical compromise to release traction whilst minimising macular hole development (460–464). A systematic review by Meng et al reported no functional difference or discrepancy in complication rates between PPV with ILM peeling compared to no ILM peeling, although the former may contribute to better anatomical resolution of MFS (465). Similarly gas tamponade was not found to have significant benefit and may increase the rate of post-operative complication (465). Meta-analyses by Wu et al and Wang et al indicate that superior visual outcomes and lower rates of complication are achieved with a fovea-sparing ILM peeling technique (466,467).

In the last 5 years, there has been a trend towards combining PPV with posterior scleral reinforcement (e.g. scleral imbrication, macular buckling or supra-choroidal injection), with reports of good functional (80%) and anatomical (65-93%) success rates. This appears to be most effective for those with axial lengths in excess of 30mm, but carries additional risks of extrusion, choroidal atrophy and neovascularisation (435,468–474).

Although the visual improvements are more marked in those with pre-operative FD, it has been suggested that the anatomical benefits of surgery for those with early PTMH or MFS only may preserve vision long-term (388,450,452). However, considering the low rates of MFS progression (71-88%) and reportedly high rates of anatomical (82-100%) and functional (61-70%) success following intervention, it would seem that a initial conservative approach is merited in most instances (385–388,450,452,453,475). The precise optimal timing for intervention remains unclear; Shimada et al recommend that, at stage 3 of FD development, there is sufficient evidence for progression to consider surgery, while minimising the risk of post-operative FTMH (436).

Worse pre-operative vision, greater schisis extent, presence of pre-macular structures, EZ disruption and thinner central foveal thickness may all hold some predictive value for post-operative outcomes, but these remain to be fully elucidated (385–387,389,439,440,475). In general, the surgical approach ought to be tailored towards the primary inducive factor, which may pre-retinal, retinal or scleral in origin.

In summary, MFS is a common disorder in high myopia, which carries a favourable long-term prognosis. Several anatomical features are pertinent to our understanding of the pathophysiology and the stratification of those at risk of progression. Firstly, posterior staphyloma is significantly associated with formation of an outer layer retinoschisis. Secondly, development of inner layer retinoschisis is highly suggestive, but not pathognomic, of an inward tractional element (e.g. a pre-macular structure). Thirdly, the extent of the schisis, microstructural changes and the presence of pre-macular structures appear to be predictive of poorer prognosis. Finally, pathoanatomical natural history studies suggest that the development of the schisis precedes the formation of FD and FTMH. The findings on OCT further support the notion that MFS is a highly complex and diverse condition, and management must be individualised according to visual function, vitreoretinal morphology and the surgical techniques at one’s disposal.

The paucity of clinical biomarkers in MFS challenges the ability to provide accurate risk stratification or the delivery of timely surgical intervention, when merited. In this chapter, I evaluate both functional and anatomical characteristics, including qualitative and quantitative OCT features, in eyes with myopic foveoschisis at baseline and during the course of follow-up, to explore its natural history and to measure associations with the development of FD.

3.2 Methods

A retrospective, observational study was performed at a tertiary ophthalmic centre. Patients with MFS, who presented between January 2008 and January 2020, were identified through electronic records.

Patients were identified according to the search terms 'myopia' or 'myopic' + 'schisis' or 'traction' + 'maculopathy', as used in electronic clinical letters. All adult patients with documented evidence of SE ≤-6.00 dioptres (D) or AL ≥26.5mm were included, in whom there was OCT evidence of schisis affecting the macula area and available VA data. Patients were excluded if there was co-existent retinal or ocular pathology affecting VA (including presence of chorioretinal atrophy, CNV or pre-existing FTMH) or a history of vitreoretinal surgery, preceding the first visit to our service. In order to avoid loss of valid data, measurements from both eyes were taken, so depending on the degree of intraclass correlation, a hierarchical design could be considered to control for inter-eye correlation, as appropriate.

This study is divided into two phases: In phase 1, baseline data are analysed for all patients with MFS and, in phase 2, follow-up data are analysed for those eyes, without FD at presentation, for which there were available data at least 1 year after initial presentation or until the point of development of a FD.

Data collected included demographic information (age, sex and ethnicity), eye-specific data (laterality, SE), as well as both qualitative and quantitative OCT

parameters. Qualitative features included the presence of pre-macular structures, such as ERM, EP, VMT and ILM detachment. Other recorded features included the presence of ILH, OLH and FD.

Horizontal extent of MFS was classified according to Shimada et al's S0-S4 classification (Figure 3-8) (385). In addition, grade of MTM was categorised using the ATN classification system, incorporating the modifications proposed by Li et al (Figure 3-9) (442–444). OCT images were classified by two clinician graders, and in the event of disagreement, further classification was provided by a third clinician.

Quantitative OCT parameters were collected using the proprietary linear measuring software in the Topcon 3D OCT-1000 ImageNet programme. These included CRT, AvRT, CSH and CT (see 2.3.6.1). SA is a similar, but quantifiable, metric to schisis extent; it was estimated by thresholding the colour thickness map (as described in 2.3.6.2).

3.3 Results

3.3.1 Phase 1: Baseline analysis

3.3.1.1 All cases:

530 highly myopic patients were identified, of whom 154 patients (218 eyes) with MFS met the inclusion criteria and were included in the final analysis. The mean (±SD) age was 59.0 (±11.2) years and logMAR VA of 0.22 (±0.23) at baseline. With the exception of SE, which showed a between-eye correlation coefficient of 0.78, all other variables were not strongly correlated between patient eyes (all <0.30), therefore these parameters were considered independent and included from both eyes in all further analyses. Baseline VA was not associated with age, sex or ethnicity on simple linear regression analysis. Patient and eye characteristics are summarised in Table 3-1; 34 unaffected fellow eyes are included for comparison. Affected eyes had a significantly worse baseline VA, and more negative SE, as well as a greater

proportion of pre-macular structures than unaffected fellow eyes ($p<0.001$), which remained statistically significant, following removal of those with FD or FTMH ($p=0.002$, Figure 3-10). Incidence of PS was comparable between the groups ($p=0.127$).

Table 3-1: Summary of baseline characteristics of all patients with MFS

Patients (n=154)	**Mean ±SD / n (%)**
Age (years)	59 ±11
Female sex	116 (75%)
Ethnicity:	
White	81 (53%)
South-East Asian	22 (14%)
Other Asian	13 (8%)
Black	10 (6%)
Other/mixed	12 (8%)
Not disclosed	16 (10%)
Laterality of affected eye(s):	
Right eye only	51 (33%)
Left eye only	39 (25%)
Both eyes	64 (41%)

Eyes (n=252)	**Affected eyes (n=218)**	**Unaffected fellow eyes (n=34)**	***p-value***
Baseline VA (logMAR)	0.22 ±0.23	0.09 ±0.16	***<0.001***
Spherical Equivalent (D)	-13.2 ±4.5	-10.5 ±3.9	***<0.001***
Vitreoretinal features:			
Any pre-macular structure	166 (76%)	14 (41%)	***<0.001***
Vitreo-macular traction	30 (14%)	0	***0.021***
Epiretinal membrane	136 (62%)	14 (41%)	***0.019***
Epiretinal proliferation	7 (3%)	0	*0.289*
ILM detachment	37 (17%)	0	***0.009***
Inner lamellar hole (ILH)	57 (26%)	0	***0.001***
Outer lamellar hole (OLH)	8 (4%)	0	*0.256*
Foveal detachment (FD)	12 (6%)	0	*0.161*
Posterior staphyloma	167 (77%)	30 (88%)	*0.127*

In Table 3-2, all eyes are categorised according to both the S0-S4 schisis and the modified ATN grading systems, alongside healthy fellow eyes. Quantitative OCT parameters are reported for 156 cases with S1-4 and T1-3 only. There were no between-group differences for age or sex for schisis extent. However, SE was significantly lower and logMAR VA was significantly worse in the S4 group ($p=0.035$ and $p<0.001$ respectively). In addition, S4 was significantly associated with presence of ILM detachment ($p<0.001$). By comparison, a significantly greater proportion of those with S2 schisis had evidence of ERM and ILH ($p=0.010$ and $p<0.001$ respectively), but a significantly lower incidence of PS ($p<0.001$) and ILM detachment ($p=0.011$).

There was no significant between-group difference in age for T1-4 on the ATN classification. 12 eyes (5.5%) had a FD (T3) at presentation, of which 11 (92%) had S4 schisis extent, while the remaining 1 case had S3 schisis. VA was significantly worse in those with FD ($p<0.001$, Figure 3-10) and there was a significant association demonstrated between the presence of FD and S4 schisis extent on Pearson chi-squared analysis ($p<0.001$). All cases of FD were associated with the presence of PS, compared to 76% of those without FD ($p=0.039$). The baseline functional and qualitative anatomical characteristics for those eyes with 'MFS only' and those with 'MFS + FD' are summarised in Table 3-3.

Table 3-2: Baseline characteristics according to existing MFS staging criteria

	Schisis classification				Modified ATN classification				Healthy fellow eyes
Characteristic	**S1**	**S2**	**S3**	**S4**	**T1**	**T2**	**T3**	**T4**	
Eyes (n)	73 (33%)	37 (17%)	66 (30%)	42 (19%)	16 (7%)	185 (85%)	12 (6%)	5 (2%)	34
Age (years)	58 ±11	60 ±10	59 ±12	58 ±12	64 ±12	59 ±11	60 ±11	53 ±9	58 ±10
Spherical Equivalent (D)	-13.6 ±4.1	-12.0 ±4.3	-12.6 ±4.5	-14.6 ±4.8	-11.8 ±3.3	-13.2 ±4.4	-15.6 ±5.7	-11.2 ±4.0	-10.5 ±3.9
Baseline VA (logMAR)	0.11 ±0.15	0.19 ±0.17	0.22 ±0.22	0.43 ±0.28	0.14 ±0.17	0.19 ±0.19	0.62 ±0.32	0.57 ±0.34	0.09 ±0.16
All pre-macular structures	51 (70%)	32 (87%)	46 (70%)	37 (88%)	12 (75%)	141 (76%)	10 (83%)	3 (60%)	14 (41%)
Vitreo-macular traction	6 (8%)	3 (8%)	13 (20%)	8 (19%)	4 (25%)	25 (14%)	1 (8%)	0	0
Epiretinal membrane	46 (63%)	30 (81%)	37 (56%)	23 (55%)	9 (56%)	118 (64%)	6 (50%)	3 (60%)	14 (41%)
ILM detachment	9 (12%)	1 (3%)	9 (14%)	18 (43%)	4 (25%)	29 (16%)	4 (33%)	0	0
Inner lamellar hole	5 (7%)	20 (54%)	19 (29%)	13 (31%)	3 (19%)	49 (26%)	5 (42%)	0	0
Outer lamellar hole	0	0	1 (2%)	7 (17%)	0	0	8 (67%)	-	0
Full thickness macular hole	0	1 (3%)	3 (5%)	1 (2%)	-	-	-	5 (100%)	0
Foveal detachment	0	0	1 (2%)	11 (26%)	-	-	12 (100%)	-	0
Posterior Staphyloma	57 (78%)	18 (49%)	54 (82%)	38 (90%)	8 (50%)	144 (78%)	12 (100%)	3 (60%)	30 (88%)
Dome-shaped macula	8 (11%)	2 (5%)	3 (5%)	1 (2%)	0	14 (8%)	0	0	0
OCT parameters:	(n=51)	(n=31)	(n=43)	(n=31)	(n=12)	(n=133)	(n=11)	-	(n=23)
Central retinal thickness (µm)	190 ±40	240 ±91	228 ±75	395 ±163	225 ±81	239 ±107	427 ±160	NR	204 ±37
Average retinal thickness (µm)	273 ±38	267 ±34	293 ±46	446 ±71	277 ±37	302 ±73	460 ±87	NR	258 ±16
Central schisis height (µm)	N/A	130 ±64	153 ±85	349 ±118	78 ±23	190 ±113	368 ±163	NR	N/A
Subfoveal choroidal thickness	46 ±32	83 ±54	65 ±48	48 ±41	55 ±40	62 ±47	33 ±13	NR	109 ±71
Schisis area (mm^2)	NR	3.2 ±4.4	6.8 ±6.1	22.1 ±4.8	8.9 ±3.4	8.6 ±8.8	22.3 ±5.6	NR	N/A

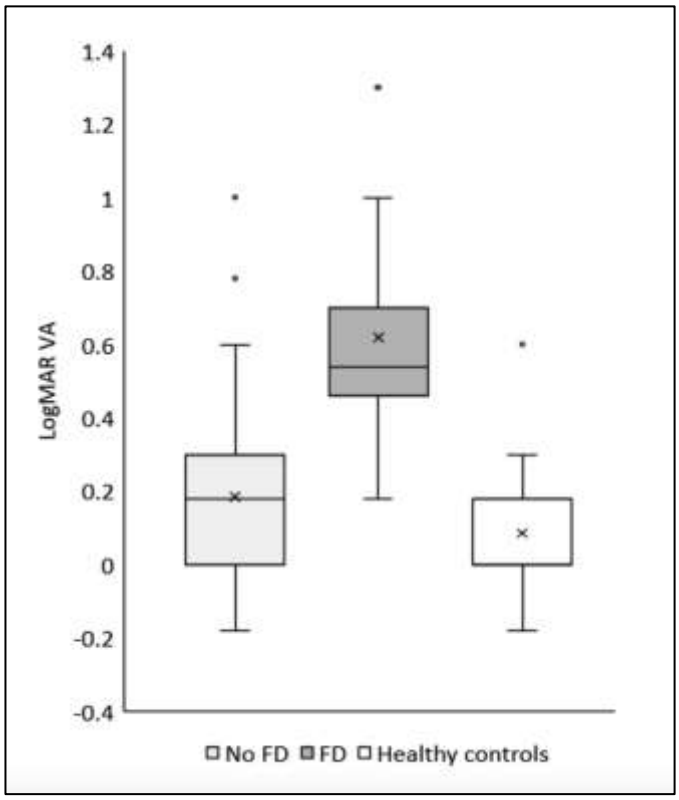

Figure 3-10*: *Comparison of baseline logMAR VA between eyes with MFS only, MFS and FD and healthy fellow eyes

5 eyes (2.3%) had a FTMH (T4) at presentation, which was associated with worse VA (p=0.008), but no association with other demographic features. Due to uncertainty regarding the antecedent pathoanatomical process in such cases, these eyes are not included in any further analyses.

Table 3-3: Baseline functional and anatomical characteristics according to FD status in MFS

Characteristic	**MFS only**	**MFS + FD**	***p-value***
Eyes [n(%)]	201 (94%)	12 (6%)	-
Spherical Equivalent (D)	-13.1 ±4.4	-15.6 ±5.7	*0.152*
Age (years)	59 ±12	60 ±11	*0.630*
VA (logMAR)	0.18 ±0.19	0.62 ±0.32	***<0.001***
Schisis extent			
S1	73 (36%)	0	*0.005*
S2	36 (18%)	0	*0.102*
S3	62 (31%)	1 (8%)	*0.084*
S4	30 (15%)	11 (92%)	***<0.001***
All pre-macular structures	151 (76%)	10 (83%)	*0.435*
Vitreo-macular traction	29 (14%)	1 (8%)	*0.475*
Epiretinal membrane	127 (63%)	6 (50%)	*0.267*
ILM detachment	33 (16%)	4 (33%)	*0.135*
ILH	52 (26%)	5 (42%)	*0.190*
OLH	0	8 (73%)	***<0.001***
Posterior Staphyloma	152 (76%)	12 (100%)	***0.039***

3.3.1.2 Fovea-involving (S2-4) cases:

Following removal of cases with FTMH (T4) and those with non-fovea involving MFS (S1), 140 patients remained with fovea-involving schisis. The comparative characteristics, including qualitative data, where available, of those with and without FD are summarised in Table 3-4; In this subgroup, baseline VA was significantly associated with age (p=0.037, β=0.004), while VA, schisis extent and presence of PS all remained significantly different between those with and without FD on sub-analysis.

Table 3-4: Baseline functional and anatomical characteristics according to FD status in patients with fovea-involving MFS

Characteristic	**MFS only**	**MFS + FD**	***p-value***
Eyes [n(%)]	128 (91%)	12 (9%)	-
Spherical Equivalent (D)	-12.8 ±4.5	-15.6 ±5.7	*0.118*
Age (years)	59 ±12	60 ±11	*0.717*
VA (logMAR)	0.23 ±0.20	0.62 ±0.32	***<0.001***
Schisis extent			
S2	36 (28%)	0	
S3	62 (48%)	1 (8%)	
S4	30 (23%)	11 (92%)	***<0.001****
All pre-macular structures	102 (80%)	10 (83%)	*0.556*
Vitreo-macular traction	23 (18%)	1 (8%)	*0.353*
Epiretinal membrane	81 (63%)	6 (50%)	*0.272*
ILM detachment	24 (19%)	4 (33%)	*0.197*
ILH	47 (37%)	5 (42%)	*0.480*
OLH	0	8 (73%)	***<0.001***
Posterior Staphyloma	95 (74%)	12 (100%)	***0.034***
OCT parameters	(n=94)	(n=11)	
Central retinal thickness (μm)	263 ±120	427 ±160	***<0.001***
Average retinal thickness (μm)	314 ±79	460 ±87	***<0.001***
Schisis height (μm) [if present]	185 ±113	368 ±163	***<0.001***
Schisis area (mm^2)	8.6 ±8.7	22.3 ±5.6	***<0.001***
**chi-squared analysis comparing distribution of schisis extent between groups*			

Regarding quantitative OCT parameters, the presence of FD was significantly correlated with greater CRT, AvRT, CSH and SA (all p≤0.001) on Mann Whitney-U comparison, in 105 eyes with available Topcon OCT data (Figure 3-11). On logistic regression modeling, all OCT metrics were significantly associated with the presence of FD (all p<0.01); the strongest association was demonstrated with AvRT (OR=1.02

[95%CI: 1.01-1.02], p<0.001, pseudo-R^2=0.31) and SA (OR=1.21 [95%CI: 1.08-1.35], p=0.001, pseudo-R^2=0.30). That is to say, for example, that each 1mm^2 increase in SA is estimated to result in a 1.21 times increased odds of presence of FD. These results indicate that individual anatomical features may explain up to an estimated 30-35% of the variance in the presence of FD at baseline.

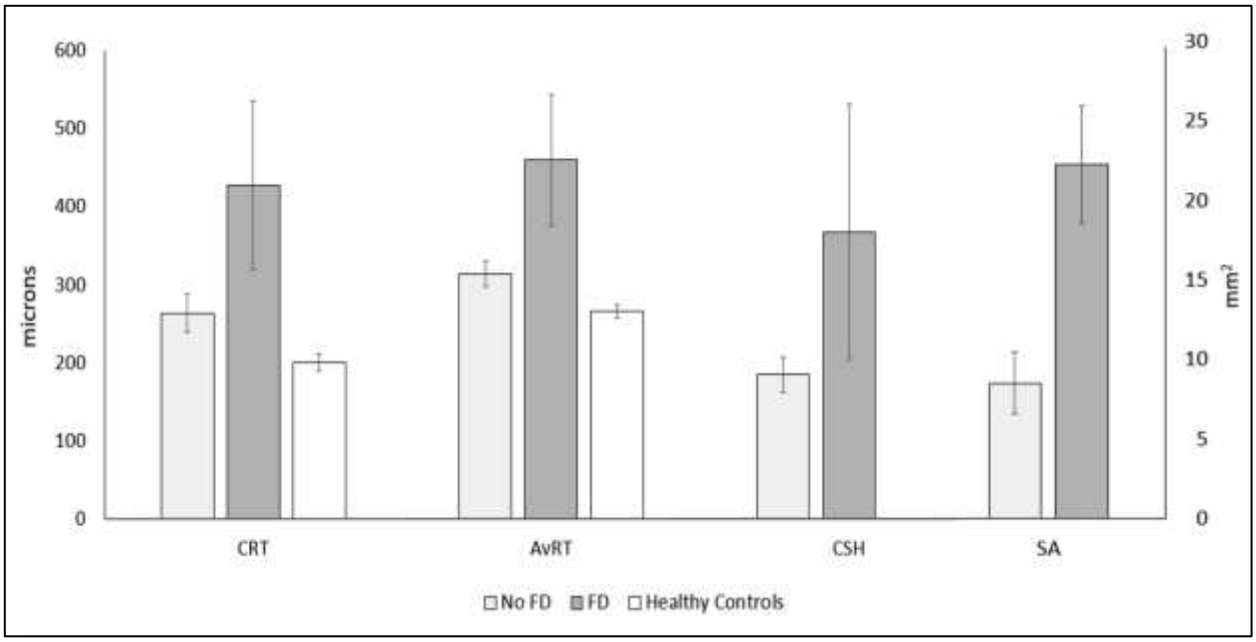

Figure 3-11*: *Comparison of OCT qualitative metrics between patients with MFS only, MFS and FD and healthy fellow eyes

On within-group analysis of 128 patients with MFS and no FD, the association between age and VA remained significant (p=0.018, β=0.003). 94 patients with MFS only and Topcon OCT imaging underwent subgroup analysis to investigate the effect of schisis morphology on visual acuity. On age-adjusted multivariate regression modeling, worse VA was significantly associated with greater CSH (p=0.037, β=0.0004, R^2=0.11), albeit with a small effect size, but not with CRT (p=0.591), AvRT (p=0.125) or SA (p=0.062).

ANCOVA comparison of schisis extent (S2-4), with age-adjustment, revealed a significant between-group difference for VA in those with MFS only (p=0.004); S4 was associated with significantly worse VA than both S2 (p=0.027) and S3 (p=0.003) on Bonferroni pairwise testing, but no difference between S2 and S3 (Figure 3-12). In

addition, S4 schisis showed significant correlation with presence of ILM detachment compared to S2-3 (47% vs 11%, p<0.001) on chi-squared analysis.

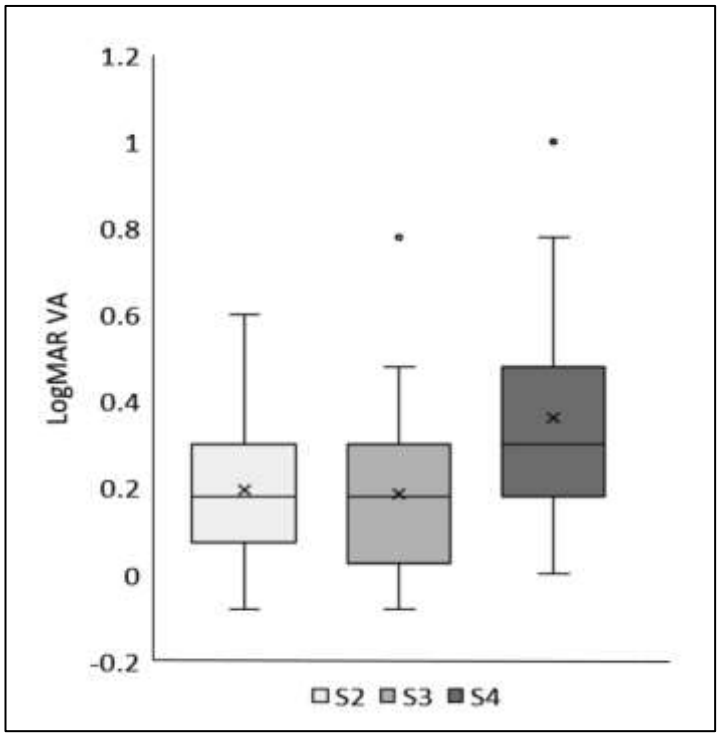

Figure 3-12*: *Comparison of logMAR VA in patients with MFS only, according to schisis extent (S2-S4)

3.3.2 Phase 2: Longitudinal analysis

3.3.2.1 All cases:

118 eyes with MFS from 88 patients had available follow-up data for at least 1 year or until the point of development of FD (mean 4.6 ±2.6 years). During this period, 5 eyes (4%) developed a new FD, all of which occurred on a background of S4 schisis (Figure 3-13), after a mean period of 3.4 (±2.8) years.

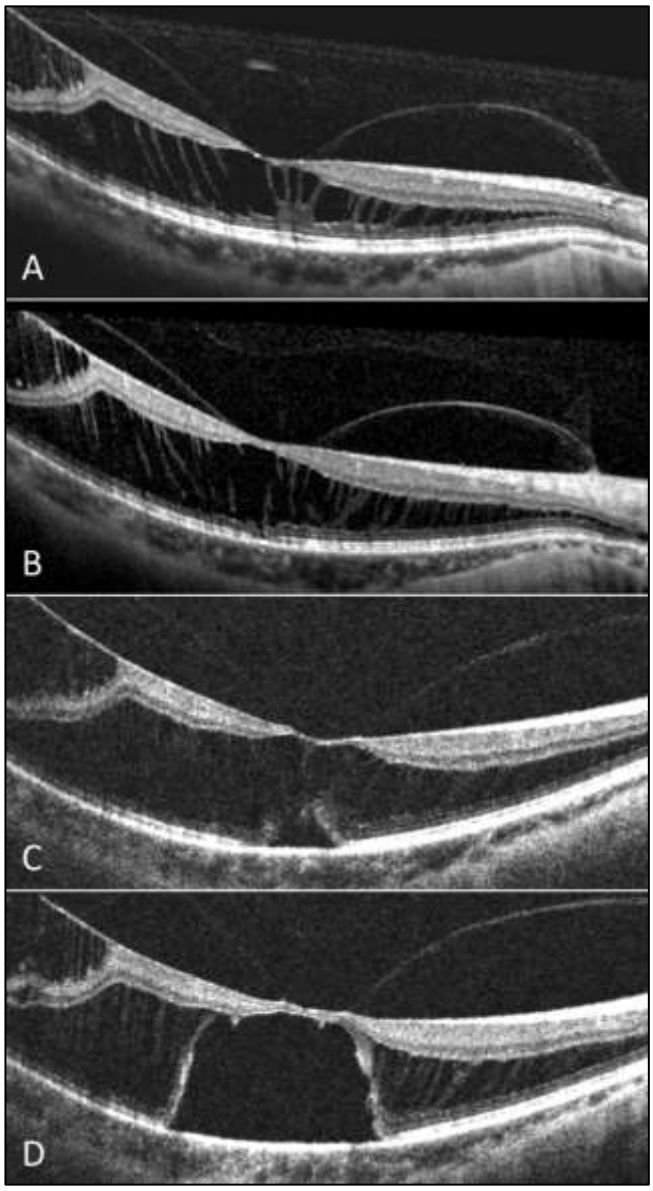

Figure 3-13: Longitudinal observation of FD development: (A) widespread schisis with evidence of both VMT and ILM detachment; (B) EZ disruption; (C) formation of small OLH with early FD; (D) FD enlarges horizontally and vertically

Development of FD was associated with a drop in VA (0.44 ±0.36), while those that did not develop FD demonstrated a non-significant mean change in vision (0.02 ±0.18, p=0.282) over 4.7 (±2.6) years. Presence of FD at follow up was significantly associated with worse final VA (p<0.001, Figure 3-14).

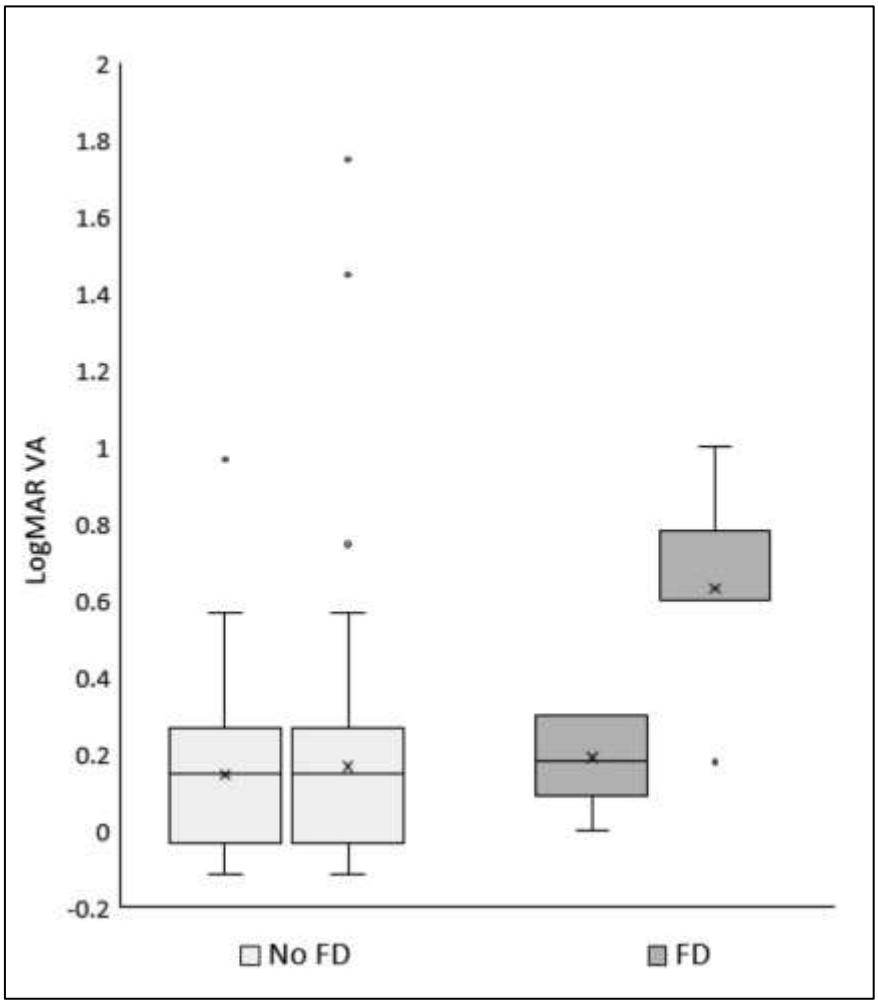

Figure 3-14: Comparison of baseline and final logMAR VA in eyes with MFS that did not and did develop FD during the course of follow-up

Table 3-5: Phase 2: Baseline and follow-up characteristics according to FD status in all eyes with MFS

Characteristic	MFS only (n=113)		MFS + FD (n=5)		
	Baseline	**Final**	**Baseline**	**Pre-FD development**	**Final**
Age (years)	58 ±11	62 ±11	46 ±11	49 ±13	49 ±13
VA (logMAR)	0.18 ± 0.19	0.20 ±0.27	0.19 ±0.12	0.37 ±0.16	0.63 ±0.30
Duration	-	4.7 ±2.6	-	2.9 ±2.7	3.4 ±2.8
ATN classification grade					
T0	-	1 (1%)	-	-	-
T1	7 (6%)	8 (7%)	0	0	-
T2	107 (94%)	105 (92%)	5 (100%)	5 (100%)	-
T3	-	-	-	-	5 (100%)
T4	-	-	-	-	-
Schisis extent					
S0	-	1 (1%)	-	0	0
S1	45 (40%)	42 (37%)	0	0	0
S2	21 (19%)	23 (20%)	0	0	0
S3	31 (27%)	30 (27%)	1 (20%)	0	0
S4	16 (14%)	17 (15%)	4 (80%)	5 (100%)	5 (100%)
Posterior staphyloma	92 (81%)	-	5 (100%)	-	-
ILM detachment	14 (12%)	-	4 (80%)	-	-

The functional and qualitative anatomical characteristics for both groups are summarised in Table 3-5, according to baseline and follow-up. In addition, the characteristics are reported for the visit immediately prior to development of FD under 'pre-FD development'. At baseline, there was no significant between-group difference in age or logMAR VA. All cases of FD developed on a background of S4 schisis, which represents a significant association on Fisher's exact testing (p=-

0.004). In turn, the presence of S4 schisis remained significantly associated with ILM detachment (p=0.042).

3.3.2.2 Fovea-involving (S2-4) cases:

Following removal of cases with non-fovea-involving (S1) MFS at baseline, 73 patients remained with fovea-involving schisis, of whom 5 (7%) developed FD. The comparative characteristics of those with and without FD at baseline and final follow-up are summarised in Table 3-6, including within- and between-group comparisons. Quantitative parameters for 48 eyes with matched longitudinal Topcon OCT data are included, of which 4 (8%) developed FD.

Despite the small numbers, there was a significant between-group difference detected for AvRT, CSH and SA at baseline and all parameters at follow-up (Figure 3-15). On logistic regression analysis, all OCT metrics were associated with FD development, with AvRT demonstrating the strongest association (OR=1.04 [95%CI 1.00-1.08], p=0.046, pseudo-R^2=0.59). In absolute terms, all of the eyes that developed FD had an AvRT >450µm during the course of observation, which represented a significant association on Fisher's exact testing (p<0.001). All OCT metrics remained significantly associated with the presence of ILM detachment (all p<0.01).

Table 3-6: Phase 2: Baseline and follow-up characteristics according to FD status at final visit in eyes with fovea-involving MFS

Characteristic (n/mean ±SD)	**MFS only**	**MFS + FD**	***p-value***
Number (%)	68 (93%)	5 (7%)	-
Baseline age (years)	59±10	46 ±11	*0.084*
Duration of follow-up (months)	4.7 ±2.6	3.4 ±2.8	*0.615*
VA (logMAR)			
Baseline	0.23 ±0.20	0.19 ±0.12	*0.563*
Final	0.26 ±0.31	0.63 ±0.30	***0.047***
p-value	*0.138*	*0.250*	
OCT parameters:	(n=44)	(n=4)	
Central retinal thickness (µm)			
Baseline	268 ±111	351 ±150	*0.265*
Final	229 ±90	485 ±284	*0.105*
p-value	***0.019***	*0.250*	
Average retinal thickness (µm)			
Baseline	312 ±72	429 ±60	***0.007***
Final	309 ±79	551 ±121	***<0.001***
p-value	*0.631*	*0.125*	
Central schisis height (µm)			
Baseline	186 ±110	314 ±56	***0.049***
Final	186 ±142	514 ±152	***0.001***
p-value	*0.913*	*0.125*	
Schisis area (mm^2)			
Baseline	8.8 ±8.5	22.7 ±4.2	***0.014***
Final	8.1 ±8.1	25.8 ±3.0	***<0.001***
p-value	*0.483*	*0.125*	

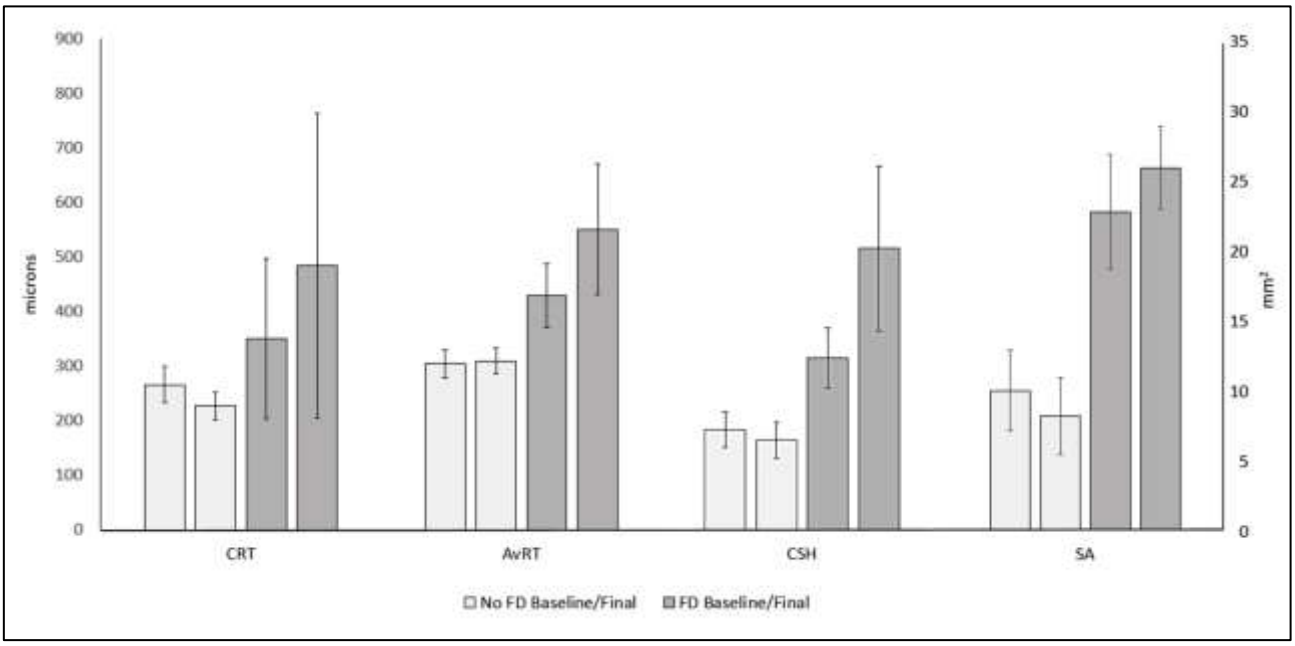

Figure 3-15: A comparison of baseline and final quantitative OCT metrics in MFS according to foveal detachment status at final visit

3.3.2.3 Fovea-involving MFS cases:

In 68 eyes with fovea-involving MFS (i.e. S2-4) at baseline that did not develop FD during follow-up, there was a non-significant change in VA from 0.23 (±0.20) to 0.26 (±0.31), over a period of 4.7 (±2.6) years (p=0.138). 21% demonstrated a reduction in S0-4 schisis extent (Figure 3-18), while 6% increased (Figure 3-16). There were 8 cases of spontaneous resolution of fovea-involving MFS, but only 1 case demonstrated global resolution of macular foveoschisis. The change in S0-4 schisis extent over time represents a significant change in frequency distribution on Fisher's exact testing (p=0.036). Variation in VA related to improvement or worsening of schisis extent, did not reach significance on Kruskall-Wallis analysis (p=0.083).

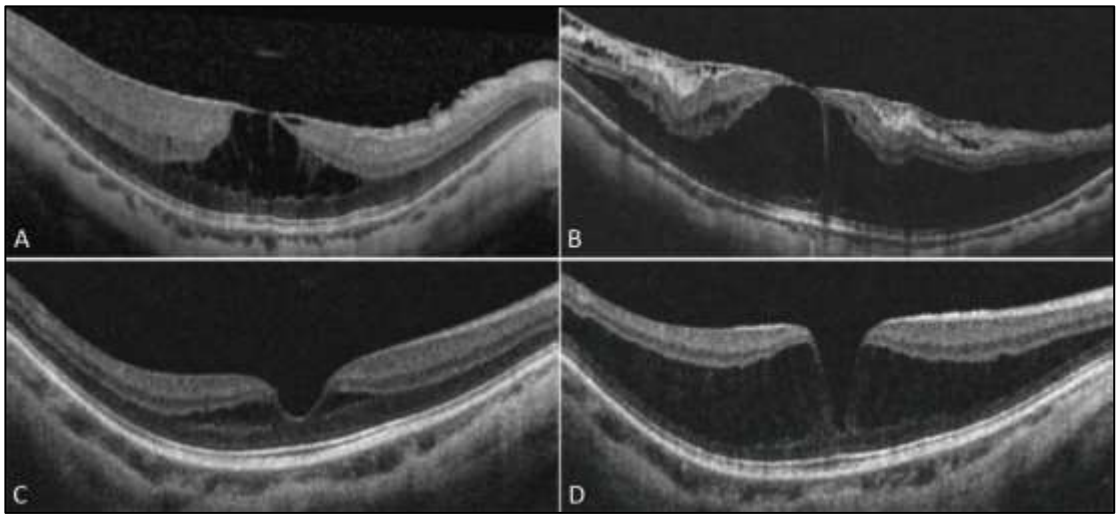

Figure 3-16: Increase in schisis extent: (A&B) Increase in schisis extent with contraction of ERM; (C&D): Widening of outer schisis cavity associated with staphyloma

In 44 eyes with OCT data, there was a significant reduction in CRT height (p=0.019), but non-significant change in AvRT, CSH or SA over a mean period of 4.8 (±2.7) years' follow-up. Although final AvRT, CSH and SA were found to be associated with final VA (all p≤0.02), the effect sizes were small (β=0.002, 0.001 and 0.020 respectively), indicating minimal contribution to the variance in VA. Neither the duration of disease, nor relative change in OCT parameters from baseline were found to be associated with change in VA in eyes with MFS only during the follow-up period.

3.3.2.4 Surgery

Although not specifically relevant to the study, it is worth mentioning that 14 eyes underwent surgery for MFS-related disease during the study period. Of these, 7 (50%) had FD or FTMH at the time of surgery, with a mean (±SD) pre-operative VA of 0.65 ±0.24; the remaining 7 cases had presence of VMT or ERM only, and a mean (±SD) pre-operative VA of 0.51 ±0.25. Final visual outcome after 6 months was broadly similar between the groups (0.48 ±0.47 and 0.50 ±0.44 respectively). Of the operated eyes, 2 cases were complicated by iatrogenic FTMH formation, while one

pre-existing macular hole developed a MHRD. The numbers in this study cohort were too small and heterogeneous to investigate the effects of surgery in MFS but serve to illustrate the potential risks of surgical intervention in this patient group.

3.4 Discussion

This study reports on the associations between baseline and longitudinal OCT features and anatomico-functional characteristics in 218 eyes with MFS. I found that greater schisis extent is significantly associated with worse VA, as well as the baseline presence or subsequent development of FD. Sub-group analysis revealed that quantifiable OCT parameters, such as AvRT, are also associated with FD in MFS.

The demographic characteristics and natural course of the disease in our cohort are consistent with those reported in the literature (372,385–387,392–394,476,477). The natural history of MFS is generally stable, following an uncomplicated clinical course in 71-87% of cases (372,385–387,392,418,444). In the absence of FD, I observed functional deterioration to be rare; 111/113 (98%) of eyes retained vision within ≤0.30 logMAR of baseline, over an average of 4.7 years' follow-up. The overall incidence of FD in both phases of this study was 7.8%, which is in keeping with previous findings of between 3-24%, with the variance likely partly explained by both the demography and distribution of cases studied, as well as the increasing utilisation of OCT to detect asymptomatic MFS (372,385,387,392,418,444).

In Shimada et al's 4-stage progression to FD in MFS, whereby focal irregularities in the outer retina precede the development of an outer lamellar hole and FD (see Figure 3-6), the interval between the stages is reportedly short, but offers a potentially optimal opportunity for surgery (436). The prevalence of FD at presentation in this study supports the assertion that it develops rapidly on a background of minimally symptomatic foveoschisis. An alternative pathway for development of FTMH in MTM has been postulated, which occurs via initial formation of an ILH (437,444). This mechanism of FTMH is probably similar to that of

idiopathic FTMH formation in emmetropic eyes (i.e. via focal VMT) and is supported by our finding that those with S2 schisis have a higher rate of ERM and ILH at baseline, despite a lower incidence of posterior staphyloma (437,438,444). I propose that FTMH should only be considered a stage in MFS progression if it occurred via FD, which would indicate that it comprised part of the continuous, mechanical process described by Shimada et al.

While the precise underlying pathomechanism of MFS remains subject to debate, the presence of PS is generally accepted to predispose eyes to its development (372,378,392,393). My data support this finding, showing an overall prevalence of 77% in our cohort, increasing to 100% in those that were complicated by FD. OCT studies have suggested that outer layer retinoschisis (OLR) is ubiquitously present in eyes with MFS and is anatomically related to the presence of PS (372,478). OLR is typically observed in HFL and is characterised by the presence of columnar components, which are obliquely orientated centrally, becoming increasingly verticalised in the more peripheral macula (as in Figure 3-9B) (383,392,393). These columnar elements are likely to contain MC and photoreceptor processes, which are horizontally orientated in HFL under normal circumstances, but appear to afford some redundancy in cases of tractional foveopathy, stretching to permit retention of retinal function (100,335,394,428,479).

More recently, evidence increasingly supports a role of pre-macular structures (PMS) in both the development and progression of MFS (383,388–390,408). The prevalence of PMS in MFS is reportedly between 46-83% (372,391,407,428,480); in this study I found PMS to be present in 76% of eyes, a significantly higher proportion than in unaffected fellow eyes (41%). Inner layer retinoschisis (ILR) is reported to co-exist in up to half of eyes with MFS, predominantly located between the inner plexiform layer and ILM, and may be attributable to the forces exerted by PMS at the VMI (372,384,394,428,432). In particular, ILM detachment, a characteristic phenomenon thought to represent a consequence of ILM non-compliance in myopic eyes, was noted to be present in 17% of eyes in this study, increasing to 44% of those with S4 schisis extent (427,430,433,481). ILM detachment is often observed as a cord-like

elevation, spanning from the parafovea to the vascular arcade, separated from the outer retina by a sub-ILM cavity, containing vertically orientated columnar elements (Figure 3-4) (372,394,419,433). The ILM is tethered at the retinal vessels, whereat insertion of vitreoretino-vascular bands into sclerotic arterioles and adjacent neuro-glial-vascular units results in multilayer paravascular abnormalities, such as microfolds, cysts and lamellar defects (Figure 3-5D) (58,415,416,418,419,421). Because the MC processes outside the parafoveal region are already vertically orientated at rest, it follows that ILM detachment can initiate ILR by generating a broad centripetal force, early in the disease process (Figure 3-17A&B) (372,404). When combined with posterior elongation of the globe, this results in progressive transmission of forces throughout macula and both horizontal and vertical extension of the OLR (Figure 3-17C). Eventually, excessive verticalisation of the centermost MC processes leads rupture of the MCC stalk, outer retinal disruption and FD formation due to the unopposed tension from the zMCs (Figure 3-17D) (100). This mechanical theory may account for the finding in this study that ILM detachment is associated with S4 schisis extent and AvRT, while both characteristics, in addition to PS, are significantly associated with FD development.

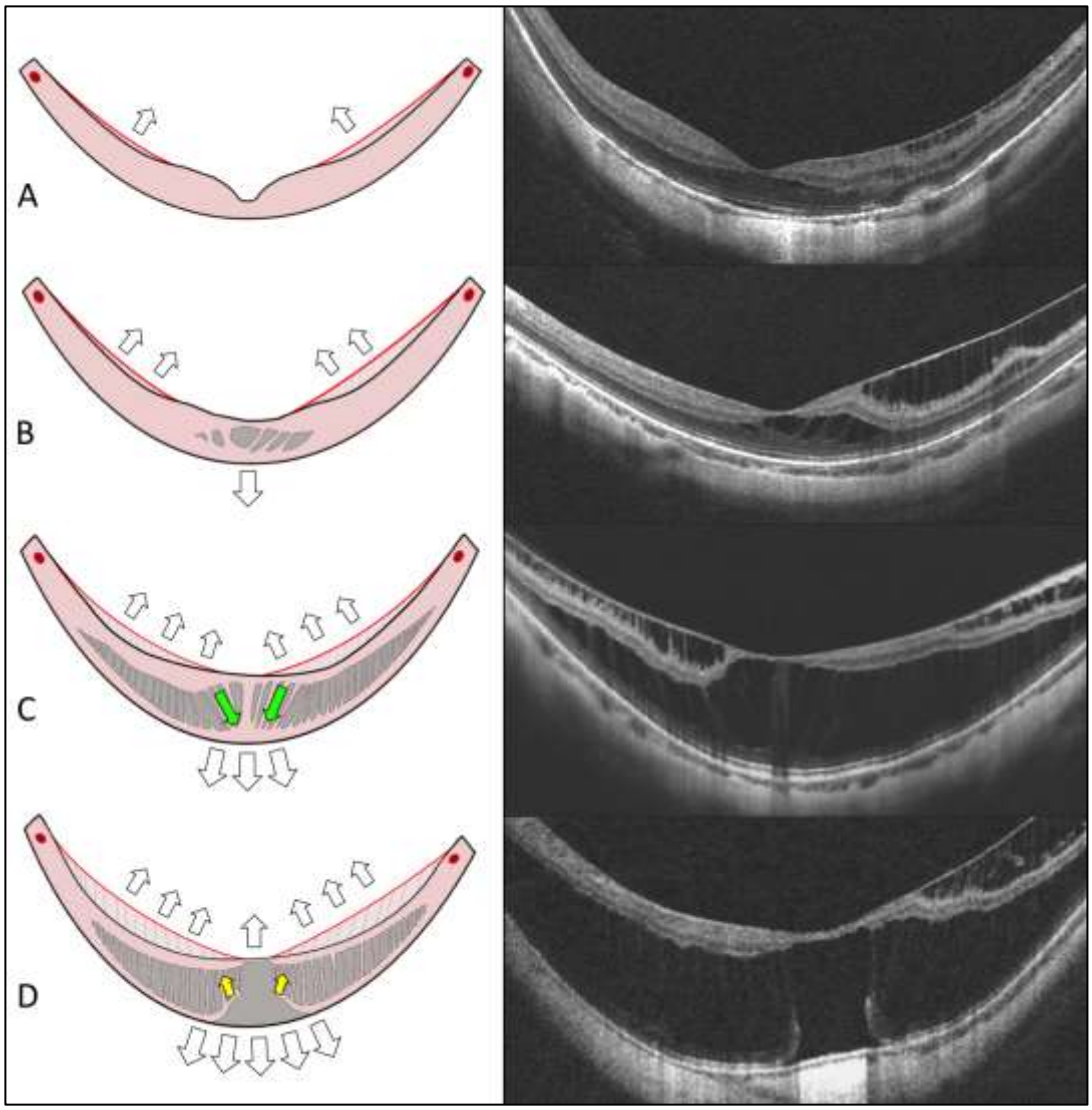

Figure 3-17: A diagram demonstrating the centripetal forces exerted on the retina by ILM detachment and centrifugal forces from PS formation (white arrows): (A) Non-compliant ILM acts as a chord, with a net inward force manifesting as inner layer retinoschisis in the perifoveal region; (B) increased inwards traction, combined with PS progression results in development of foveal outer layer retinoschisis; (C) broad inner retinal traction causes progressive stretching of the relatively elastic retina, resulting in widening of the schisis cavity and verticalisation of zMC processes. Forces transmitted within the retina are concentrated at the fovea (green arrows); (D) the tensile capacity of the MC processes is reached and the elastic limit of the retina is exceeded, leading to development of OLH and FD. Subsequently the inward traction is partially relieved and the outer schisis cavity collapses centrally

The association between schisis parameters and ILM detachment raises the question as to whether schisis extent is itself a risk factor for progression, or rather a surrogate measure of the breadth and magnitude of the forces exerted by PS and PMS. Further clues as to the relevance of ILM detachment can be found by studying those eyes that exhibit improvement of foveoschisis (385). We observed several cases of reduction in schisis extent following spontaneous avulsion of ILM detachment (Figure 3-18). Notwithstanding this, the presence of ILM detachment was not a prerequisite for progression to FD, and since both S4 schisis and AvRT were associated with FD development in this study, it suggests that they remain, in themselves, useful clinical biomarkers for risk of progression in MFS.

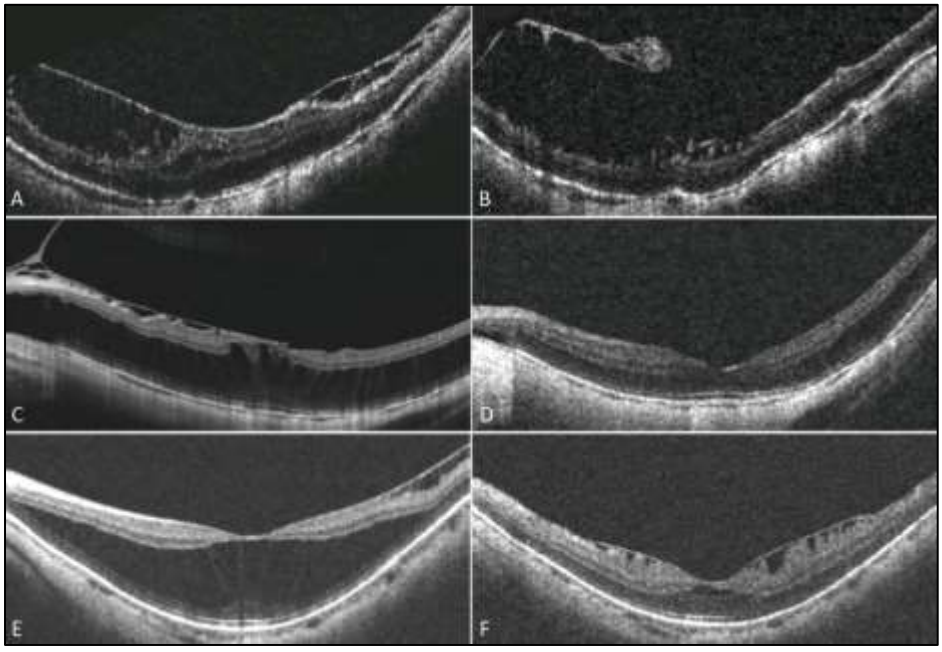

Figure 3-18: Spontaneous improvement in MFS: (A&B): Resolution of MFS associated with avulsion of ILM; (C&D): improvement associated with avulsion of ERM; (E&F): improvement associated with relaxation of ILM detachment

The relationship between extent of schisis and progression of MFS has previously been described (372,385,386). In 2013, Shimada et al found that a greater proportion of eyes with S4 schisis had a higher risk of anatomical and visual deterioration than those with S1-3 (43% vs 8%). However, the same subgroup also demonstrated a higher rate of spontaneous improvement (11% vs 3%), preventing

the conclusion of a significant effect (385,386). In this study, which defined the endpoint of progression as the development of FD, I found that 15/16 (94%) of all FDs developed on a background of S4 schisis, representing a statistically significant association. With respect to those eyes with MFS that did not develop FD, there remained a significant association with S4 schisis extent and worse VA at baseline and follow-up. It is plausible that those cases with extensive schisis are already undergoing microstructural changes, preceding the development of FD (386)(385,386); indeed, 20% of eyes with S4 in phase 2 went on to develop FD during follow-up. These findings suggest that eyes with S4 schisis and reduced VA are at higher risk of anatomico-functional deterioration (440,475). However, this assumption must be measured against the fact that spontaneous improvement in MFS is possible, negating a need for surgery.

In attempt to explore the relationship between schisis morphology and anatomico-functional behaviour more precisely, this study also investigated quantitative OCT metrics in MFS. There is a lack of consensus in the literature as to the association between CRT or CSH with VA in MFS, presumably due to the remarkable capacity of the retina to retain function in the presence of OLR (386,389,482). In the mathematical model of zMC stiffness in MFS (as a function of the angle Θ, subtended between the horizontal and vertical components of the MC), Govetto et al demonstrated that increasing verticalisation of the intra-schitic processes (up to a maximal displacement of 471µm) was associated with worse VA (100). I found that, in those eyes with MFS but no FD, greater AvRT, CSH and SA were all associated with worse VA at final follow-up. However, the estimated effect size was very low in all these models, suggesting that they contribute minimally to the observed variance in VA in MFS. This indicates that, in the absence of FD, OCT metrics are not powerful predictors of function in MFS.

By contrast, there were significant associations between OCT parameters and FD development at both baseline and follow-up. In particular, AvRT was associated with increased odds of FD at baseline, accounting for an estimated 31% of the variance in phase 1, increasing to 63% in phase 2 (i.e. at the point of FD development). This

discrepancy between baseline and follow-up may reflect the observation that the schisis cavity collapses following development of FD (385,394,417). In absolute terms, an AvRT ≥450µm was significantly associated with subsequent FD development in this study. If risk stratification were based on this parameter alone, 18% of eyes in this study cohort would be considered 'high-risk', 44% of which would have benefitted from early detection of progression during the study period. This novel finding indicates that, as biomarkers, OCT metrics may contribute to more accurate models for predicting progression to FD in MFS. It ought to be noted that the parameters in this study have been calculated using Topcon OCT and are not directly translatable to other systems.

Table 3-7 provides a proposed monitoring system for MFS, based on the qualitative and quantitative risk factors of schisis extent and AvRT. The objectives at each review are to assess for deterioration in VA and early changes on OCT, suggestive of progression (see Figure 3-6). At this point, discussion of the risks and benefits of surgical intervention may be appropriate. Although care was taken to avoid the risk of observer bias during the calculation of OCT quantitative metrics, this scoring system has not been validated, neither internally nor externally and, as such, remains uncorroborated.

Table 3-7: Proposed MFS Monitoring Scoring System

Characteristic	**Threshold**	**Score**
Schisis extent	S0-2	0
	S3-4	1
Average retinal thickness (µm)	<450	0
	≥450	1
Total score	**Suggested monitoring frequency**	
0	12 months	
1	6 months	
2	≤3 months	

The optimal approach and timing of surgery in high-risk eyes remains unclear, due to a lack of prospective, controlled studies. Anatomical and functional success has been reported using a variety of internal and external (or combined) approaches, and the prevalence of both PS and ILM detachment in this study support a role for a tailored approach in progressive MFS (140,404,452,453,455,457,458,472,473,483). The low rate of progression in MFS makes it challenging to justify pre-emptive intervention, while complications, including FTMH and MHRD have been described at rates between 0-19% (although this risk appears to be somewhat mitigated by the use of fovea-sparing ILM peeling) (452,464,475,486–488). Evidence indicates that, besides pre-operative VA, the presence of FD is strongest predictor associated with poor final visual outcome (440,450,489). It follows, therefore, that any clinical biomarkers capable of anticipating the development of FD would be inherently valuable. This study was not designed to investigate surgical outcomes in MFS, but the existing evidence supports a role for early intervention, while also revealing a risk of operative complication, in this patient group. Both factors ought to be taken into consideration when applying the above-proposed scoring system in clinical practice.

There are potential limitations to this study due to its retrospective, observational design, introducing a risk of information and reporting bias, as well as confounding. For example, AL was not routinely measured in all patients and has previously been associated with MFS (372,379,390). However, both SE and CT measurements (which have been shown to be significantly correlated with AL) were found to be consistent with existing reports (490,491). The complications of high myopia are not limited to MFS and, while several potentially confounding factors, such as CNVM, macular atrophy and retinal detachment, were excluded from this study, there are other microstructural and physiological features of high myopia that have not been considered here (386,439). Co-factors such as these will all ultimately influence both prognostication and clinical decision-making (386,390,439). The potential for observer bias was reduced by the inclusion of multiple graders for qualitative data, however the quantification of OCT metrics was performed by a single grader only and therefore both reported associations and the grading system requires further validation before they may be suitable for clinical application. Regardless, this real-

world clinical dataset comprises one of the largest studies of the natural history and associations of MFS to-date.

3.5 Conclusion

In conclusion, the findings of this study confirm that MFS is a relatively common and generally stable condition; in the absence of FD, VA does not significantly change over time. The findings presented support the assertion that schisis extent is associated with poorer anatomico-functional outcomes, while also identifying novel associations with ILM detachment, lending further evidence to support the relevance of PMS in the pathomechanisms of MFS. Furthermore, greater AvRT has been shown to be significantly associated with FD development. This novel association indicates that quantitative OCT parameters may represent viable biomarkers for predicting progression in cases of MFS.

I propose that vigilant observation is merited in eyes with widespread MFS, for evidence of functional or anatomical progression, alongside careful scrutiny of OCT metrics. To this end, I have proposed a simple OCT-based scoring system to aid risk stratification and guide follow-up intervals, with a view to facilitating earlier identification of progression and planning timely intervention accordingly.

CHAPTER 4

A RETROSPECTIVE OBSERVATIONAL STUDY OF THE ANATOMICO-FUNCTIONAL BEHAVIOUR OF FOVEOMACULAR RETINOSCHISIS IN OPTIC DISC PIT MACULOPATHY

"You must unlearn, what you have learned"

– Yoda

4.1 Introduction

First described in 1882 by Weithe, and further characterised by Reis in 1908, optic disc pits (ODP) are congenital focal cavities within the optic nerve, with a reported prevalence of approximately 1/11,000 (492–497). ODPs typically present as unilateral, focal, white-grey, round or oval depressions at the temporal aspect of the optic nerve, and are usually an isolated ophthalmic finding (Figure 4-1) (498–501). An association with the presence of a cilioretinal artery has been reported in up to 60% of cases (501).

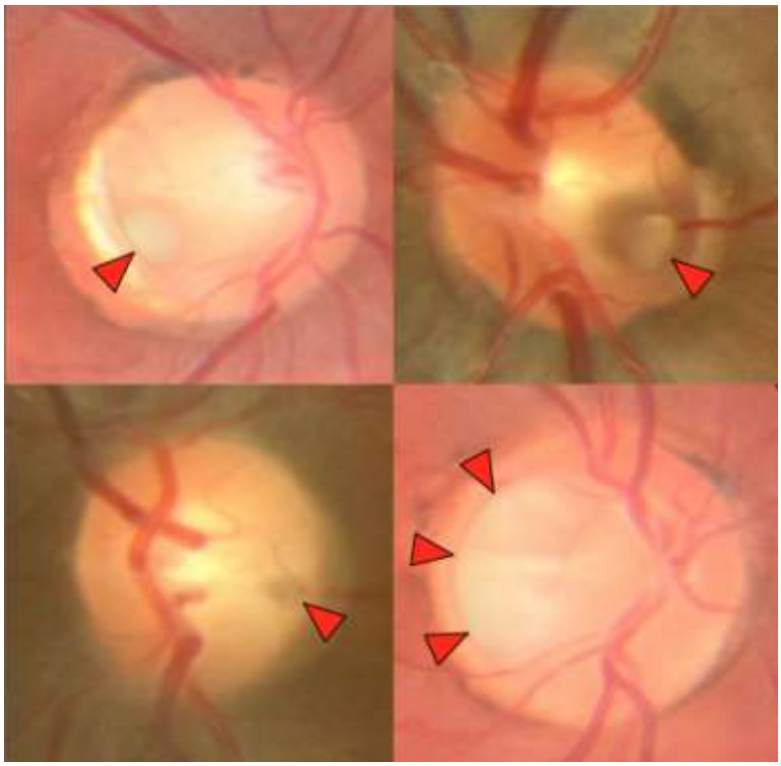

Figure 4-1: Various morphologies of optic disc pits (red arrowheads denote location of pit)

ODPs are commonly asymptomatic, although may be associated with visual field defects due to axonal loss at the neuroretinal rim adjacent to the pit (501). However, in 25%-75% of cases, an ODP can be complicated by the dynamic accumulation of intra- and/or subretinal fluid at the macula, an entity known as optic disc pit maculopathy (ODP-M) (Figure 4-2) (3,494,501–503). The mean reported age of

presentation with ODP-M is 27-36 years, although the condition has been described in children, particularly following blunt trauma to the eye in question (4,494,497,501,504–514).

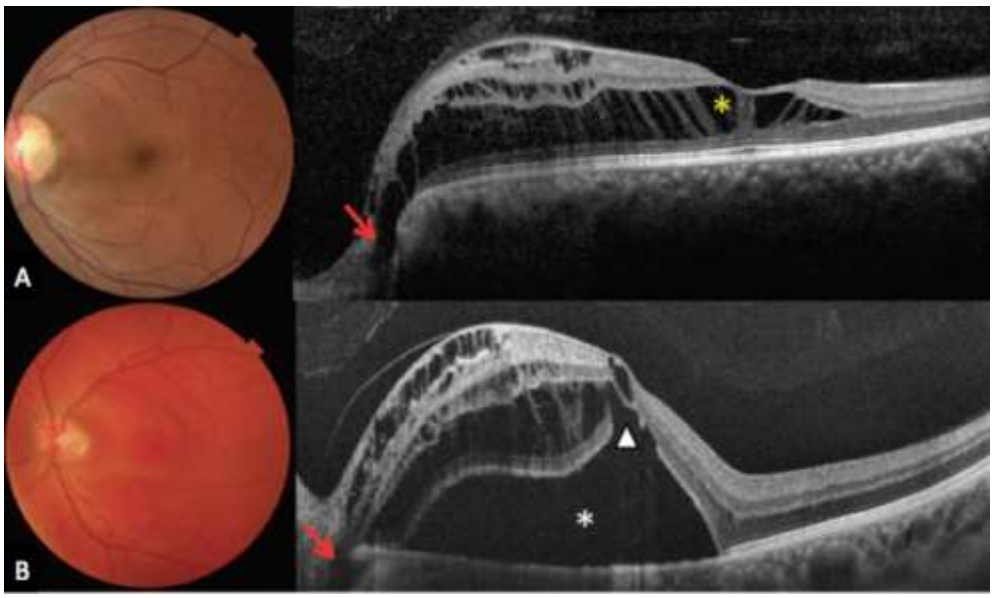

Figure 4-2: Examples of 2 eyes with ODP-M: (A): multi-layer IRF accumulation primarily in HFL (yellow asterisk), as well as the INL, GCL and sub-ILM; (B): multi-layer IRF and SRF (white asterisk) accumulation, with OLH (white arrowhead). Red arrows denote location of ODP

4.1.1 Pathogenesis

The embryological basis of ODP formation is not fully understood, but thought to be related to defects in the migration and differentiation of mesodermal elements into the lamina cribrosa during oculogenesis (96,499). ODPs are sometimes termed ‘atypical colobomas’ and were described by Gass as “failed complete resolution of the peripapillary neuroectodermal folds during development of the primordial optic nerve papilla” (515). Histologically, herniation of dysplastic neuroectodermal (retinal) tissue, surrounded by a connective tissue capsule, is observed through the lamina cribrosa, towards the subarachnoid space (SAS) (Figure 4-3C) (515–517). Nerve axons may traverse the anterior aspect of the pit, and frequently a

diaphanous, translucent glial membrane is noted to overlie the pit, which is closely associated with strands of condensed vitreous (517–521). OCT and histological studies have demonstrated the presence of holes within this diaphanous membrane, which are thought to allow the passage of fluid into the retina, resulting in maculopathy (Figure 4-3A,B,D) (517,522–526). The precise source of the IRF and SRF in ODP-M remains controversial and no single unifying theory has been proven beyond doubt.

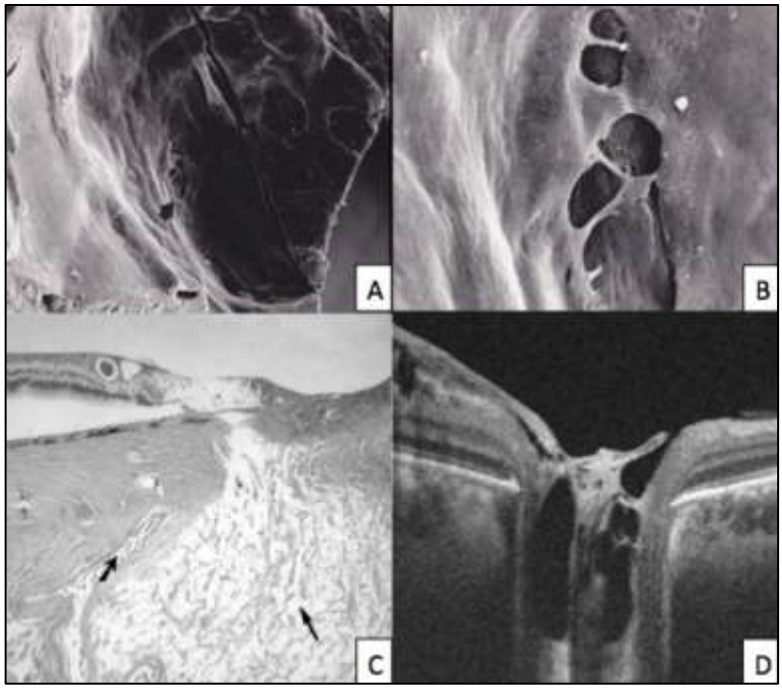

Figure 4-3: ODP morphology; (A&B): scanning electron microscopy of ODP, demonstrating defects in the overlying diaphanous membrane; (C): Histological cross section through ODP, showing herniation of dysplastic retina (long arrow) separated from the SAS by a dural connective tissue sheath (short arrow); (D): OCT of the optic nerve head demonstrating multiple pits and overlying membrane. Credit: (A&B): Christoforidis et al (2012), Clinical Ophthalmology 2012:6 1169-1174 (517) [originally published by and used with permission from Dove Medical Press Ltd]

Sugar first postulated that maculopathy might arise due to the passage of liquefied vitreous via the optic pit to the subretinal space (SRS) (Figure 4-4) (502,527). Ferry demonstrated the presence of vitreous mucopolysaccharides within the pit in 1963

(516), while Brown et al reported that India ink injected into the vitreous of collie dogs was seen to migrate into the SRS (528). These findings, alongside various case reports describing the migration of intra-ocular silicone oil, heavy liquid or gas into the intraretinal space (IRS) or SRS in various congenital optic nerve head disorders, or successful drainage of fluid through the membranous defect over the pit, support the theory of a vitreous source for ODP-M (520,525,529–532).

Figure 4-4: A proposed mechanism of ODP-M formation; vitreous traction on the diaphanous membrane creates a hole, though which liquefied vitreous passes into through the ODP and into the SRS. Credit: Bonnet (1991) (525) [image reproduced with permission of the rights holder, Springer Nature]

An alternative fluid source theory implicates the migration of cerebrospinal fluid (CSF) from the SAS around the optic nerve (533–535). Using histological specimens, Gass demonstrated the protrusion of a multi-loculated pit into the distended SAS, which was separated from the SRS by multiple thin, bridging septae (515). Unable to visualise a direct communication between the vitreous and the SRS, he concluded that a route from the SAS and the SRS seemed a more plausible aetiology. Indeed, some imaging and surgical reports have endorsed the possibility of a direct connection between these spaces in congenital disc anomalies (533,534,536–539). However, other histological and OCT studies, that also noted this proximity between the pit and the SA space, have reported the meningeal sheath to be intact, refuting the notion of a direct communication between vitreous and CSF (516,517,540,541).

A third fluid origin that has been postulated relates to vascular abnormalities around the pit causing leakage into the SRS (542,543), but this theory is currently afforded little weight, considering lack of angiographic permeability observed in the majority of patients (501).

Regardless of the source of the fluid, the exact mechanism by which the fluid migrates into the IRS and SRS is also subject to debate. In most cases, the development of maculopathy has been reported in young adults, usually presenting in the 3rd or 4th decade of life, around the age that vitreous liquefaction begins (513). It is therefore conceivable that vitreous syneresis and epipapillary traction play a role, initiating the development of the defect in the diaphanous membrane over the cavity and allowing passage of fluid from the vitreous into the retina (517,518,520). Indeed, many of those with observed ODP-M did not have evidence of complete vitreous separation (501), while spontaneous resolution of ODP-M has been noted after PVD (525,544). Furthermore, treatment of ODP-M with either PPV and induction of PVD or macular buckling has been shown to lead to resolution of ODP-M, supporting a role for vitreous traction (545–552). There are several OCT and surgical reports witnessing vitreous strands adherent to the ODP margin (522,540,553,554), which have even been demonstrated to have a seemingly dynamic tractional effect on the pit (523,555,556).

It ought to be noted, however, that this pathomorphology is not universally observed, and vitrectomy with induction of PVD alone does not always appear to definitively resolve the maculopathy (522,547,557,558). This mechanistic theory is also somewhat confounded by the observation that maculopathy may occur in young children, long before vitreous syneresis is observed (504,509,511,514,547,559). Some studies suggest that this precocious behaviour of ODPs in children could be related to blunt trauma causing transient, excessive, peripapillary vitreous traction in this demographic (509,510). Due to the strong vitreous adhesion in children, induction of PVD is more difficult, somewhat incentivising observation over early surgical intervention (560). There are several reports of childhood ODP-M exhibiting spontaneous resolution of ODP-M (504,512–

514,559,561,562), which may indicate that presentation in this age group is attributable to a separate pathomechanical process, perhaps with a distinct natural course.

Jain and Johnson attempted to provide a unifying theory for the pathophysiology of ODP-M by proposing the role of dynamic pressure gradients across the communicating spaces (563). They suggest that fluctuations of the translaminar pressure gradient between the SAS and the intraocular space, due to positional and exertional variations, could account for the migration of fluid. This could be a result either of a direct communication between the SAS and the pit, or, if the pit is separated by a connective tissue capsule, it could act as a 'bulb-syringe', drawing fluid from the vitreous body when the translaminar pressure gradient falls and then regurgitating it into the IRS as the gradient rises again. In this way, continuous aliquots of fluid could be forced into the retina, giving rise to ODP-M (Figure 4-5). Theoretically, this would account for the presence of either, or both, vitreous and CSF within the retinal spaces (563). This notion of a translaminar pressure differential is supported by the described phenomenon of intraocular vitreous debris being sucked into the pit and expelled again with changes in IOP, as well as the observed migration of intraocular oil into the SAS (523,534,564). It might even be argued that the aforementioned observations of adherent vitreous strands at the ODP margin could be explained as vitreous incarceration from the pressure differential.

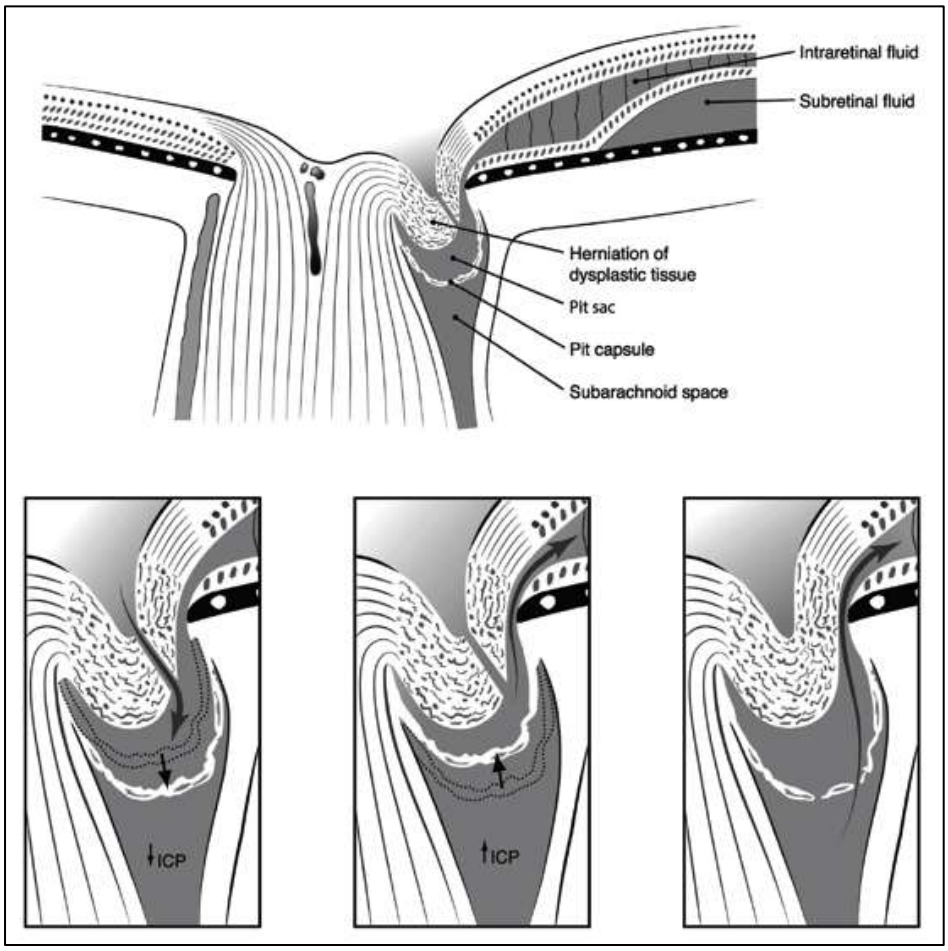

Figure 4-5: A proposed mechanism for ODP-M formation; (bottom left): vitreous fluid is 'sucked' into the pit during a drop in intracranial pressure (ICP); (bottom middle): During rise in ICP, the fluid is expelled from the pit and into the retina; (bottom right): if there are defects in the capsule, it is conceivable that CSF could pass directly into the retina. Credit: Jain and Johnson (2014) (563) [images reproduced with permission of the rights holder, Elsevier]

In fact, it is likely that a combination of many factors contribute to the variable observed features and fluid trajectories in ODP-M. A 'multiple mechanism' theory is supported by advanced OCT imaging studies of pit, which appears to demonstrate a variety of morphologies, with various connections observed between the vitreous cavity, the retina and the SAS (538,565).

4.1.2 Differential diagnoses

It is worth noting that several other developmental optic disc anomalies can predispose to the formation of macular retinoschisis and ought to be distinguished from ODP-M. These include optic disc coloboma, morning glory syndrome (MGS) and tilted disc syndrome (531,533,566–570). These conditions share similarities with the pathoanatomy of ODPs, albeit a result of distinct developmental defects. In the case of coloboma, there is a chorioretinal and/or scleral defect due to incomplete closure of the embryonic optic fissure, into which the thinned and atrophic retina extends, forming an intercalary membrane (571). Breaks in this membrane can manifest in schisis or neurosensory detachment (Figure 4-6A) (554,567,572,573). MGS is a less well-understood developmental disorder, characterised by an enlarged funnel-shaped excavation of peripapillary sclera, central herniation of neural tissue and abnormal radial vascular patterning. In this case, the poorly differentiated papillary tissue frequently allows continuity between the excavation margin and both the SAS and SRS (Figure 4-6B) (569,574–576).

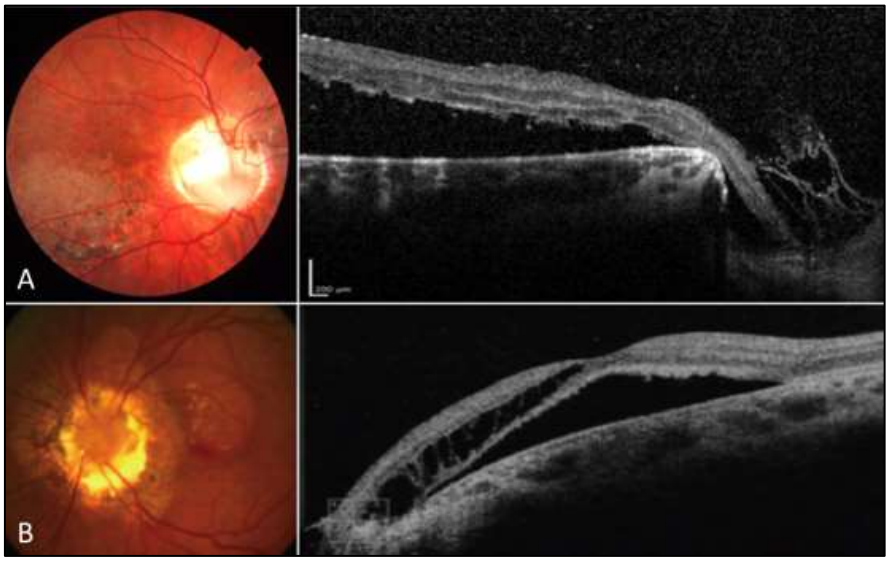

Figure 4-6: (A): Neurosensory detachment associated with optic nerve coloboma; (B): foveoschisis and detachment associated with morning glory syndrome. Credit: (B) Cañete-Campos et al (2011) (566) [images reproduced with permission of the rights holder, Elsevier]

Another form of acquired retinoschisis that has been described is glaucoma-associated retinoschisis (GAR), which is characterised by peripapillary or macular schisis in the context of neuroretinal tissue loss (577–582). Studies report the presence of fluctuating peripapillary retinoschisis (PPRS) in around 6% of subjects with primary open angle glaucoma, which was confined to the RNFL and GCL in the majority cases, but occasionally also involved HFL.

The underlying mechanism of GAR remains unresolved. A potential mechanical basis, as a result of posterior displacement of the lamina cribrosa, opposed by anterior traction at the vitreo-papillary interface, has been proposed, although significant evidence of vitreous traction has not been demonstrated (578,579,583,584). Another theory relates to the presence of structural defects in the lamina cribrosa, such as so-called 'occult' or acquired disc pits and laminar disinsertions, which may be revealed following peripapillary RNFL loss and may predispose to the development of GAR through intraretinal ingress of liquefied vitreous (Figure 4-7) (579,585–592).

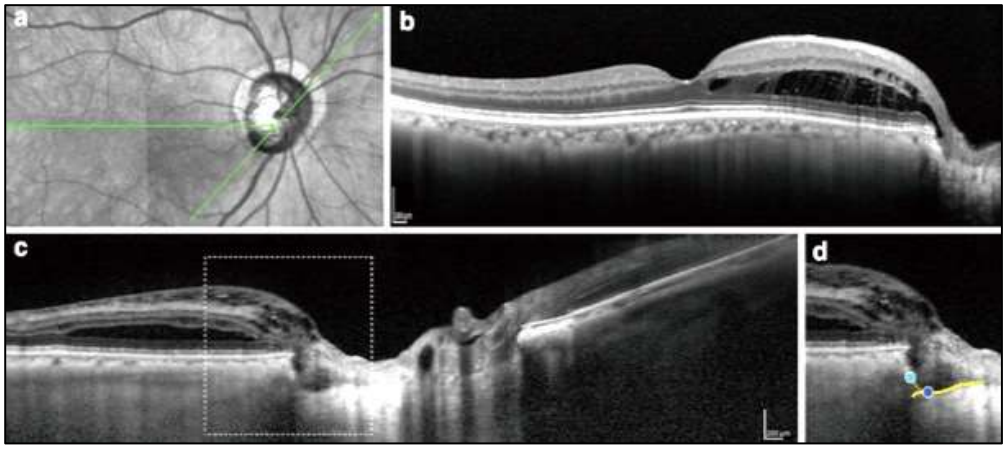

Figure 4-7: (a): Near-infrared (NIR) and (b-d) OCT in PPRS; (b): maculoschisis involving HFL and INL, continuous with optic nerve; (c): multi-layer schisis inferiorly; (d): posteriorly displaced disinsertion of lamina cribrosa (yellow line/dark blue circle) from expected location (light blue circle). Credit: Yoshitake et al (2014) (589) [images reproduced with permission of the rights holder, Springer Nature]

Several reports have indicated that such cases of macular retinoschisis may either spontaneously resolve or improve following vitrectomy with ILM peeling and/or gas tamponade, if persistent (580,593–599). Proteomic analysis of the macular fluid associated with GAR has confirmed the presence of vitreous as the source of the retinal fluid in one case (600).

Reports have also indicated that the presence of PPRS and serous detachment may be associated with IOP fluctuations, even in the absence of significant glaucomatous optic neuropathy (583,594,598,601,602). One proposed mechanism is that sustained increases in IOP may cause development of 'micro-holes' in the peripapillary ILM, allowing penetration of liquefied vitreous into the peri- and retrolaminar spaces (578,598,601,603). Indeed, several case reports have demonstrated resolution of schisis following filtration surgery (598,602).

GAR is an important differential in cases of suspected ODP-M and other acquired forms of FRS. In fact, two conditions may even be superimposed, wherein the presence of ODP-M on a background of glaucoma can give rise to an appearance of irreversible visual field progression, which may actually be amenable to intervention and visual recovery (604–606).

Finally, another similar and recently described condition, which may manifest as peripapillary retinoschisis, is peripapillary pachychoroid syndrome (PPS), a subgroup within the novel pachychoroid disease spectrum. This disorder is characterised by a thickened nasal macular choroid with dilated vessels in Haller's layer, optic disc crowding and juxtapapillary intra- or subretinal fluid accumulation (607). One postulated mechanism for PPS is that peripapillary choroidal congestion may lead to increased hydrostatic pressure in the choroidopial venous system, causing compartment syndrome-like optic nerve compression. This in turn may cause RPE dysfunction, optic nerve swelling and peripapillary fluid accumulation (Figure 4-8) (607). This concept is supported by the observation that the intraretinal cysts may fluctuate with changes in both central venous and intraocular pressure (608,609).

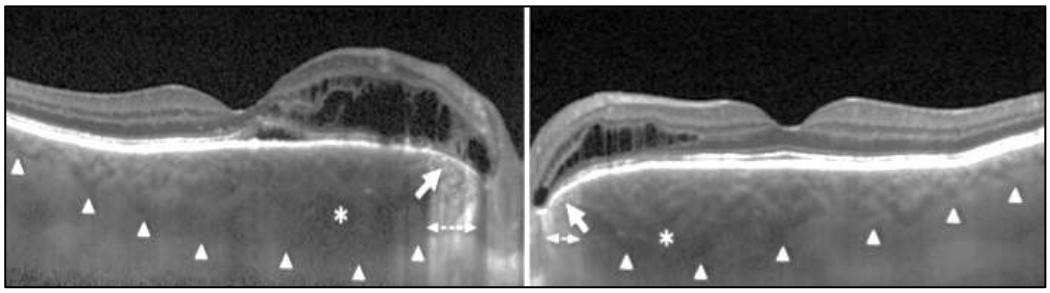

Figure 4-8: Peripapillary pachychoroid syndrome: IRF and SRF accumulation in association with outer retina atrophy (solid arrows), nasal macular choroidal thickening (arrowheads) and dilated large choroidal vessels (asterisks). Credit: Phasukkijwatana et al (2018) (607) [images reproduced with permission of the rights holder, LWW]

4.1.3 Natural history

Until recently, the understanding of the natural history of ODP-M has been based predominantly on the work of Brown et al in the 1970s-80s, as well as the findings of Sobol et al and Theodossiadis et al in the 1990s (501,505,506,610–613). Brown et al followed up 20 cases of untreated ODP-M, over a mean period of 4.5 years, demonstrating a mean decline in logMAR VA from 0.48 to 0.60. At the final review, 55% of cases had a VA ≥0.70 (501). Sobol et al and Theodossiadis et al reported smaller cohorts, but with worse visual outcomes, ranging from mean VA of 1.16 to 1.33 (505,506). Table 4-1 details the largest natural history studies of ODP-M to date. In the majority of cases, the functional prognosis for ODP-M was shown to be poor, with a mean reported final visual outcome of 0.72 logMAR (497,501,504–506). This evidence has supported the widespread belief that, in the absence of surgical intervention, the visual prognosis for ODP-M is generally unfavourable.

Table 4-1: Summary of previous ODP-M natural history studies

Authors	Year	n	Baseline VA (logMAR)	Final VA (logMAR)	Change in VA (logMAR)	Mean follow-up (years)
Sugar	1967	10	0.46	0.35	-0.09	3.9
Brown et al	1980	20	0.48	0.60	0.12	4.5
Sobol et al	1990	15	0.43	1.16	0.68	8.3
Theodossiadis et al	1992	8[§]	1.09	1.33	0.24	9.0
Steel et al	2018	43	0.49	0.55	0.06	1.0
AVERAGE			**0.54**	**0.72**	**0.17**	**5.5**
[§]8 previously untreated patients from 16 total in study						

More recently, in a 2018 prospective population-based study, Steel et al collected observations for 43 cases followed for 1 year, noting a small decline in VA, from a mean baseline of 0.49 to a final acuity of 0.55 (497). After 1 year of follow-up, 81% of eyes enrolled in the study remained anatomically stable or improved, albeit the presence of SRF at baseline appeared to convey a higher risk both anatomical and functional decline. Moreover, those in whom surgery was deferred achieved a similar gain in vision to those receiving prompt intervention, implying that an initial period of observation may be a reasonable approach in this patient group. This evidence challenges the existing paradigm that ODP-M always carries a predictable and poor prognosis (497).

In terms of anatomical natural history, Lincoff et al first described a schisis-like appearance in cases with ODP in 1988, postulating that maculopathy was initiated via ingress of fluid into the inner retina at a point of continuity with the pit, which could subsequently spread to the outer retina, resulting in development of OLH and/or neurosensory detachment (see Figure 4-2B) (3). This assessment appears to have been remarkably accurate, according to further characterisation of ODP-M using OCT, which support this concept of a 'bilaminar structure', in which macular detachment develops secondary to a pre-existing overlying schisis, usually observed in HFL (see Figure 4-2A) (519,522,536,614–619).

There exists some controversy as to whether the presence of OLH is a pre-requisite for progression from IRF to SRF accumulation in ODP-M, or whether fluid can 'percolate' between compartments, without a direct communication (4,620). Roy et al reported that all studied cases of ODP-M had outer layer retinoschisis (OLR), 91% of which had additional SRF; of these 69% had an OLH (507). They proposed that the most likely mechanism was that the OLR formed initially, from where fluid 'seeped' bidirectionally into both the inner retinal layers (ILR) and SRS, obviating the need for a direct communication.

To date, the most comprehensive investigations into the anatomical variants and the structure-function relationship have been undertaken by Steel et al (497,508). Using similar terminology for fluid layer classification to Roy et al, Steel et al reported retrospectively on 36 patients with ODP-M in 2016, alongside 98 cases from the literature, and prospectively on 68 patients in 2018 (497,508). Retrospectively, it was noted that between 77-95% of reported cases had SRF with OLR and/or ILR, while only 5-22% had IRF only. As with Roy et al, no cases were found to have SRF in isolation and, in this study, OLH was only seen in 50% of cases. It was also noted that the combination of SRF and multi-layered retinoschisis (MLR) was associated with a worse VA at baseline.

Prospectively, however, only 43 (61%) of cases had SRF compared to 27 (39%) with IRF alone. Again, no cases demonstrated SRF in isolation. Cases with SRF at baseline were reported to have a higher likelihood of progression than IRF only (27% vs 9%), and a lower rate of spontaneous improvement (7% vs 30%). Over 1-year's follow-up of 53 cases, 43 (81%) improved or remained stable anatomically, including 21/30 (70%) of those with SRF at presentation. While change in mean VA during the study period was negligible, those with SRF at baseline had significantly worse VA than those with IRF only (0.69 vs 0.33 logMAR). This led to the suggestion that patients without SRF retain good vision and may be observed, while the structure and function of those eyes with SRF rarely improved without surgery.

The findings of some of the largest observational OCT-based studies of ODP-M to date are summarised in Table 4-2 (4,497,507,508,538). Overall, the most common

fluid configuration identified was MLR+SRF (42%), followed by IRF only (29%) and OLR+SRF (24%). Collectively, 71% demonstrated presence of SRF, while cases involving either ILR+SRF or SRF only were uncommon (5%). A recent meta-analysis by Meng et al, the pooled incidence for each fluid distribution was: SRF only in 10%, IRF only in 14% and a combination of the two in 69% (465). The pooled incidence of OLH was 53%; notably the measures of heterogeneity were high in all cases.

Table 4-2: Distribution of fluid accumulation in ODP-M

Authors	Year	n	IRF only	OLR+SRS	ILR+SRS	MLR+SRS	SRS only
Imamura et al	2010	16	5 (31%)	1 (6%)	0	9 (56%)	1 (6%)
Roy et al	2013	32	3 (9%)	12 (38%)	0	17 (53%)	0
Michalewski et al	2014	20	8 (40%)	3 (15%)	0	9 (45%)	0
Steel et al	2016	36	8 (22%)	16 (44%)	0	12 (33%)	0
Steel et al	2018	70	27 (39%)	9 (13%)	3 (4%)	26 (37%)	5 (7%)
TOTAL		**174**	**51 (29%)**	**41 (24%)**	**3 (2%)**	**73 (42%)**	**6 (3%)**

Since OLR is present in up to 89-95% of cases, it follows that this is most commonly the primary affected layer, as previously suggested (3,507,618,621). It is well reported, however, that macular detachment may occur in the absence of antecedent retinal schisis, presumably due to direct communication between the pit and the SRS (519,558,620,622).

Given the apparent lack of clarity concerning the variability in both anatomical and functional natural history in ODP-M, it remains challenging to discern the relative merit or ideal timing of intervention in these cases.

4.1.4 Therapeutic approaches

Besides the dilemma of *when* to operate, the optimal intervention itself also remains controversial. Various studies have proposed a role for juxtapapillary laser (JPL), with the intention of creating a chorioretinal scar as a barrier for fluid ingress into the

retina (515,526,613,623–625,525). In isolation, this approach has only partial success and frequent recurrence has been observed, probably due to the co-existence of serous detachment, which limits retina-RPE adhesion (3,525,526). Intravitreal gas injection, on its own or in combination with JPL has also been successful in some cases (626–628). Theodossiadis et al have reported several cases of macular bucking with a sponge explant, demonstrating success rates of up to 85% (551,552,629–632). However, this approach is technically more difficult and may be prone to higher rates of complication and delayed macular atrophy.

Today, PPV, with removal of the posterior hyaloid, is the mainstay of treatment for ODP-M. The rationale is centred on the assumption that there is a tractional element to the pathogenesis of ODP-M, but this approach also affords the opportunity for adjunctive therapy, such as JPL, ILM peeling and gas tamponade. Good anatomical outcomes, ranging from 45-92%, have been reported using 23- or 25-gauge vitrectomy with or without various combinations of the above approaches (491,494,540–544,627–636). In a multicentre series of 51 cases, Avci et al reported that, by median 5 months' follow-up, 44 (86%) patients achieved complete resolution of serous macula detachment with a gain of ≥0.30 logMAR seen in 84% and a final VA ≤0.30 in 61%. They reported 12% rate of intraoperative complication, with 14% requiring additional surgery (640). The role of newer techniques, such as epipapillary membrane peeling, removal of fibroglial tissue from the pit, inner retinal fenestration and radial optic neurotomy, remains to be seen (643–645). Approaches to cover or 'stuff' the pit, with ILM, autologous platelets or fibrin glue have also shown promising early results (456,646–653).

It should be noted that the rate of surgical failure and re-operation is not insignificant in the management of ODP-M, and many studies also report a protracted period of up to 2 years for complete resorption of SRF (547,548,557,614,620,635,638,644,654).

In summary, ODP-M is an uncommon disorder and robust evidence as to its natural history and precise anatomico-functional behaviour is in short supply. There is neither general consensus on the precise pathophysiological mechanisms, nor are

there any prospective trials to definitively guide treatment. There is, however, a growing understanding of a latent period in the disease, during which patients can retain excellent visual function, in the presence of marked FRS. With an estimated annual incidence of 1-2 per million in the UK, ODP-M is a rare disorder and therefore challenging to study (497); less than a third of cases have IRF only at presentation. As such, understanding of the precise anatomico-functional natural history remains largely unresolved.

In this chapter, I investigate the demographic, structural and functional characteristics of a large cohort of patients, to explore the natural history and anatomico-functional correlations of FRS in ODP-M.

4.2 Methods

A single-centre, retrospective, observational study was performed by review of electronic records of patients who presented at a tertiary ophthalmic hospital trust with new or existing ODP and ODP-M between January 2001 and January 2020.

Patients were included for whom VA at initial presentation, fundus imaging and demographic data were available. In this study, ODP-M was defined as any serous detachment or splitting of the macular retina in the presence of an ODP, with absence of alternative explanatory aetiology. Data were not included from those with history of laser or surgical treatment for ODP-M prior to presentation or other concurrent ocular pathology affecting vision.

Demographic data were compiled, including age, sex and, where specified, ethnicity., In the event of bilaterality, one eye was selected (using a random number generator) and the fellow eye was removed from the final analysis. Considering the low chance of bilateral ODP-M (and therefore data loss), this approach was considered appropriate in order to minimise potential confounding or statistical error due to within-patient inter-eye correlation. ODP characterisation, including pit number, size

and location, was performed using *en face* fundus images (e.g. colour photograph or near-infrared reflectance image) from the Topcon 3D OCT-1000 or Heidelberg Spectralis sd-OCT. Further qualitative OCT data collected included the presence of IRF, SRF +/- OLH (OLH is defined as a partial thickness disruption of the outer retina, including the ELM). The quantitative OCT data gathered comprised CRT, AvRT, CSH and SA, as defined in 2.3.6.1 and 2.3.6.2, using Topcon OCT only.

Data analysis for this study is divided into 3 phases: Phase 1 consists of an analysis of all patients with ODP-M to explore baseline demographic, functional characteristics and ODP physiognomy; Phase 2 examines further morphological sub-categorisation and comparison is undertaken in those with available OCT data; Phase 3 explores longitudinal changes, including a comparison of the quantitative functional and anatomical changes over time, in patients with centre-involving FRS with data over ≥12 months or until the point of progression.

4.3 Results

4.3.1 Phase 1: Baseline characteristics of all patients with ODP-M

A total of 312 patients were identified with a diagnosis of ODP, of whom, 119 patients (38%) had a recorded diagnosis of maculopathy. Of these cases with ODP-M, 87 (73%) patients were included in the final analysis (the remaining 32 did not have complete available baseline functional and anatomical data). The patient and pit characteristics for this cohort are summarised in Table 4-3. No demographic or pit features showed any association with baseline acuity on univariate analysis.

Table 4-3: Summary of baseline characteristics of all patients with ODP-M

Characteristic	**n=87 eyes**
Baseline age (mean years ± SD)	35.1 ±18.2
Sex	55 (63%) female
Ethnicity	
White	45 (68%)
Asian	10 (11%)
Black	4 (5%)
Other	7 (8%)
Not-specified	21 (24%)
Affected eye(s)	
Right	33 (38%)
Left	54 (62%)
Baseline logMAR VA (mean / median)	0.38 / 0.30
Optic disc characteristics	**n=89 pits**
Number of pits/optic disc	
One	85 (98%)
Two	2 (2%)
Location of pit	
Temporal	56 (63%)
Infero-temporal	20 (22%)
Inferior	5 (6%)
Infero-nasal	2 (2%)
Nasal	1 (1%)
Supero-temporal	2 (2%)
Central	3 (3%)
Pit size (disc diameter)	0.31 ±0.14
Presence of cilioretinal artery	
Yes	16 (18%)
No	72 (82%)

4.3.2 Phase 2: Morphological categorisation of patients with ODP-M

Of those 87 patients in phase 1, 50 (57%) had available Topcon 3D OCT imaging at baseline. From this cohort, the anatomical configuration of ODP-M was classified into three novel subtypes, based on observed OCT characteristics at baseline visit. 'Type 1a' ODP-M describes those with IRF only (Figure 4-9A). 'Type 1b' refers to those with IRF and an OLH +/- SRF (Figure 4-9B). At baseline, types 1a and 1b affected 17 (34%) and 14 (28%) of eyes respectively.

'Type 2' ODP-M comprised those with SRF (i.e. macular detachment) at presentation, with or without superjacent IRF, but an absence of OLH (Figure 4-9C). This configuration was observable in 19 eyes (38%). The baseline demographic and functional characteristics are summarised according to the above morphological subtypes in Table 4-4, wherein 35 healthy fellow eyes are also included for comparison.

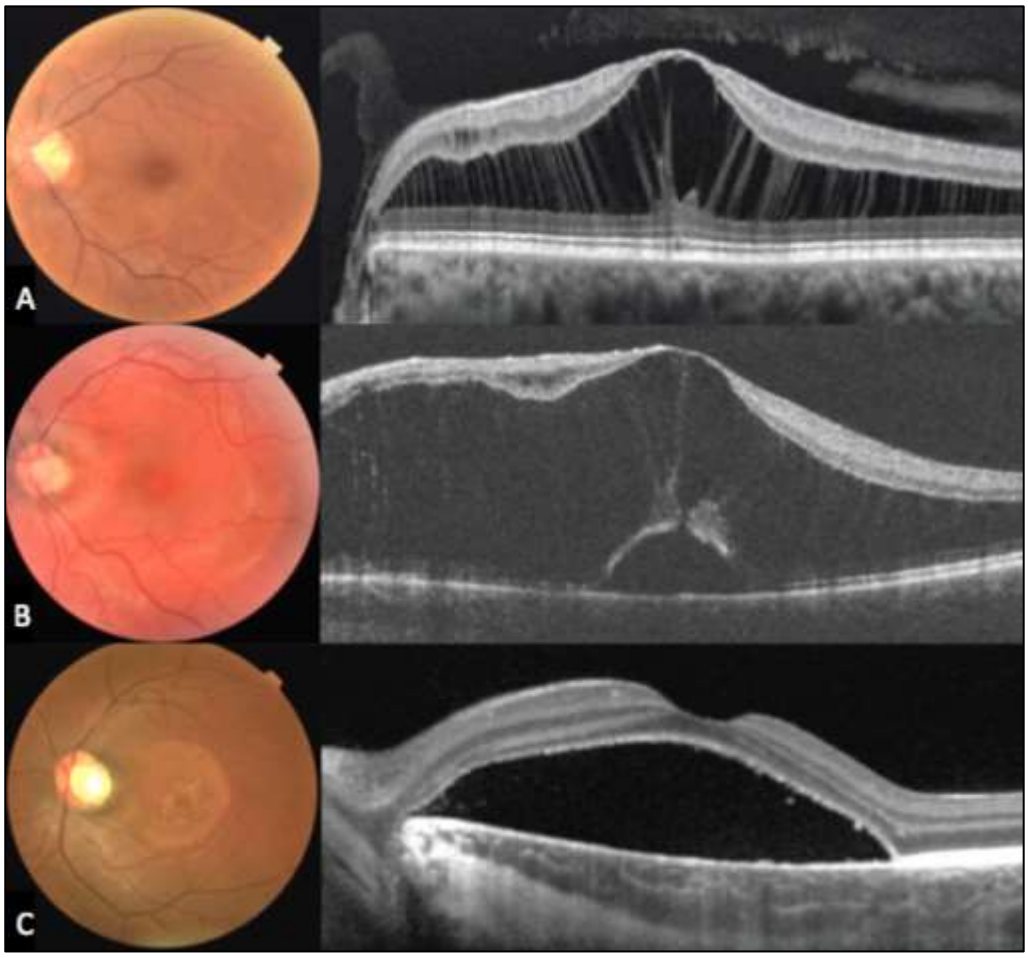

Figure 4-9: Examples of proposed subtypes of ODP-M: (A) 'type 1a' ODP-M, characterised by FRS without OLH or SRF; (B): 'type 1b' ODP-M, characterised by FRS with OLH +/- SRF; (C) 'type 2' ODP-M, characterised by SRF without OLH

Table 4-4: Comparison of baseline characteristics between ODP-M morphological subtypes and healthy fellow eyes

Characteristic (n/mean ±SD)	Type 1a	Type 1b	Type 2	Healthy fellow eyes
Number	17 (34%)	14 (28%)	19 (38%)	35
Baseline age (years)	39 ±13	35 ±10	19 ±14	33 ±13
Female sex	9 (53%)	7 (50%)	13 (68%)	18 (51%)
Right eye	7 (41%)	3 (21%)	7 (37%)	25 (71%)
Baseline VA (logMAR)	0.20 ±0.24	0.71 ±0.39	0.39 ±0.32	-0.04 ±0.05

Linear regression analysis revealed no overall association between age and VA at baseline, but there was a significant difference in the age at presentation between the types of ODP-M on ANOVA ($p<0.001$) (Figure 4-10). The mean (median) age in both types 1a and 1b was 39 (39) and 35 (34) years respectively, compared to 19 (14) years in type 2 ODP-M (both $p\leq0.002$ on pairwise analyses). There was no significant difference in age between types 1a and 1b ($p=0.246$).

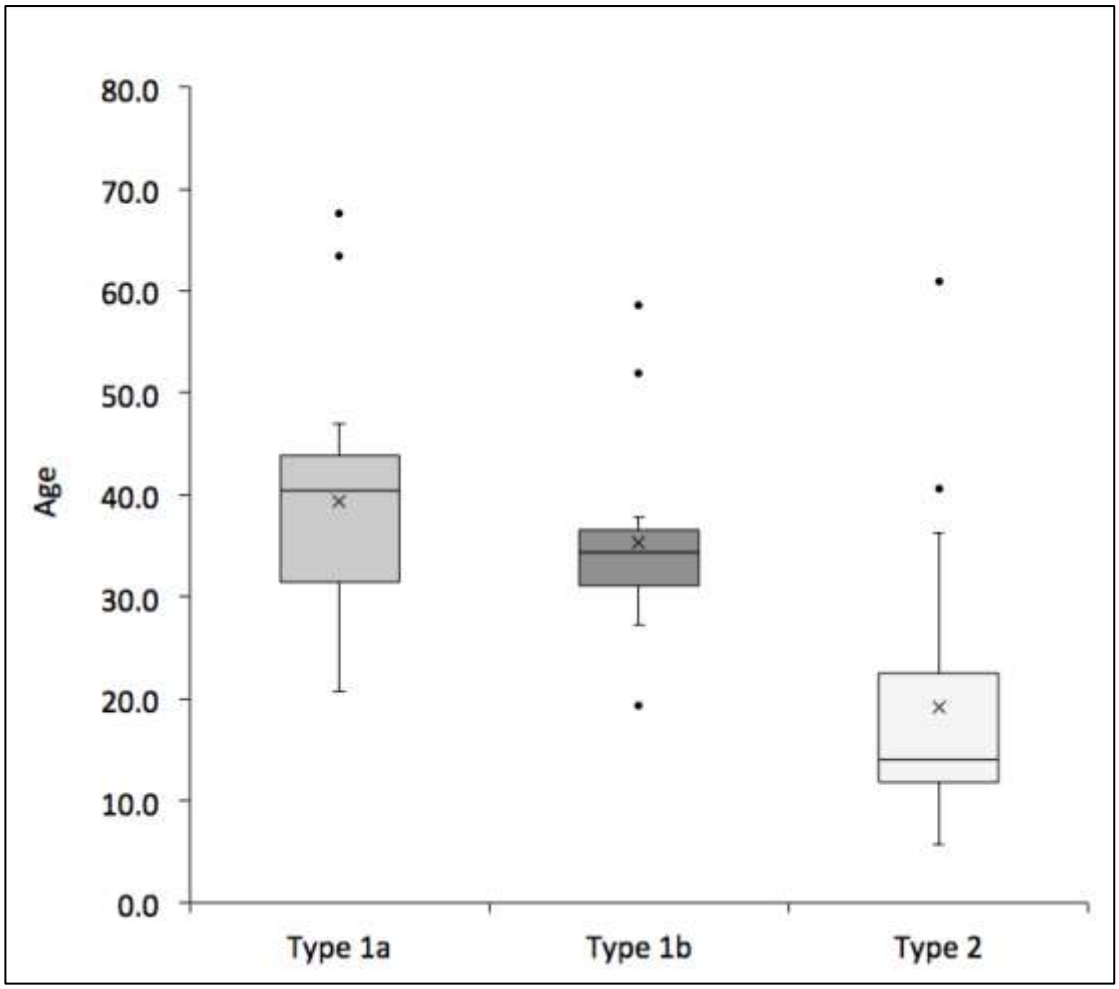

Figure 4-10: Comparison of baseline age between types 1a, 1b and 2 ODP-M

The overall mean (±SD) baseline VA in this cohort was 0.42 (±0.37). On ANOVA there was a significant between-group difference in baseline VA ($p<0.001$), with type 1b demonstrating significantly worse VA than both type 1a ($p<0.001$) and type 2 ODP-M ($p=0.023$) on subgroup analysis. Type 1a and 2 were non-significantly different

(p=0.217); all subtypes demonstrated significantly worse VA than the healthy fellow eyes (p<0.001) (Figure 4-11).

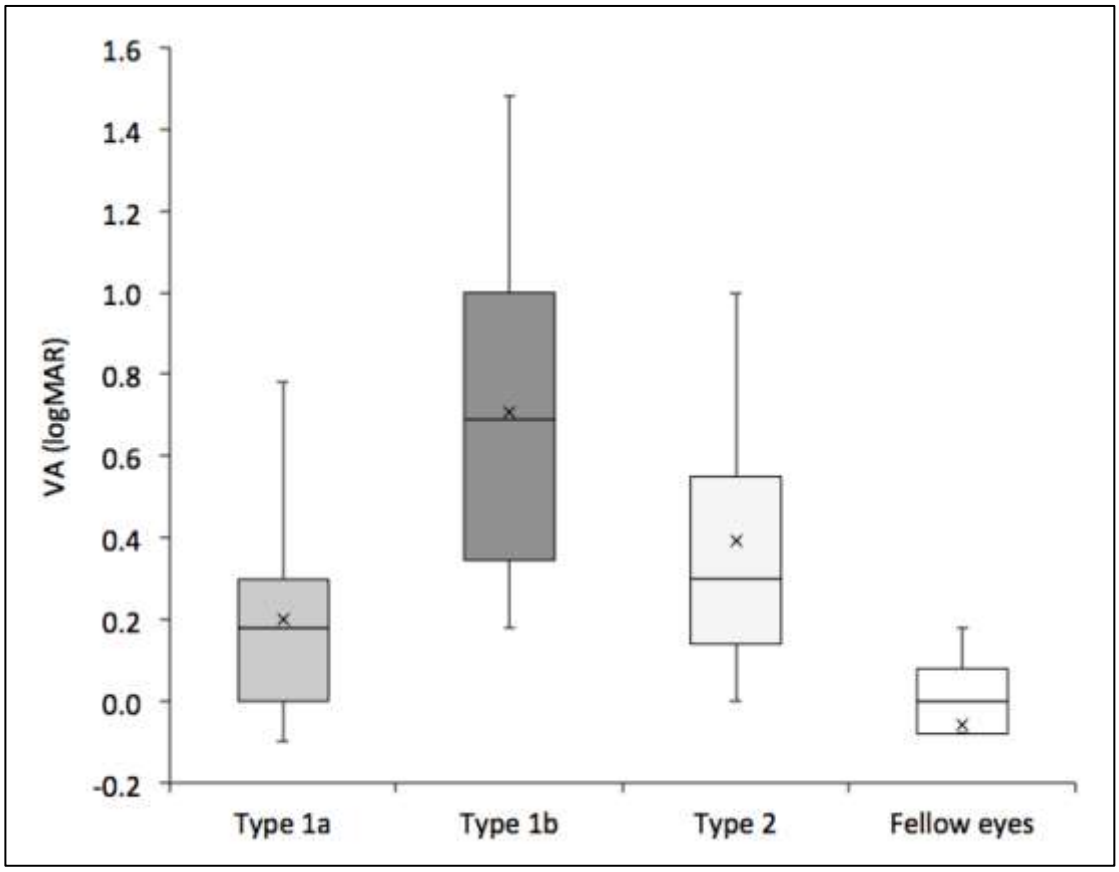

Figure 4-11: Comparison of baseline VA between types 1a, 1b, 2 ODP-M and healthy fellow eyes

Morphological comparison of retinal layers involved was undertaken, according to the classification system devised by Roy et al (see Table 4-2). These data are displayed in Table 4-5. Overall, 80% demonstrated a morphology including the presence of OLR, while those with either IRF only or SRF made up 34% and 14% respectively. A significant association was found between worse VA and the presence of either OLH or SRF (p<0.001 and p=0.002 respectively), but not IRF (p=0.921), on simple linear regression. However, only OLH survived multivariate regression analysis with Bonferroni correction, indicating an independent association with poorer visual function (p=0.008, β=0.312).

Table 4-5: Distribution of fluid accumulation in ODP-M

Group	OLR only	MLR only	OLR+SRF	ILR+SRF	MLR+SRF	SRF only
Type 1a	4	13	-	-	-	-
Type 1b	-	-	6	0	8	0
Type 2	-	-	7	3	2	7
All eyes (%)	4 (8%)	13 (26%)	13 (26%)	3 (6%)	10 (20%)	7 (14%)

A further sub-comparison of the functional and quantitative anatomical characteristics between eyes with types 1a and 1b ODP-M, alongside 28 healthy fellow eyes, was undertaken (Table 4-6). Although all OCT measurements were greater in those eyes with type 1b than 1a ODP-M, statistical significance was only reached on between-group comparison for AvRT (p=0.021) (Table 4-6; Figure 4-12).

On within-group analysis of type 1a ODP-M, there was a significant negative correlation between VA and CRT, AvRT, CSH (all $p \leq 0.01$, $\beta < 0.002$) and SA ($p=0.009$, $\beta=0.016$), all with relatively small effect sizes. In contrast, VA was not correlated with any of the OCT-derived parameters in the type 1b subgroup.

Table 4-6: Comparison of baseline characteristics of types 1a and 1b ODP-M and healthy fellow eyes

Characteristic (mean ±SD)	Type 1a	Type 1b	*p-value*	Healthy fellow eyes
Number [n(%)]	17 (55%)	14 (45%)		28
Baseline age (years)	39 ±13	35 ±10	*0.246*	37 ±12
Baseline VA (logMAR)	0.20 ±0.24	0.71 ±0.39	***<0.001***	-0.05 ±0.04
Central retinal thickness (µm)	503 ±222	691 ±361	*0.186*	206 ±26
Average retinal thickness (µm)	368 ±85	507 ±176	***0.021***	270 ±14
Central schisis height (µm)	352 ±239	617 ±356	*0.062*	-
Schisis area (mm^2)	13.9 ±8.8	19.7 ±6.6	*0.074*	-

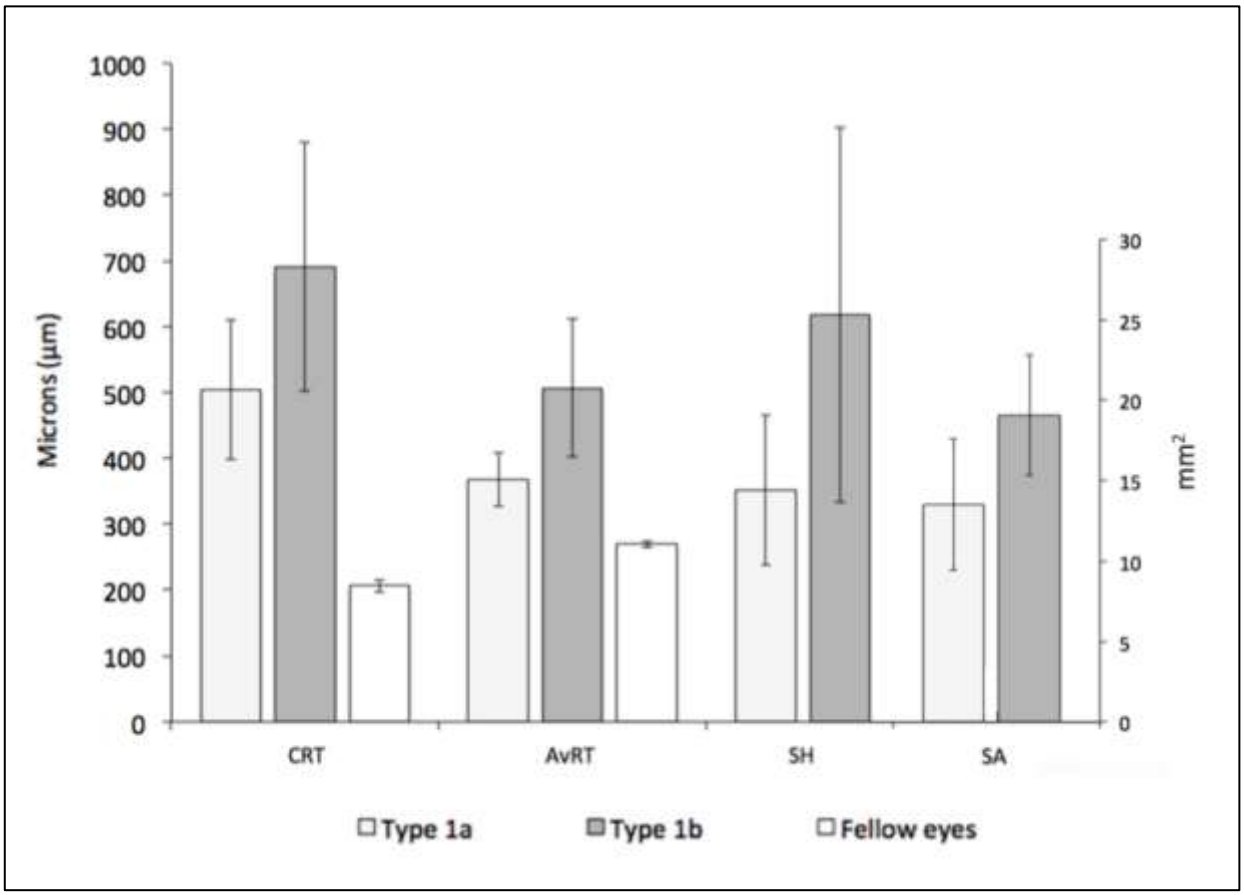

Figure 4-12*: *Comparison of quantitative OCT parameters between types 1a, 1b ODP-M and healthy fellow eyes

4.3.3 Phase 3: Longitudinal analysis

37 eyes were followed up, of which 22 (59%) remained under observation for ≥12 months (mean 3.1 ±2.0 years), while 15 (41%) underwent surgery (comprising PPV +/- adjunctive procedures) following a mean period of 0.9 (±1.6) years. The longitudinal data are summarised, according to baseline ODP-M subtype, in Table 4-7.

Of those eyes that remained under observation, there was a non-significant mean (median) change in VA of -0.03 (-0.10) logMAR (p=0.216), with no significant between-group difference in final VA between ODP-M subtypes (p=0.757). The overall rate of complete resolution in observed eyes was 32% (see Figure 4-13).

4 eyes with type 1a developed a new OLH +/- SRF (i.e. progressed to type 1b) and underwent vitrectomy, in addition to 6 with OLH at baseline. Therefore, a total of 10 eyes with type 1b ODP-M and 5 eyes with type 2 ODP-M morphologies received surgery. A significantly greater proportion of eye with type 1b at baseline underwent surgery, relative to types 1a or 2 ($p=0.012$ on Fisher's exact testing). Moreover, there remained an independent association between worse final VA and the presence of OLH, but not SRF, on multivariate regression analysis ($p=0.016$, $\beta=0.265$).

Following a mean post-operative period of 2.7 (±2.6) years, a final mean (median) VA of 0.42 (0.48) was achieved. This represented a significant improvement in those who underwent surgery ($p=0.008$), but final VA remained significantly worse than that of the observed group ($p<0.001$). The overall rate of complete resolution in operated eyes was 73% (see Figure 4-14F), which was a significantly greater proportion than that of the observed cohort on Fisher's exact testing ($p=0.015$).

This study was not designed to investigate surgical outcomes, so these results serve only to illustrate the comparative anatomico-functional course between observation and intervention in these cases of ODP-M.

Table 4-7: Comparison of anatomical and functional outcomes in observed and operated eyes with ODP-M

Baseline ODP-M morphology	**Type 1a**		**Type 1b**		**Type 2**	
Characteristic [n(%)]/mean ±SD)	**Observation**	**Surgery**	**Observation**	**Surgery**	**Observation**	**Surgery**
Number	11 (73%)	4 (27%)*	1 (13%)	7 (88%)	10 (71%)	4 (29%)
Baseline age (years)	41 ±15	34 ±11	52	36 ±11	16 ±11	27 ±23
Baseline VA	0.12 ±0.17	0.39 ±0.36	0.18	0.77 ±0.30	0.28 ±0.30	0.50 ±0.28
Pre-op VA	-	0.85 ±0.19	-	0.81 ±0.24	-	0.57 ±0.25
Final VA	0.11 ±0.11	0.27 ±0.25	0.18	0.51 ±0.11	0.23 ±0.33	0.42 ±0.29
Duration of f/up (years)	3.2 ±2.3	2.3 ±2.7	3.4	0.3 ±0.3	2.9 ±1.8	0.5 ±0.5
Complete resolution of IRF/SRF	1 (9%)	4 (100%)	1 (100%)	4 (57%)	5 (50%)	3 (75%)

**Eyes with type 1a that developed OLH±SRF (i.e. progressed to type 1b); IRF - intraretinal fluid; SRF - subretinal fluid*

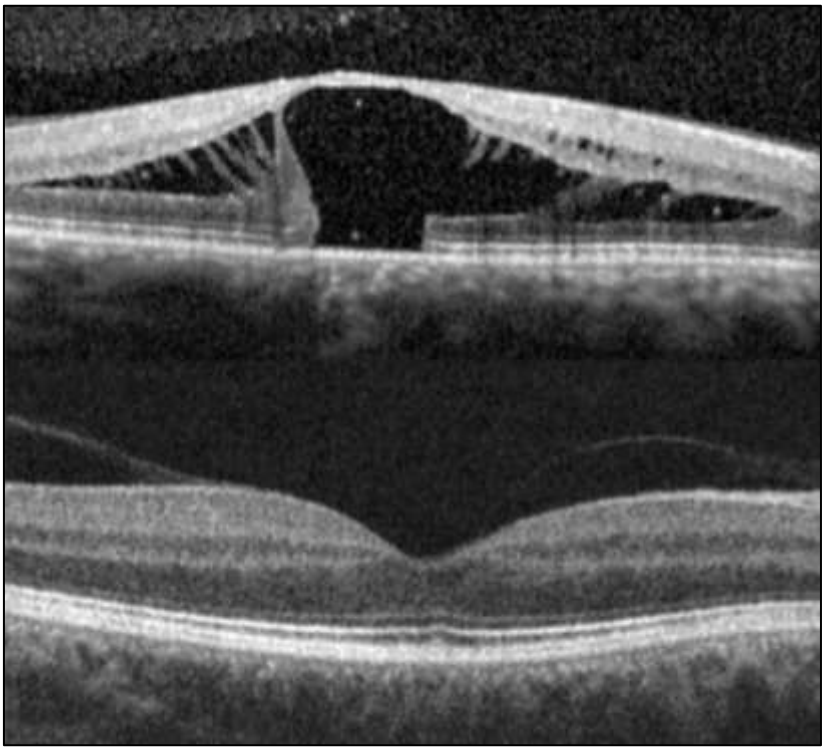

Figure 4-13: Spontaneous resolution of type 1b ODP-M

4.3.3.1 Longitudinal analysis of type 1a ODP-M (FRS only)

Those with centre-involving type 1a ODP-M were deemed to meet the definition for FRS secondary to ODP-M and underwent further longitudinal anatomico-functional association analysis in phase 3. The presence of OLH and/or SRF (i.e. in types 1b and 2 ODP-M) in approximately two thirds of cases at presentation appears to represent the end-point ODP-M progression and further inclusion would confound investigation of the natural history of FRS in ODP-M.

15 patients with type 1a ODP-M had follow-up for ≥12 months or to the point of development of OLH/SRF. The baseline and follow-up characteristics for those eyes that did and did not develop OLH are summarised in

Table 4-8, including the between- and within-group statistical comparisons. For the purpose of this table, 'final' follow-up is defined as either the most recent visit or, in the event of development of OLH ± FD, the point at which this was first identified.

Table 4-8: Comparison of eyes that remained with FRS only (type 1a) during follow-up with those that developed OLH (type 1b)

Characteristics (mean ±SD)		**Type 1a**	**Type 1b**	***p-value***
Number [n(%)]		11 (73%)	4 (27%)	-
Duration of follow-up (years)		3.2 ±2.3	2.3 ±2.7	-
Visual acuity (logMAR)	Baseline	0.12 ±0.17	0.39 ±0.36	*0.273*
	Final	0.11 ±0.11	0.85 ±0.19	***0.002***
	p-value	*0.543*	*0.125*	
Central retinal thickness (µm)	Baseline	430 ±151	643 ±327	*0.280*
	Final	336 ±119	933 ±69	***0.002***
	p-value	***0.024***	*0.250*	
Average retinal thickness (µm)	Baseline	334 ±66	416 ±105	*0.111*
	Final	310 ±62	500 ±55	***0.003***
	p-value	*0.131*	*0.375*	
Central schisis height (µm)	Baseline	264 ±157	530 ±348	*0.229*
	Final	171 ±128	609 ±181	***0.003***
	p-value	***0.015***	*0.875*	
Schisis area (mm^2)	Baseline	11.2 ±8.1	15.5 ±8.3	*0.226*
	Final	7.6 ±8.4	22.5 ±2.9	***0.040***
	p-value	*0.123*	*0.125*	

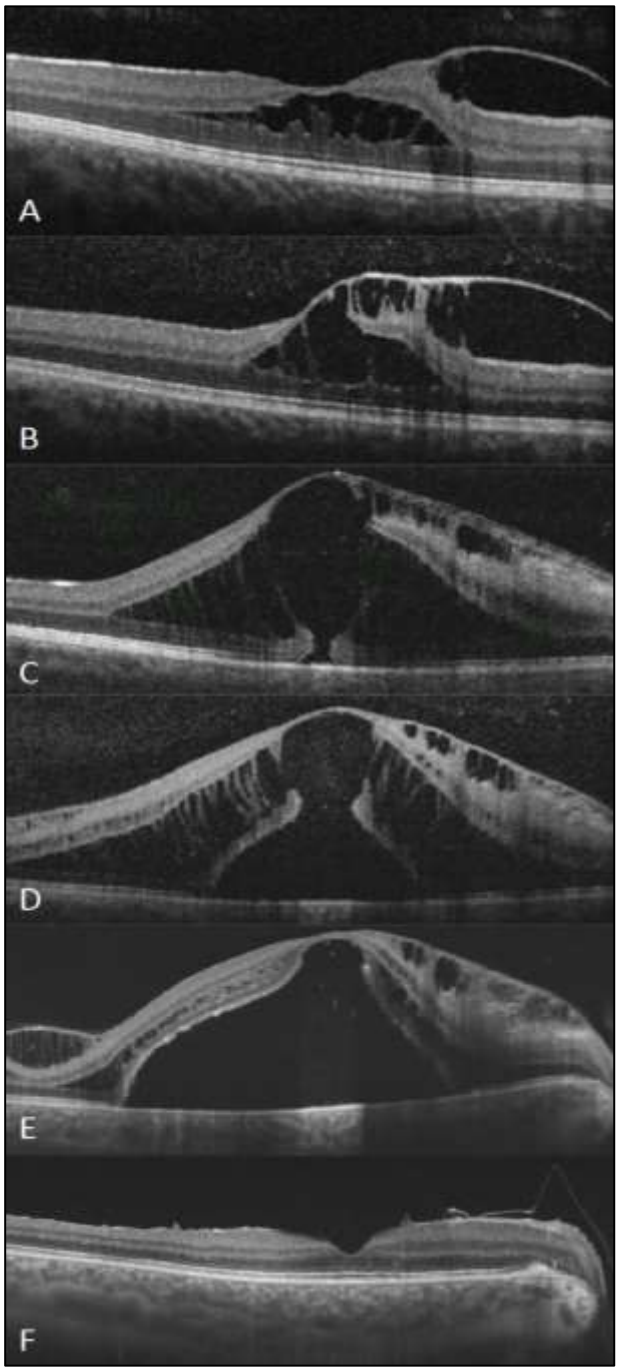

Figure 4-14: Progression from type 1a to type 1b ODP-M. (A) Baseline visit: FRS only (logMAR VA 0.18); (B) 36 months: enlargement of FRS with disruption to inner foveal anatomy; (C) 42 months: development of foveal pseudocyst with enlargement of FRS and formation of OLH; (D) 45 months: development of foveal detachment, with collapse of schisis cavity centrally; (E) 49 months: enlargement of detachment with almost full resolution of FRS (VA 0.78); (F) 19 months post-operatively: complete resolution of IRF/SRF with final VA of 0.30

4.3.3.1.1 Between-group functional analysis

VA was worse at baseline in those eyes that ended up progressing to type 1b, than those that did not (0.12 vs 0.39), but this did not reach statistical significance (p=0.273). However, at the point of development of OLH ± FD, this difference became significant (0.11 versus 0.85, p=0.002).

In the absence of development of OLH ± FD, patients with type 1a ODP-M demonstrated a non-significant change in VA from baseline to follow-up (p=0.828), over a mean (±SD) duration 3.2 (±2.3) years (Figure 4-15).

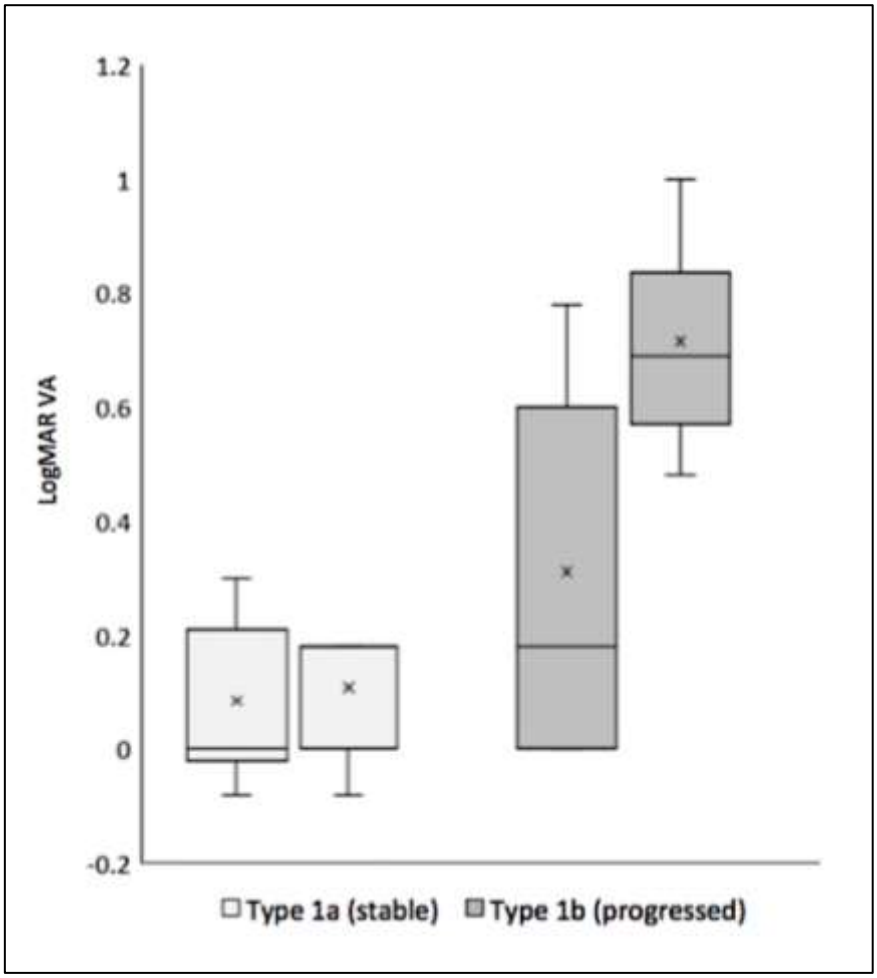

Figure 4-15: Comparison of baseline VA and final VA in stable type 1a ODP-M (FRS only) and those that progressed to type 1b ODP-M (OLH ± FD)

All 4 patients who developed OLH ± FD during follow-up underwent surgery within an average period of 6 months. After mean post-operative follow-up period of 1.8 years, VA had improved from a mean (median) pre-operative acuity of 0.85 (0.89) to 0.27 (0.24); all eyes achieved complete anatomical resolution following intervention.

4.3.3.1.2 Between-group anatomical analysis

With reference to Table 4-8, differences in quantitative anatomical characteristics were also noted between the groups at baseline, but these did not reach statistical significance. Over the course of follow-up, however, a significant difference was identified in CRT, AvRT, CSH and SA, between those eyes that progressed and those that did not, as measured at the point of OLH ± FD development (all $p \leq 0.003$). On logistic regression modeling, final CRT >641 predicted progression to type 1b perfectly; final CSH was significantly associated with FD development (odds ratio (OR): 1.02 [95%CI: 1.01-1.03, pseudo-R^2: 0.74); final AvRT, however, was not significantly associated with progression (p=0.176).

In terms of SA, those eyes that progressed to type 1b had a greater final mean area than those that did not (22.5 vs 7.6 mm^2), representing a significant between-group difference for both final areas, as well as absolute increase in area over time (both p=0.040). On logistic regression analysis, final area and absolute change were associated with progression to type 1b (OR: 1.32 [95%CI:1.13-1.52], pseudo-R^2: 0.49, p<0.001 and OR: 1.37 [95CI: 1.12-1.67], pseudo-R^2: 0.40, p=0.002 respectively). That is to say that for each $1mm^2$ greater final area, or $1mm^2$ *increase* in area over time, the odds of progression are estimated to increase by 1.32 or 1.37 respectively.

The relative changes in OCT parameters between the two groups are displayed in Figure 4-16.

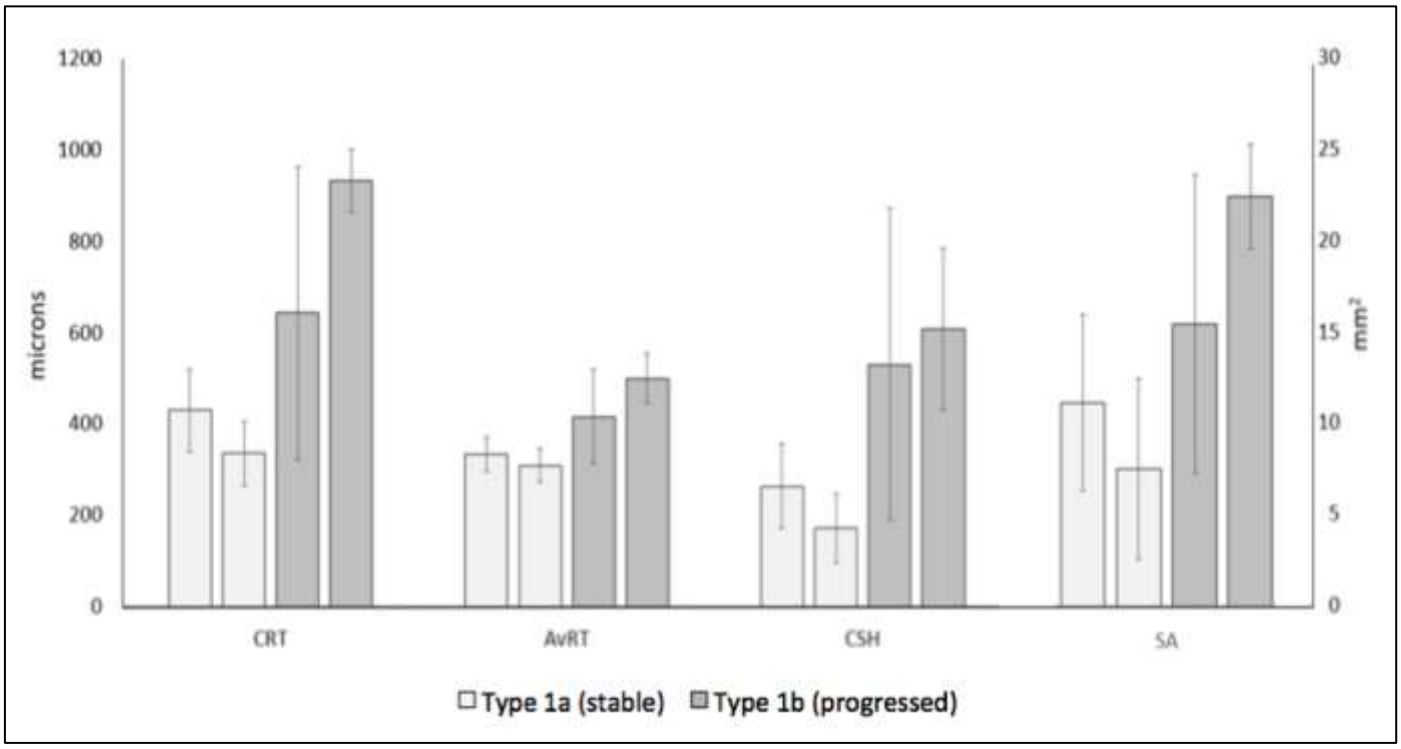

Figure 4-16: Comparison of baseline and final OCT parameters, grouped by stable type 1a and progression to type 1b ODP-M at final visit

4.3.3.1.3 Within-group analysis

At final follow-up, in those patients with type 1a ODP-M that did not progress to type 1b, there was a non-significant change in VA from 0.09 to 0.11 logMAR (p=0.978). A reduction in all OCT metrics was observed, which reached significance for CRT and CSH (p=0.024 and p=0.015 respectively) and these metrics were no longer associated with VA. Moreover, larger *relative* decreases in CRT, AvRT and CSH *were* all significantly associated with improvement in VA, with a reasonable effect size (all p≤0.050; β=0.004, β=0.008 and β=0.002 respectively). That is to say that, in the absence of progression, a 50% reduction in CRT or CSH might be expected to manifest in a mean improvement of 0.18 [95%CI:0.01-0.35] or 0.11 [95%CI:0.002-0.21] logMAR respectively (Figure 4-17). In this study population, however, there was a mean change of only -18% and -29% in CRT and CSH respectively, which was associated with a non-significant change in VA of 0.02 (±0.15). This is partly

explicable by both the floor effect of reduction in OCT parameters, as well as the ceiling effect for improvement in VA.

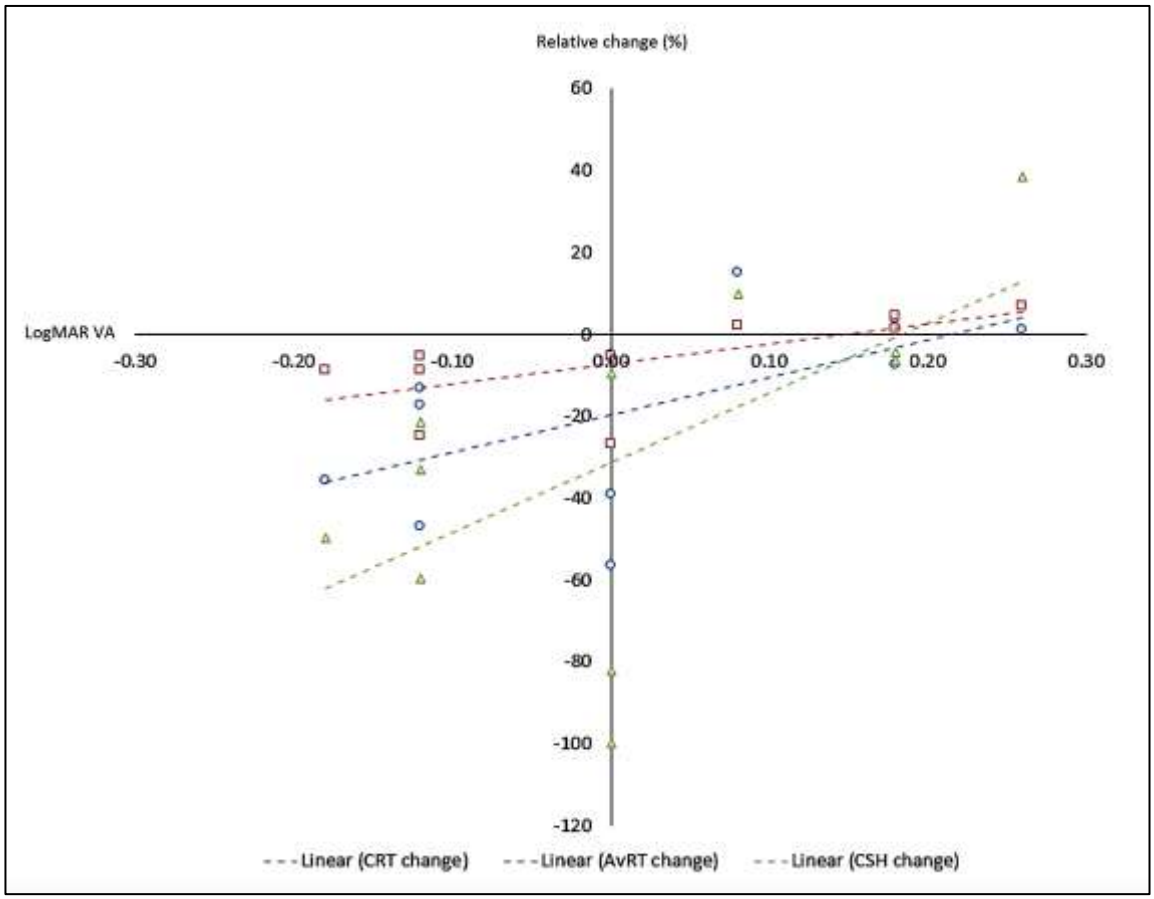

Figure 4-17: Regression co-efficient for percentage change in CRT (blue line), AvRT (red line) and CSH (green line) and change in VA in eyes with type 1a ODP-M (FRS only)

In terms of change in schisis area, there was a non-significant mean reduction from 11.2 to 7.6 mm^2 in those with stable type 1a ODP-M (p=0.123). However, it was noted that absolute and relative decreases in SA were significantly associated with improvement in VA (p=0.017, β=0.015 and p<0.001, β=0.001). This means that a $1mm^2$ decrease in SA is estimated to be associated with a mean VA improvement of 0.02 [0.003-0.03] logMAR, while a 50% decrease in SA is estimated to result in an improvement of 0.07 [0.04-0.09] logMAR (Figure 4-18). The latter is has an R^2 of 0.62, indicating that the variance in this parameter is estimated to be responsible for approximately 62% of the variance in VA seen in this subgroup, which is the highest

of all parameters investigated in cases of non-progressive FRS. In this study, the mean observed change in stable type 1a ODP-M SA during follow-up was -3.6mm^2 or -16%, associated with a mean improvement of just 0.01 logMAR. Complete spontaneous resolution of FRS was only noted in 1 eye (Figure 4-19).

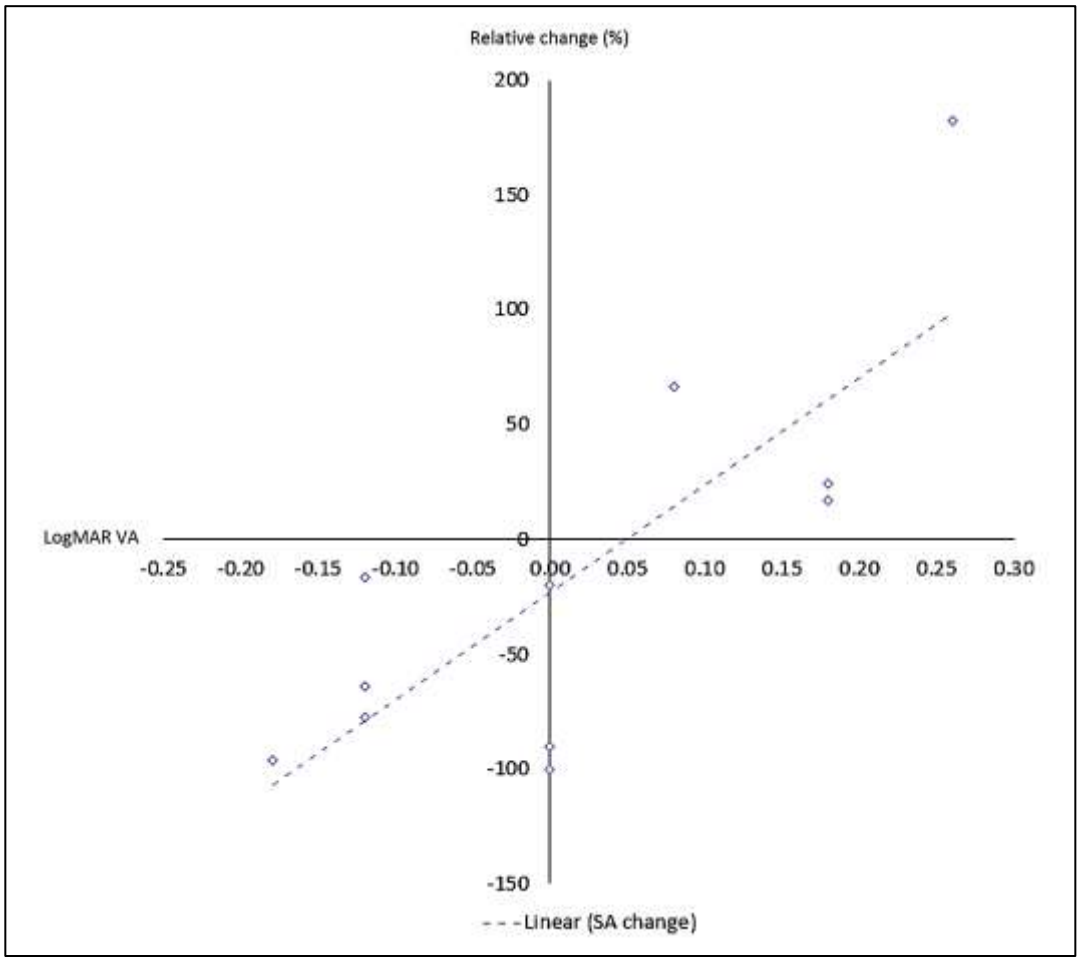

***Figure 4-18*: Regression co-efficient for percentage change in SA and change in VA in eyes with type 1a ODP-M (FRS only)**

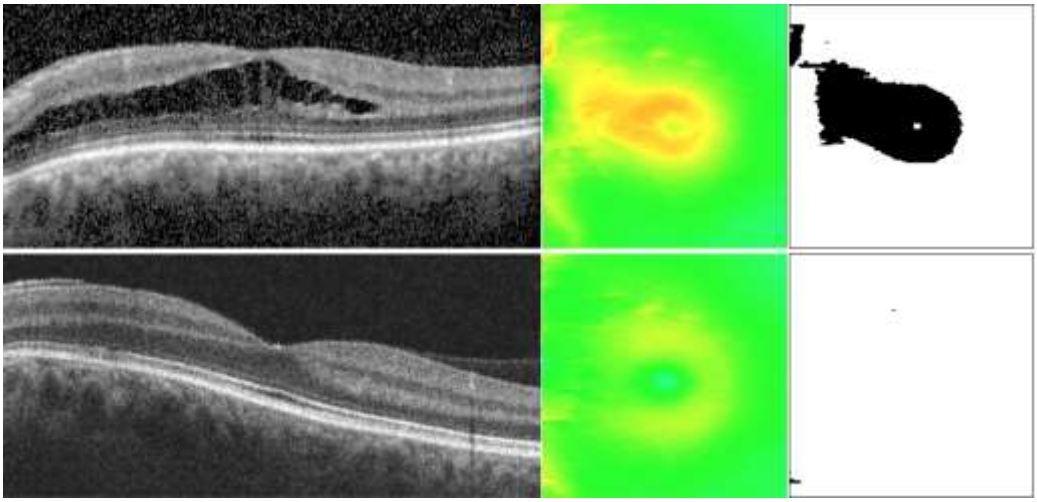

Figure 4-19*: *OCTs and colour thickness maps demonstrating spontaneous resolution of type 1a ODP-M, as observed over 46 months

By contrast, in those eyes that progressed to type 1b, there was a mean increase in SA of 7.1 (±6.6) mm^2 or 80% (±88%), with an associated reduction in VA of 0.33 (±0.22), which did not constitute a significant association (Figure 4-20). Indeed, at the time of progression, there were no within-group significant associations between VA and any anatomical parameters, indicating that, following development of OLH ± FD, the magnitude of anatomical deformation ceases to have further effect on visual function.

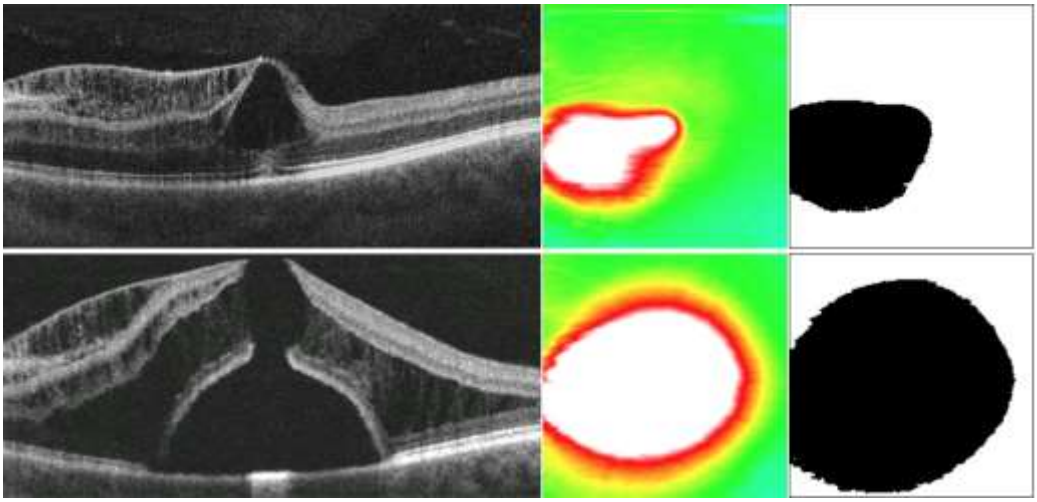

Figure 4-20*: *Progressive enlargement of schisis area, with associated development of type 1b ODP-M morphology, as observed over 3 months

4.4 Discussion

4.4.1 Baseline characteristics of ODP-M

The presence of retinoschisis or serous detachment of the macula has been reported in between 25%-75% of patients with ODP, however these figures are likely to be an over-representation as the tendency of patients with visually significant maculopathy to access hospital eye services is higher than those with asymptomatic disc pits (494,525,610,612,655). In this sample, I found the prevalence of maculopathy to be 38% amongst those with a documented diagnosis of ODP.

In phase 1, analysis of 87 patients revealed mean age at presentation to be 35 years, with a slight preponderance of female sex (63%) and left eye laterality (62%). Previous OCT-based studies have reported a mean age of 28-35 years, female sex in 19-67% and left eye affected in 42-67% (4,497,507,508). Table 4-9 summarises the baseline characteristics from some of the largest case series of ODP-M to date. I also found a predominance of white ethnicity (relative to the local demographic ratios), which is in keeping with previous reports (497,501,508). The reasons for these associations with ODP-M remain unclear.

I noted that the majority of pits were located temporally, which is consistent with existing evidence, suggesting that temporal pits are more likely to give rise to maculopathy (494,501,504,525). Brown et al found a trend for larger pits to be associated with maculopathy, reporting an average pit size of 0.32 disc diameters (DD) in those with macular involvement (compared to 0.23 in those without) (501). The finding of a mean pit size of 0.31 DD in ODP-M is consistent with this premise. Finally, it has been proposed that there is a higher frequency of cilioretinal artery (CRA) associated with an ODP, with reports ranging from 59-63% prevalence (501,506). However authors admit that the displacement of a vessel by a pit can give the illusion of a CRA (494,501,502), which I found was often the case when observed on *en face* imaging; the prevalence of CRA in this study was 18%, which is more in keeping with the estimated population frequency of 15-32% (656–658).

Table 4-9: Baseline characteristics in ODP-M: comparison with published results

Authors	Year	n	Mean age	Female sex	Right eye	Temporal pit[†]	Mean pit size	Baseline VA (logMAR)	OLH ± FD present at baseline
Kranenburg	1960	16	34	19%	44%	94%	0.29	0.89	69%
Sugar	1967	12	35	50%	33%	*NR*	*NR*	0.60	75%
Brown et al	1980	39	31	*NR*	*NR*	95%	0.32	0.60	100%
Sobol et al	1990	15	32	53%	47%	87%	*NR*	0.43	100%
Theodossiadis et al	1992	8[§]	28	38%	NR	88%	0.20	1.09	63%
Imamura et al	2010	16	36	44%	44%	*NR*	*NR*	0.80	69%
Roy et al	2013	32	28	41%	*NR*	*NR*	*NR*	0.85	91%
Steel et al	2016	36	33	42%	58%	100%	*NR*	0.80	78%
Steel et al	2018	70	35	50%	44%	96%	*NR*	0.61	61%
AVERAGE			**32**	**44%**	**44%**	**95%**	**0.27**	**0.74**	**78%**
Present Study	2021	87	35	63%	38%	87%	0.31	0.38	66%[‡]

NR = not reported; [§]8 previously untreated patients from 16 total in study; [†]includes infero-/superotemporally located pits; [‡]data from 51 patients with baseline OCT scans, in whom mean baseline VA was 0.35 (4,494,497,501,504–508)

4.4.2 Morphological categorisation of ODP-M

In phase 2, I have re-categorised ODP-M according to the location of retinal fluid accumulation and presence or absence of OLH. Previous reports have quoted the proportion of eyes with ODP-M that involved any SRF accumulation as between 60-91%, while those with IRF only constitute around 9-40% of cases (4,497,507,508,538,659). My findings in phase 2, that 66% of eyes had types 1b or 2 ODP-M at baseline, compared to only 34% with type 1a, is in keeping with this. Moreover, the observations that the majority of cases (84%) had evidence of IRF at presentation and that 27% of those with IRF only (type 1a) at baseline progressed to develop SRF, support the proposed anatomical order of events, whereby fluid initially collects in the IRS, before migrating to the SRS (465,507,538,618). However, while all cases of type 1a ODP-M that progressed to 1b did so in the presence of new OLH development (indicating that this is the mechanism through which SRF propagates from pre-existing IRF), 19 eyes had SRF *without* OLH (i.e. type 2 ODP-M). Indeed, in this study, only 42% of all those with SRF were found to have an OLH, in keeping with previous reports (507,508). This configuration was evident at baseline, suggesting that the SRF may have arisen *de novo, i.e.* as a result of direct communication between the ODP and the SR space, rather than through percolation from other retinal layers.

A novel finding of this study was that there are significant differences in age between those presenting with the different abovementioned fluid configurations (mean age of 38 years in types 1a/b versus 19 years in type 2). 7 eyes (14%) within the type 2 subgroup were noted to have SRF only, which is a similar proportion to that previously reported in the OCT era (0-14%) (497,507,508,549,659,660). Interestingly, all of these cases were observed in patients younger than 25-years-old (mean age of 17 years) and, in several cases, a direct communication between the SRF and ODP could be visualised (Figure 4-21). Moreover, 13/14 (93%) of all cases observed in patients <20-years-old were type 2 ODP-Ms.

There are several reports of spontaneous ODP-M occurring in children that demonstrate the presence of SRF at baseline (512–514,559,560,620). Some authors

have previously postulated that there may be multiple distinct mechanisms in ODP-M (538,620); in their series of five subjects, for example, Skaat et al presented 2 children with neurosensory detachment without IRF and suggested that fluid may emanate directly from the optic nerve to the SRS (620). It is possible that this discrepancy is attributable to the differences in both vitreous and axial length between the child and adult eye. For example, the posterior precortical vitreous pocket (PPVP), which comprises premacular liquefied vitreous, is not observable until age 3 and continues to enlarge into adolescence (43,661). Moreover, a thick vitreous septum separates the PPVP from Cloquet's canal post-natally; channels between the two are rarely observed before age 5, while they are present in 50% of 11 year-olds and almost all adult eyes (661). Finally, changes in the scleral extracellular matrix and axial elongation persist into early adolescence and are likely to be linked to the observed changes in vitreous morphology (395). The lack of vitreous liquefaction, combined with an absence of communication between the pre-macular and pre-papillary bursae, mean that vitreous synchysis and epipapillary traction are unlikely to represent a primary pathomechanism in children with ODP-M (i.e. in the absence of significant trauma). It is reasonable, therefore, to consider that an alternative mechanism, such as a direct communication between the pit and, say, the subarachnoid space, could result in the early manifestation of type 2 ODP-M. The precise pathophysiology and source of fluid in these cases remains to be elucidated, but this concept indicates that management approaches may need to be adapted to address variable underlying mechanisms, on the basis of observed ODP-M morphology. For example, primary ingress of fluid into the SRS (type 2 ODP-M) might be better suited to juxtapapillary laser treatment, while types 1a and 1b may benefit more from vitrectomy or inner retinal fenestration.

Without the aid of histochemical analysis, however, this notion of pathomechanical variation remains theoretical, and the potential benefit of a modified surgical approach is speculative. Further research is required to clarify this hypothesis. It is notable that those with type 2 ODP-M had, on average, better baseline VA than those with type 1b, while a greater proportion of cases also demonstrated complete spontaneous functional and anatomical resolution of maculopathy, indicating that

there may be a role for surveillance in cases of type 2 ODP-M with good visual function.

This sub-categorisation system is also hypothetical, as we cannot be certain of the antecedent anatomical progression. It is possible that type 2 cases are preceded by type 1 morphologies, but the absence of OLH, alongside the longitudinal evidence from phase 2, support the theory of two distinct pathomechanisms.

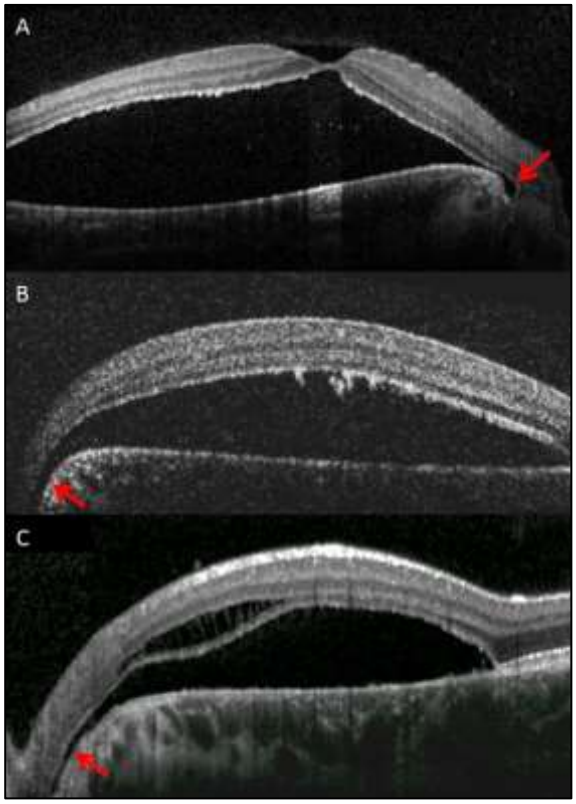

Figure 4-21: **Examples of type 2 ODP-M with direct communication between the SRS and the ODP (red arrows). (A&B): SRF in a 12 and 23-year-old patient respectively; (C): SRF with OLR in a 15-year-old patient**

4.4.3 Anatomico-functional characteristics of ODP-M

Compared to other observational case series, the reported mean baseline VA of 0.38 logMAR in this study is generally better than that previously described. This is partly explicable by the relatively high proportion of cases with IRF only, compared to some

of the other natural history studies. In 2018, Steel et al reported an association between the presence of SRF and a worse baseline vision, which was also the case in this study (497). Since most natural history studies predate the use of OCT, it follows that they comprise a higher proportion of patients with SRF, and therefore the reported VA would be worse at presentation. On the basis of these findings, the visual prognosis for ODP-M is generally considered to be poor, in the absence of intervention (494,501,505,506,640).

In fact, in this study, the majority of cases did not undergo surgical intervention and, in the observed cohort, VA was maintained, although the rate of spontaneous complete resolution was relatively low (32%), in keeping with previous reports (502). Those eyes that presented with, or progressed to poor VA, demonstrated significant improvement following intervention, with a high rate of complete resolution of retinal fluid (73%), again consistent with existing evidence (548,549,640). Of note, the majority of cases that presented with, or progressed to, type 1b ODP-M were observed to undergo functional deterioration, necessitating surgery in 73%, compared to a minority of those eyes that retained type 1a or type 2 morphology throughout (0% and 36% respectively). Indeed, the presence of OLH was significantly associated with having surgery, as well as independently associated with worse VA at baseline and final follow-up. This indicates that the presence of SRF is not, in itself, a feature that predisposes to worse VA and higher rates of progression, as suggested, but rather the presence of OLH +/- SRF (508,662). In this study, a greater proportion of type 2 ODP-M tolerated observation and several were observed to undergo spontaneous resolution (Figure 4-22). As such, there is perceived merit in distinguishing the morphological subtype 1b from type 2 ODP-M.

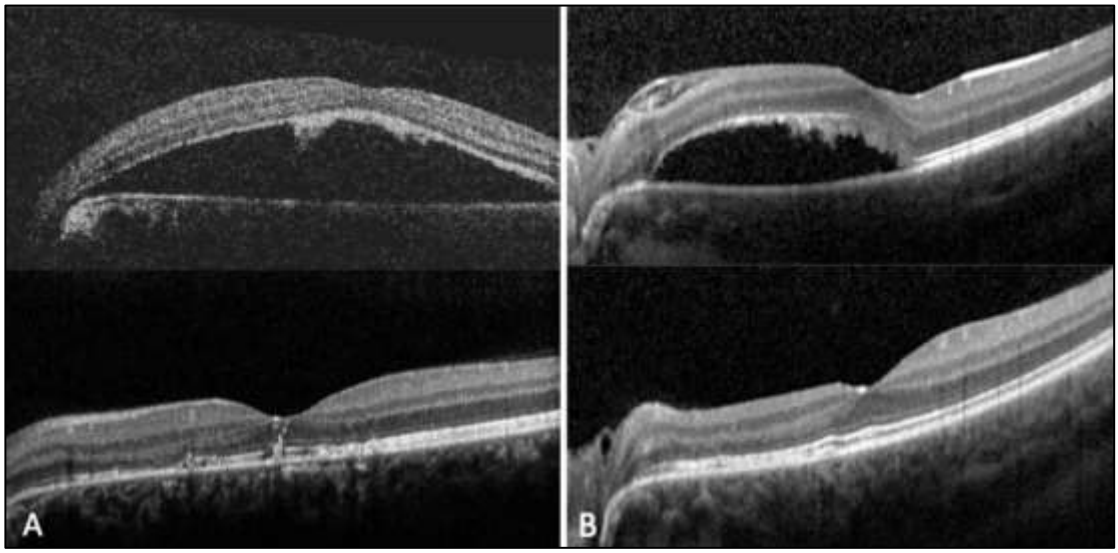

Figure 4-22: Examples of complete resolution of type 2 ODP-M in a 24-year-old and 5-year-old respectively

It is becoming increasingly apparent that there is a stable subgroup of eyes with ODP-M that maintain good visual function. For example, Steel et al reported on a subgroup of 23 cases with IRF only, with a mean VA of 0.33 logMAR at baseline, which demonstrated a non-significant change in VA of only -0.02, over a follow-up period of 1 year. My findings in phase 3 support this, insofar as those with type 1a ODP-M at presentation had a mean VA of 0.12 and the majority of these cases (73%) did not progress, while retaining good visual function, over a mean observation period of 3.2 years. This suggests that the presence of FRS in ODP-M is not, in itself, functionally significant or an indication for surgical intervention.

In phases 2 and 3, I also explored the baseline and longitudinal changes in morphology of type 1 ODP-M, with regards to quantitative OCT parameters. At baseline, I found that not only was greater AvRT associated with the presence of OLH ± FD (type 1b ODP-M), but increases in all OCT metrics were also associated with worse VA in those eyes with FRS only (albeit with relatively small effect size). This suggests that degree of retinal deformation is related to functional decline prior to the development of an OLH and FD. This is further supported by the observation that, over the course of follow-up, the eyes that progressed to type 1b demonstrated an increase in all OCT metrics, while those that did not progress showed significant improvement in both CRT and CSH measurements. Although

functional and anatomical differences between these two groups were noted at baseline, they did not reach statistical significance until the final visit. The numbers in this analysis were too small to draw definitive conclusions from, but it is conceivable that there is a latent period, prior to the development of OLH or FD, wherein subtle anatomical changes anticipate progression. The observed early decline in VA associated with enlargement of the schisis may represent microstructural changes and could serve as a useful clinical predictor for progression. In absolute terms, a CRT >650µm predicted progression perfectly, while 4/5 of the eyes with a CSH >400 progressed to FD. The fact that those with type 1a ODP-M at baseline only make up a small proportion of all cases (34%) indicates that if progression to type 1b is to take place, it is liable to be a rapid sequence of events (as is often observed in MFS).

In view of the above findings, I propose a monitoring scoring system for patients with type 1a ODP-M, as detailed in Table 4-10. The objective of each review is to determine if there has been a significant deterioration of VA or if there is evidence of anatomical progression on OCT, both of which could be assessed in a semi-virtual setting. At the point at which progression is detected, early discussion of surgical intervention is warranted. I have chosen CRT as it was highly correlated with progression but is also easily and reproducibly measured using most OCT software packages. While CSH and SA are also novel and interesting parameters, which showed association with progression, they is not currently automatically calculated on most OCT systems. It ought also to be noted that the suggested monitoring scoring system has not been validated internally or externally and, as such, remains hypothetical. Moreover, the parameters have been derived using Topcon OCT metrics and are not directly translatable to other OCT devices.

Table 4-10: Proposed ODP-M Monitoring Scoring System

Characteristic	Threshold	Score
Central retinal thickness (µm)	<400	0
	400-600	1
	>600	2
Total score	**Suggested monitoring frequency**	
0	12 months	
1	6 months	
2	≤3 months	

If this scoring system were applied to the cohort of this study, it would result in only 6/15 (40%) cases undergoing the most frequent screening interval (≤3 monthly) at some point during follow-up but allow the detection of early progression in 4 of those eyes during the study period.

The above association between CRT and observed anatomico-functional decline, as well as longitudinally observed progression in specific cases (see Figure 4-14), can be related to our understanding of the foveal ultrastructure (see 1.2.4.3). Considering there is a relative lack of extraretinal forces at play in ODP-M (unlike in VRI disorders and MFS), inner foveal disruption is rarely observed. Instead, retinal deformation primarily occurs through progressive internal anteroposterior force vectors, resulting in rapid and excessive compensatory verticalisation of MC processes (Figure 4-23A&B). At the point at which the tensile limit of the MCs of the MCC is met (which appears to be at around 400µm), rupture of the MCC vertical stalk is observed, with formation of a foveal pseudocyst and OLH (Figure 4-23C). Following this, the unopposed centrifugal force vectors of the z-shaped MCs lead to progressive development and enlargement of a FD, with subsequent relaxation of stretched MCs in HFL and collapse of the schisis cavity (Figure 4-23D&E). This collapse explains why no difference is seen between eyes with type 1a and 1b ODP-M at baseline, but is demonstrated when studied longitudinally. Therefore, although

aetiologically distinct, ODP-M appears to share both functional and morphological similarities to the tractional foveopathies discussed in chapters 1 and 3, with respect to its mechanical effects on the retinal ultrastructure and, in particular, the foveal MC subpopulations.

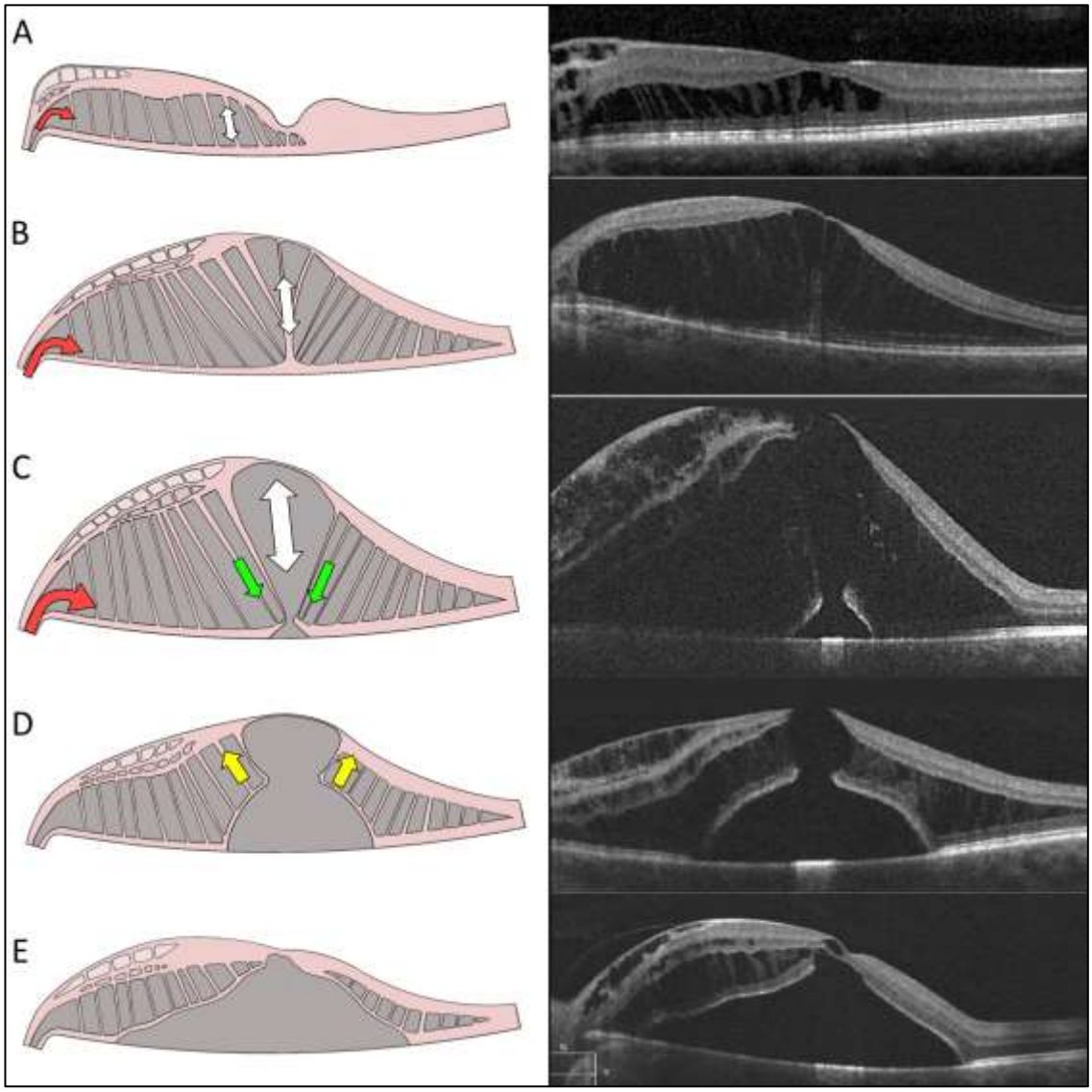

Figure 4-23*: *A diagram demonstrating the potential stages and underlying mechanics of the anatomical natural history of ODP-M; (A): early ingress of fluid (red arrow) causing formation of schisis cavities, predominantly in HFL, with bevelling of zMC complexes; (B): progressive fluid accumulation and vertical stretch of the MCC (white arrow); (C): rupture of the MCC stalk with formation of foveal pseudocyst and OLH, combined with concentration of inward traction along unopposed zMCs (green arrows), leads to early development of FD; (D):

enlargement of FD with collapse of overlying schisis cavity (yellow arrows); (E): Enlargement of detachment and resolution of foveomacular retinoschisis

Although spontaneous macular reattachment with visual recovery has been described in up to 25% of cases of ODP-M with SRF, I found the rate of complete spontaneous resolution of type 1a ODP-M to be low at 9% (1/11), which is consistent with the findings of Steel et al in 2016 (504,505,508,511,513,663–666). The rate of spontaneous resolution of type 2 ODP-M was, by contrast, higher at 50% (5/10) of observed cases, lending further weight to the possibility of a distinct pathomechanism in these cases.

Numerous studies have reported on the benefits of various vitreoretinal surgical approaches in the management of ODP-M and there is clearly an indication for intervention in certain cases (497,547,549,631,633,635,638,640,651,659,667–670). For example, in this study, patients with types 1b and 2 ODP-M who underwent surgery demonstrated functional and anatomical recovery. However, surgery carries a risk of iatrogenic damage, operative failure with need for repeat surgery, as well as cataract formation (465). Risk stratification of cases of ODP-M through enhanced understanding of the pathomechanics may avoid subjecting patients to unwarranted surgical risk, as well as optimising the timing of surgery, in those who would serve to benefit from intervention.

As with Chapter 3, there are potential limitations to the retrospective, observational design of this study, including the risk of introducing bias and the possible presence of confounding variables, as well as the chance of selection bias as to the prevalence of this condition in the general population, as a consequence of it being performed at a tertiary ophthalmic unit. There is potential for observer bias as analysis of quantifiable OCT metrics was performed by a single grader only, therefore the proposed associations and grading system require further validation before they might be suitable for clinical application. Despite relatively small numbers with follow-up data, I have demonstrated significant and novel findings, with respect to the demographic and longitudinal anatomico-functional characteristics of ODP-M. Large-scale prospective studies are required to establish causality and validate the

proposed risk-stratification of cases, while further characterisation of OCT changes may reveal additional useful prognostic markers.

4.5 Conclusion

In summary, I have recategorised ODP-M according to fluid distribution and demonstrated a significant age difference between those with types 1a/b and 2 ODP-M at presentation, thus supporting the possibility of alternative pathoanatomical mechanisms in ODP-M, whereby SRF can arise *de novo* in younger patients and may therefore be amenable to distinct management approaches.

Furthermore, contrary to current practice and understanding, the results of this study suggest that there may be a relatively good prognosis for observation in many of the eyes with ODP-M that present with either IRF only (type 1a) or SRF without OLH (type 2). I found that the majority of cases of type 1a ODP-M demonstrated no anatomical or functional progression over more than 3 years' follow-up. Despite the fact that complete resolution of FRS is rare in the absence of surgical intervention, VA is maintained, indicated that chronic presence of schisis does not carry significant visual morbidity in ODP-M.

Finally, I have identified that, in the event that progression to OLH ± FD (type 1b) occurs, it is preceded by significant and measurable retinal deformation, as well as a decline in VA. It is likely that OCT parameters represent useful clinical biomarkers for risk stratification in ODP-M. Based on my findings, I have proposed a simple OCT-based scoring system to guide follow-up intervals, with a view to enabling early identification of progression and planning timely intervention, where necessary.

CHAPTER 5

A RETROSPECTIVE OBSERVATIONAL AND CROSS-SECTIONAL STUDY OF THE ANATOMICO-FUNCTIONAL BEHAVIOUR OF IDIOPATHIC FOVEOMACULAR RETINOSCHISIS

"The situation has become much more complicated"

– Qui Gon Jinn

5.1 Introduction

The presence of FRS has been described in the absence of evidence of genetic mutation, vitreoretinal traction, myopia or optic nerve head anomaly. In 2014, Ober et al coined the term 'stellate nonhereditary idiopathic foveomacular retinoschisis' (SNIFR) in an attempt to provide a unifying classification under which to categorise these unusual cases, without an explanatory pathophysiological mechanism (671). Their series comprised 22 eyes of 17 subjects, without optic nerve head abnormalities, angiographic leakage, nor a positive genetic test or family history for XLRS. There was a preponderance of female subjects and a mean age of 61 years. Subjects were reported to have a stellate appearance at the macula, with splitting within the OPL and ONL (i.e. HFL) (Figure 5-1). Almost all subjects demonstrated anatomical and functional stability over the course of their follow-up; the mean VA at baseline was approximately 0.10 logMAR, which was unchanged in the vast majority (one eye developed FD during the follow-up period). Interestingly, despite the cohort having a mean age of >60 years and having predominantly myopic refractions, only 3/19 (16%) had evidence of complete vitreous separation on OCT. This was not considered relevant and the authors concluded that, while the mechanism was not clear, "it indicates that factors other than traction alone can play a role in foveomacular schisis-like maculopathy in the absence of a known *RS1* mutation" (671).

Since the term was coined, further case reports of SNIFR have been published, using the acronym to describe various manifestations of FRS of uncertain origin (338,339,672–685). However, several of these cases were associated with other ocular or macular pathology, potentially influencing the validity of whether these truly represent an 'idiopathic' process (338,339,684,685). Other cases did not show features consistent with Ober et al's description, such as a multi-layered schisis cavity, direct continuity with the optic nerve head (in some cases with angiographic leakage) and VMI disorders, raising the suspicion for alternative diagnoses (677,679,681–683).

As such, there have really only been 12 further reports (of 18 eyes) in the literature, consistent with a probable diagnosis of SNIFR (672–681,683,686). Almost all of these cases were observed in female subjects, with a mean age of 59 years and VA of 0.10 logMAR. Reported cases of SNIFR appear to have favourable functional profiles and share similar anatomical configurations, namely FRS at the level of HFL (672,674,675).

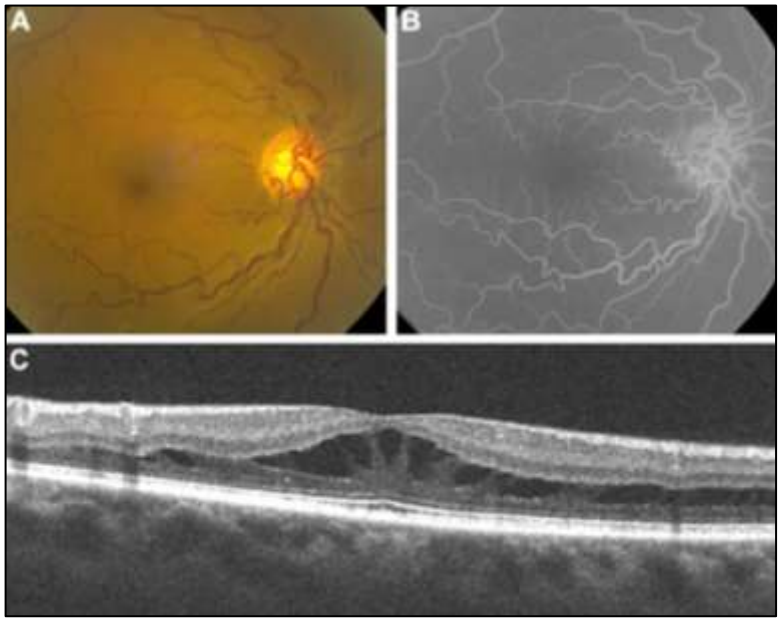

Figure 5-1: Features SNIFR; (A) Photograph showing perifoveal stellate appearance, fluorescein angiography demonstrating absence of vascular leakage; (C): OCT reveals retinal schisis at the level of HFL. Credit: Ober et al (2014) (671) [images reproduced with permission of the rights holder, Elsevier]

5.1.1 Pathogenesis

The precise pathomechanism of SNIFR remains unresolved. Ober et al originally suggested that the condition was neither heritable nor tractional (671). However, more recently, structural *en face* imaging has since revealed a 'spoke-wheel' pattern of schisis distribution, reminiscent of that demonstrated by Govetto et al in cases of tractional FRS (see Figure 1-32) (335,672,674). Fragiotta et al used OCT-A to demonstrate an absence in vascular flow signal in the schisis cavity in a single

patient, suggesting that a relative lack of bridging vessels between the intermediate and deep capillary plexi (in the INL and OPL respectively) may underlie the pathoanatomical schisis morphology in SNIFR (673). Notwithstanding the fact that this theory remains to be demonstrated on a larger cohort, the deep capillary plexus is located in the superficial OPL, therefore if the schisis is posterior to this (in HFL), we would not necessarily expect to visualise any flow signal in this location (687,688); to date, this theory has not gained widespread acceptance (675,686,689).

In their study, Ober et al noted that, in 3 eyes with peripheral OCT, there was evidence of additional involvement of the IPL peripherally (reported as a bullous peripheral retinoschisis clinically) (671). Subsequent to this, Ahmed et al also noted the presence of peripheral retinoschisis in both the affected and the fellow eye of one subject with unilateral SNIFR (674). They proposed that this may represent "the eventuality of SNIFR occurrence including peripheral involvement without central affection of the other eye", but conceded that they could not determine the chronology of the concurrently observed schisis distributions in their report. Mandell et al also noted the presence of widespread peripheral retinoschisis in one subject with bilateral SNIFR, with reported a significantly reduced b:a wave ratio on scotopic ERG (675).

5.1.2 Peripheral retinoschisis

'Senile' or peripheral retinoschisis (PRS) is the condition for which the term 'retinoschisis' was first used by Wilczek in 1935 (1,690,691). An acquired disorder, PRS is thought to affect up to 7% of people over the age of 40 years, the vast majority of whom are asymptomatic and non-progressive, despite a consistent association with absolute scotomata over the affected retina (2,692–697).

PRS arises due to the coalescence of cystic cavities, which in turn result from the erosion of neuroretinal and glial support elements within areas of peripheral cystoid degeneration. Cystoid degeneration can be broadly categorised into two types, based on histology: 'typical' and 'reticular' (694,698–702). Typical cystoid

degeneration (TCD) appears as tiny, outer retinal cysts at the ora serrata. This type of degeneration is ubiquitously observed in the peripheral retina beyond 8 years of life, tending to appear first as temporal inner retinal stippling, before extending posteriorly and circumferentially (698,700,701). In contrast, reticular cystoid degeneration is less common, affecting approximately 13% of adult eyes (703). Clinically, it is observed posterior to, but continuous with TCD, manifesting as a more finely flecked inner retinal surface, in a net-like pattern. Here, the cysts primarily form in the inner retina (694,699,703,704).

In both instances, degeneration can progress to form a more extensive retinoschisis cavity (705). Typical PRS manifests as a fusiform split at the level of the outer retina (OPL and adjacent nuclear layers), separated by septa comprising aggregations of glia-axonal tissue. Clinically, it can be difficult to appreciate on biomicroscopic examination, but the retina is described as a having a 'pitted' appearance, often with glistening white dots on the ILM surface, probably representing endplate remnants of ruptured MCs (Figure 5-2A&B) (696,699,704). Typical retinoschisis is often bilateral and rarely progresses or extends posteriorly (698,704). By comparison, reticular PRS is less common and often unilateral. Characteristically demonstrating an ovoid bullous architecture, it appears as a lace-like, vessel-containing inner layer overlying honeycomb-like excavations in the outer layer, separated at the level of the NFL (Figure 5-2C&D). While there is always a co-existent band of TCD found anteriorly, the reticular PRS may extend further posteriorly than the typical type and is more prone to complication, such as the development of inner and outer leaf holes and subsequent 'schisis-detachments' (693,696,699,704,705). It has been suggested that, in both types of retinoschisis, there is extensive degeneration of the neuroretinal architecture, which results in absolute scotomata (698).

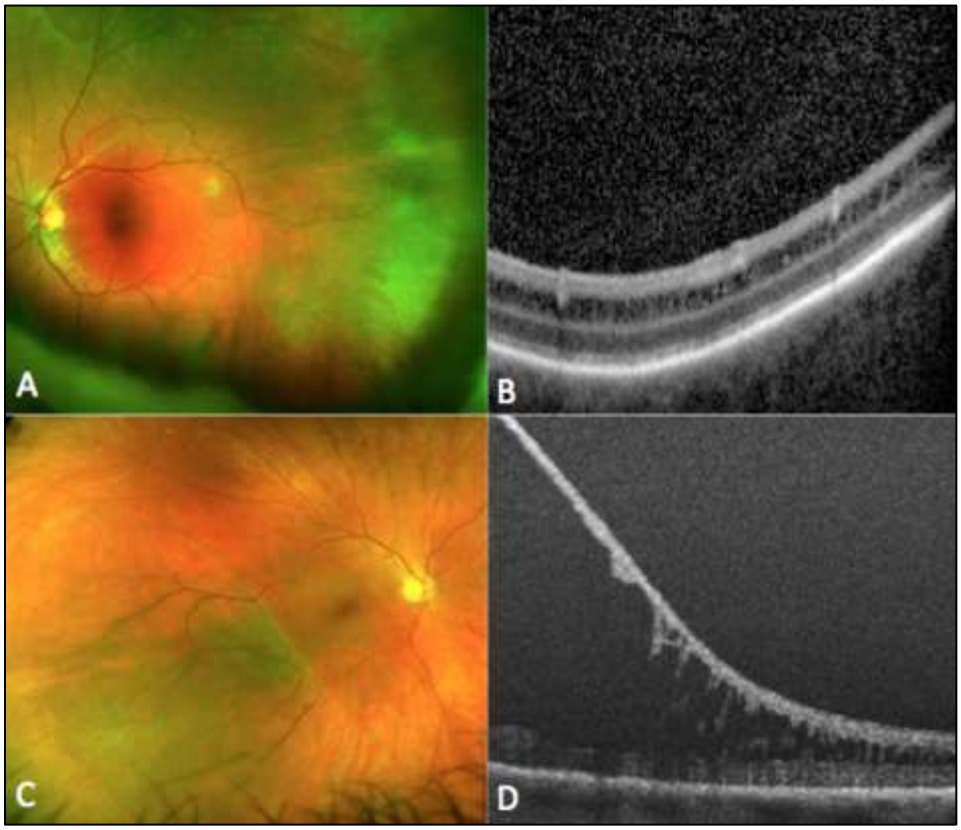

Figure 5-2: Widefield imaging and OCT of (A&B) typical and (C&D) reticular PRS

In reality, there is significant clinical overlap between the two types of PRS *in vivo* (706–712). For example, Landa et al described a case that appeared as bullous retinoschisis clinically, but had separate schisis cavities that appeared both within the outer *and* inner retina (707). Yeoh et al observed this arrangement in 4 patients and termed it a 'double-schisis cavity' (Figure 5-3) (708). Eibenberger et al found that 11/47 (23%) eyes had evidence of such morphology, without clear predilection for either bullous or flat retinoschisis configurations (711).

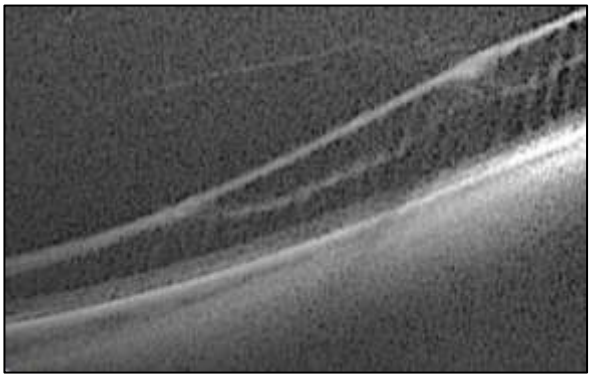

Figure 5-3: OCT of PRS, demonstrating multi-layered schisis involving both inner and outer retina

There is a growing body of evidence that vitreoretinal traction may play a role in the pathogenesis of PRS. In addition to direct visualisation of the vitreous cortex on OCT, there have been suggestions that angiographic leakage and non-perfusion in the vicinity of peripheral schisis could be caused by localised hydrostatic and/or tractional mechanisms (712–714). PRS has also been shown to have an association with hypermetropia and nanophthalmos and, although the nature of this relationship remains unresolved, it might be related to reduced scleral outflow or choroidal congestion, which can impair posterior segment drainage, in turn disrupting MC function (2,715,716). Alternatively, it could represent abnormal biomechanical behaviour at the peripheral vitreoretinal interface in the long-sighted eye. Choudhry et al have demonstrated an intimate relationship between the inner leaf of the schisis cavity and the posterior hyaloid on widefield imaging (710) (Figure 5-4).

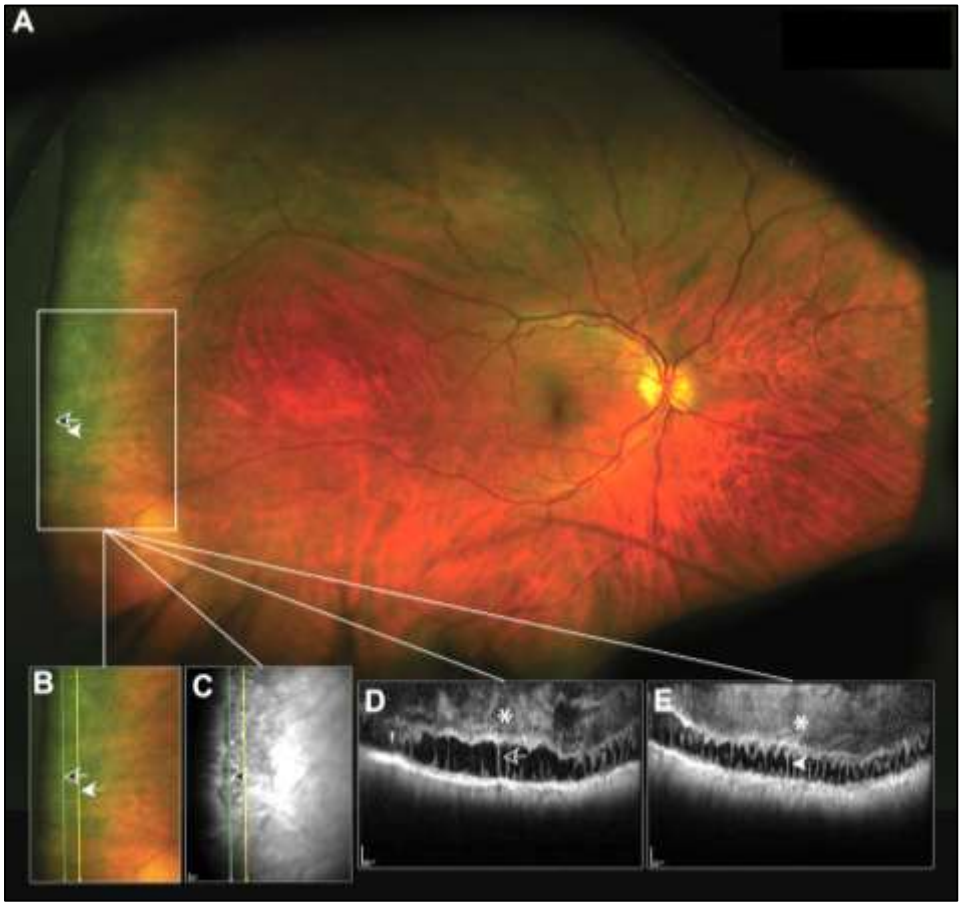

Figure 5-4: Imaging montage of typical PRS; (A): UWF colour image (B&C): colour and NIR inset; (D&E): schitic cavity within OPL/INL, closely approximated to condensed vitreous cortex (asterisks). Credit: Choudhry et al (2016) (710) [image reproduced with permission of the rights holder, Elsevier]

Byer has extensively characterised the functional and anatomical natural history of PRS (693,717). He reported that, over a mean period of 9 years, 3.2% of patients showed some evidence of posterior extension of the retinoschisis, while new areas of schisis developed in 10%. The most posterior extension was reported to 3 DD from the macula. 9 eyes (4.1%) demonstrated spontaneous improvement, with 5 eyes (2.2%) resolving entirely. Despite a reported high rate of eyes with post-equatorial extension of retinoschisis (66-77%) (693,718), involvement of the macula in PRS is exceptionally rare, in the absence of schisis-detachment (693,697,718–722). The reported incidence of schisis-detachment is 6.4%, although this only results in progressive and symptomatic disease in around 0.05%-2.2% (693,695,723,724).

It is widely accepted that degenerative PRS is a common and predominantly clinically insignificant condition, which, despite the association with peripheral absolute scotoma, carries an excellent long-term functional prognosis without treatment. Although the precise mechanisms underlying the disorder remain obscure, considering the current evidence, posterior extension of PRS does not appear to have a known association with FRS.

In summary, SNIFR serves as a diagnosis of exclusion in cases of FRS, for which there is no convincing alternative explanation. The condition appears to affect (predominantly female) patients at around the 6-7th decade of life, manifesting with FRS in HFL and conveying a good visual prognosis. OCT and *en face* imaging reveal a schisis morphology that is similar to those seen in cases of acquired mechanical FRS (335). To-date, theories concerning observed associations with vitreous attachment and PRS are limited by small sample sizes and, as such, the precise pathoanatomical mechanism of SNIFR remains elusive (674).

In this chapter I evaluate the visual and structural characteristics, longitudinal anatomico-functional behaviour and clinical associations in cases of unexplained or 'idiopathic' foveomacular retinoschisis (IFRS), in order to further explore the underlying pathophysiology and natural history of this disorder.

5.2 Methods

A single site retrospective, observational study was performed to identify patients with evidence of FRS without a known predisposing disorder. Patients were included, who presented to a tertiary ophthalmic hospital trust between January 2010 and January 2020, with centre-involving macular schisis. Cases were identified through review of electronic case notes, using the search terms "schisis", "retinoschisis", "maculoschisis" and "foveoschisis", and correlation with historical OCT imaging. Exclusion criteria included patients under 18-years-old; those with significant ocular co-pathology or alternative pre-disposing features (such as high

myopia or posterior staphyloma, optic nerve anomalies, ERM or focal VMT); or having had identification of a genetic mutation associated with FRS.

Where documented, the following data were collected: demographic characteristics (age, sex, ethnicity), VA at baseline and final visit, SE, AL, reported visual symptoms and ophthalmic examination findings, including evidence of PRS. In cases where data for SE or AL were not available, high myopia was excluded if there was an absence of staphyloma on OCT or myopic retinal features on fundus imaging (as per the International photographic classification and grading system, Ohno-Matsui et al, 2015) (363). Serial OCT imaging was reviewed to determine PVD status and peripheral extension of retinoschisis. OCT images were obtained using the Topcon 3D OCT-1000, Heidelberg Spectralis sd-OCT and Zeiss Cirrus 5000 HD-OCT devices. Measured quantitative OCT parameters included CRT, AvRT, CSH and SA, as defined in 2.3.6.1 and 2.3.6.2. For quantitative analysis, only images from Topcon 3D-OCT were used to avoid confounding from inter-device variability.

The study is divided into 3 phases: Phase 1 investigates the baseline demographic, functional and anatomical characteristics in those with IFRS. Phase 2 explores the longitudinal functional and anatomical changes in those with ≥12 months' follow-up. Finally phase 3 comprises a cross-sectional study of a subset of 9 eyes from 7 patients, who underwent additional anatomico-functional testing. This includes OCT imaging (Zeiss Cirrus 5000), Optos California widefield scanning laser ophthalmoscopy (Optos, Marlborough, MA), microperimetry (MAIA, CentreVue, Padova, Italy), Humphrey perimetry (Carl Zeiss Meditec) and, where available, biometry (IOLMaster 700, Carl Zeiss Meditec) and autorefraction (ARK-510A, NidekCo. Aichi, Japan). Composite OCT images were created using open-source graphics editing software (GNU Image Manipulation Program).

5.3 RESULTS

1,221 patients, identified using the pre-specified search terms, had macula-involving retinoschisis, of whom 1,194 (98%) were excluded for other predisposing factors (as

detailed in Table 5-1). 35 eyes from the remaining 27 patients were considered to meet the criteria for categorisation as IFRS, of which 5 eyes were excluded from further analysis due to the existence of significant ocular co-pathology, including amblyopia, branch retinal vein occlusion and AMD.

Table 5-1: Pathologies associated with foveomacular retinoschisis

Pathology subgroup	Precise pathology	No. of patients
Mechanical	High myopia	531
	Vitreo-retinal interface disorders	243
	Optic disc pit	53
	Other peri-papillary disorders	15
Degenerative	Age-related macular degeneration	13
	Degenerative retinoschisis-detachment	12
Inherited	X-linked retinoschisis	170
	Enhanced s-cone syndrome	16
	Macular dystrophy	14
	Retinitis pigmentosa	5
	Best disease	5
	Other inherited	20
Inflammatory/vascular	Cystoid macular oedema	27
	Diabetic macular oedema	13
	Central serous chorioretinopathy	9
	Macular telangiectasia	5
	Other inflammatory/vascular	9
Neoplastic	Melanoma	19
	Naevus	7
	Other intra-ocular tumours	7
Iatrogenic	Nicotinic acid maculopathy	1
Idiopathic	Idiopathic foveomacular retinoschisis	27
Total		1221

5.3.1 Phase 1: Baseline characteristics of patients with idiopathic FRS

30 eyes (from 26 patients) were included in the phase 1 analysis. The mean (±SD) age at presentation was 60.1 (±15.6) years and 65% were female. The mean VA at baseline was 0.09 (±0.21), which was non-significantly different to that of fellow healthy eyes (0.00 ±0.12, p=0.081, Figure 5-5). 17/26 (65%) of patients were asymptomatic throughout, while 8 (31%) reported mild to moderate distortion or blurring. 1 eye (patient 8) had reported long-standing unexplained poor vision, despite normal electrodiagnostic tests. Baseline patient characteristics are summarised below in Table 5-2; Individual patient data are provided in further detail in Table 5-4).

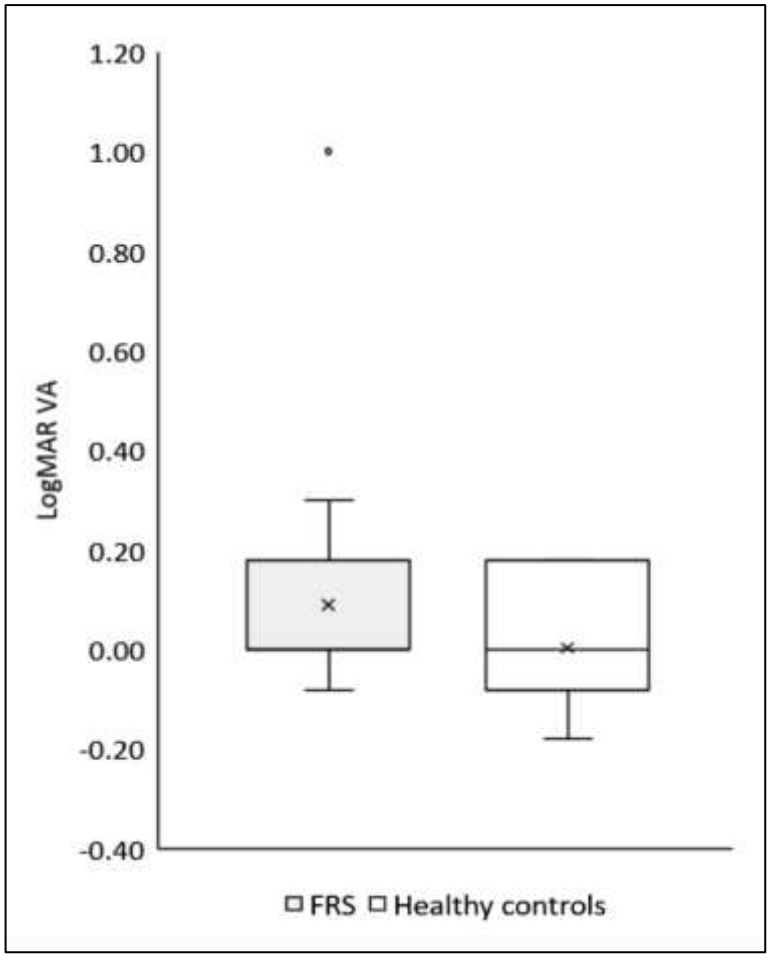

Figure 5-5: Comparison of logMAR VA between patients with IFRS and healthy fellow eyes

Table 5-2: Baseline patient characteristics for patients with idiopathic FRS

Characteristic (n(%)/mean ±SD)	**n=30 eyes**	
Age (years)	60.1 ±15.6	
Female sex	17 (65%)	
Ethnicity		
White	16 (57%)	
Black	3 (11%)	
Chinese	3 (11%)	
Other Asian	1 (4%)	
Not recorded	5 (18%)	
Right eye	13 (43%)	
Spherical equivalent (D)	-0.68 ±3.15	
Axial length (mm)	23.63 ±0.97	
	Affected eyes	**Fellow eyes**
Number of eyes	30	15
Visual acuity (logMAR)	0.09 ±0.21	0.00 ±0.12
Foveomacular retinoschisis	30 (100%)	0
Peripheral retinoschisis		
Present	18 (60%)	7 (47%)
Absent	2 (7%)	0
Not checked	10 (33%)	8 (53%)
Complete posterior vitreous detachment	4 (13%)	9 (60%)

One patient had a negative genetic test for RS1 mutation, while the remainder did not undergo testing based on a lack of anatomical or functional evidence for an inherited retinal disease phenotype, on specialist clinical assessment. 17/26 (65%) had a family history documented at the time of assessment, of whom 15 (88%) had no relevant history, while the remaining 2 patients were siblings. Approximately half of all eyes (12/27) had data for refractive SE or AL.. 7 patients also underwent ancillary electrodiagnostic testing, all of which were reported as grossly normal, although 2 reports mentioned patchy irregularity affecting the temporal retina on multifocal electroretinogram (mfERG).

All affected eyes had OCT evidence of FRS, which, in each case, involved HFL and extended beyond the limits of the macular cube scan temporally (Figure 5-6). 20 affected eyes had a contemporaneous comment regarding examination of the peripheral retina, of which 18 (90%) had recorded features of PRS on examination, one of which had a stable schisis-detachment. 27/30 (90%) affected eyes were also noted to have incomplete or anomalous separation of the posterior hyaloid on OCT.

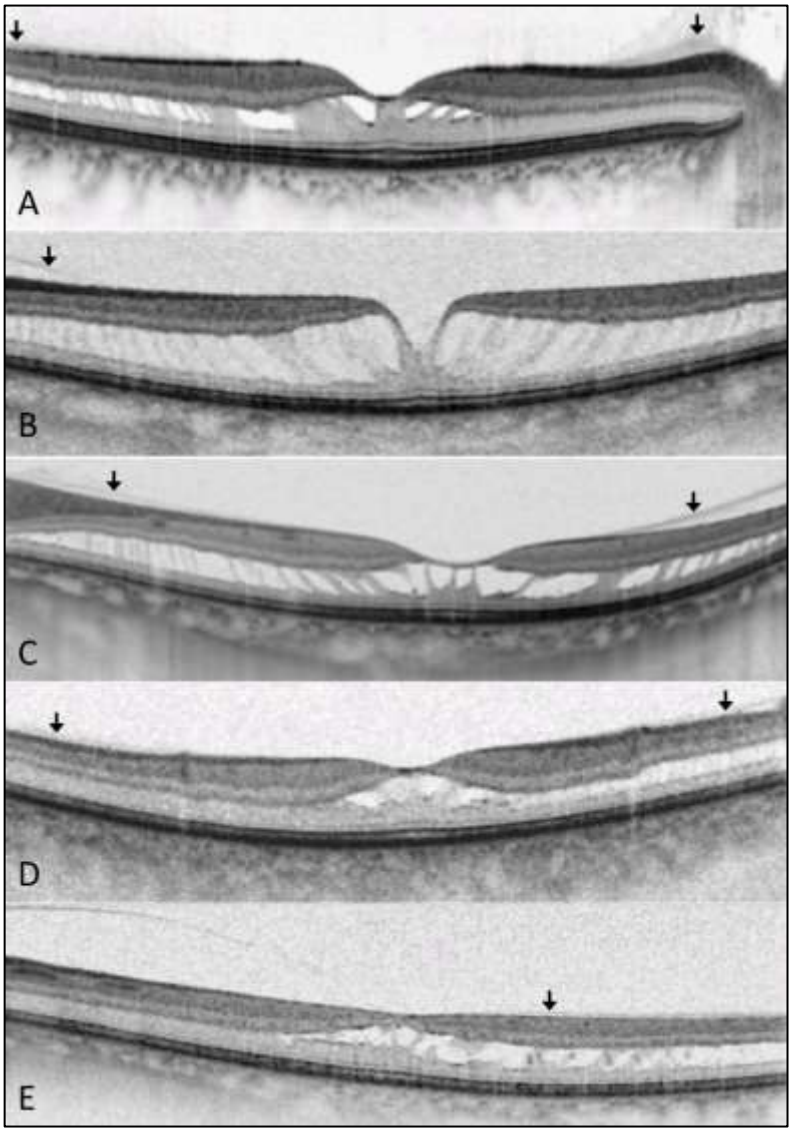

Figure 5-6: Examples of IFRS on OCT: (A-E): schisis cavity affects HFL only and extends into the temporal retina beyond the limits of the 6mm macular cube scan. Attachment of the posterior hyaloid is denoted by the black arrows. Credit: Bloch et al (2021) (725) [image reproduced with permission of the rights holder, LWW]

Furthermore, 15 patients had fellow eyes unaffected by FRS or other macular pathology, 7 (47%) of which also had documented evidence of PRS while only 6 (40%) had incomplete separation of the posterior hyaloid on OCT. This represented a significant association between absence of PVD and presence of FRS on chi squared testing with Fisher's exact test (p=0.002). Of note, 3 patient fellow eyes were not included due to a history of full thickness macular hole (FTMH) and 1 with lamellar macular hole, suggestive of prior disorder of the VMI.

5.3.2 Baseline quantitative OCT analysis

25/30 eyes (83%) had a Topcon OCT at baseline. The OCT parameters, including CRT, AvRT, CSH and SA, as well as comparative healthy fellow eye parameters, are summarised in Table 5-3 and Figure 5-7 below. There were significant differences in CRT and AvRT between affected and healthy fellow eyes at baseline (both p<0.001), but no difference in VA. There were no associations found between OCT parameters and VA in cases of FRS.

Table 5-3: Baseline OCT-based characteristics in eyes with idiopathic FRS and healthy fellow eyes

Characteristic [mean ±SD]	**Idiopathic FRS**	**Healthy fellow eyes**	***p-value***
Number of eyes	25	11	-
Age (years)	61 ±14	63 ±14	*0.559*
Visual acuity (logMAR)	0.09 ±0.22	0.00 ±0.12	*0.125*
Central retinal thickness (µm)	311 ±117	205 ±17	***<0.001***
Average retinal thickness (µm)	313 ±50	266 ±14	***<0.001***
Central schisis height (µm)	173 ±109	N/A	-
Schisis area (mm^2)	8.6 ±9.7	N/A	-

Table 5-4: Detailed IFRS patient characteristics

No.	Sex	Baseline age (yrs)	Eye	Ethnicity	SE (D)	AL (mm)	FRS	PRS	Complete PVD	Baseline VA (logMAR)	Final VA (logMAR)	Follow-up duration (months)	Symptoms	Comment
1	F	51	OS	White	+1.00	22.15	Y	Y	N	-0.08	0.00	53	Mild distortion	Eccentric mfERG abnormality
2	F	58	OS	Black	+0.50	22.55	Y	Y	N	-0.08	0.00	32	Asymptomatic	
3	M	70	OS	White	+2.00	NR	Y	Y	N	0.30	0.18	20	Mild blurring	
4	F	54	OD	White	-5.00	24.12	Y	Y	N	0.00	-	-	Asymptomatic	
			OS	White	-4.75	24.32	Y	Y	N	-0.08	-	-	Asymptomatic	
5	M	53	OD	White	+2.50	NR	Y	Y	N	0.00	-0.08	112	Mild distortion	
			OS	White	+2.50	NR	Y	Y	N	0.00	-0.08	112	Mild distortion	
6	M	20	OS	Chinese	-4.50	25.17	Y	Y	N	0.00	-	-	Asymptomatic	
7	F	25	OD	Chinese	-2.50	23.65	Y	Y	N	0.00	-	-	Mild distortion	
8	F	41	OD	White	NR	NR	Y	NR	N	1.00	1.48	134	Poor vision	Normal ERG
9	F	74	OS	Black	+2.25	NR	Y	NR	N	0.00	0.20	18	Asymptomatic	
10	F	60	OD	White	NR	NR	Y	Y	N	0.18	-0.08	118	Asymptomatic	
11	F	65	OS	White	NR	NR	Y	N	N	0.00	0.00	77	Asymptomatic	
12	M	70	OS	White	NR	NR	Y	NR	Y	0.18	0.00	29	Difficulty in dim light	Normal ERG
13	M	74	OS	NR	NR	NR	Y	Y	Y	0.00	-	-	Asymptomatic	
14	F	61	OS	NR	NR	NR	Y	N	N	-0.08	0.00	47	Asymptomatic	mfERG abnormalities peripherally
15	F	60	OD	Asian	NR	NR	Y	Y	N	0.00	-	-	Asymptomatic	
16	F	37	OS	Chinese	Emmetropia	23.27	Y	Y	N	0.18	-	-	Asymptomatic	Normal ERG
17	M	70	OD	Black	Hyperopia	NR	Y	NR	N	0.00	0.18	22	Mild distortion	
18	F	56	OD	White	+1.50	NR	Y	Y	N	0.00	0.00	29	Asymptomatic	
19	F	84	OD	White	NR	NR	Y	NR	Y	0.30	0.30	24	Blurred vision	
20	M	65	OD	NR	NR	NR	Y	NR	N	0.00	0.18	24	Asymptomatic	
			OS		NR	NR	Y	NR	N	0.00	0.18	24	Asymptomatic	
21	M	63	OD	Black	NR	NR	Y	NR	N	0.18	-	-	Asymptomatic	
			OS		NR	NR	Y	NR	N	0.18	-	-	Asymptomatic	
22	F	60	OD	White	NR	NR	Y	Y	N	0.00	0.00	14	Asymptomatic	
23	F	84	OS	NR	Pseudophakia	NR	Y	Y	N	0.30	0.30	26	Mild blurred vision	
24	F	71	OD	NR	Pseudophakia	23.77	Y	NR	N	0.00	0.18	17	Asymptomatic	
25	M	66	OS	White	Mild myopia	NR	Y	Y	N	-0.08	-	-	Asymptomatic	Normal ERG
26	F	71	OS	White	NR	NR	Y	Y	Y	0.18	0.18	79	Asymptomatic	Normal ERG

NR: not recorded

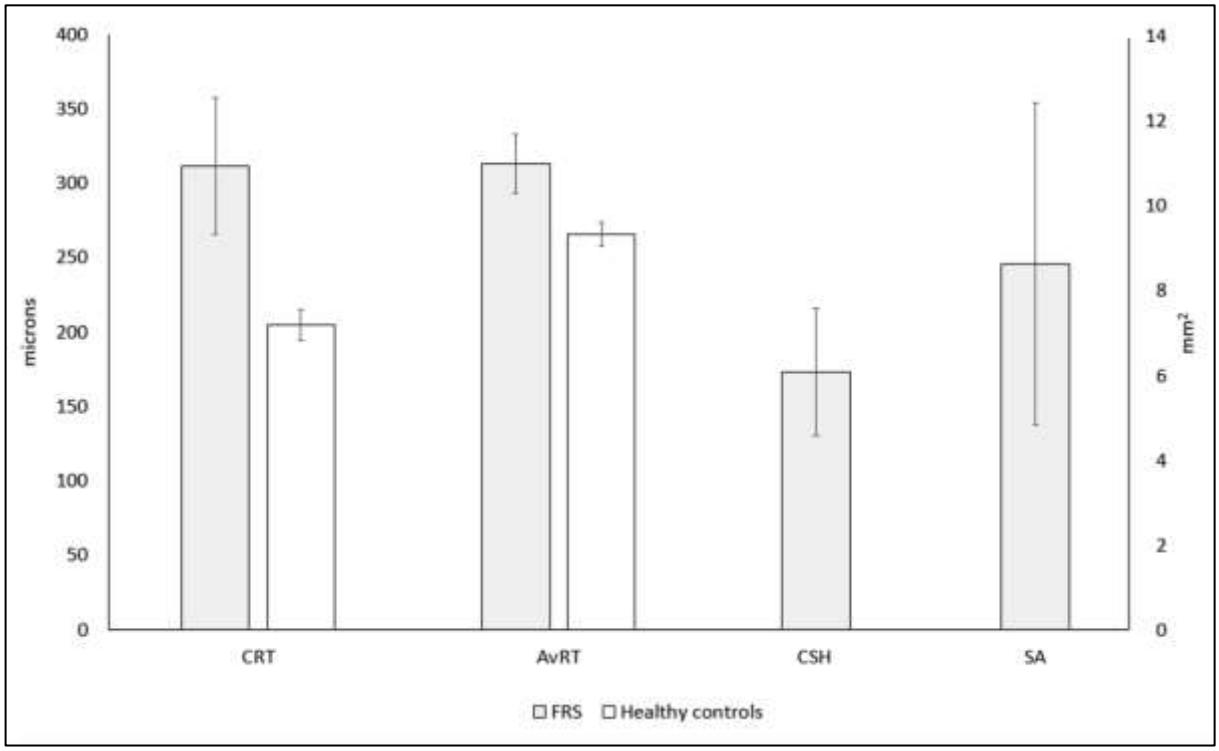

Figure 5-7: Comparison of quantitative OCT parameters in those with idiopathic FRS, compared to healthy fellow eyes (where applicable)

5.3.2.1 Subgroup analysis by age

Age followed a biphasic distribution, with 3 patients (6, 7 and 16) below 40-years-old at presentation, and the remaining 22 patients ranging from 41 to 84-years-old (Figure 5-8). Notably, all 3 patients in the younger age range were of Chinese ethnicity, two of whom were siblings; Patients 6 and 16 had suffered previous FTMHs in the fellow eyes, aged 20 and 17 respectively.

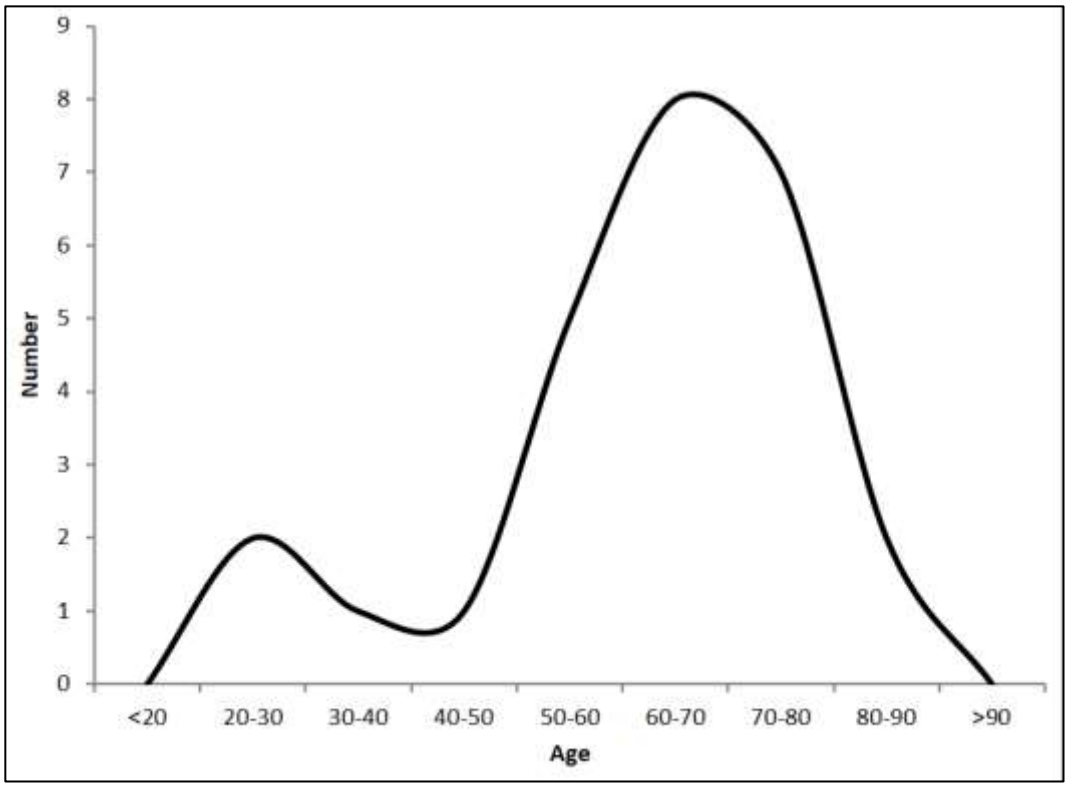

Figure 5-8: Biphasic age distribution in patients with idiopathic FRS

Demographic, functional and anatomical characteristics are summarised by age group in Table 5-5. Although functionally the groups were equivalent, significant differences in OCT groups were noted (albeit with OCT data only available in 2/3 eyes in the former group and 23/27 in the latter).

Table 5-5: Subgroup analysis by age (<40 compared to >40 years)

Characteristic [n (%); mean ±SD]	<40 years	>40 years	*p-value*
Number of patients	3	22	
Age (years)	28.1 ±8.4	64.8 ±10.2	***<0.001***
Female sex (n/%)	2 (67%)	15 (65%)	
Ethnicity (n/%)			
White	0	16 (64%)	
Black	0	3 (12%)	
Chinese	3 (100%)	0	
Other	0	1 (4%)	
Not recorded	0	5 (20%)	
Visual acuity (logMAR)	0.06 ±0.10	0.09 ±0.22	*1.000*
Central retinal thickness (µm)*	598 ±48	286 ±82	***0.007***
Central schisis height (µm)*	405 ±95	153 ±85	***0.013***
Average retinal thickness (µm)*	435 ±29	303 ±35	***0.007***
Schisis area (mm^2)*	27.5 ±0.7	7.0 ±8.1	***0.020***
**these parameters were only available for 2/3 eyes in group 1 and 23/27 in group 2*			

5.3.3 Phase 2: Longitudinal functional and anatomical follow-up

In 20 eyes (67%) with ≥12 months' follow-up data, mean VA at baseline was 0.11 ±0.25, and 0.16 ±0.34 at final follow-up (mean (±SD) duration of 4.2 ±3.3 years). This represents a non-significant change (p=0.260). Duration of follow-up was not associated with change in VA. These results are presented in Figure 5-9.

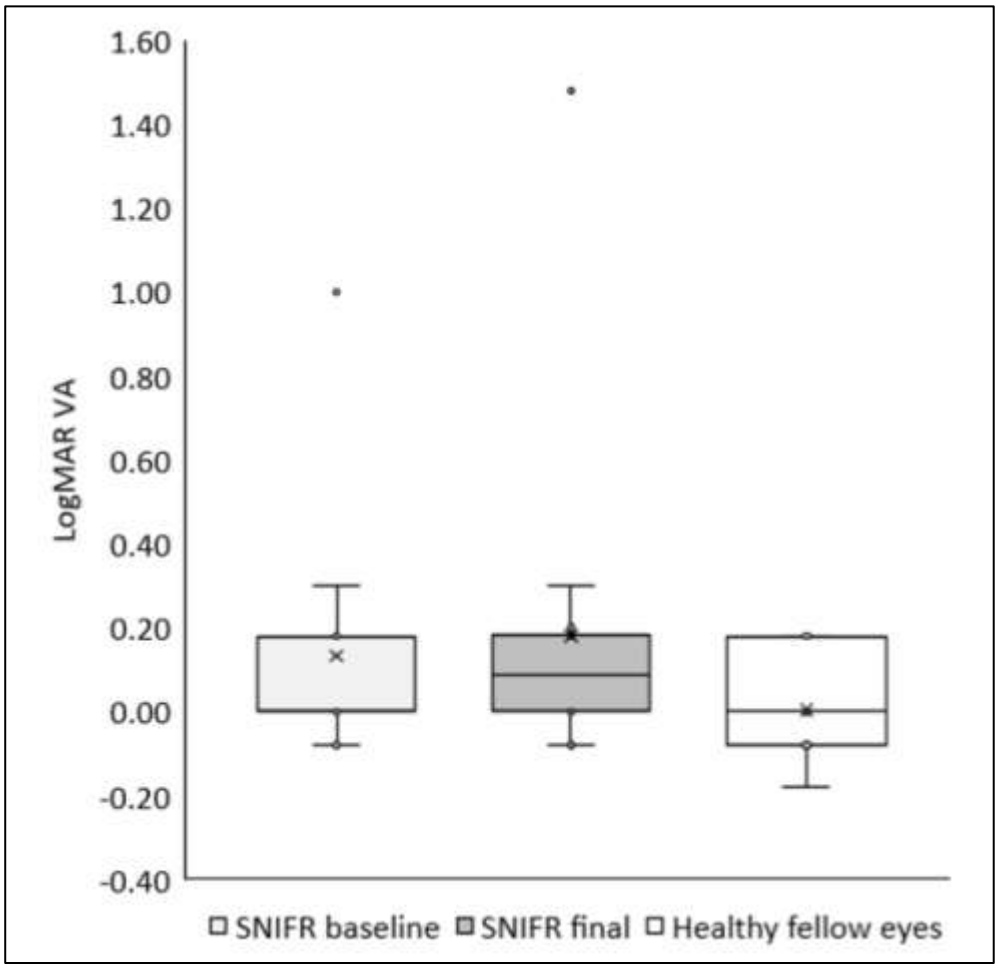

Figure 5-9: Within-group comparison of baseline and final VA in patients with idiopathic FRS, compared to healthy fellow eyes

Table 5-6: Longitudinal characteristics in patients with idiopathic FRS (n=14)

Characteristic [mean ±SD]	Baseline	Final follow-up	*p-value*
Visual acuity (logMAR)	0.11 ±0.28	0.18 ±0.39	*0.414*
Central retinal thickness (µm)	300 ±92	232 ±47	***0.012***
Average retinal thickness (µm)	306 ±35	286 ±37	*0.070*
Central schisis height (µm)	177 ±86	110 ±71	***0.025***
Schisis area (mm^2)	7.7 ±7.1	3.4 ±6.5	*0.058*

Of those patients with functional follow-up data, 14 eyes also had Topcon OCT imaging available at both baseline and final follow-up of ≥12 months, from which quantitative comparison could be made. Over a mean (±SD) period of 4.3 ±3.0 years, there was a significant decrease in CRT (mean -67µm, p=0.012) and CSH (mean -67µm, p=0.025), with a trend towards significant decreases in AvRT and schisis area (mean -20µm, p=0.070 and -4.3mm^2, p=0.060 respectively). There was no significant association with extent of change in OCT parameters and change in VA or duration of follow-up. These results, along with pairwise analysis, are presented in Table 5-6 and Figure 5-10.

During follow-up, 5 cases were observed to have undergone spontaneous complete PVD, with associated reduction in schisis height on OCT (see Figure 5-19A&B). However, given the overall pattern of longitudinal improvement across the cohort, PVD was not itself found to be significantly associated with a greater magnitude of change in either OCT parameters or VA.

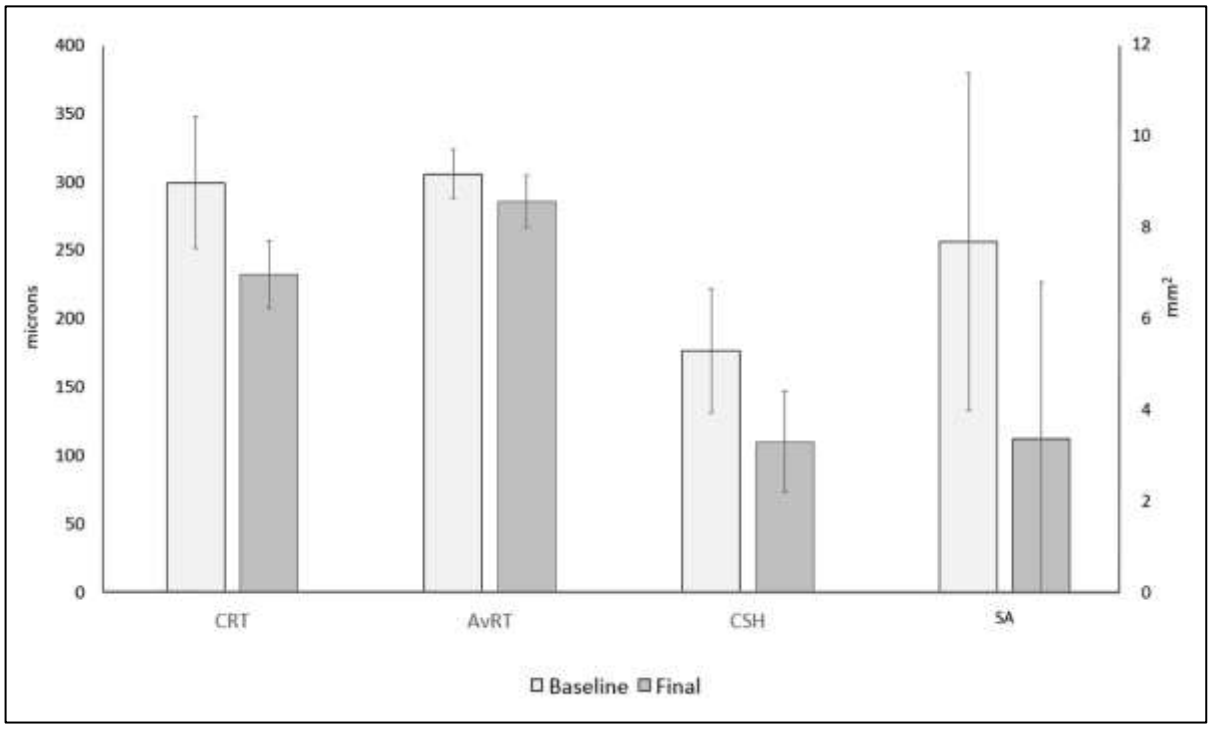

Figure 5-10: Baseline and final OCT parameters in patients with idiopathic FRS

5.3.4 Phase 3: Cross-sectional study

9 eyes (from patients 1-7) underwent further cross-sectional examination, multimodal imaging and functional testing. With reference to 5.3.2.1, two of these patients (6 and 7) belonged to the '<40 years' subgroup and are discussed separately below.

On biomicroscopic examination, all 7 eyes (from patients 1-5) demonstrated a stellate appearance at the macula and had peripheral features suggestive of PRS, including microcystoid degeneration and absolute scotoma. On the composite widefield OCT scans, the FRS was evident at the level of HFL and was continuous with PRS (and, in 1 case, schisis-detachment), at which point the schisis cavity appears to widen, involving different or multiple retinal layers (Figure 5-11C, Figure 5-12A&C & Figure 5-13B,G,L). Peripheral extension of the schisis cavity was observed in all cases on minimal intensity *en face* OCT projections (Figure 5-11E, Figure 5-12B,D, Figure 5-13C,H,M & Figure 5-14). All affected eyes had evidence of

posterior hyaloid attachment, to varying degrees, at the posterior pole, while the fellow eye in 4 unilaterally affected patients showed complete vitreous separation, but in conjunction with features of PRS (Figure 5-15). Functional peripheral loss was further demonstrated on 7 eyes with 60-4 ± 30-2 static visual field (VF) testing (Figure 5-11G & Figure 5-13E,J,O). In all cases, microperimetry demonstrated normal macular function, with a mean (±SD) average sensitivity 28.5 (±1.0) dB (Figure 5-11F & Figure 5-13D,I,N).

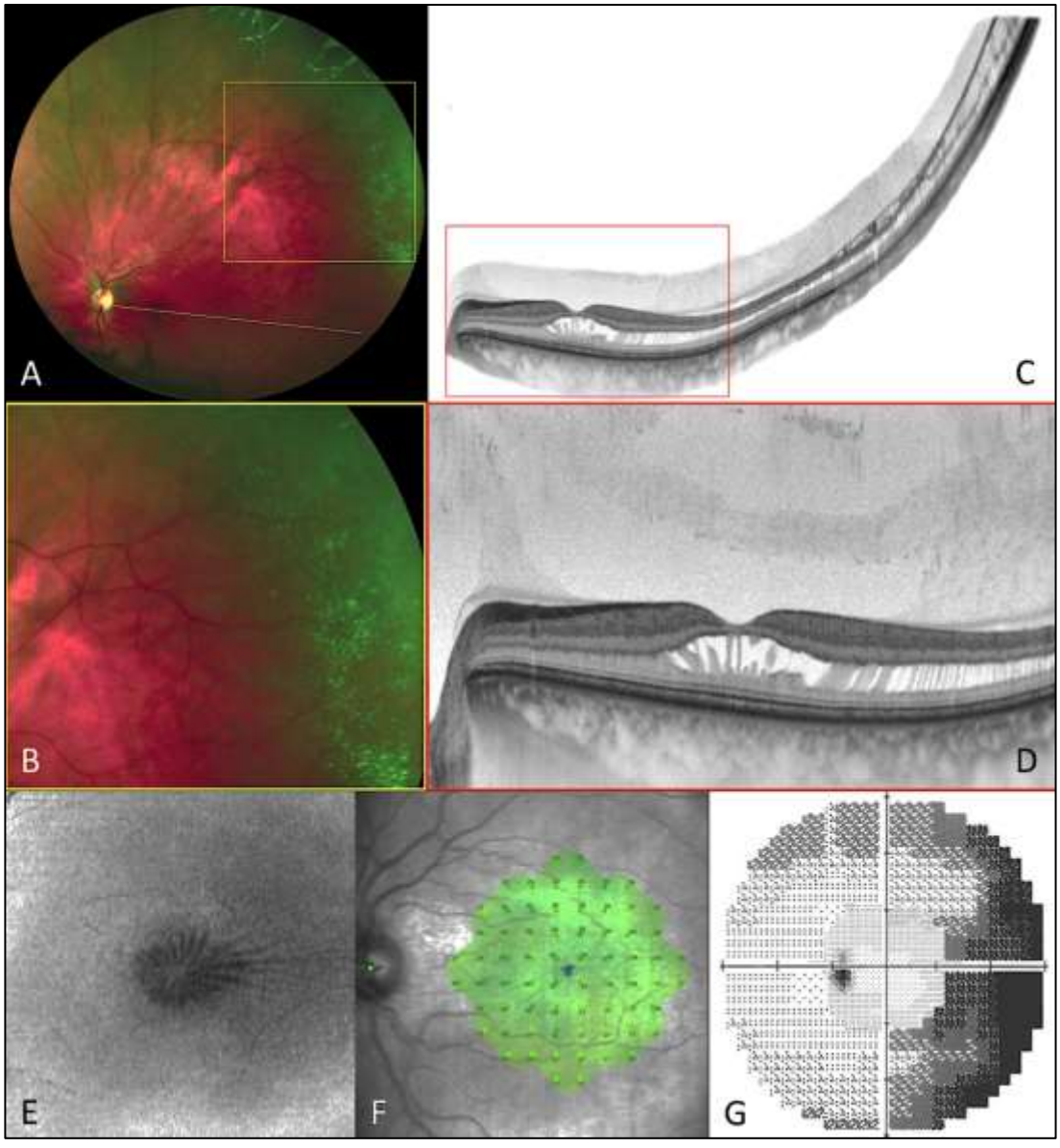

Figure 5-11: Images from patient 1 (OS): Optos widefield SLO imaging (A&B) reveals microcystoid changes in the temporal peripheral retina; widefield composite OCT (C) demonstrates continuity between the central FRS and PRS, with

posterior cortical vitreous attachment (D); en face projection of the mid-retina (E) shows the 'spoke-wheel' distribution of the schisis cavity; microperimetry (F) is normal, with evidence of scotoma in the nasal peripheral VF (corresponding to the temporal retinal changes) on 60-4 static perimetry (G). Credit: Bloch et al (2021) [images reproduced with permission of the rights holder, LWW]

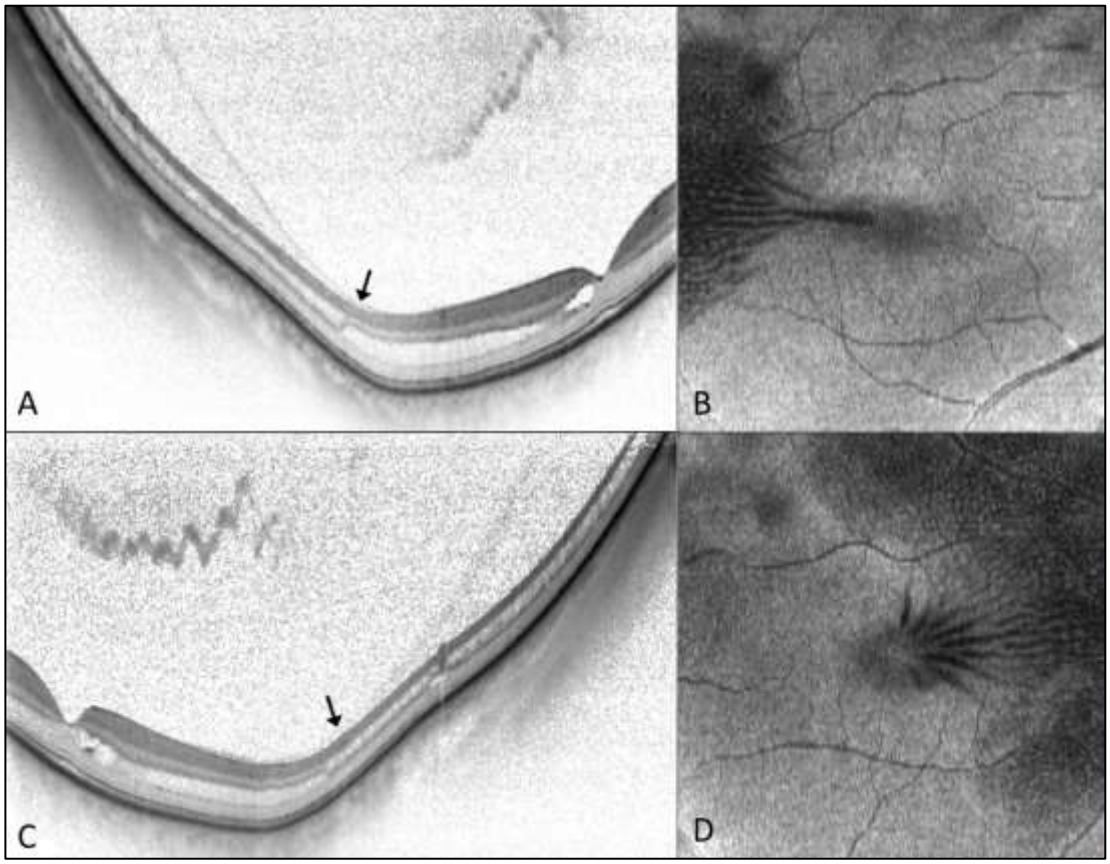

Figure 5-12: Images from patient 5 (OU): Widefield OCT (A&C) reveals a transition from HFL to the INL, with persistent attachment of the posterior hyaloid (black arrows); en face projection of the mid retina demonstrates the 'spoke-wheel' distribution of the schisis cavity, extending temporally (B&D). Credit: Bloch et al (2021) [images reproduced with permission of the rights holder, LWW]

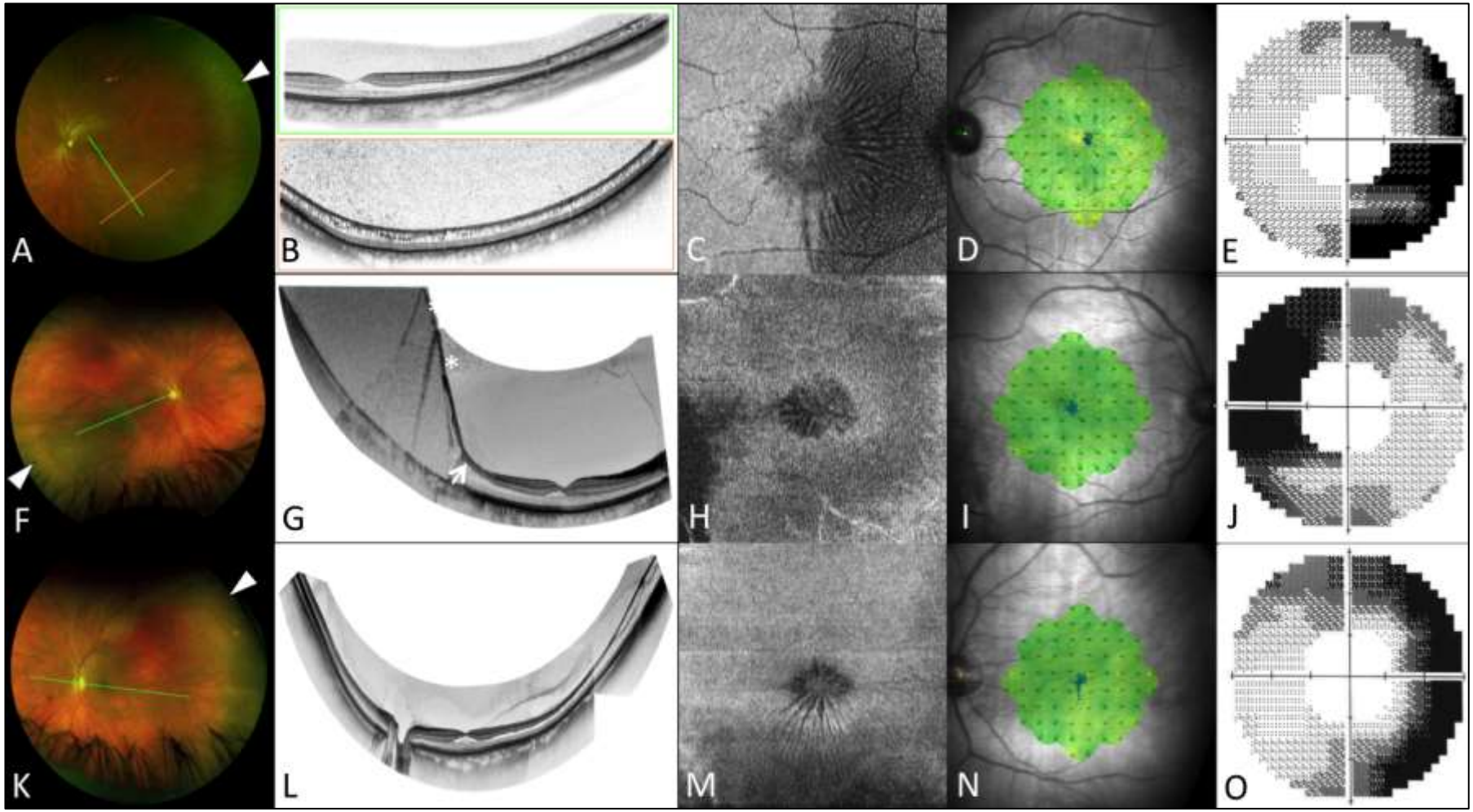

Figure 5-13: Images from patients 2 (OS) and 4 (OU): Optos widefield SLO imaging (A,F,K) demonstrates peripheral microcystoid changes (white arrow heads); widefield OCT composites (B,G,L) reveal continuity with peripheral retinoschisis (B&J) and schisis-detachment (F, arrow); asterisks denote mirror artefacts on OCT; En face projections of the mid-retina demonstrating the 'spoke-wheel' distribution of the schisis, extending peripherally (C,H,M); microperimetry (D,I,N) is normal, while 60-4 static perimetry (E,J,O) shows loss of sensitivity in the nasal VF. Credit: Bloch et al (2021) [images reproduced with permission of the rights holder, LWW]

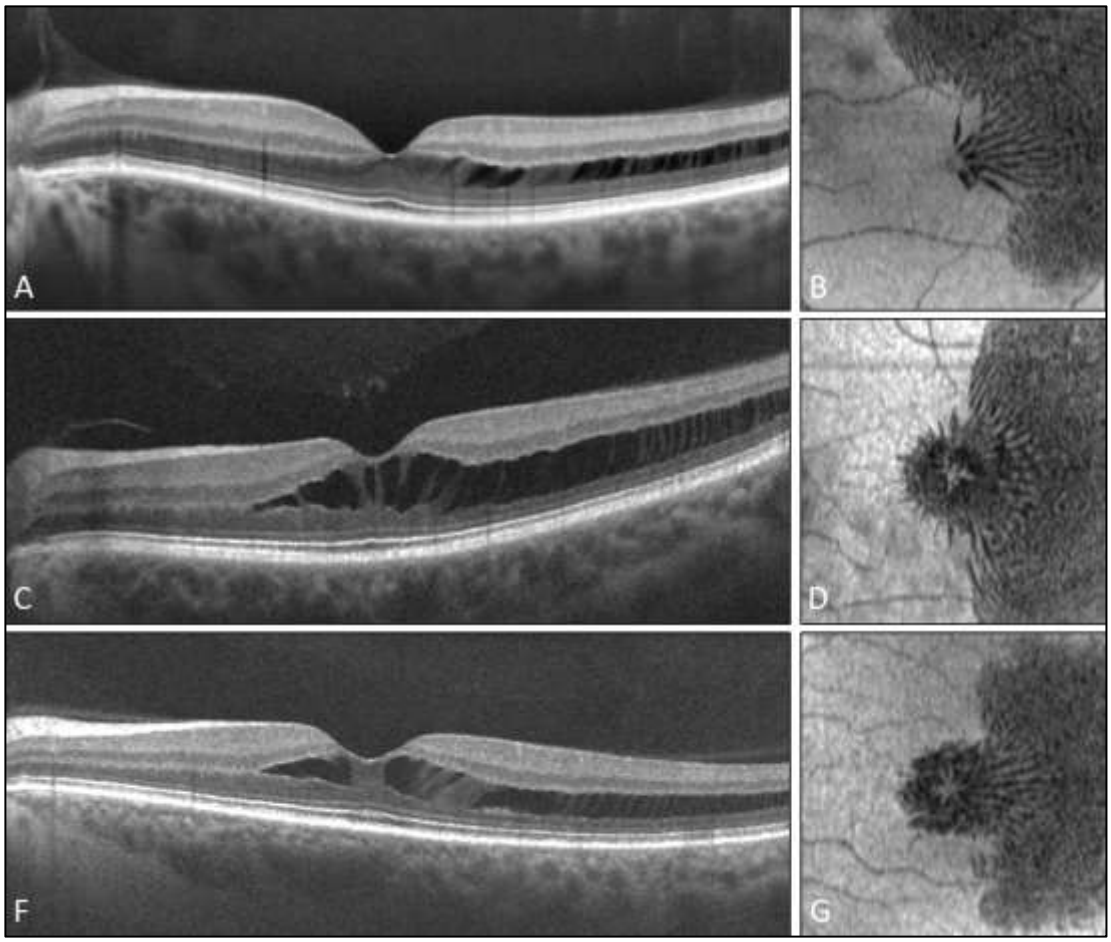

Figure 5-14: OCT (A,C,F) and minimal intensity en face projections (B,D,G) demonstrating the extent of schisis in cases of IFRS

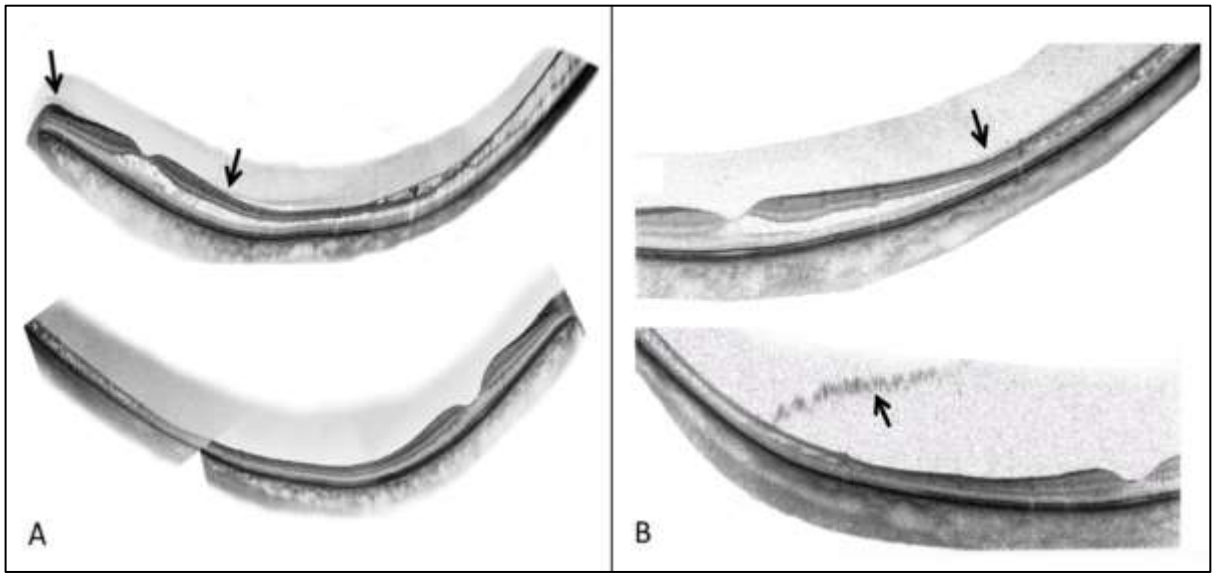

Figure 5-15: Comparison of affected and fellow eyes in patients 1 (A) and 2 (B): black arrows denote posterior hyaloid face

Patients 6 and 7 are siblings and also formed part of the '<40 years' subgroup. Due to the demographic and anatomical differences (see Table 5-5), I have reported these cases separately as part of the cross-sectional study. Examination of patient 6 revealed macular striae and loss of foveal contour (Figure 5-16A&B), with a glistening appearance in the peripheral retina. OCT revealed widespread FRS with partial detachment of the posterior hyaloid (Figure 5-16C&D). The presence of a large PPVP was suggestive of overlying vitreous liquefaction, while lamellar vitreoschisis indicated a mismatch in the degree of liquefaction anterior and posterior to the hyaloid face.

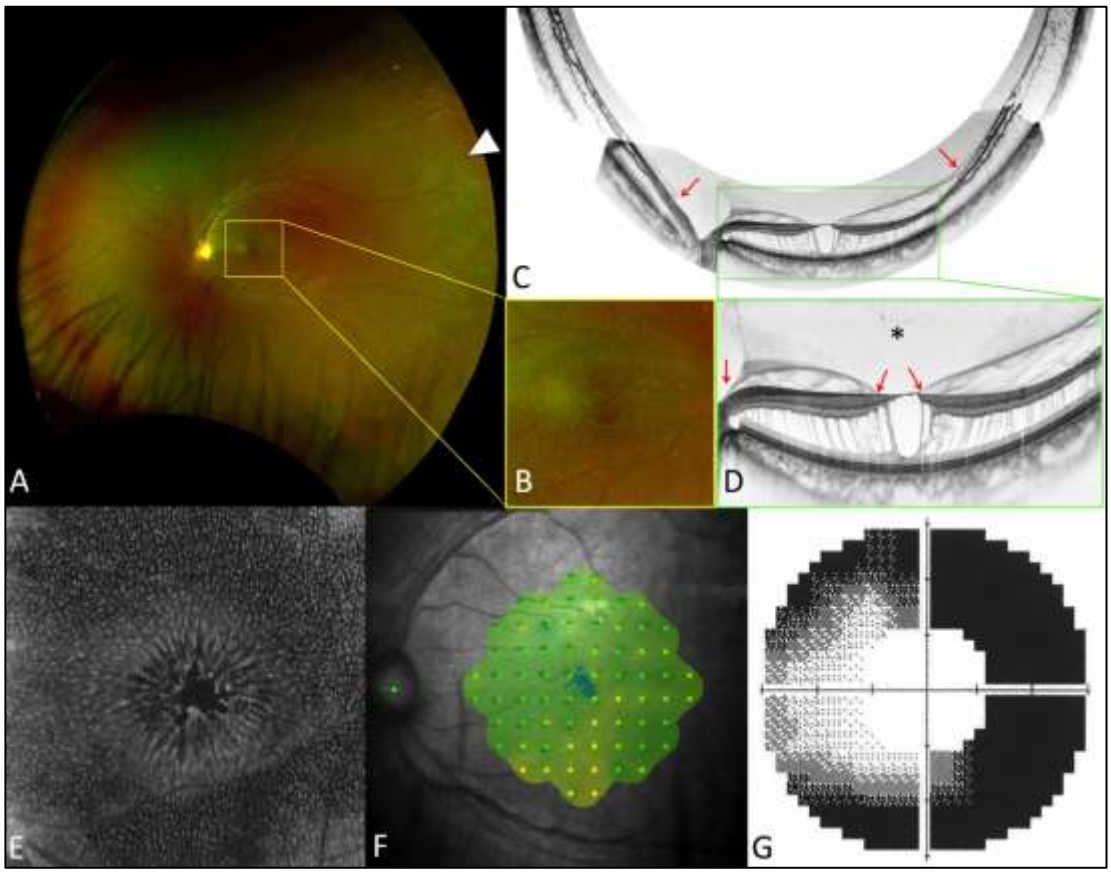

Figure 5-16: Images from patient 6: Optos widefield pseudocolour image (A) showing features of microcystoid degeneration (white arrowhead), with inset (B) showing foveal striae (B); composite and high-definition OCT scans (C&D) demonstrating enlarged posterior pre-cortical vitreous pocket (asterisk),

anomalous PVD with vitreoschisis (red arrows), traction and FRS; En face projection (E) showing FRS extent; microperimetry (F) and 60-4 Humphrey VF (G) demonstrate good central function with peripheral absolute scotoma, most marked in the nasal field

OCT of the peripheral retina in both patients revealed multi-layer PRS, more marked in patient 6 (Figure 5-16C and Figure 5-17C), once again associated with posterior hyaloid attachment. Functional testing showed good central retinal function (Figure 5-16F & Figure 5-17F), while, in patient 6, there was an extensive absolute scotoma (Figure 5-16G). Visual acuities in the affected eyes were normal in both cases (logMAR 0.00), while AL and SE were normal (25.17mm and 23.65) and moderately myopic (-4.50D and -2.50D) respectively.

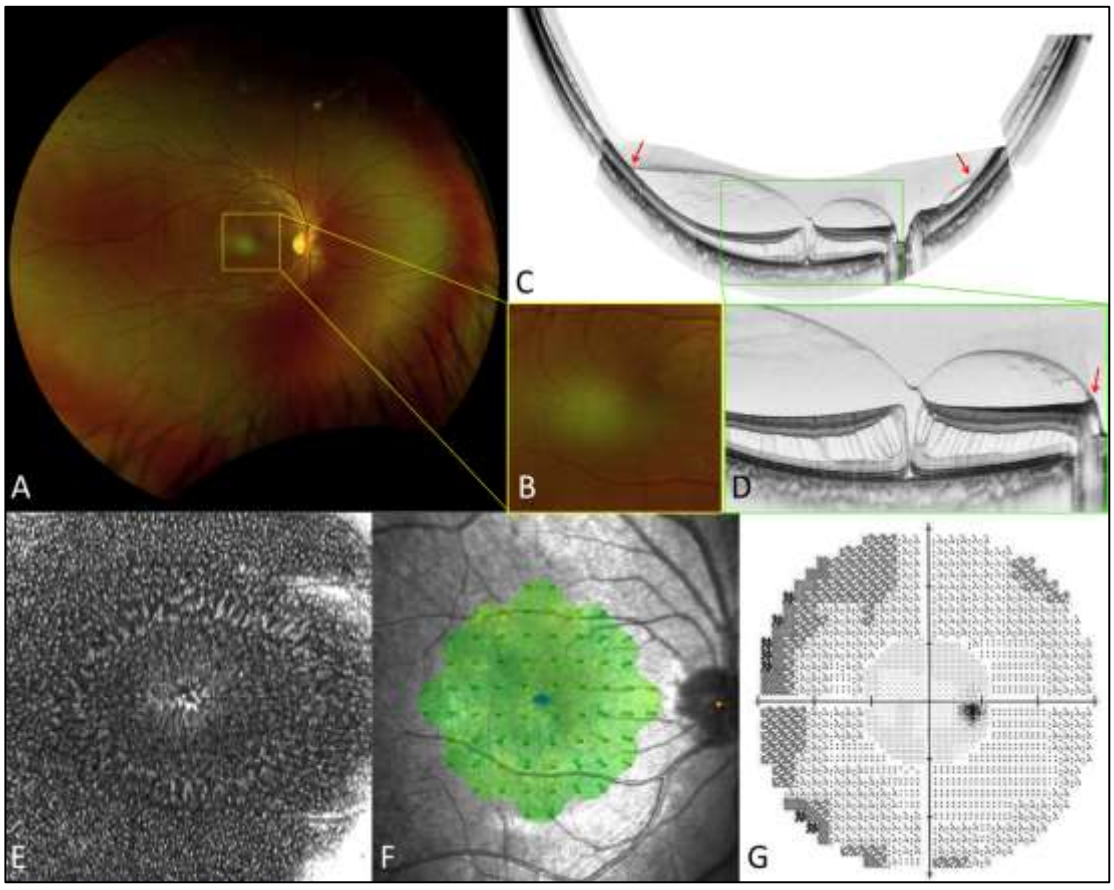

Figure 5-17: Images from patient 7 (sibling of patient 6): Optos widefield pseudocolour image (A) with inset (B) showing foveal striae (B); Composite and high-definition OCT scans (C&D) demonstrating anomalous PVD with vitreoschisis

(red arrows), traction and FRS; en face projection (E) showing FRS extent; microperimetry (F) and 60-4 Humphrey VF (G) demonstrate good central function with mild nasal VF loss

Examination of patient 7's fellow eye revealed complete separation of the posterior cortical vitreous at the fovea, with an absence of FRS, but shallow PRS associated with attachment of the posterior hyaloid (Figure 5-18).

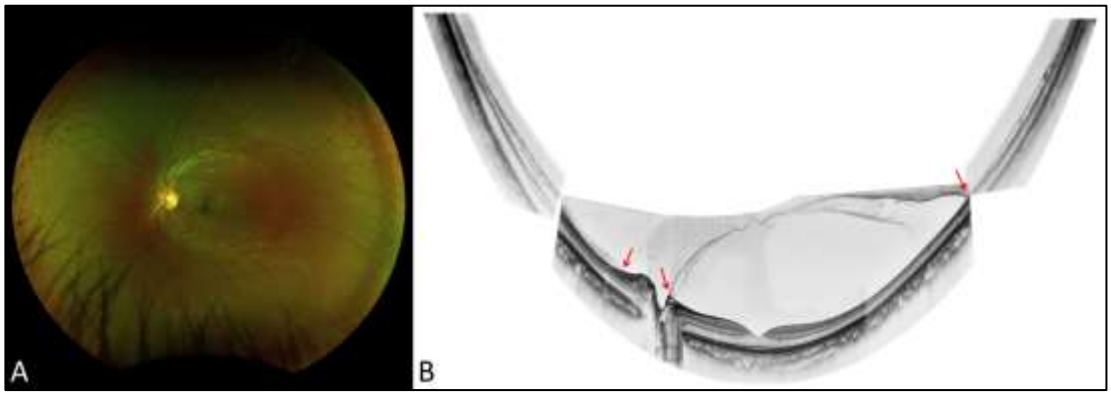

Figure 5-18: Fellow eye of patient 7 (A&B), revealing complete separation of posterior vitreous cortex over the macula, with reattachment at the mid-periphery associated with shallow PRS

In view of a potentially inherited mechanism in patients 6 and 7, the patients' (non-consanguineous) parents were also examined. Their mother had developed a FTMH aged 48, surgery for which was unsuccessful, while their father was a borderline high myope with a prior ophthalmic history of retinal tear only. On examination and imaging, neither parent had contemporaneous features of retinoschisis or evidence of anomalous vitreoretinal behaviour. Genetic testing was performed on both affected patients, which did not reveal any point mutations on a retinal dystrophy panel, including *RS1* and *CRB1* testing.

5.4 Discussion

In this chapter, I have presented a combination of retrospective and cross-sectional, observational data from 30 eyes affected with idiopathic foveomacular retinoschisis. Mean age at presentation of 60.1 years and slight female preponderance is in keeping with previous reports and supports the notion that vitreous liquefaction and anomalous PVD, which is known to occur earlier and more frequently in female patients, may play a role (671,726).

Of those with contemporaneous documentation, 90% had evidence of PRS in addition to FRS. Moreover, in those who underwent cross-sectional functional testing, a discrepancy was noted in the anatomico-functional behaviour between the areas affected by retinoschisis centrally and peripherally. All of our patients' microperimetric findings support the consensus in the literature that SNIFR does not, for the most part, lead to significant loss of macular function (671). However, it appears that there is a transition zone, in the mid-periphery, where both the anatomical and functional characteristics of the retinoschisis changes, from a cavitation solely within HFL to one including the INL and, in some cases, also the NFL (see Figure 5-11Figure 5-12 & Figure 5-13). At approximately this point, the 60-4 static perimetry demonstrates the presence of a dense VF defect. Here, the retinoschisis is behaving in a functional manner that one would traditionally expect with acquired PRS, i.e. with a negative absolute scotoma. While it is reassuring that the central retina appears to be spared such degeneration, the loss of peripheral field could challenge the purportedly benign course of SNIFR. The precise mechanism by which acquired retinoschisis causes absolute scotoma in the periphery is unclear, but may be attributable to erosion of the neuroretinal and glial support elements during coalescence of microcystoid cavities (705,727). Natural history studies of PRS have previously shown central involvement to be extremely rare, however these studies pre-date the widespread use of high-resolution OCT (693,695). In Ober et al's 2014 retrospective study, 6 eyes from 4 patients were demonstrated to have concurrent PRS, while several subsequent case studies, which have attributed findings of FRS to SNIFR, have also demonstrated evidence of

concurrent extramacular schisis (although these features were not considered of primary relevance in these reports) (672,674,675,679).

Another novel observation is the large proportion of eyes with anomalous or incomplete PVD (86%) compared to those unaffected fellow eyes (42%). Furthermore, the presence of VMI abnormalities in 5 excluded or fellow eyes lends further support to the possible role of anomalous PVD in patients predisposed to developing the features of SNIFR. In Ober et al's study, a total of 19 eyes (86%) were reported *not* to have evidence of PVD (despite an average age of 61 in a predominantly myopic cohort) (671). This is consistent with other case reports of SNIFR in the literature, of which 80% do not have complete vitreous separation (672–676,678–681,683). Since the publication of this study, a further case report has also demonstrated resolution of FRS following release of VMA (680).

It is also notable that the unaffected fellow eyes of several patients had evidence of PRS, but without FRS. This asymmetric finding has been described previously in a single case by Ahmed et al., who ascribed it to possible "early stage of stellate nonhereditary idiopathic retinoschisis without foveal involvement" (674). This hypothesis presumes that SNIFR is preceded by PRS, which extends to involve the central retina. The observation of concurrent PRS and FRS, as in these cases of SNIFR, indeed lends credence to the plausibility of a common pathophysiological mechanism, but the developmental chronology remains to be clarified. In this study, I found a significantly greater proportion of fellow eyes with PRS but without FRS had evidence of complete PVD. Given the relative frequency at which PRS is observed in the general population, it could be postulated that the concomitant manifestation of FRS might only be rarely observed, in the context of a co-existent adherent posterior cortical vitreous. A widefield imaging study by Choudhry et al in 2016 revealed structural approximation of the peripheral posterior cortical vitreous face with the inner retina in a case of senile retinoschisis (Figure 5-4). However, the precise relevance of vitreous behaviour in PRS remains unclear (710).

Further clues to the pathoanatomy of SNIFR can be investigated by studying the longitudinal natural history. In phase 2 of this study, 20 eyes underwent follow-up of

≥12 months, during which time there was significant reduction in CRT, CSH and a trend towards a reduction in both SA and AvRT. Throughout this period, there was no significant change in VA. Considering the aforementioned association between posterior hyaloid attachment and FRS, we might expect spontaneous PVD to have played a role in the observed anatomical improvement (680). However, only 25% of cases were observed to undergo PVD (based on review of OCT) and this did not manifest in greater improvement than those with residual posterior cortical vitreous attachment, due to the overall trend for spontaneous resolution (Figure 5-19). This does not necessarily support or counter the notion of a tractional aetiology, since other dynamic changes in the VRI, such as anomalous PVD, including vitreoschisis or syneresis, cannot be discounted. It does, however, indicate that SNIFR is generally a functionally stable condition, regardless of chronicity. One patient in this study underwent pars plana vitrectomy, although it was abandoned due to a perceived high risk of iatrogenic damage due to the mobility of the inner schitic retina during internal limiting membrane peeling. There is not a strong indication from this study, or the literature, that surgical intervention is likely to be functionally beneficial (and in fact may be detrimental), although resolution of schisis following vitrectomy +/- induction of PVD would lend further support to the notion of a tractional aetiology (680,684).

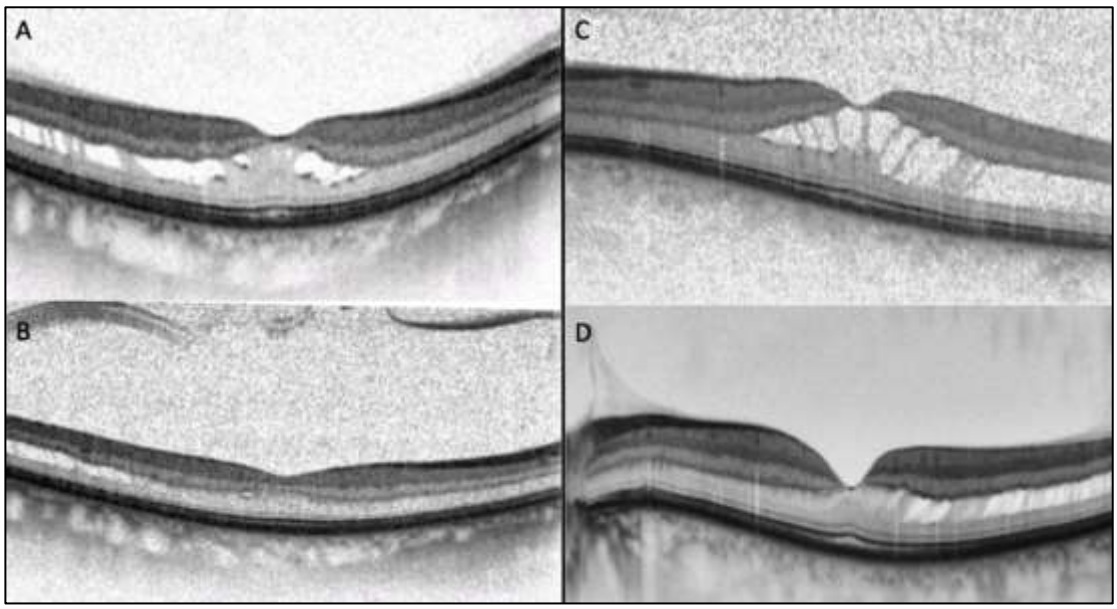

Figure 5-19: Longitudinal follow-up of 2 patients with idiopathic FRS: (A&B) improvement of FRS with evidence of PVD; (C&D): improvement in schisis in the absence of observed PVD

The pathoanatomical mechanism by which tractional macular disorders, such as ERM or VMT, lead to the formation of FRS has been discussed in 1.3. It is proposed that, under normal conditions, the combined action of a specialised MC subpopulation in the MCC and 'typical' zMCs in the foveal walls, form and maintain the foveal ultrastructure (99). The orientation of the zMCs appears to provide a degree of anatomical compliance, allowing the retention of function in the presence of significant foveal deformation. On OCT, anteroposterior and tangential traction (such as those observed in tractional disorders of the VMI) manifests with progressive beveling of columnar retinal elements (thought to include MC processes), which obliquely span the schisis cavity. This anatomical phenomenon is thought to be responsible for the radiating 'spoke-wheel' pattern, as seen on *en face* imaging (100,335). VA is preserved at the point that the MC processes are in a beveled orientation, only deteriorating once the processes become fully verticalised. At this stage, it is presumed that the tensile capacity of the MCs is overcome and, as a result, mechanical disruption of the fovea may occur, as demonstrated in both MFS and ODP-M (98–100,141).

While our cases do not have angiographic data to support an absence of exudative macular edema, the OCT and *en face* images are highly supportive of a similar pathoanatomical mechanism in IFRS. Furthermore, the discrepancy observed between the anatomico-functional behaviour of the retina centrally and peripherally could potentially be explained by a difference in MC morphology. Outside the macula, MCs are vertical in their resting state (Figure 1-9). As such, retinal deformation through traction would be expected to occur earlier in this subpopulation, which may result in the observed multi-layer retinoschisis and associated functional decline (presumably as a result of early neuro-glial disruption) (9,22). This anatomic variability is best observed on the *en face* images (e.g. Figure 5-16E), where the 'spoke-wheel' pattern of the beveled MC processes, centred on

the fovea, progressively verticalises into the perifoveal and mid-peripheral retina, giving rise to a 'speckled' appearance. This indicates that the zMCs of the fovea provide an important protective role, in allowing a degree of retinal deformation, while protecting central visual function.

With the exception of patient 7 (Figure 5-17), there were no cases of development of FD or P/FTMH during the follow-up period in this study, nor was VA significantly reduced in affected eyes. This supports the assertion that functional decline is only observed in the context of excessive MC stretch, (i.e. >400µm, as seen ODP-M), but not in the cases of IFRS, where the mean (±SD) CSH was 173µm (±109) (100).

Considering all these findings together, I suggest that not only is there an association between central and peripheral retinoschisis in idiopathic FRS, but that this disorder demonstrates the hallmark features of a tractional pathology. Considering the age of onset and the association with persistent attachment of the posterior cortical vitreous, it appears that the most probable explanatory mechanism involves abnormally adherent posterior hyaloid in the presence of normal vitreous synchysis and syneresis. The natural history is favourable for good long-term anatomical and functional outcomes, caveated with the potential for a significant reduction in peripheral VF, related to PRS. The merit of regular monitoring in cases of IFRS is questionable, but annual surveillance would appear to be a reasonable and safe approach.

5.4.1 Differentiating SNIFR from other causes of FRS

SNIFR is essentially a descriptive diagnosis only and one of exclusion. In view of a potentially tractional mechanism, it is important to distinguish SNIFR from other mechanical causes of FRS, which may share morphological characteristics. In particular, the presence of high myopia, VMT or an ERM may indicate an alternative mechanism (100,335,337,385); continuity with the optic nerve ought to raise suspicion of ODP-M or glaucoma-associated retinoschisis (508,582). Inherited retinal

disease should be considered as a possible cause in all young patients with cystoid spaces and IS/OS disruption on OCT (258,288,308).

Additionally, in 2019, Sun et al. reported a series of 17 eyes from 10 Chinese subjects, the majority (80%) of whom were female, of mean age 41 years, with mild myopia (-1.25 to -5.00) (728). In the first report of its kind, they described a condition, distinct from SNIFR, which manifests with rapid progression from FRS to the development of P/FTMH and/or FD, with a mean vision at presentation of 0.88 logMAR (Figure 5-20A&B). 13/17 of eyes underwent PPV, ILM peeling and gas tamponade, followed by a visual recovery to a mean of 0.18 logMAR. At the time of surgery, they noted "remarkable liquefaction of the core vitreous" and had difficulty inducing PVD due to "tight vitreo-macular attachment, and poor ILM compliance".

Based on these findings by Sun et al, I performed a sub-analysis of those patients who were <40-years-old (see 5.3.2.1); three patients were identified, all of whom were of Chinese origin and two of whom were siblings. Although all these patients demonstrated good central macular function, similar to those with SNIFR, the distinct demographic characteristics, as well as a evidence of early-onset VRI disorders (fellow eye FTMHs in patients 6 and 16 and vitreoschisis in patients 6 and 7), is supportive of Sun et al's suggestion of another clinical disorder, distinct from SNIFR, which follows a more progressive course. The findings in this study also suggest that this pathology manifests with a larger schisis height and extent than SNIFR. Similar to SNIFR, the FRS may extend to involve the peripheral retina, causing retinoschisis that may lead to functional loss, to a seemingly varying degree. Yassur et al have previously reported the co-existence of both peripheral retinoschisis and FRS in such cases, which were often, but not exclusively, young, moderate myopes, while Yang and Chen demonstrated a similar morphology in a single case report of a 41-year-old Chinese woman (296,729). Despite Sun et al.'s description of a lack of PRS in their group, they published 2 images demonstrating extramacular schisis (Figure 5-20C) and it would be interesting to know the results of both anatomical and functional investigations of the peripheral retina in this cohort (728).

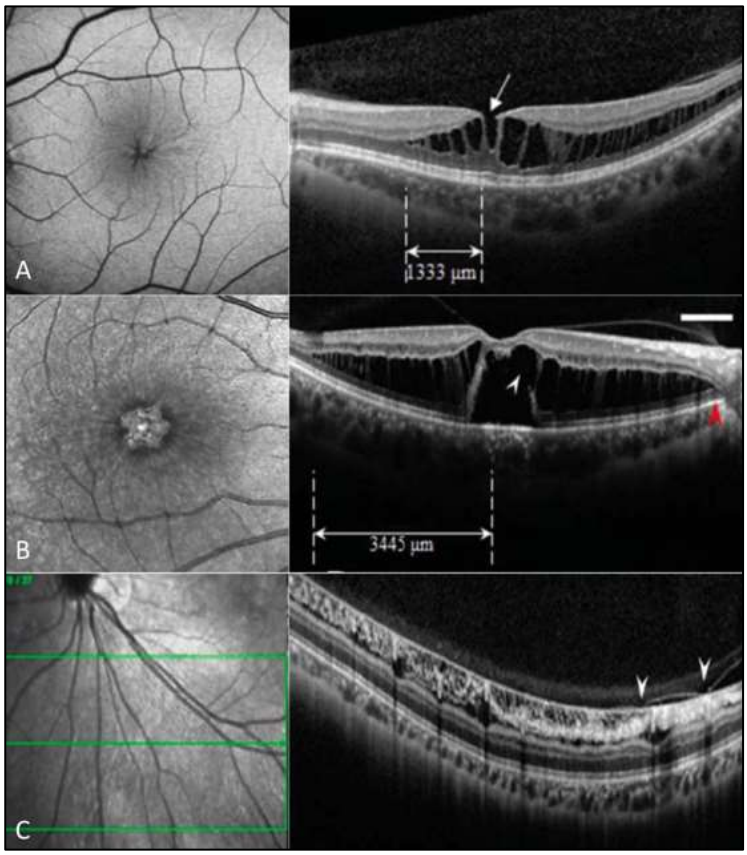

Figure 5-20: Near-infrared and OCT imaging from Sun et al's cohort; (A): FRS with small inner lamellar defect (white arrow); (B): FD with OLH (white arrow head); (C): extramacular schisis with persistent vitreous adhesion over retinal vessels (white arrowheads). Credit: Sun et al (2019) (728) [images reproduced with permission of the rights holder, LWW]

Based on presence of this disorder in siblings, it is conceivable that patients affected with IFRS may have a familial predisposition. Several case reports have also reported a possible familial trait for FRS in young, often related, female individuals, which has been postulated to follow either an autosomal recessive or a dominant mode of inheritance (277–279,296,297). In 1988, Han et al reported FRS with peripheral degeneration in a 56-year-old, whose 4 daughters also all showed evidence of cystoid degeneration or PRS (279). These findings appear to challenge the inclusion of 'non-hereditary' in the term SNIFR. Although no genetic mutations were observed in the *RS1* or *CRB1* genes in these siblings, further genome-wide association studies may reveal whether those with IFRS have an inherent predisposition.

I agree that this disorder, reported by Sun et al, is a distinct clinical entity to SNIFR (as described by Ober et al), but postulate that they may share common features, in particular a lack of complete PVD with tight vitreomacular adherence. Perhaps the difference in patient demographic reflects the premature vitreous liquefaction and longer AL in Sun et al's cohort, compared to the normal age of liquefaction at which those patients with SNIFR seem to be affected. As opposed to SNIFR, traction in this sub-cohort causes more rapid and pronounced stretch of the zMCs of the fovea (e.g. CSH 405μm vs 153μm), resulting in the observed mechanical decompensation. Due to the different natural history and management approach, it is important to distinguish the two disorders. To reflect this distinction, I suggest the term 'stellate progressive liquefaction-induced foveomacular retinoschisis' (SPLIFR). In Table 5-7 I have detailed the comparative features of both SNIFR and SPLIFR, based on the findings from this study and existing evidence in the literature (671–675,677–679,728). Those with SPLIFR are, on average, younger, more myopic and have a higher rate of progression to P/FTMH +/- FD (81% vs 2%) than those with SNIFR. There is a greater proportion of bilateral cases in SPLIFR, than in SNIFR. The sex distribution is similar between groups, with a greater propensity for female patients to be affected in both cases.

Table 5-7: Comparison of features in 'SNIFR' and 'SPLIFR'

Characteristic [n (%); mean ±SD]	**'SNIFR'**	**'SPLIFR'**
Number of subjects	47	14
Number of eyes	58	21
Mean age (range)	62 years (36-85)	23 years (15-41)
Sex	38/47 (81%) female	11/14 (79%) female
Right eye affected	33/58 (57%)	11/21 (52%)
Laterality	11/47 (23%) bilateral	7/14 (50%) bilateral
Spherical equivalent	-5.00 to +2.25 (n=10)	-5.00 to -1.25 (n=19)
Axial length	22.15 – 24.32 (n=6)	23.09 – 25.17 (n=19)
Baseline VA (logMAR)	0.12 ±0.21	0.57 ±0.50
Familial pattern	Not demonstrated	Demonstrated
Foveomacular retinoschisis	58/58 (100%)	21/21 (100%)
Peripheral retinoschisis	26/28 (93%)*	3/3 (100%)*
Posterior vitreous detachment	10/56 (18%)*	0/21 (0%)*
Partial thickness macular hole	0/58 (0%)	10/21 (48%)
Full thickness macular hole	0/58 (0%)	6/21 (29%)
Foveal detachment	1/58 (2%)	13/21 (62%)
Total holes/detachments	1/58 (2%)	17/21 (81%)
Follow-up duration (range)	0 – 134 months	0 – 60+ months
*Only including those subjects that had a comment on the presence or absence of PVD/PRS		

This study is limited by the retrospective design, resulting in incomplete collection of data, such as SE, AL or investigations, including genetic testing, fluorescein or OCT angiography. In this regard, I am not in a position to explore certain associations, such as the relationship between refractive error and IFRS, or confirm a definite absence of inherited or exudative pathology. Furthermore, documented presence or absence of PVD and PRS was variable and, in this study, OCT was used to determine PVD status. Although inferior to ultrasonographic examination, OCT has been shown to have a high negative predictive value for PVD (730).

Overall, I have shown that forms of idiopathic FRS, which account for up to 2% of all recorded cases of FRS, appear to be associated with both PRS and anomalous or

incomplete PVD, in the largest study of this disorder to date. In these cases, retinoschisis manifests with different anatomico-functional behaviour at the macula to the periphery, exhibiting apparent long-term stability of visual acuity, despite peripheral absolute scotoma. The reason for this observed discrepancy remains unclear, but may relate to ultrastructural variations in the retina between the macula and the periphery, such as the anatomical conformation of glial support cells (e.g. MCs) or variable properties of the VRI. Further identification and characterisation of such cases using prospective multimodal anatomico-functional testing may shed further light the precise relationship.

5.5 Conclusion

In conclusion, idiopathic foveomacular retinoschisis appears to be associated with peripheral retinoshisis and incomplete or anomalous posterior vitreous detachment. At least two subtypes have been described, herein referred to as SNIFR and SPLIFR, which may share commonalities in terms of pathophysiology, but have separate demographic features and follow differing natural anatomico-functional courses. SNIFR has a favourable prognosis, with functional stability and anatomical improvement on longitudinal follow-up. By contrast, SPLIFR appears to be a rapidly progressive form of FRS, associated with functional decline, frequently meriting surgical intervention.

I propose that all patients with features of stellate FRS undergo widefield imaging and VF testing to identify any concurrent peripheral retinal disease or anomalous vitreoretinal interaction, as this may provide more insight into the precise pathomechanism of this peculiar group of vitreoretinal disorders.

CHAPTER 6

A CROSS-SECTIONAL INVESTIGATION OF ANATOMICO-FUNCTIONAL BEHAVIOUR IN FOVEOMACULAR RETINOSCHISIS

"You make it so difficult sometimes"

– Princess Leia

6.1 Introduction

Ophthalmic imaging represents a fertile environment for the application of deep learning and artificial intelligence, as illustrated by the multitude of studies already undertaken (731–734). Similarly, microperimetry is increasingly being recognised as a useful index of functionality in emerging therapeutics, such as gene therapy and stem cell-related visual restorative approaches, given its accuracy, repeatability and data-rich output (349,350,735,736). The fundamentals of MP are discussed in 2.3.3. Although both DL and MP have been applied to several disorders characterised by retinal fluid accumulation (e.g. DMO and AMD), there is relatively little research concerning the behaviour of retinoschitic pathologies.

6.1.1 Machine learning

Machine learning (ML) is a branch of computer science and artificial intelligence (AI), which describes a series of frameworks through which computer algorithms can make predictions or decisions about data, without being explicitly programmed to do so (737). The benefit of ML systems is their ability to automatically learn and improve models, based on exposure to large volumes of data. ML algorithms are typically categorised as supervised or unsupervised, depending on the use of a training dataset, with labelled examples, from which the learning algorithm can produce inferred functions to predict future events, as well as compare its output to a 'gold standard' and make adjustments accordingly (738). Deep learning (DL) is a subsection of ML, specifically referring to models that use multi-layered neural networks (NNs) to extract features from input data, assign a weight of importance at each 'hidden' layer, or series of 'nodes', from which an output is processed and passes to the next node if it reaches a given threshold. In a feed-forward network, information flows from the input to a final output, which, in the case of supervised learning, may be compared against a target output using a loss function. From this point, the backpropagation algorithm is used to derive the gradient of the loss with respect to the parameters, which are then used to adjust the latter so as to find a

local minimum of the loss (through so-called 'gradient descent'), to a point of convergence at which the model has the greatest predictive accuracy. This process of iterative optimisation, in which activation functions are used to send data forward through a network and the backpropagation algorithm is used to fine-tune the model, are the core principles governing a traditional NN (Figure 6-1), such as the multilayer perceptron (MLP) (739–742). In general, the larger the dataset and the greater the number of layers in a NN, the more complex decision-making it is capable of.

However, MLPs carry the risk of overfitting, whereby the model fits too well to the training set, such that it learns the irrelevant information (the noise) specific to the training set, at the expense of the features of interest (the signal) and therefore becomes less generalisable in its evaluation of unseen data. That is to say, that in order to reduce variance in its output, a bias will be introduced that favours the training dataset. There are several techniques to minimise a risk of overfitting in DL, such as data augmentation, through the geometric or photometric manipulation of existing images, thus increasing the volume of training data and separation of the dataset into training and testing sets, with the use of 'hold-out' or crossvalidation techniques to improve generalisability (743).

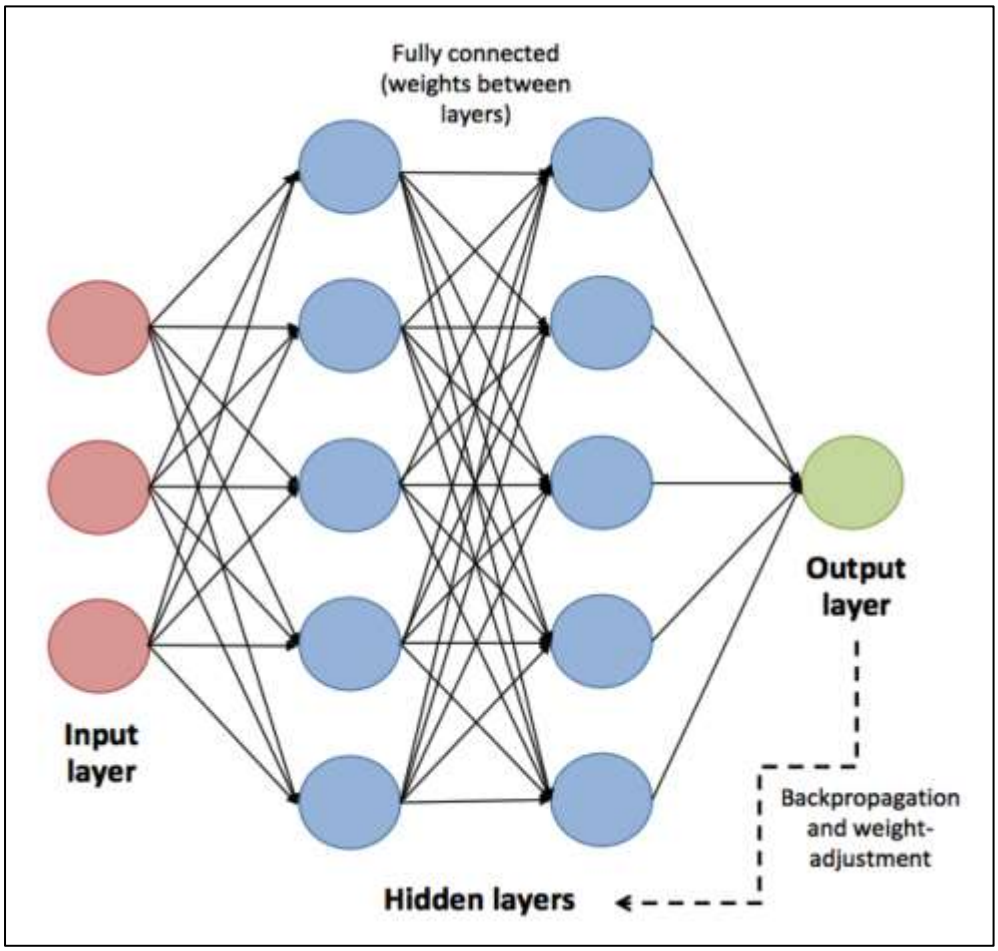

Figure 6-1: The basic architecture of a neural network

To further combat some of the shortcomings of a traditional NN in the field of image analysis, feed-forward DL NNs called convolutional neural networks (CNNs) are utilised (744). The CNN is conceptually based on our knowledge of the human visual pathway, which comprises a hierarchical, layered system of visual processing, from the retina to the visual cortex, with extensive input from higher cortical centres, such as those concerned with memory and face or object recognition. CNNs mimic this system, using multiple layers to extract features, prior to inputting the data into a classification network.

In a CNN, the input image is accepted in the form of arrays, organised into a matrix. This matrix is then filtered using smaller filter matrices, or kernels, which slide over the input data, performing elementwise multiplication over a set number of pixels and summing the resulting value into a single pixel (Figure 6-2) (745,746). The size of

the output image depends on both the size of the kernel and the number of 'strides' programmed (i.e. how many pixels the kernel moves as it slides over the input channel). A larger kernel with a higher number of strides, will result in greater downsizing of the output layer.

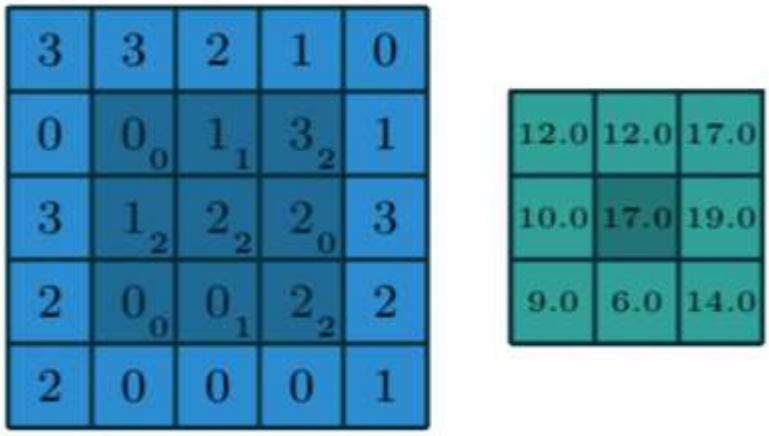

Figure 6-2: A convolution operation: The 3x3 pixel kernel (dark blue) slides across the 5x5 pixel matrix (light blue), performing an elementwise multiplication and summing the data into a single pixel (dark green), which makes up the smaller (3x3) output matrix (light green). Credit: Dumoulin and Visin (2018) (746) [images Creative Commons licensed]

These kernel settings form the parameters of the model and this process of so-called 'convolution operations' is used detect patterns in the image and produce meaningful and compressed representations of the input image's content in the form of feature map. Unlike the MLP, the CNN architecture produces 3-dimensional features maps at each layer, comprising of one 2D feature map per filter, the number of which may vary according to the number of filters per layer. Several other types of 'hidden' layers exist in a CNN pipeline, such as a rectified linear unit (ReLu) layer, wherein non-linear activation functions are applied to the feature map yielding a rectified feature map, containing only non-negative values. Next, a pooling layer downsamples the dimensionality of the rectified feature map into a 2D pooled feature map, by identifying specific values (e.g. average or maximal values) of a feature, such as an edge, corner or specific sub-feature (Figure 6-3). This whole

process may be repeated several times (e.g. AlexNet) or even several hundred times (e.g. ResNet-1202), depending on the number of convolutional layers, before a final pooled feature map is then flattened into a single linear continuous vector, and fed into a fully connected layer to classify the object in question in the output layer (Figure 6-4) (747–750).

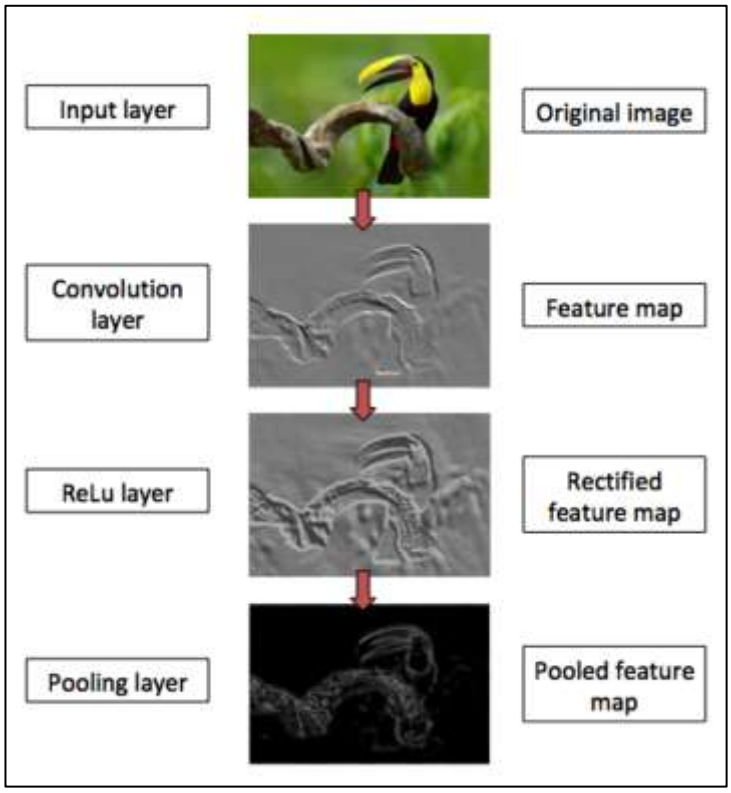

Figure 6-3: Examples of feature extraction techniques in hidden layers of a CNN. Adapted from: Biswal et al (2021) (751) [images reproduced with permission of the rights holder]

The methodology of CNNs allows the extraction of semantic meaning from each pixel position by incorporating local context from neighbouring pixels (i.e. spatial hierarchy and topological relationships), while the downsampling effect of convolution operations reduces the number of weights that need to be assigned per image. Furthermore, in contrast to MLPs, CNNs are translationally invariant, meaning that features of interest can appear anywhere in an image, without innate importance being assigned to its position in space. All these factors contribute to

superior generalisation of CNNs and computational efficiency to train larger, more powerful networks.

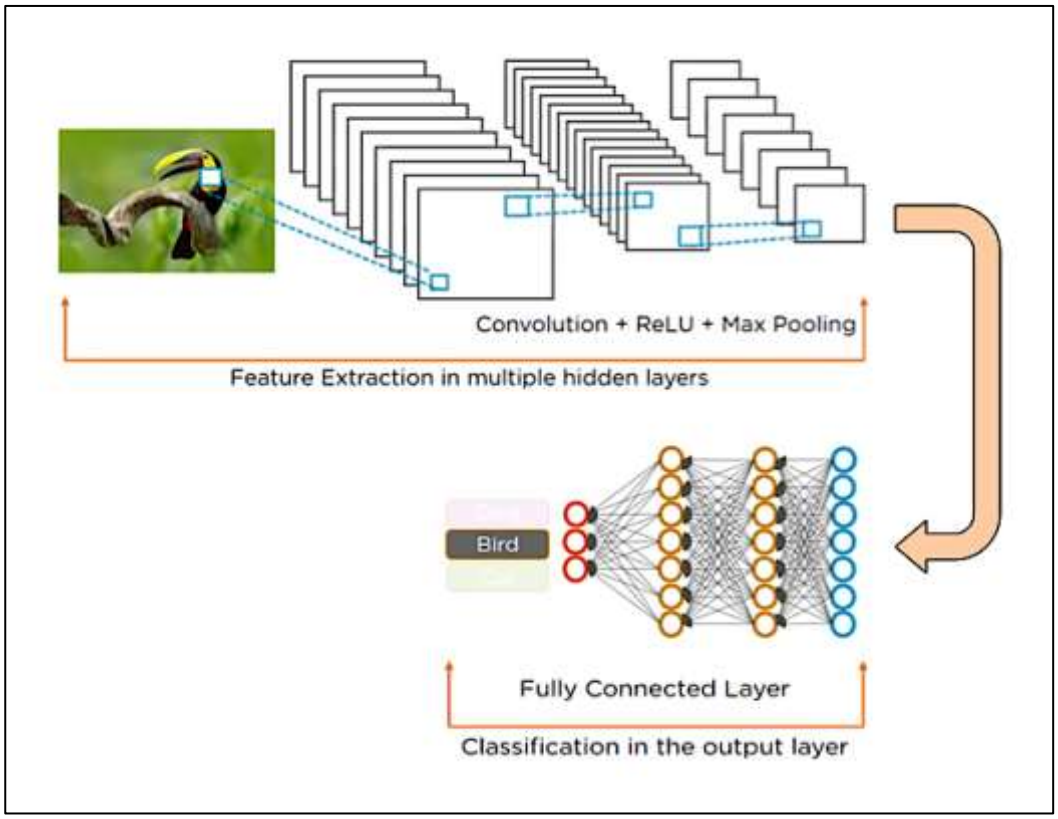

Figure 6-4: Illustration of a CNN pipeline, including a fully connected classification layer. Adapted from: Biswal et al (2021) (751) [images reproduced with permission of the rights holder]

This simplified description of CNNs becomes more complex with the introduction of encoder-decoder networks, such as in a so-called 'fully' convolutional neural network (FCNN) (752). In these networks, at the point where the CNN has downsampled the output to the smallest pooled feature vector, a FCNN is introduced, which is a convolution filter of 1x1 pixel, in the place of a fully connected layer. This map is then upsampled through deconvolutional layers, while receiving semantic inputs from equivalent layers in the encoder region (e.g. through additive or 'concatenating' skip connections), to allow interpretation of information regarding both 'what' is in the image and 'where' it is (Figure 6-5). This architecture further improves translational invariance, while permitting variation of image input

size and reducing the computational power required through successive downsampling and by negating the need for the ‘dense’ layers in a fully connected NN (753).

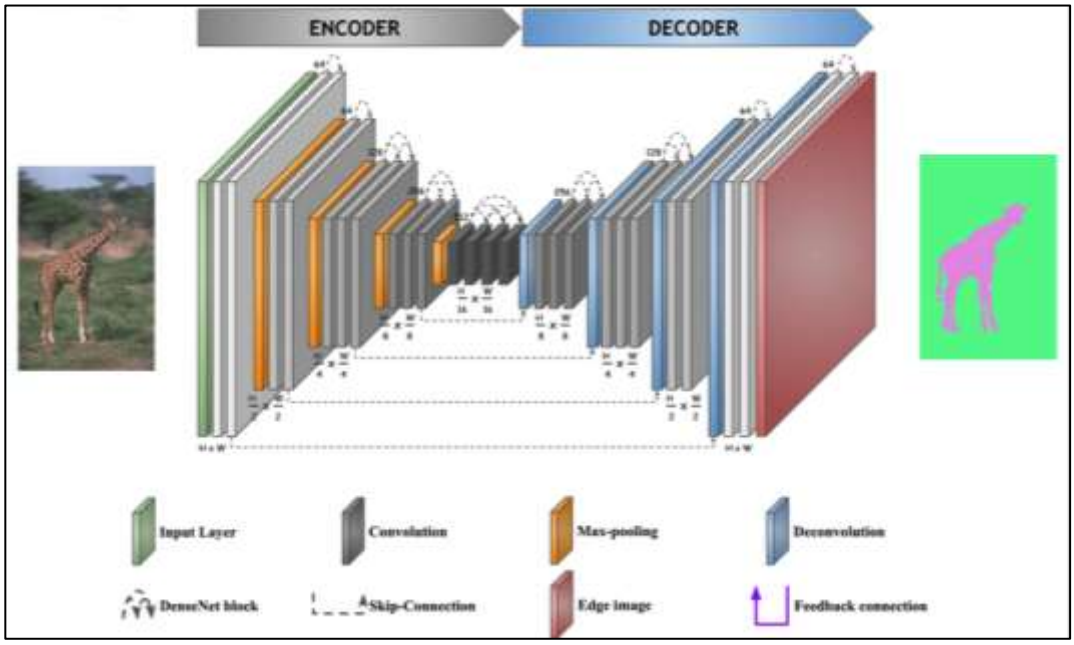

Figure 6-5: Illustration of an encoder-decoder pipeline. Adapted from: Le et al (2019) (754) [image Creative Commons licensed]

The most popular FCNN architecture for semantic image segmentation is the U-net, first described by Ronneberger et al in 2015 (Figure 6-6) (755). Another approach, invented by Google, called DeepLab, incorporates an encoder-decoder architecture, but also utilises techniques such as ‘atrous spatial pyramid pooling’ and ‘atrous convolution’ to enable encoding of multiscale information and preservation of spatial resolution (Figure 6-7) (756–758).

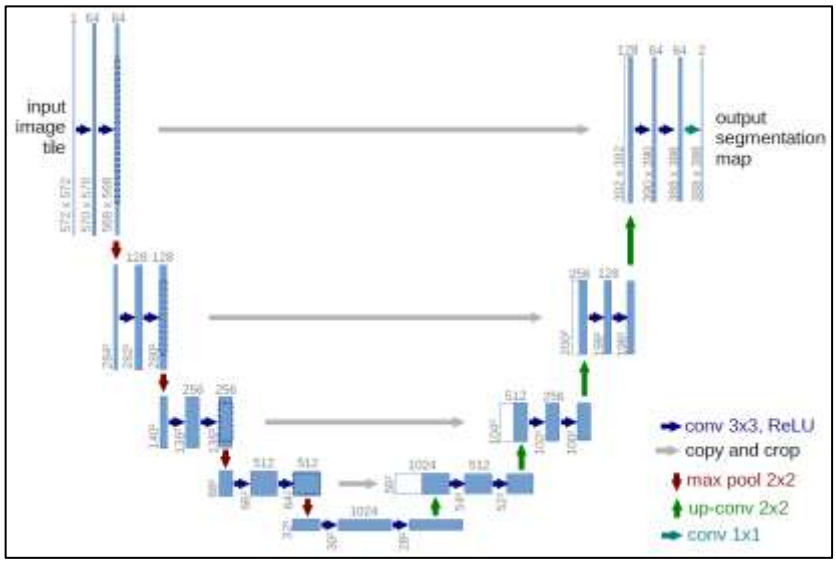

Figure 6-6: The U-net fully convolutional neural network architecture. Credit: Ronneberger et al (2015) (755) [image Creative Commons licensed]

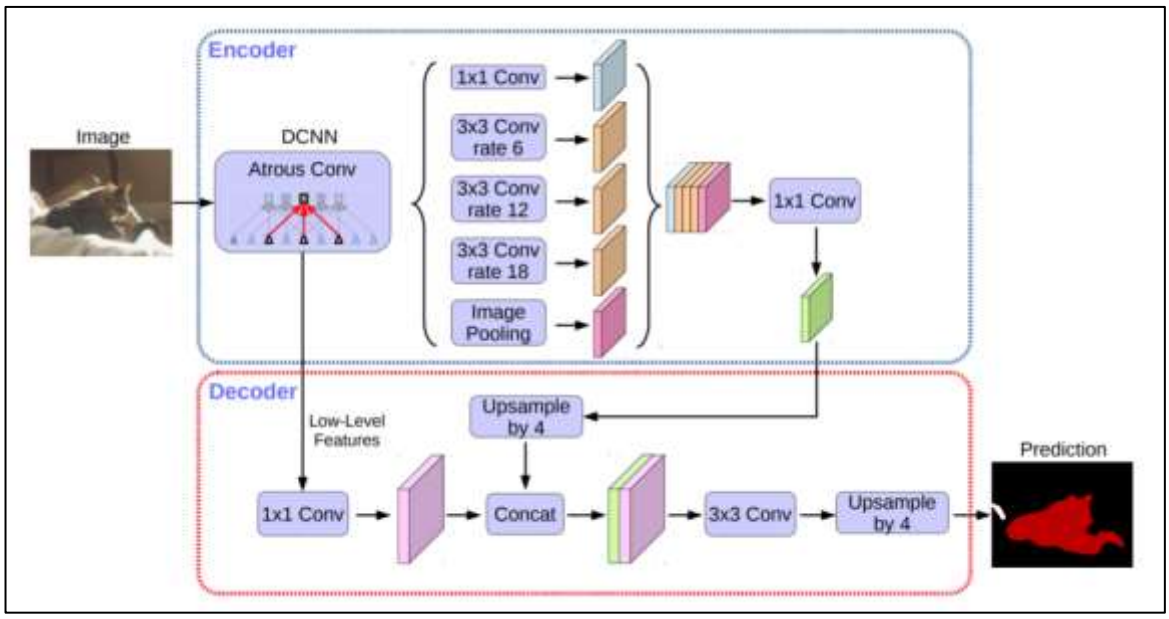

Figure 6-7: The DeepLabv3+ encoder-decoder pipeline with atrous convolutions. Credit: Chen et al (2018) (758) [image Creative Commons licensed]

Performance of a ML model is often measured using a Dice similarity coefficient (DSC), which is calculated as follows for Boolean data types:

$$\text{DICE Similarity coefficient} = \frac{2 \times \text{true positives}}{2 \times \text{true positives} + \text{false positives} + \text{false negatives}}$$

A DSC score of 1 would indicate perfect performance of a ML model, relative to a pre-defined, gold standard segmentation (the 'ground truth'). Another commonly used evaluation metric is the 'intersection over union' (IoU) score, which gives the accuracy of object detection by measuring the degree of overlap between a ground truth segmentation and a predicted segmentation, and calculating it as a ratio of the total area shared by both segmentations. As with DSC, an IoU of 1 indicates perfect overlap and thus perfect performance of the model.

6.1.2 Deep learning in ophthalmology

Deep learning techniques have the potential to play a key role in medical image analysis and have already been successfully applied in ophthalmology (731,732). Analysis of large OCT datasets has yielded high levels of specificity and sensitivity for ophthalmic disease detection and appropriate referral triaging (759–761). Various groups have developed specific DL models to identify the presence of IRF and SRF on OCT, the majority of which focus on common diseases, such as DMO and AMD (733,734).

Several studies have achieved impressive results for binary segmentation of intraretinal fluid, with DSC scores ranging between 0.73-0.79 (762–766). Other approaches have attempted to classify multiple different fluid layers in the same model. For example, as part of the MICCAI RETOUCH challenge in 2017, Lu et al devised the winning model for multiclass retinal fluid segmentation using a U-net architecture, yielding DSC scores of 0.753 and 0.750, for IRF and SRF detection

respectively, when using OCT data captured on the Zeiss Cirrus sd-OCT (765). Since then, further refinement of these NN architectures has led to even better performance for IRF and SRF segmentation (767–770). Recently, Alsaih et al published their results for fluid segmentation with various models, demonstrating that DeepLabv3+ (trained using ResNet-101 and Xception feature extraction methods or 'backbones' and the ADAM optimizer algorithm) outperformed most other approaches, when applied to the RETOUCH database, achieving a DSC of 0.78-0.86 for IRF and 0.81-0.88 for SRF, depending on the OCT acquisition device in question (Figure 6-8) (771).

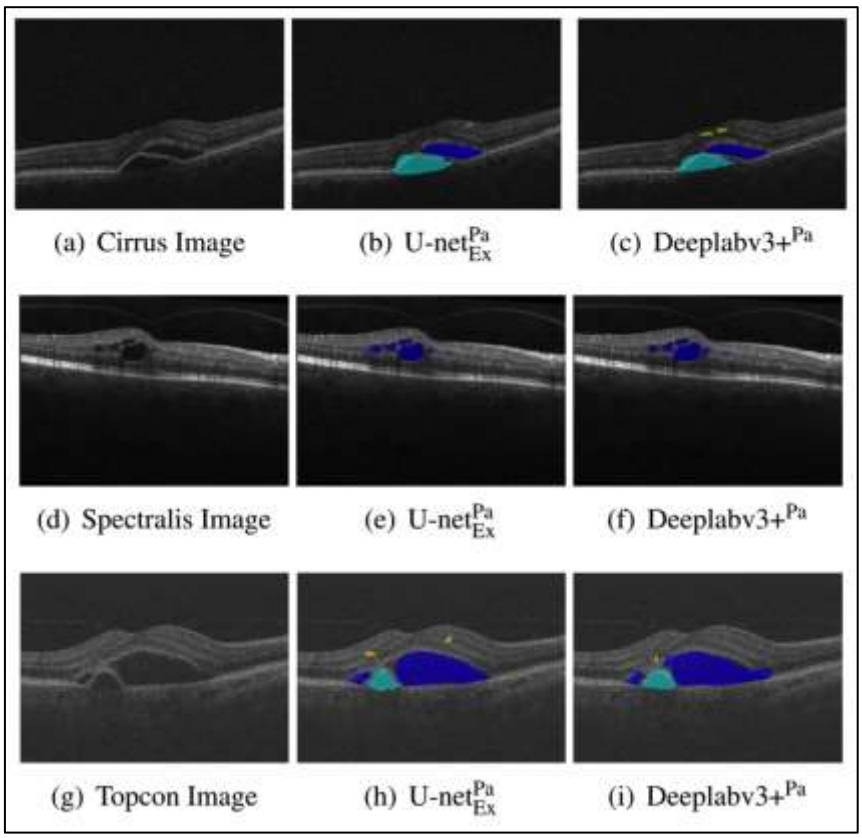

Figure 6-8: Network outputs of U-net and DeepLabv3+ models using OCT images from various acquisition devices in the RETOUCH dataset. Credit: Alsaih et al (2020) [image Creative Commons licensed] (771)

Ajaz et al (2021) and Schmidt-Erfurth et al (2021) have comprehensively reviewed the myriad of approaches and challenges using DL for OCT-derived fluid segmentation (733,734). For the purposes of this thesis, it is important to note that

the current benchmark for IRF and SRF segmentation using the Cirrus 5000 sd-OCT is a DSC of 0.78 and 0.81 respectively (771).

To-date, the majority of DL models have focused on semantic segmentation of IRF and SRF in DMO and AMD. This is, to my knowledge, the first study to use a deep convolutional network to perform per-slice semantic segmentation of the OCT volumes, in order to achieve automated IRF and SRF segmentation, in the context of foveomacular retinoschisis.

In chapters 3-5, I have explored the natural history and anatomico-functional correlates in three acquired forms of foveomacular retinoschisis, using retrospective study designs. I have demonstrated correlations between OCT-derived metrics and both VA and risk of progression to end-stage disease. Finally, in the cases of MFS and ODP-M, I have investigated the potential application these parameters as an aid to clinical decision making, devising a scoring system to optimise monitoring intervals.

In this chapter, I study the application of DL and MP in the modelling of the anatomico-functional behaviour of FRS, to further explore the precise relationship and potential role of quantifiable biomarkers.

6.2 Methods

A single-centre, cross-sectional case-control study was undertaken to investigate the relationship between FRS pathomorphology and macular function. In the initial phase of this study, subjects with evidence of macular IRF and/or SRF were identified and recruited at clinical visits to a tertiary ophthalmic hospital trust between February 2019 and January 2020. Underlying pathologies included ERM, MTM, ODP-M, IFRS and XLRS. All subjects had a Zeiss Cirrus 5000 OCT 6x6mm macular cube scan, comprising 128 2D B-scan slices, each made up of 512x1024 pixels.

6.2.1 Development of deep learning model

A deep convolutional neural network was used to perform semantic segmentation of IRF and SRF from OCT slices. A dataset was created by annotating a sparse set of 10 (out of 128) slices from OCT volumes of 25 eyes with IRF, SRF or both, resulting in 250 image-annotation pairs. All slices were annotated by a single ophthalmologist; a further 10 images were annotated by a second ophthalmologist to calculate inter-human observer agreement. Data from 5 subjects were held out as a validation set; therefore, the model was trained on 200 examples. Each annotation contained per-pixel labelling for 3 classes: IRF, SRF and background, the latter represented by every other non-fluid pixel in the image. To speed up training, annotations of ILM and RPE layers were obtained and used to crop each OCT slice to a smaller region of interest, tightly around the retina; this was performed by coarsely segmenting the retinal boundaries using thresholding.

The model architecture was DeepLabv3+ with a ResNet101 backbone, which was initialised using ImageNet pre-trained weights (758). This initialisation was crucial for achieving good performance given the limited training examples used. The model was trained for a total of 10K steps using the ADAM optimizer with a batch size of 4 and employing data augmentation using intensity jittering, random flipping and blurring (772). The Lovasz Softmax loss function was used as it yielded better results than the default choice of Cross-Entropy loss (773). The performance of the model was evaluated on the held-out validation set and the DSC/IoU score of each class was calculated (Table 6-1). The DL model yielded similar performance for IRF segmentation (DSC 0.865 and IoU 0.762), when compared to the agreement between human annotators (DSC 0.900 and IoU 0.790).

Table 6-1: Network output on held-out validation set

Metric	Mean	Background	Any fluid	IRF	SRF
IoU	0.8713	0.9674	0.8233	0.7620	0.8846
DICE	0.9290	0.9834	0.9018	0.8649	0.9387

Examples of the network output are given in Figure 6-9, while Figure 6-10 demonstrates the model performance for IRF segmentation during training.

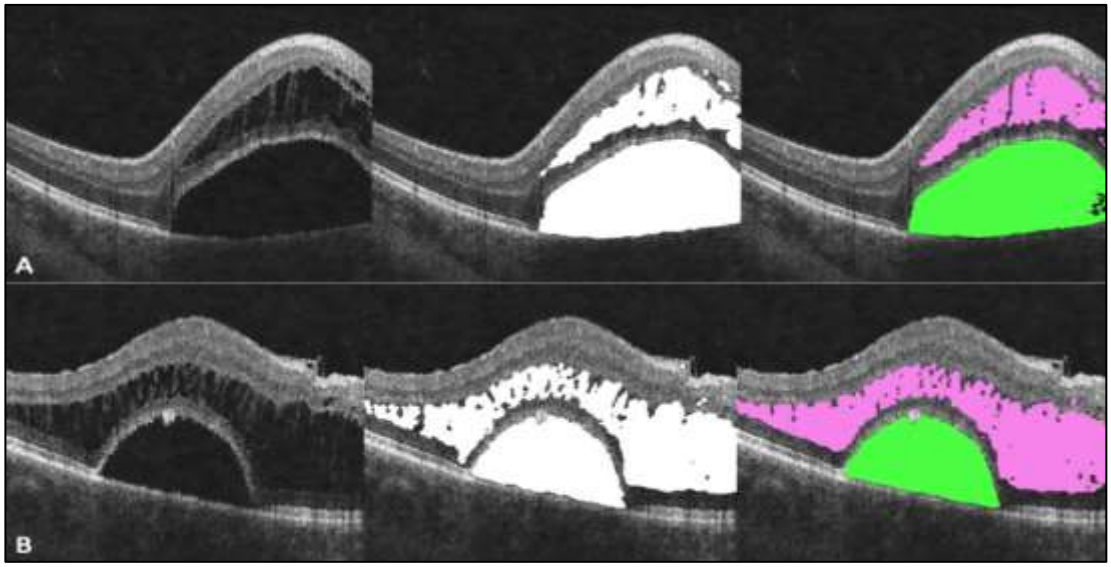

Figure 6-9: (A&B) Segmentation examples from two different eyes (A&B); original OCT images with IRF and SRF (left); human-annotated and labeled references (middle); model segmentation outputs (right)

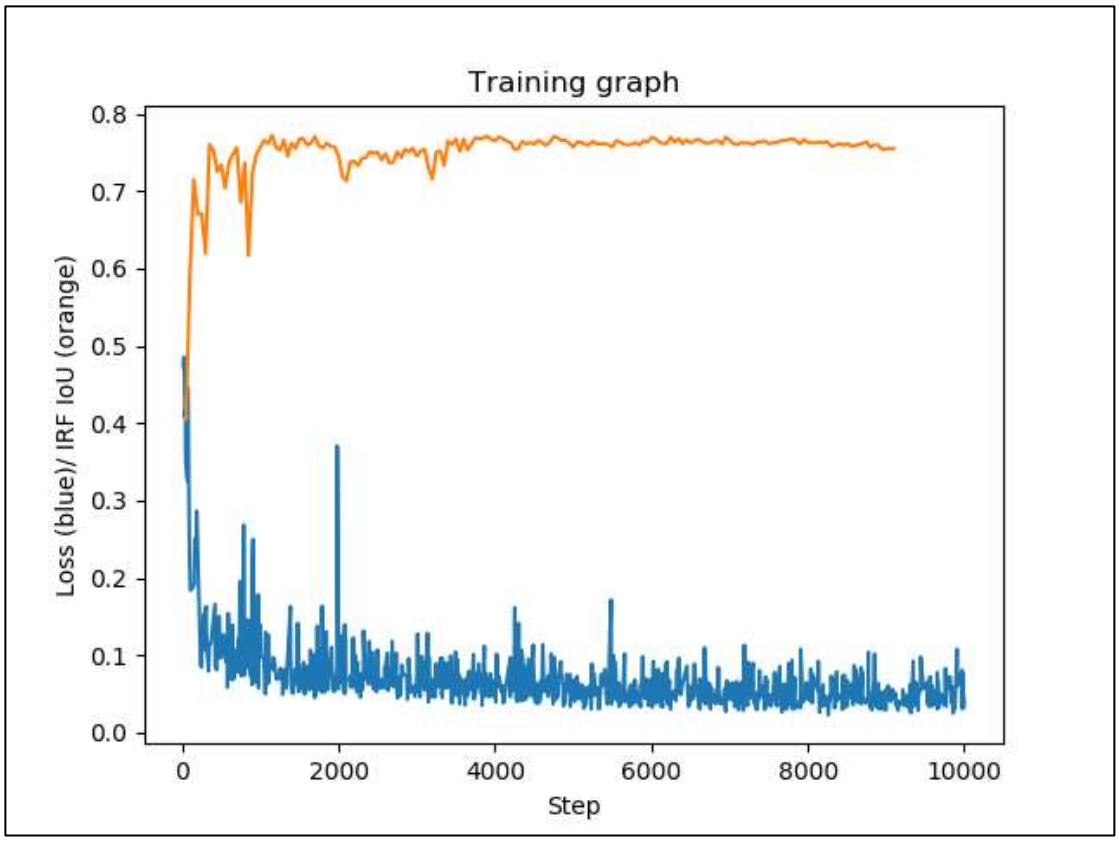

Figure 6-10: Evolution of loss (blue) and Intraretinal fluid IoU during the course of training. Loss values reach a plateau at around 5000 optimisation steps, which coincides with a plateau of generalisation performance on the validation set as indicated by the saturation of IoU score

6.2.2 Application of deep learning model

In the following phase of the study, subjects with acquired FRS and IRF only (i.e. MFS, ODP-M or IFRS) were included. Eyes with VMT, complex ERM, FTMH or FD were excluded. Additional exclusion criteria included previous retinal laser or surgical intervention or concurrent ocular pathology affecting vision. Eyes that were used in the development of the DL model were included, where the above criteria were met. Subjects with X-linked retinoschisis were also included, to illustrate the different anatomico-functional behaviour of congenital FRS.

Subjects with FRS had a Cirrus 5000 OCT scan, from each of which the above DL model segmented 128 2D slices (Figure 6-11).

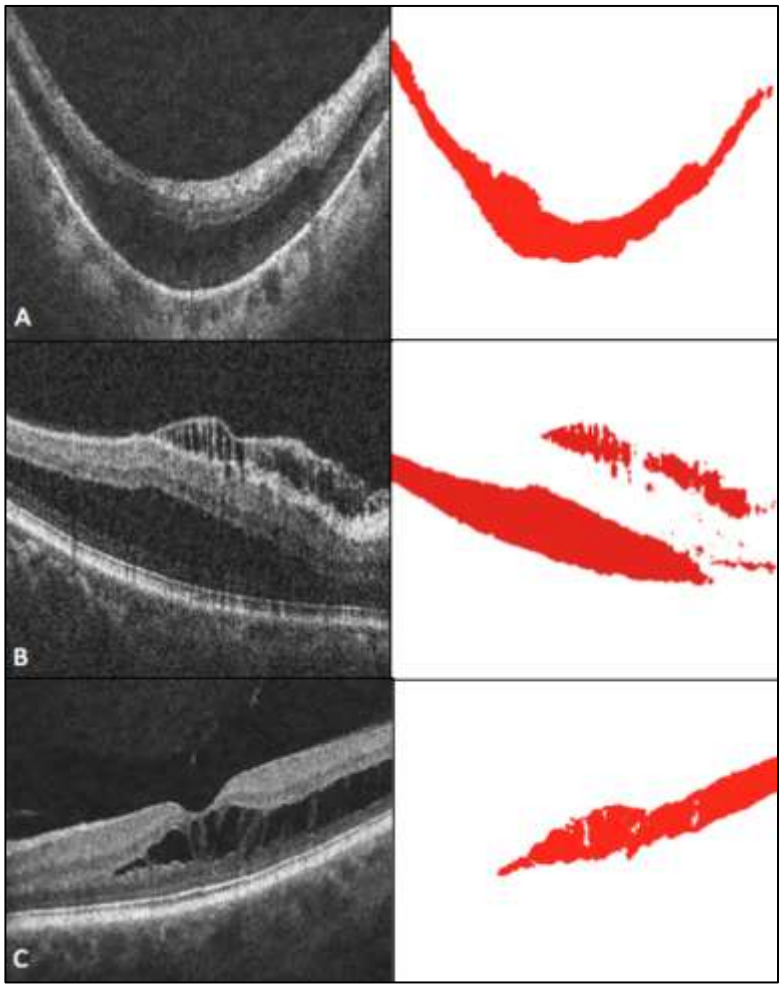

Figure 6-11: Network output in cases of (A) MFS, (B) ODP-M and (C) IFRS; original OCT B-scan (left); model segmentation (right)

Following this, aggregation of 2D segmentations into 3D volumes was performed using FIJI™ image analysis software. The annotated image stack was resliced along the z-axis projection to give an *en face* stack of images, using bilinear interpolation between slices to create a 3D aggregation comprising isotropic voxels with 1:1:1 ratio. The resulting *en face* images had a resolution of 512x512 pixels, corresponding to the 6x6mm border, meaning that each pixel corresponded to a diameter of approximately 11.7µm (Figure 6-12B). 3D renderings of the schisis cavity could be visualised using the '3D projection' plug-in in FIJI™ (Figure 6-12C).

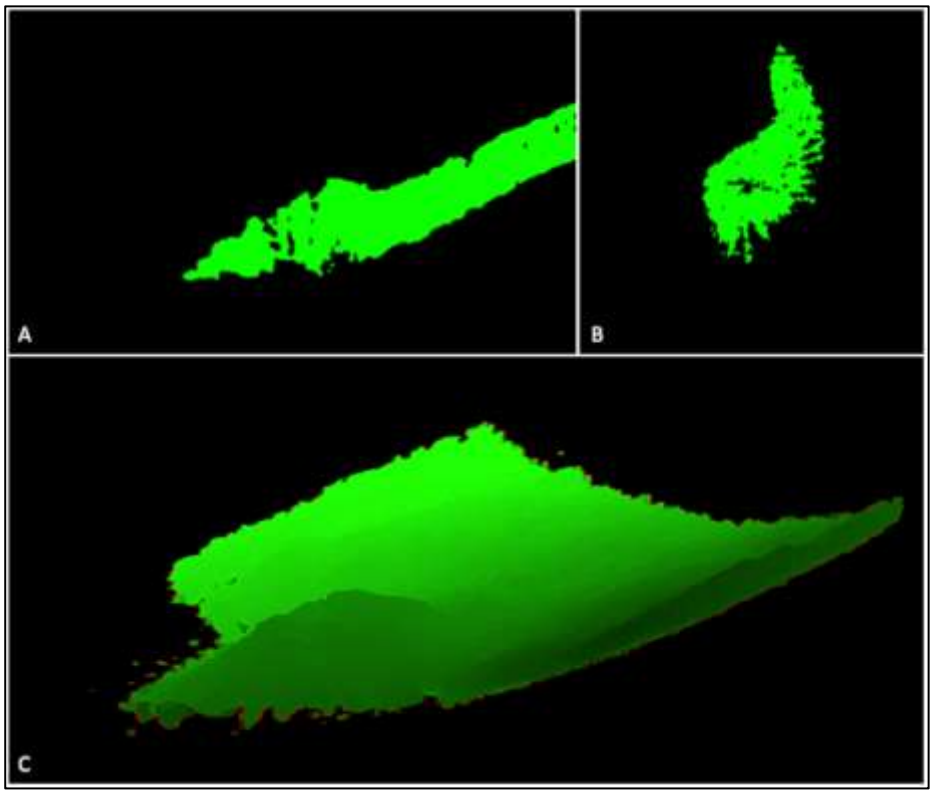

Figure 6-12: Visualisations of the segmented schisis cavity: (A): cross-sectional view; (B): en face slice; (C): 3D-projection

Schisis area was estimated by creating a 'sum slices' z-projection, which can be binarised and the thresholded pixels counted and measured as a proportion of whole 2D area (which is a known area of 36mm^2 OR 36 million µm^2). Schisis volume is estimated by counting all annotated voxels in stack, as a proportion of total voxels in 3D volume (which equates is a known volume of 72mm^2 or 72 billion µm^3).

6.2.3 Microperimetry

All included subjects also underwent MAIA microperimetric assessment (Centervue, Padova, Italy). A detailed description of MAIA MP and its output parameters is provided in 2.3.3. Age-matched controls were included as a comparison group.

In order to measure anatomico-functional associations between microperimetric stimuli and schisis morphology, the MP grid was registered to the *en face* schisis

segmentation by aligning retinal vessel regions-of-interest (ROIs) between the near-infrared reflectance image corresponding to the macular cube and the fundus image corresponding to the MP grid (Figure 6-13C-E).

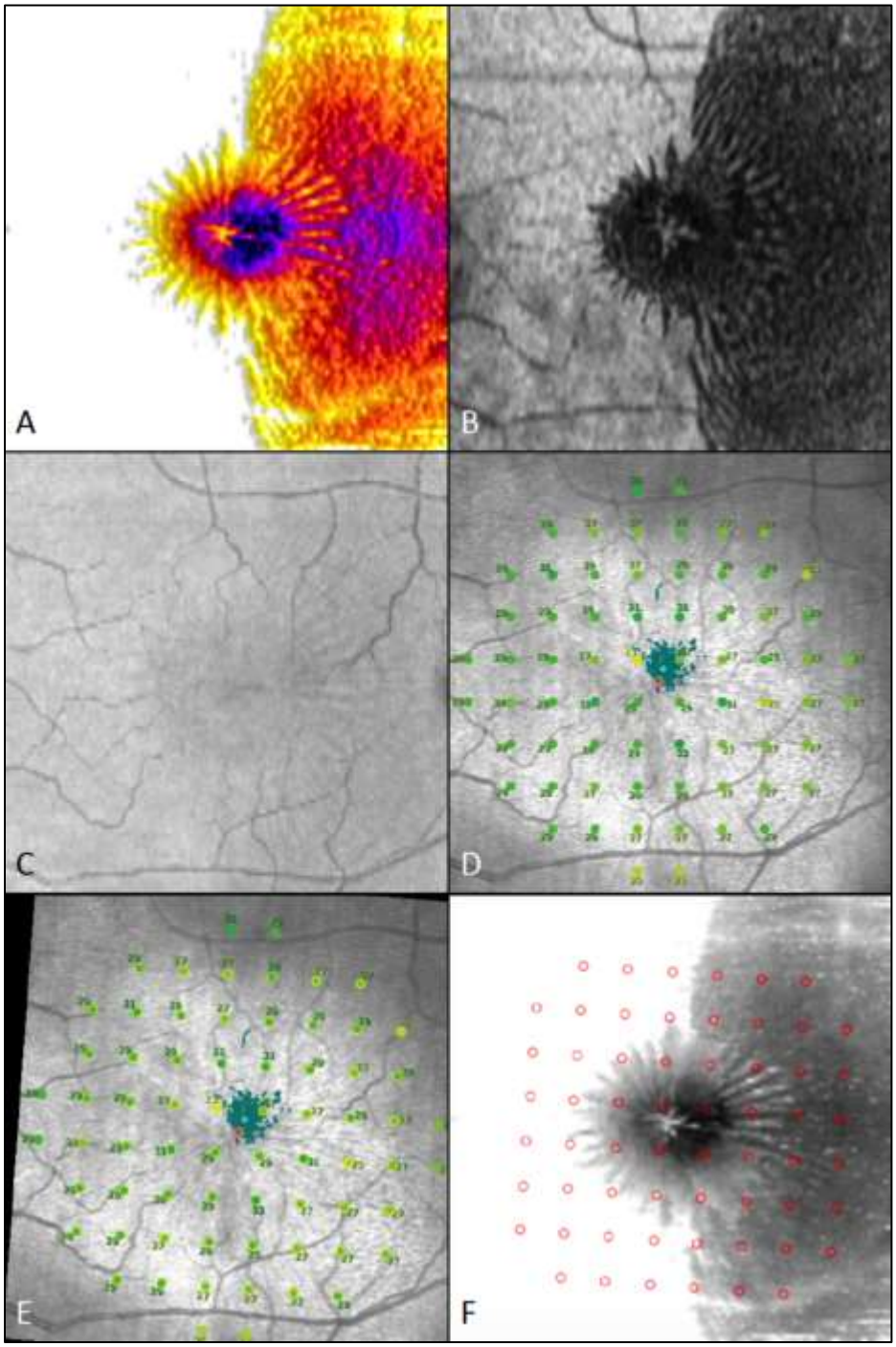

Figure 6-13: En face multimodal imaging in a case of FRS; (A): sum-projection of en face segmentation slices to create heat map (with fire LUT); (B): minimal-intensity projection using Zeiss Cirrus 5000 proprietary software; (C): en face near-infrared

(NIR) image from Cirrus OCT; (D): MAIA microperimetry grid with registered cSLO fundus image; (E): microperimetry grid after registration to NIR image, with circular ROIs demarcated; (F): ROIs projected onto sum-projection of en face schisis segmentation

Each MP stimulus is based on a Goldmann III stimulus of $4mm^2$ (25.6 arcminutes), which corresponds to a diameter of approximately 120µm on the retina. We can estimate therefore that, if the stimulus has a circle of radius 60µm, the projected area of a $4mm^2$ stimulus on the retina would be approximately $11{,}000\mu m^2$. On the *en face* image, 5 pixels corresponded to approximately 58.5µm, so a circle with this radius would have an area of $10{,}751\mu m^2$, which is a close approximation to the estimated projected MP stimulus size on the retina.

Using this information, I drew circular ROIs of 5-pixel radius over each of the centremost 60 MP stimuli loci, which I then projected onto the registered *en face* segmentation map (Figure 6-14A). A cylinder ROI can be extended from this circle, through the whole *en face* segmentation, to calculate the number of annotated voxels (Figure 6-14B). This allowed estimation of the local schisis volume at each MP stimulus location, using the known parameters of the whole cube. For example, we know the entire stack contained 66,974,720 voxels and has a volume of 72 billion μm^3. If a given cylindrical ROI contains 1000 thresholded voxels, we know this equates to 0.0015% of the total voxel number or a local schisis volume (LSV) of $1{,}080{,}000\mu m^3$. From here, the estimated local schisis height (LSH) within this ROI can be calculated, using the equation: $LSH = LSV \div \pi r^2$. In this example therefore, the LSH = 1,080,000 ÷ 10,751 = 100.4µm.

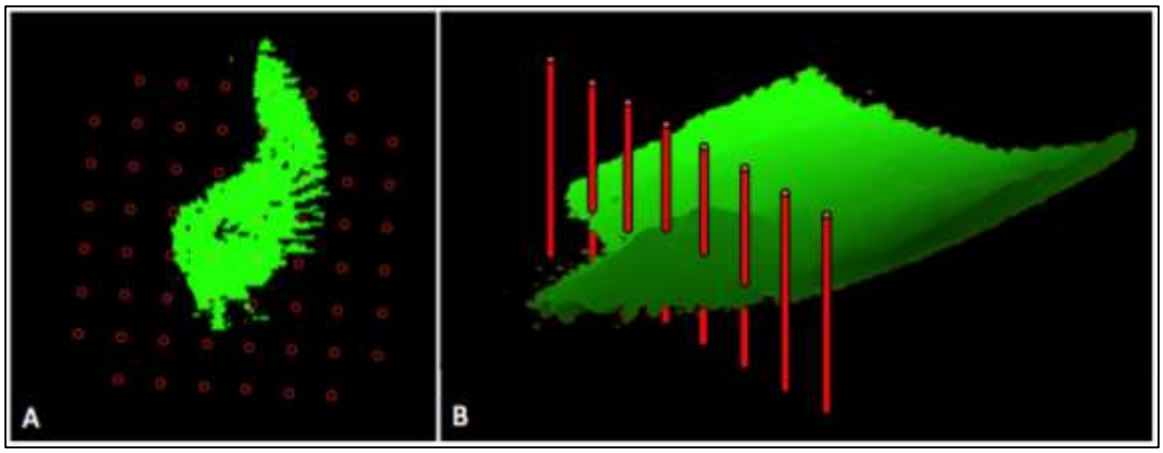

Figure 6-14: ROIs for calculating schisis metrics; (A): en face view with projected ROIs from MP grid; (B): illustration of the ROIs in 3D space as a cylinder

Associations between microperimetric parameters, including average threshold microperimetric sensitivity (ATS), fixation metrics (P1, P2, BCEA63% and BCEA95%) and schisis morphological parameters, including schisis volume (SV), SA and AvRT were measured. The anatomico-functional relationships were analysed at 'full-field' level (referring to the global indices of schisis morphology and MP) and according to 'pointwise' sensitivity (PWS) at each of the centremost 60-loci from the microperimetry grid. Associations were measured between PWS and the estimated local schisis height.

6.3 Results

21 eyes from 18 subjects with acquired FRS were included in the final analysis, alongside 21 age-matched control eyes. Of the affected eyes, 11 were used in the training and testing of the DL model, while the remaining 10 were previously unseen.

6.3.1 'Full-field' analysis

Comparison of ATS and fixation metrics revealed non-significant differences between those subjects with FRS and control eyes for all parameters. Details of the two groups are included in Table 6-2.

Table 6-2: Characteristics of FRS and healthy control eyes

Characteristic (mean ±SD)	FRS eyes (n=21)	Control eyes (n=21)	*p-value*
Age (years)	59.0 ±9.1	59.2 ±9.5	*0.995*
Female sex (%)	52	43	*0.256*
ATS (dB)	26.9 ±1.7	27.6 ±1.1	*0.191*
P1 (%)	94.4 ±6.6	94.5 ±6.8	*0.985*
P2 (%)	98.3 ±3.2	99.0 ±1.8	*0.677*
BCEA63%	1.2 ±1.6	0.9 ±0.8	*0.906*
BCEA95%	3.4 ±4.9	2.7 ±2.4	*0.695*
Schisis volume (mm^3)	2.0 ±2.1	-	-
Schisis area (mm^2)	18.6 ±10.8	-	-
Average retinal thickness (µm)	325 ±66	-	-

However, on age-adjusted linear regression analysis of those subjects with FRS, ATS was significantly associated with SV (in mm^3) ($p=0.016$, $\beta=-0.337$ (95%CI: -0.06 to -0.60) R^2: 0.28), but not with SA or AvRT (both $p>0.05$). This model estimates that, for every 1mm^3 increase in SV, there would be an observed reduction of 0.34dB (95%CI: 0.06 to 0.60dB) in ATS. In addition, fixation parameters were significantly, negatively correlated with both SV and AvRT, but not SA. These results are summarised in Table 6-3.

Table 6-3: Associations between anatomical parameters and microperimetric indices

Microperimetric Index	Schisis volume (mm^3)	Schisis area (mm^2)	Average retinal thickness (µm)
Average threshold Sensitivity	***p=0.016*** β=-0.337 R^2: 0.28	*p=0.212*	*p=0.386*
PRL_initial (P1)	***p=0.037*** β=-1.342 R^2: 0.28	*p=0.068*	***p=0.019*** β=-0.038 R^2: 0.24
PRL_final (P2)	***p=0.033*** β=-0.763 R^2: 0.33	*p=0.078*	***p=0.030*** β=-0.020 R^2: 0.25
BCEA63%	***p=0.021*** β=0.414 R^2: 0.40	*p=0.071*	***p=0.033*** β=0.010 R^2: 0.29
BCEA95%	***p=0.023*** β=1.228 R^2: 0.39	*p=0.074*	***p=0.034*** β=0.030 R^2: 0.29

6.3.2 Pointwise sensitivity analysis

To address the issue of clustering, such as that resulting from inter-subject variability in MP sensitivity, a mixed-effects, multi-level linear regression model was used, with level 1 representing the sensitivity values at individual loci and level 2 representing the subject. LSH was included as a level 1 predictor variable. Fixed effects modeling of LSH at level 1 revealed a significant association with PWS ($p<0.001$, $\beta=-0.004$) (Figure 6-15). However, when the intercepts and slopes of the regression lines were allowed to randomly vary, each demonstrated significant inter-subject variability ($p=0.002$ and $p=0.009$ respectively), with no covariance found between the intercept and slope ($p=0.452$) (Figure 6-16). Moreover, an intraclass correlation coefficient of 0.36 suggests that there is a significant clustering effect of PWS values at the level of the subject.

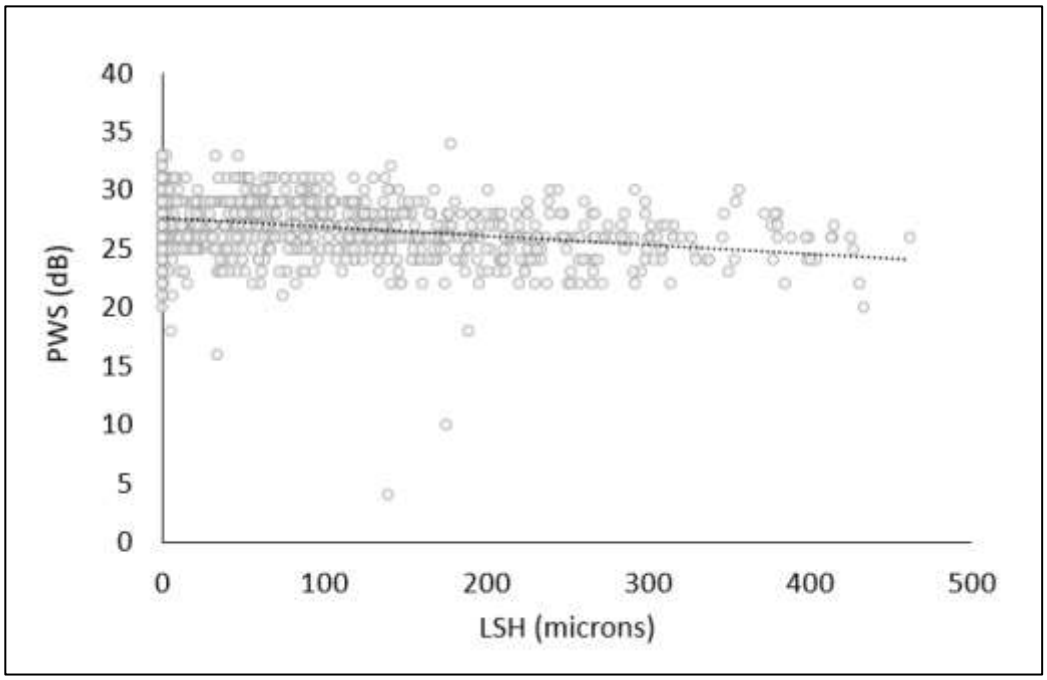

Figure 6-15: Associations between PWS and LSH, before accounting for the clustering effect at subject level

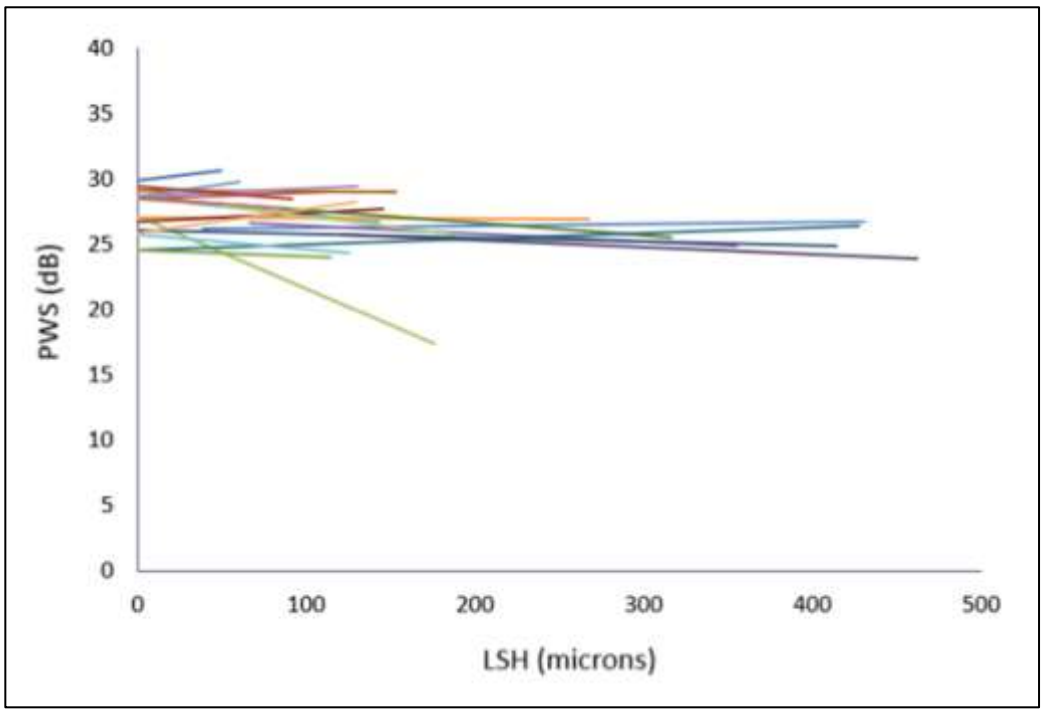

Figure 6-16: Illustration of the inter-subject variability in intercepts and slopes of regression lines

To account for this clustering effect, fixed-effects modelling of mean LSH and age as level 2 predictor variables was performed, which demonstrated a persistent significant association between mean LSH and PWS (p=0.002, β=-0.012) at subject level (Figure 6-17). That is to say that, for every 100µm increase in mean LSH, the mean PWS is estimated to fall by 1.2dB.

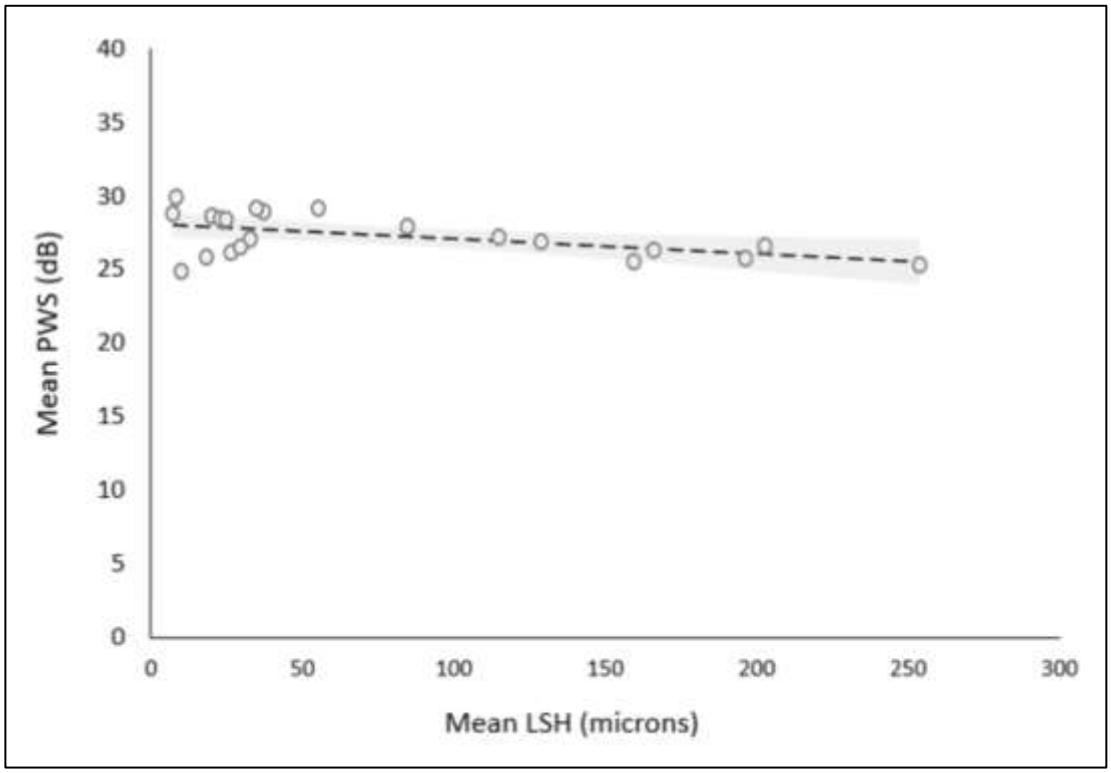

Figure 6-17: Association between mean LSH and mean PWS, using multilevel fixed effect modelling to overcome clustering at subject-level

6.3.3 Sub-analysis by eccentricity and schisis height

PWS was further sub-categorised according to eccentricity (i.e. central 1.4-4.2˚, middle 5.1-5.8˚ and outer 7.1-8.6˚ regions, see Figure 6-18). Table 6-4 displays the subject mean PWS values by eccentricity across a range of LSH sub-categories (0µm, 1-100µm, 101-200µm and >200µm), alongside the results from healthy control subjects. In control subjects, there is a correlation between increasing eccentricity and diminishing sensitivity (p=0.009). However, in those eyes affected by schisis, this

correlation is no longer noted, suggesting that the presence of schisis disproportionately affects sensitivity closer to fixation. There was a significant difference in mean PWS between healthy control eyes and FRS eyes for the central 4.2˚ (p=0.041), but not for the middle (p=0.060) or outer regions (p=0.300). (Figure 6-19).

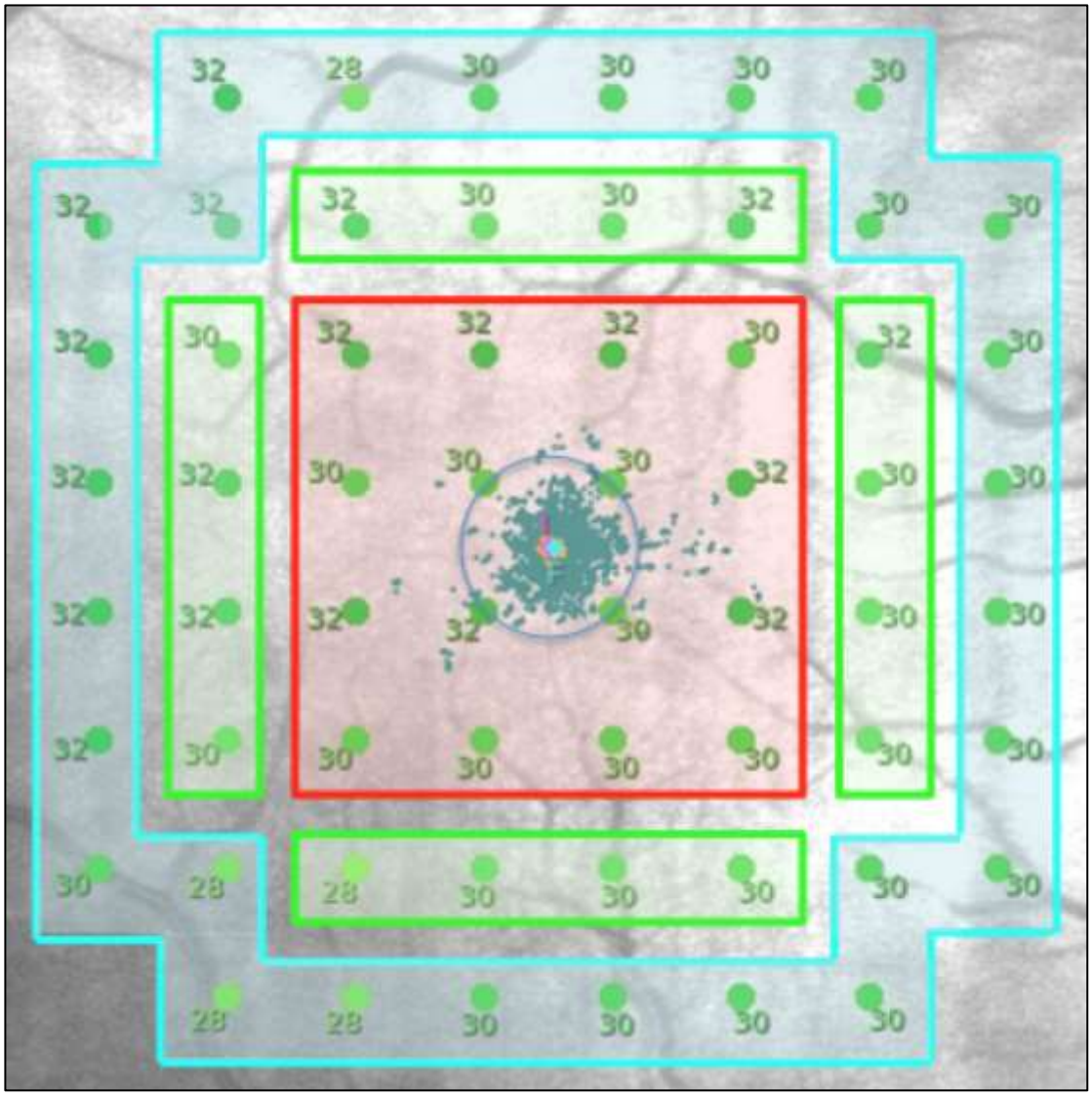

Figure 6-18: Sub-categorisation according to locus eccentricity: Central 1.4-4.2˚ (red), middle 5.1-5.8˚ (green) and outer 7.1-8.6˚ (blue) regions of interest

Table 6-4: The relationship between mean LSH and PWS, sub-categorised by eccentricity, with healthy control eyes for comparison

Schisis height	Eccentricity			*p-value*	All points
	1.4-4.2˚	**5.1-5.8˚**	**7.1-8.6˚**		
All heights	27.5 ±1.6	27.2 ±1.5	27.0 ±1.7	*0.575*	27.1 ±1.6
0µm	28.6 ±1.5	28.0 ±1.6	27.2 ±1.9	*0.161*	27.5 ±1.9
1-100µm	27.6 ±2.0	27.3 ±1.5	27.1 ±2.0	*0.820*	27.2 ±1.8
101-200µm	26.6 ±2.1	26.2 ±1.8	25.9 ±2.5	*0.883*	26.2 ±2.7
>200µm	26.2 ±1.2	25.8 ±0.9	25.7 ±2.1	*0.831*	25.8 ±0.9
p-value	***0.016***	***0.005***	*0.187*		*0.123*
Healthy control eyes	28.3 ±1.3	27.8 ±1.0	27.2 ±1.1	***0.009***	27.7 ±1.1

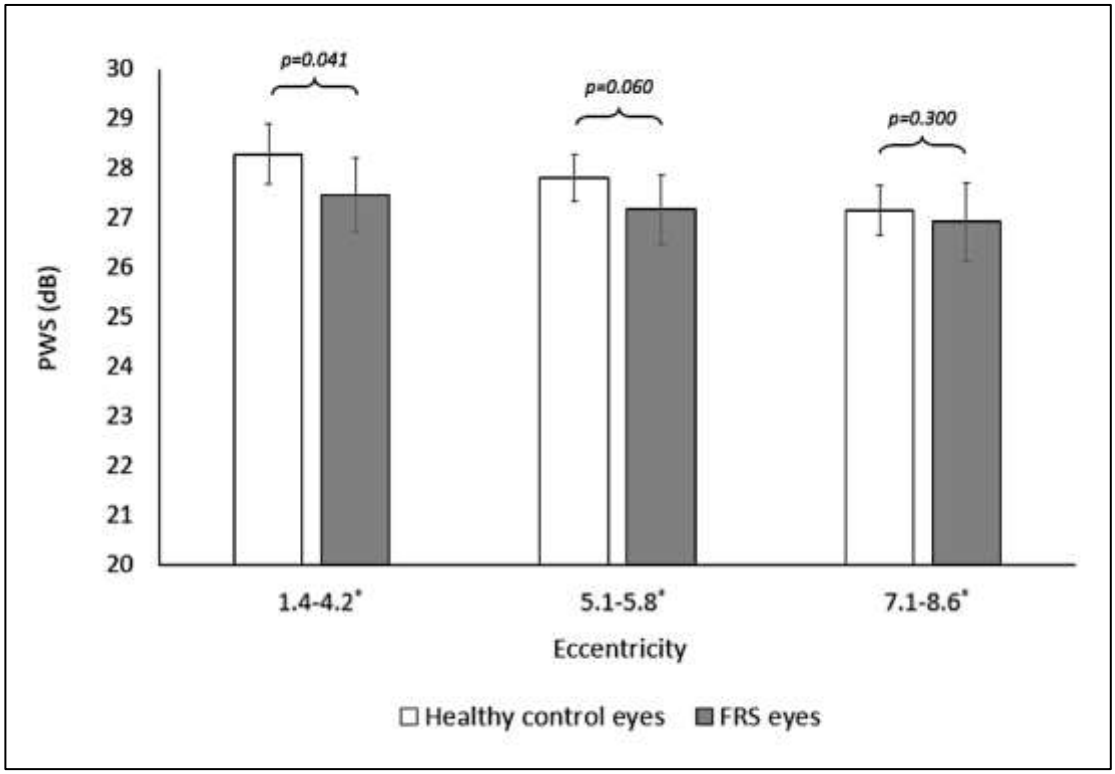

Figure 6-19: A comparison of PWS between healthy control eyes and FRS eyes, demonstrating a significant difference for the central 4.2˚ only

Figure 6-20 demonstrates that, on pairwise analysis of the schisis height categories, there is no difference between healthy control eyes and affected eye loci with 0µm

LSH (p=0.924), while loci with >100µm LSH demonstrated significantly worse mean PWS than both control and affected eye loci and 0µm LSH respectively. When modelled as a continuous variable, using an age-adjusted multivariate regression analysis, mean LSH was significantly associated with mean PWS in the central 4.2˚ only ($p<0.001$, $\beta=-0.010$, R^2: 0.45). This indicates that, following adjustment for age, this model is estimated to explain almost half of the variance in sensitivity, with each 100µm increase in mean LSH expected to yield a -1.0dB in central mean PWS.

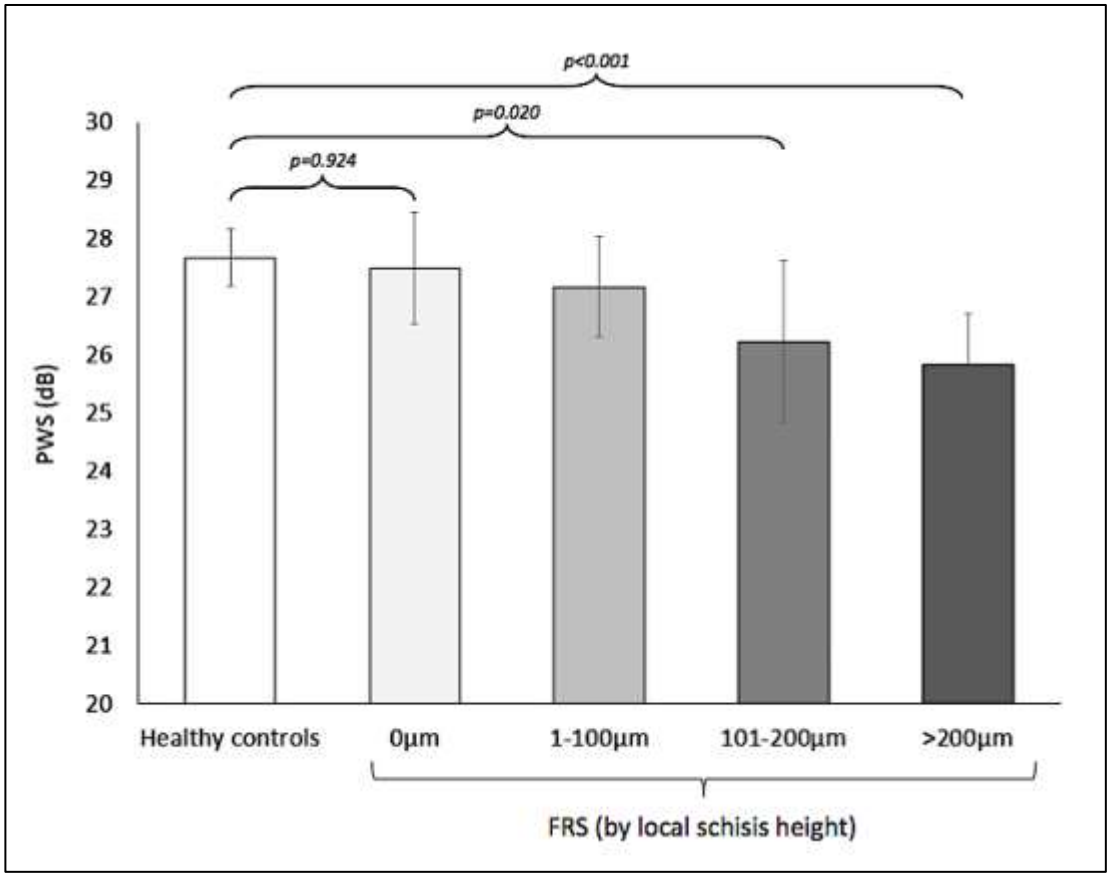

Figure 6-20: A comparison of mean PWS between healthy controls and FRS subjects, with sub-categorisation according to LSH. This demonstrates that regions with LSH >100 have significantly worse PWS than both healthy control eyes and FRS eyes with 0µm LSH

These findings support LSH as a significant predictor variable for PWS and imply that the strength of association for LSH decreases with increasing eccentricity from

fixation. The collective relationship between eccentricity, LSH and PWS is shown in Figure 6-21.

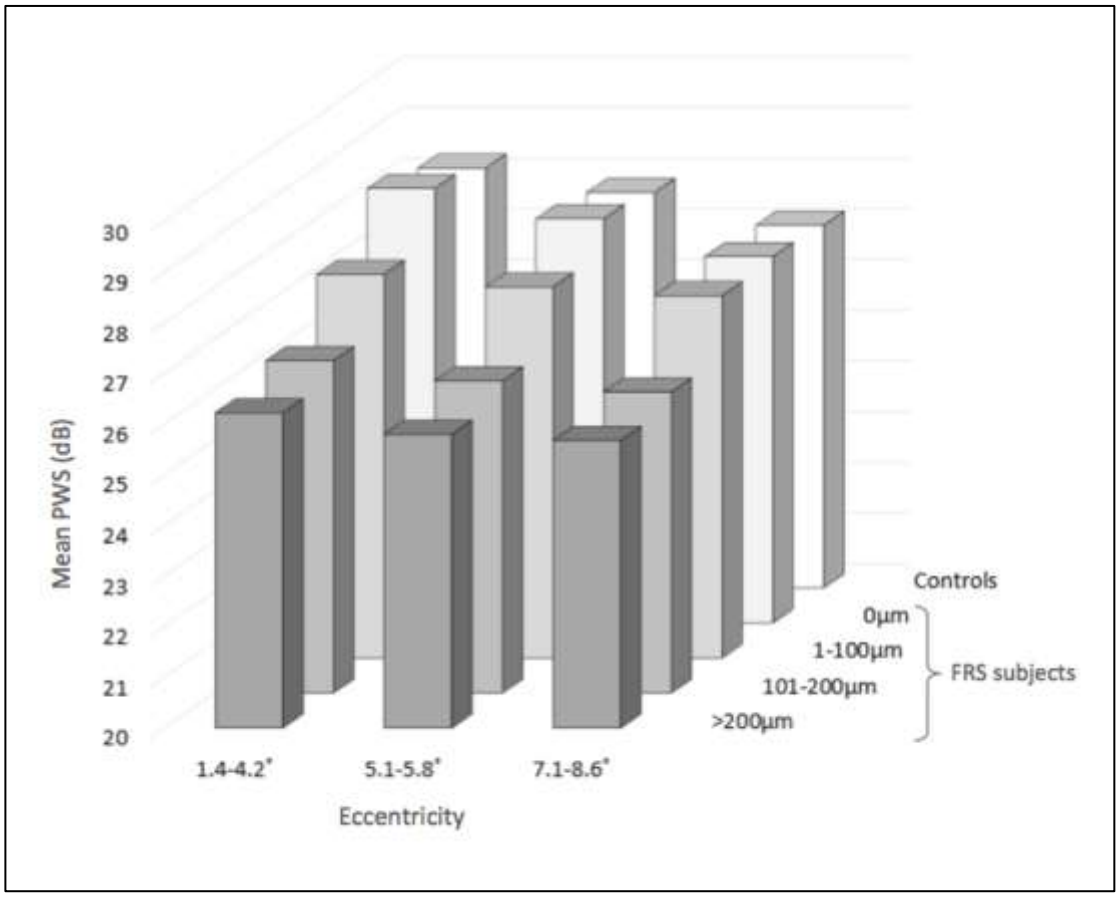

Figure 6-21: The relationship between mean PWS (y-axis), eccentricity (x-axis) and LSH sub-categories (z-axis), for both FRS subjects and healthy controls

6.3.4 Sub-analysis by pathology type

Meaningful statistical analysis according to pathology subtype was not possible due to small subject numbers in each group; high inter-subject variability is likely to confound results at this level. Comparison of mean schisis height and ATS values, subgrouped by pathology are provided in Table 6-5 and Figure 6-22, for descriptive purposes. It is noted that the anatomico-functional profiles of MFS and ODP-M are similar, while IFRS demonstrates better functional and anatomical characteristics in this small cohort. 9 eyes with XLRS are included in this analysis, as a negative control,

to illustrate that non-acquired FRS does not demonstrate the same anatomico-functional relationship, due to its dissimilar pathomechanism; unlike the other conditions, it is not a biomechanical foveopathy.

Table 6-5: Comparison of functional and anatomical characteristics according to underlying pathology

Pathology	MFS	ODP-M	IFRS	XLRS
Number of eyes	10	4	7	9
VA (logMAR)	0.16 ±0.19	0.14 ±0.09	0.05 ±0.12	0.45 ±0.15
Pointwise sensitivity (dB)	26.2 ±1.3	26.7 ±1.2	28.7 ±1.0	24.9 ±3.8
Local schisis height (µm)	89 ±87	100 ±95	38 ±42	32 ±57

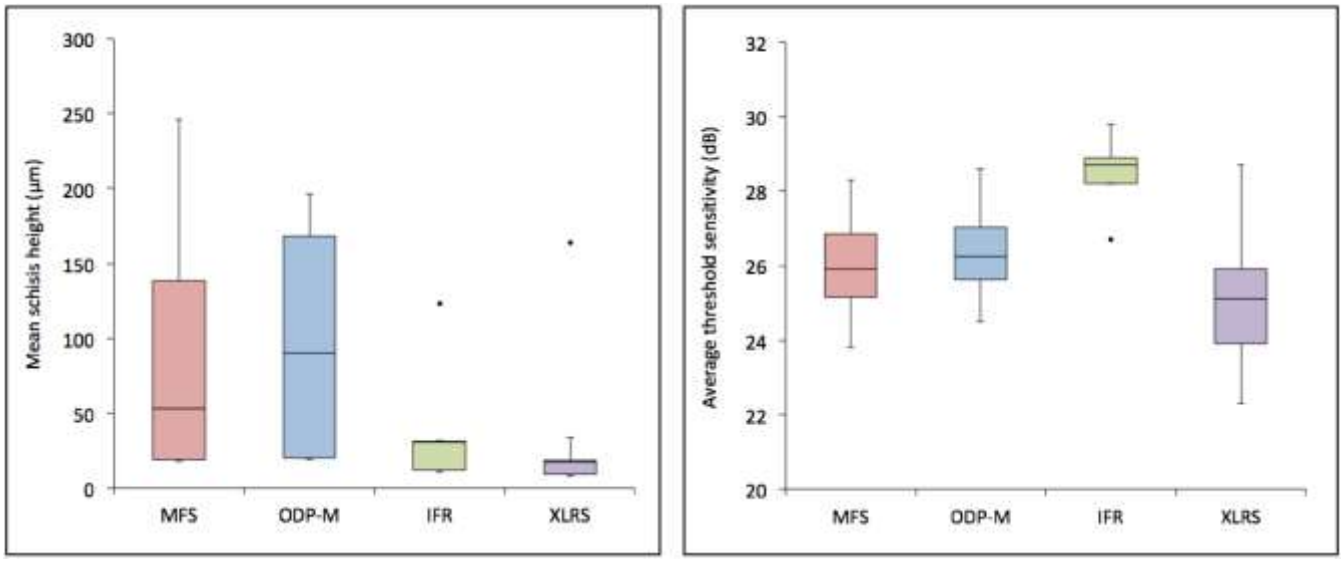

Figure 6-22: Comparison of anatomical (left) and functional (right) metrics according to pathology subtype. Round markers denote outliers

6.4 Discussion

In this chapter, I have devised an exploratory study to investigate novel approaches to image analysis and the measurement of anatomico-functional associations in FRS, using emerging techniques in the fields of computer science and psychovisual

testing. Notably, the findings of this study demonstrate a negative correlation between schisis volume and average threshold microperimetric sensitivity, with a reasonable effect size, although the R^2 values of 0.28-0.40% indicate that the observed variance in function in FRS remains largely unexplained. This may be justified, in part, by the small sample size and high inter-subject variability.

There was also negative correlation found between pointwise MP sensitivity at a given locus and the local schisis height. This relationship was susceptible to a clustering effect seen at individual subject level, but the association remained significant once this was accounted for. Analysis revealed that this correlation only became significant relationship at LSH >100µm, indicating that there may be a non-linear anatomico-functional relationship between schisis morphology and macular function. This supposition is supported by the work of Govetto et al, who modelled MC stiffness in foveoschisis as a function of the angulation of foveal MCs (see 1.2.4.5), demonstrating a non-linear correlation between MC straightening (and therein an increase in vertical schisis height) and worsening VA (100). It would seem a reasonable assertion that there is a threshold at which the limit of the MC elastic modulus is overcome, leading to cytostructural changes, which begin to affect visual function.

On sub-analysis by eccentricity with adjustment for age, only the centremost 4.2˚ demonstrated significant association between mean LSH and PWS. It is notable that the central region had a greater mean LSH than the peripheral macula (102µm versus 60µm, p=0.007), as well a greater proportion of measured points affected by schisis, as compared to the outer 5.1-8.6˚ (mean 72% versus 56%, p=0.003). However, unlike mean LSH, proportional involvement (i.e. schisis extent) did not significantly contribute to the multivariate model for variance in mean PWS, suggesting that magnitude, as opposed to mere presence of schisis, is the critical factor. This theory is also supported by the fact that schisis volume, but not schisis area, was correlated with average threshold sensitivity.

This discrepancy between the anatomico-functional behaviours of the central and peripheral macula, in response to external forces can be related back to the

arrangement of MCs within the macula (1.2.4.3). The zMCs of the foveal walls (within the centermost 1500µm of the macula) have the greatest redundancy for stretch, providing a dampening affect in response to broad tractional forces (as observed in Figure 6-23). However, once the aforementioned threshold for zMC stretch is reached (at around 400µm), stiffening occurs with transmission of forces to the outer retina and early functional deterioration. Initially, this appears to manifest as a subclinical reduction in function that is unappreciable on conventional coarse acuity testing (presumably due to the local density of photoreceptors in this region), but *is* detectable on MP. By contrast, the MCs of the more peripheral macula do not have the compliance to undergo the same degree of deformation and, as such, local function appears to be relatively retained. It would appear, therefore, that the capacity for stretch within the central macula, which conveys a degree of protection against mechanical disruption of the macula, is related to a non-linear functional disturbance, which becomes measurable after around 100µm deformation. Notwithstanding the fact that there is a measurable functional decline with increasing schisis height, it is apparent that a normal level function is retained in eyes with FRS, even in the face of marked retinal deformation.

Depending on the nature of the external force, the MC subpopulations will be affected to different degrees in different pathologies. This variability, according to the underlying pathomechanism, will be discussed further, with respect to the MC subpopulations, in chapter 7. The inclusion of eyes with XLRS serves to demonstrate that the anatomico-functional relationship differs in such cases where FRS arises as a result of a pathomechanism other than biomechanical deformation of the retina.

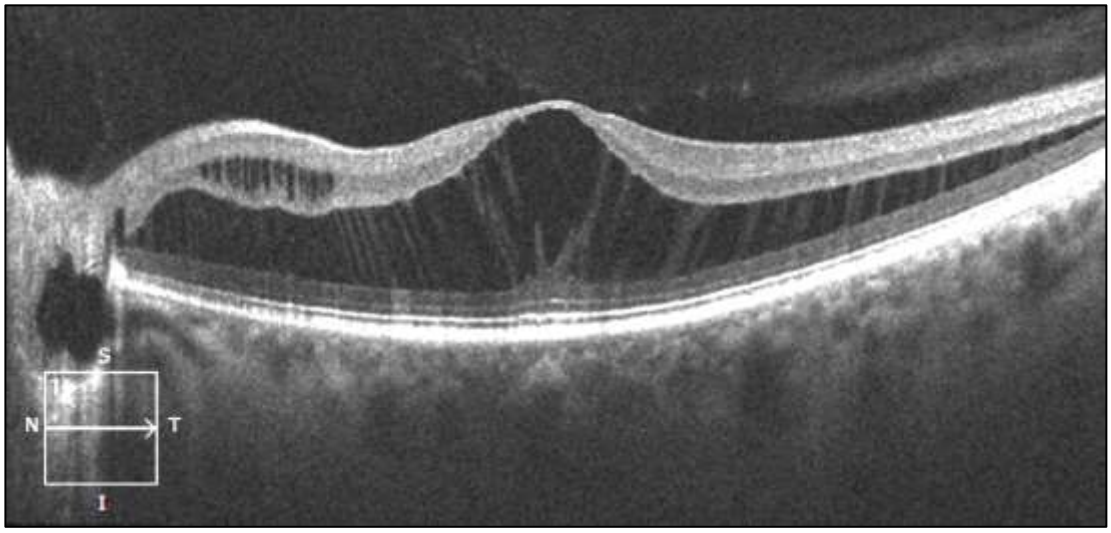

Figure 6-23: A case of FRS in ODP-M demonstrating greater retinal deformation at the fovea and parafovea, as compared to the surrounding macula

The application of a deep learning algorithm in the segmentation of IRF and SRF is not conceptually new, but this is the first time it has been used to quantify schisis dimensions in FRS, as well as being combined with microperimetric testing to measure anatomico-functional correlation. The model developed in this study performed comparably with existing pipelines for the segmentation of IRF and superiorly for SRF, using Zeiss Cirrus 5000 OCT (765,771). It is likely that automated segmentation using DL approaches will facilitate the diagnosis, monitoring and clinical decision-making for retinal disease in the very near future (733,761,774,775). It promises to deliver a reduction in the clinical burden for patients and physicians alike, since assessments can be undertaken in community or semi-virtual settings, while ever-expanding datasets will allow for continual learning and recognition of features that are imperceptible to humans (776,777). As FRS becomes more prevalent, in particular in the context of high myopia, this will be a powerful tool in the management of this clinical workload. As has been shown with common disorders, such as DMO and AMD, this is likely to provide a safe and cost-effective alternative to human graders (778–781). This study has demonstrated that a DL

model can generate agreement with a ground truth that is similar to that of a human ophthalmologist, in the context of FRS.

In this study, the majority of variance in microperimetric indices could not be explained by age-adjusted schisis metrics alone, indicating other, unknown, contributory factors to the functional variance. Microperimetric assessment has previously been used in the context of ERM foveoschisis, MFS and ODP-M, although usually as a monitoring tool for individual cases (212,408,482,512,604,782,783). Baptista et al used Nidek MP-3 microperimetry to demonstrate that macular sensitivity in 19 eyes with MFS was non-inferior to highly myopic eyes without MFS (482). It's plausible, therefore, that some of the variance in ATS in FRS in this study could be attributed by factors pertaining to the underlying pathology, irrespective of the presence of FRS. Larger normative datasets with age-, refraction- and pathology-matched cohorts are necessary before MP can be reliably applied as a monitoring tool in FRS. Moreover, evidence as to the effects of surgery on functional stability is required, before perimetric assessment could be justifiably used to trigger the decision to intervene. This is especially pertinent, since the clinical relevance of the anatomico-functional relationship is debatable, despite the correlation between greater schisis height or volume and worse perimetric indices, as these functional parameters remain within the reported 'normal range'. This suggests that, in isolation, FRS is unlikely to manifest as a visually significant loss of function, thereby supporting the proposition I have made in Chapters 3-5, wherein logMAR visual acuity (albeit a coarser functional metric) was not markedly affected by the presence of FRS only and can, therefore, remain under observation. It may be the case that MP could be more usefully applied as a monitoring tool to detect early functional decline, prior to the development of gross anatomical changes, such as foveal detachment. Ripandelli et al have suggested that decreased microperimetric sensitivity and worsening fixation stability may be detectable prior to a decline in VA or gross anatomical changes (408). Indeed, this study supports this notion, insofar as I have demonstrated that there is measurable functional disturbance, in the absence of significant anatomical or VA decline, which might act as a contributory indicator in the early detection of progression in FRS. Based on this, I would suggest that, in

addition to the structural monitoring guides that I have outlined in chapters 3 and 4 (Table 3-7 and Table 4-10 respectively), MP assessment could provide a more granular insight into macular sensitivity and fixation, in cases where the magnitude of functional impact is ambiguous. However, further longitudinal research is required to determine whether there is predictive value in serial MP assessments in the early detection of progression. If found to be beneficial, the cost-implications attached to this additional testing may be offset by the capacity for MP to be performed remotely, or in a semi-virtual clinical setting.

This study is limited by small subject numbers and high inter-subject variability, which would confound analysis at the level of individual microperimetric loci, due to a clustering effect. The same limitations restrict the ability to draw comparisons between pathological subtypes, given the small sample sizes, as well as the lack of pathology- or refraction-matched controls. Nonetheless, this study has demonstrated feasibility of both DL approaches for fluid segmentation in FRS and the integration of the derived metrics with functional indices to explore anatomico-functional relationships.

6.5 Conclusions

In conclusion, this study demonstrates a significant relationship between both extent and location of foveomacular retinoschisis and macular function. The approach serves as a 'proof-of-concept' for the application of deep learning models to the anatomico-functional analysis of retinoschitic pathologies. Through the continued improvement of accurate automated segmentation tools, combined with repeatable functional tests, we can expect this type of approach to yield increasingly clinically meaningful outputs in the monitoring and management of retinal diseases in the near future.

CHAPTER 7

DISCUSSION

"Only now, at the end, do you understand"

– Emperor Palpatine

7.1 Introduction

In this thesis I have explored the anatomico-functional behaviour of foveomacular retinoschisis (FRS), in order to establish whether the relationship between structural retinal deformation and visual function can be defined. Based on the observed morphological similarities between various acquired pathologies, I hypothesised that the functional variation and progression to a common anatomical end-point in FRS may be explained by the characteristics of the schisis, irrespective of causative mechanism or chronicity. Secondary to that, based on our current understanding of the foveal ultrastructure and Müller cell subpopulations, I proposed that by modelling and measuring the biomechanical retinal deformation in acquired FRS, we may be able to predict progression, thereby improving prognostic accuracy and guiding the timing of treatment.

I have tested this hypothesis through a series of retrospective and cross-sectional observational studies, in which I have explored both the natural history of three distinct foveomaculoschitic pathologies, myopic foveoschisis, optic disc pit maculopathy and idiopathic foveomacular retinoschisis, and also measured the anatomical and functional relationships using various approaches. In this chapter I will summarise and discuss my findings, their limitations and clinical applicability.

7.2 Natural history

The natural history of FRS, as pertaining to MFS, ODP-M and IFRS, is detailed in Chapters 3, 4 and 5 respectively. The data relating to baseline and longitudinal characteristics for all eyes with fovea-involving FRS are sub-categorised according to the absence or presence of FD and summarised in Table 7-1 and Table 7-2.

Table 7-1: Baseline characteristics of fovea-involving FRS without and with FD

Pathology	**MFS**		**ODP-M***		**IFRS§**		**All eyes**		
Characteristics	No FD	FD	No FD	FD	No FD	FD	No FD	FD	*p-value*
Number of eyes [n(%)]	128 (86%)	12 (14%)	17 (55%)	14 (45%)	30 (100%)	0 (0%)	175 (87%)	26 (13%)	-
VA (logMAR)	0.23 ±0.20	0.62 ±0.32	0.20 ±0.24	0.71 ±0.39	0.09 ±0.21	-	0.20 ±0.21	0.67 ±0.36	***<0.001***
OCT parameters	No FD	FD	No FD	FD	No FD	FD	No FD	FD	*p-value*
Number of eyes [n(%)]	94 (90%)	11 (10%)	17 (55%)	14 (45%)	25 (100%)	0 (0%)	136 (89%)	25 (16%)	-
Central retinal thickness (µm)	263 ±120	427 ±160	503 ±222	691 ±361	311 ±117	-	302 ±156	558 ±310	***<0.001***
Average retinal thickness (µm)	314 ±79	460 ±87	368 ±85	507 ±176	313 ±50	-	321 ±77	475 ±147	***<0.001***
Central schisis height (µm)	185 ±113	368 ±163	352 ±239	617 ±356	173 ±109	-	204 ±144	456 ±267	***<0.001***
Schisis area (mm^2)	8.5 ±8.7	22.3 ±5.6	13.9 ±8.8	19.7 ±6.6	8.6 ±9.7	-	9.3 ±9.0	20.8 ±6.2	***<0.001***

**Types 1a/b ODP-M included, considering possible alternative pathomechanism in type 2 ODP-M. §includes both cases of 'SNIFR' and 'SPLIFR'*

Table 7-2: Longitudinal characteristics of fovea-involving FRS without and with FD

Pathology		**MFS**		**ODP-M**		**IFRS**		**All eyes**		
Clinical characteristics		No FD	FD	No FD	FD	No FD	FD	No FD	FD	*p-value*
Number of eyes [n(%)]		68 (93%)	5 (7%)	11 (73%)	4 (27%)	20 (100%)	0 (0%)	99 (92%)	9 (8%)	-
Duration of follow-up/time to FD		4.7 ±2.6	3.4 ±2.8	3.2 ±2.3	2.3 ±2.7	4.3 ±3.3	-	4.5 ±2.7	2.9 ±2.6	*0.082*
VA (LogMAR)	Baseline	0.23 ±0.20	0.19 ±0.12	0.12 ±0.17	0.39 ±0.36	0.13 ±0.24	-	0.19 ±0.21	0.28 ±0.26	*0.374*
	Final*	0.26 ±0.31	0.63 ±0.30	0.11 ±0.11	0.85 ±0.19	0.17 ±0.33	-	0.23 ±0.30	0.73 ±0.27	***<0.001***
OCT parameters		No FD	FD	No FD	FD	No FD	FD	No FD	FD	*p-value*
Number of eyes [n(%)]		44 (92%)	4 (8%)	11 (73%)	4 (27%)	14 (100%)	0 (0%)	69 (90%)	8 (10%)	-
CRT (µm)	Baseline	268 ± 111	351 ±150	430 ±151	643 ±327	300 ±92	-	300 ±127	497 ±282	*0.053*
	Final	229 ±90	485 ±284	336 ±119	933 ±69	232 ±47	-	247 ±96	709 ±307	***<0.001***
AvRT (µm)	Baseline	312 ±72	429 ±60	334 ±66	416 ±105	306 ±35	-	314 ±65	423 ±79	***<0.001***
	Final	309 ±79	551 ±121	310 ±62	500 ±55	286 ±37	-	305 ±69	525 ±92	***<0.001***
CSH (µm)	Baseline	186 ±110	314 ±56	264 ±157	530 ±348	177 ±86	-	197 ±117	422 ±258	***0.010***
	Final	186 ±142	514 ±152	171 ±128	609 ±181	110 ±71	-	167 ±129	561 ±163	***<0.001***
SA (mm^2)	Baseline	8.8 ±8.5	22.7 ±4.2	11.2 ±8.1	15.5 ±8.3	7.7 ±7.1	-	9.0 ±8.1	19.1 ±7.2	***0.002***
		8.1 ±8.1	25.8 ±3.0	7.6 ±8.4	22.5 ±2.9	3.4 ±6.5	-	6.9 ±8.0	24.2 ±3.3	***<0.001***

**Final VA was defined at most recent follow-up or by time point at which FD was first observed*

At baseline, the proportion of cases with advanced disease (i.e. OLH ± FD) varied by pathology, comprising 45% of those with ODP-M, compared to 14% and 0% of those with MFS and IFRS respectively. This indicates that there is variability in rapidity at which different FRS disorders develop and progress.

Indeed, in those for whom the natural course from FRS to FD could be observed longitudinally, I found that the rate of progression varied according to underlying pathology, with ODP-M and MFS respectively showing 27% and 8% progression to FD during follow-up, compared again to 0% in the IFRS cohort. This discrepancy between pathologies can be largely explained by the difference in underlying pathomechanisms and the relationship with the foveal MC subpopulations. Figure 7-1 demonstrates the various external biomechanical force vectors at play in the pathogenesis of FRS.

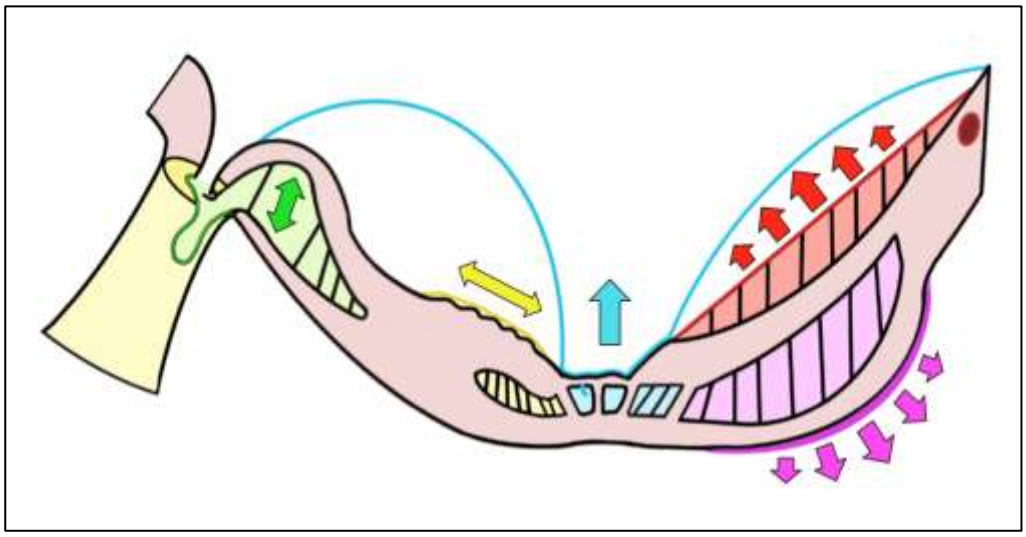

Figure 7-1: An illustration of the external biomechanical force vectors acting on the macula: green denotes the IRF accumulation of ODP-M, resulting in a net anteroposterior force vector; yellow demonstrates the tangential force vectors caused by ERM formation; blue shows the anteroposterior vector along which the posterior cortical vitreous acts following incomplete or anomalous PVD, such as in VMT or SNIFR; purple and red denote the formation of posterior staphyloma and ILM detachment in MFS and the respective centrifugal and centripetal force vectors

The observed morphology of MFS is highly variable, due to the different possible staphyloma distributions and other force vectors involved. For example, the high incidence of pre-macular structures (e.g. VMT and ERM) and the subsequent combinations of additional anteroposterior or tangential force vectors, give rise to countless configurations of MFS, the majority of which achieve long-term anatomico-functional stability. I found that MFS is associated with both the presence of posterior staphyloma and pre-macular structures (Figure 7-2), with ILM detachment in particular being related to greater average retinal thickness and schisis extent. This anatomical configuration manifests with external centrifugal and centripetal force vectors respectively, distributed across the macula. Unlike VMT or ODP-M, MFS is not typified by foveal deformation, such that stretch and rupture of the MCC are not characteristic features in the early stages. Instead, the broad forces generated by staphyloma and ILM detachment initially result in a more extensive macular schisis, manifesting progressive widespread verticalisation of the z-shaped MCs (100). Eventually, when the MCs reach their tensile capacity, forces are transmitted to the fovea, resulting in OLH and FD formation (Figure 7-5A).

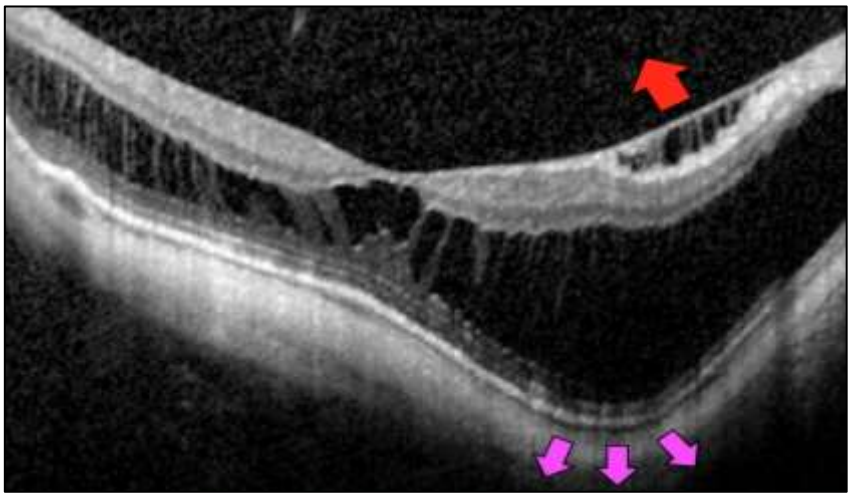

Figure 7-2: OCT in MFS; force vectors from posterior staphyloma (purple arrows) and ILM detachment (red arrow), causing broad macular schisis

In keeping with this, the most useful quantitative OCT parameter for predicting progression in MFS was average retinal thickness (AvRT); it follows that this biomarker, which relates to topographical schisis extent and, in turn, the magnitude

of externally applied forces, is most closely associated with risk of progression. Furthermore, the fact that the forces generated by axial elongation and ILM fibrosis increase very gradually, usually culminating in the 6-7th decade of life, fits with the low rate of progression (8%) over several years, as well as the average age of 59 years in this cohort.

In contrast to the complex interplay of external forces in MFS, ODP-M represents a relatively simpler pathology. It usually arises due to the generation of force vectors *within* the retina, a manifestation of the ingress of fluid at the site of a defect in the lamina cribrosa. Although approximately half of all eyes with FRS secondary to ODP-M do not progress, indicating a role for surveillance without intervention, a subset of cases are characterised by the rapid generation of high magnitude anteroposterior force vectors which, due to the relative rigidity of the sclera, cause marked deformation of the foveal architecture. In particular, elongation and rupture of the vertical MCC stalk, and early formation of a foveal pseudocyst is commonly observed (Figure 7-3). At this point, unopposed lateral traction from the zMCs leads to broadening of the schisis cavity, followed by rapid progression from OLH to FD formation in a high proportion of cases (Figure 7-5B). Considering this abovementioned natural history, it follows that there is significant association between central retinal thickness (CRT) and central schisis height (CSH) with development of FD during the follow-up period. Moreover, given the lack of extrinsic tangential or centripetal (i.e. pre-macular) tractional forces, FRS in ODP-M is purely a disorder of biomechanical retinal stretch and, as such, ILHs and FTMHs are rarely observed.

It ought to be noted, as discussed in chapter 4, that there appears to be a biphasic age distribution, with a greater propensity for children to present with a primary neurosensory detachment. This may well represent a separate pathomechanism in this age group, following a distinct natural course to that described above. However, the mean age of 39 years in this cohort of eyes with primary IRF accumulation supports the postulated role of vitreous liquefaction and epipapillary traction in the pathomechanism of ODP-M.

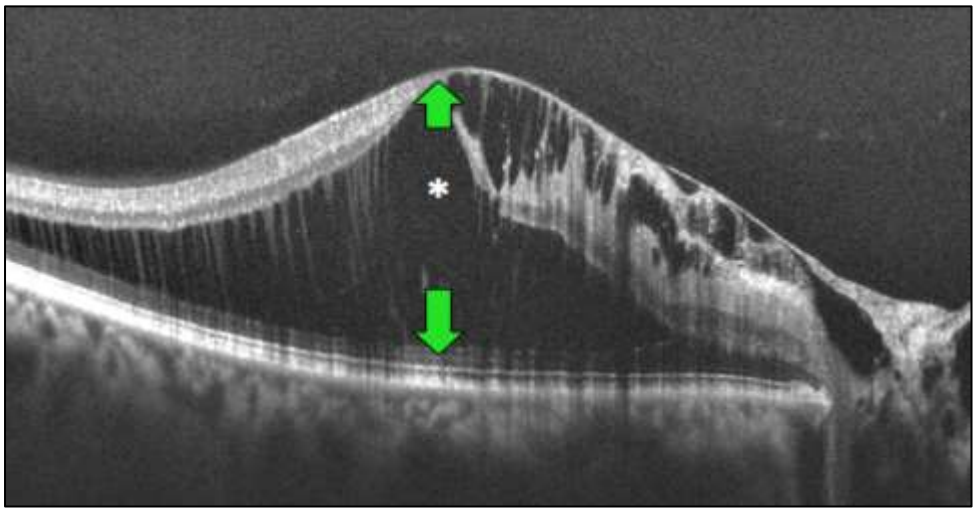

Figure 7-3: OCT in ODP-M; anteroposterior force vectors (green arrows) causing marked foveal deformation, central pseudocyst (asterisk) and multilayer schisis

Finally, study of eyes with IFRS demonstrated no cases of progression to OLH or FD. An association was found between posterior hyaloid attachment and FRS in these cases, leading me to hypothesise that IFRS occurs at the time of normal vitreous liquefaction, in the context of abnormal cortical vitreous adherence in susceptible individuals (Figure 7-4). The mean age of 64 years in this cohort is consistent with this notion. If this is the case, we may conclude that inward tractional forces from broad, anomalous PVD are sufficient to cause a small degree of macular deformation but insufficient to cause significant zMC stretch, such that there is minimal risk of progression to OLH or FD formation. Of additional interest, all eyes studied had temporal extension of FRS and association was demonstrated with peripheral retinoschisis. The precise nature of this relationship remains unclear. Longitudinal follow-up revealed that cases of IFRS tend to demonstrate morphological stability or spontaneous resolution over time (Figure 7-5C).

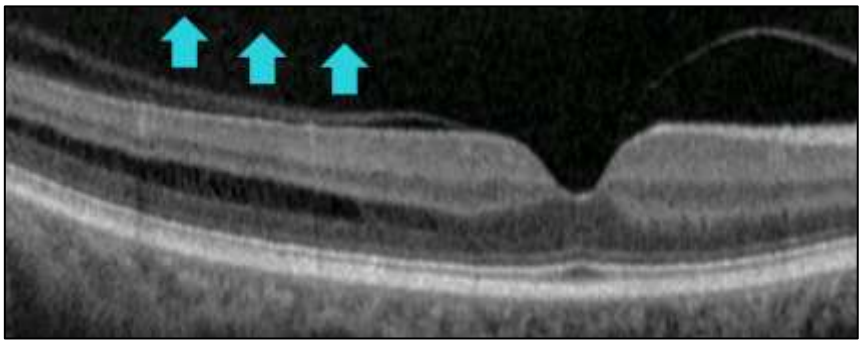

Figure 7-4: OCT in IFRS; broad posterior hyaloid attachment, with inward force vectors (blue arrows) over an area of temporal schisis, extending peripherally

A subgroup of cases with IFRS were noted to have different demographic and anatomical characteristics than the majority of the cohort. These 3 patients were younger, mildly myopic and, in all cases, Chinese. Two of the patients were siblings. When correlated with existing evidence from a series by Sun et al, I postulated that these cases represented a distinct entity to SNIFR (728). These eyes appear to have excessive vitreous synchysis and tight vitreo-macular attachment (as opposed to age-appropriate vitreous liquefaction in those cases with SNIFR), which may be compounded with low-grade myopic changes to convey a high risk of progression to the anatomical end-point of FD or macular hole. To differentiate this subtype of IFRS from SNIFR, I proposed the term 'stellate progressive liquefaction-induced foveomacular retinoschisis' (SPLIFR). Genetic testing did not identify a specific mutations in the siblings and the possibility of a heritable predisposition in SPLIFR remains unresolved.

Based on the findings of this thesis, I conclude that the natural history of pathologies affected by FRS differ according to the underlying pathomechanisms and magnitude of the relative external forces. Qualitative and quantitative anatomical parameters of interest will therefore vary in their utility in monitoring and risk stratifying cases. There is a growing body of evidence for surgical techniques in both MFS and ODP-M with high rates of success. The challenge is determining which patients serve to benefit from intervention and at what point in the course of the disease. I have identified several pathology-specific biomarkers, which may be of clinical relevance in the surveillance of MFS and ODP-M; these are discussed further in 7.4.

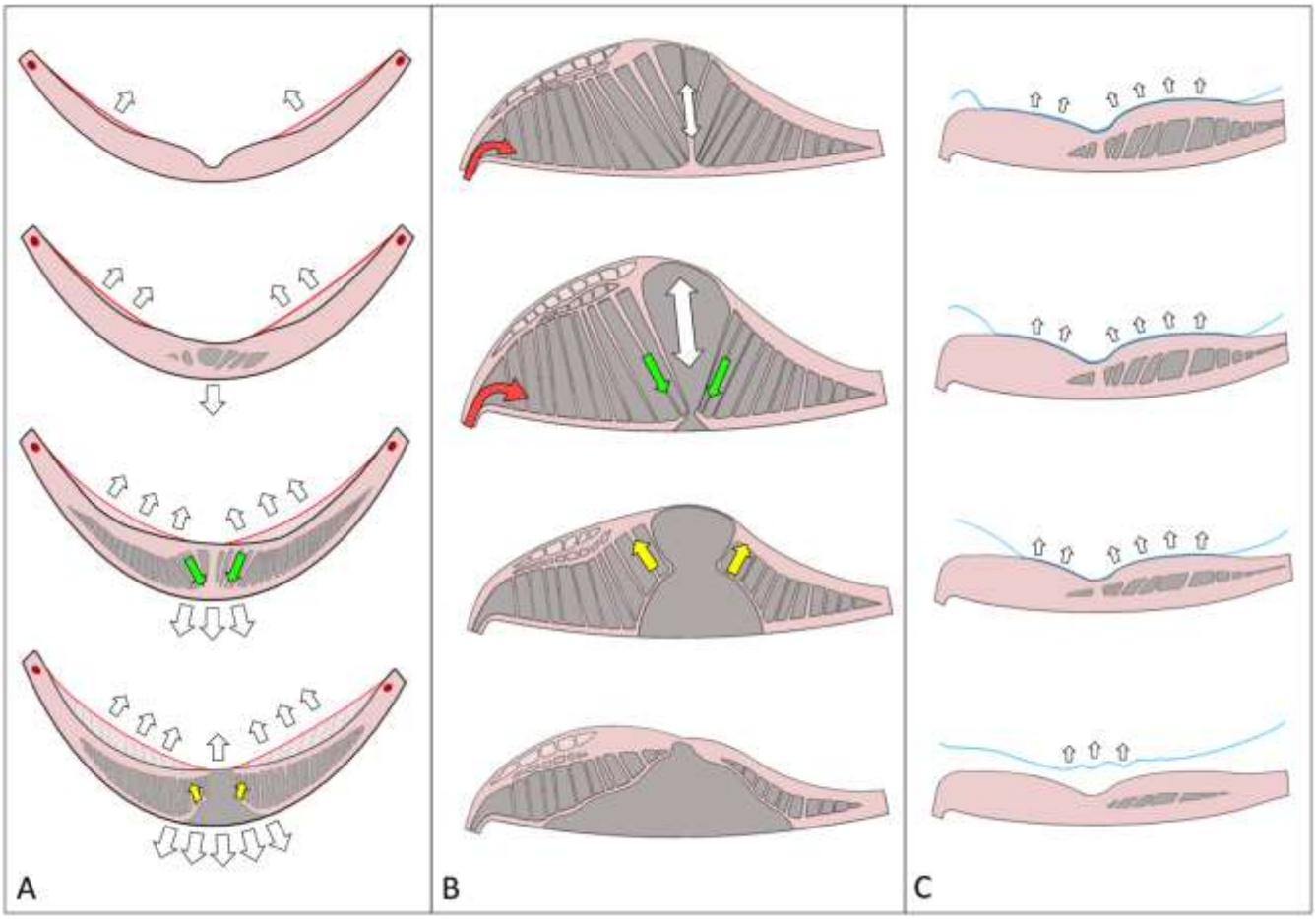

Figure 7-5: The various pathomorphologies of progressive FRS: (A): Myopic foveoschisis is typified by the presence of pre-retinal centripetal traction, combined with centrifugal scleral ectasia (white arrows) with progressive verticalisation of MCs, transmitting forces to the outer foveal retina (green arrows). Finally an OLH and/or FD develops, with unopposed action of zMCs (yellow arrows) resulting in enlargement of the FD and collapse of the schisis cavity; (B): in optic disc pit maculopathy, ingress of fluid through the lamina cribrosal defect (red arrow) may result in rapid formation of a schitic cavity, with anteroposterior force vectors (white arrows) causing foveal deformation, pseudocyst formation and eventual OLH/FD, through transmitted forces towards the outer retina (green arrows). Subsequent enlargement of the FD, through unopposed zMC traction (yellow arrows), leads to collapse of the foveal pseudocyst and schisis cavity; (C): in stellate non-hereditary foveomacular retinoschisis, anomalous PVD with residual vitreous cortical attachment is frequently observed. During vitreous syneresis, this may exert broad, low-grade centripetal traction (white arrows), causing shallow schisis formation in susceptible eyes. The natural history is one of spontaneous improvement, even in the absence of clear evidence of complete PVD.

7.3 Anatomico-functional behaviour

The next matter that I sought to address was that of the anatomico-functional behaviour of FRS, in the absence of OLH or FD. In chapter 1, I hypothesised that, regardless of aetiology or chronicity, visual function is not related to the presence of foveomacular retinoschisis *per se*, but rather to the magnitude of retinal deformation. In order to explore this, I have analysed longitudinal visual function in FRS-only subgroups within each pathology group. Moreover, I have measured associations between schisis morphology and visual function, using several approaches. The longitudinal, observational data relating to FRS-only cases are summarised in Table 7-3.

In each pathology subgroup, there was no significant change in visual function during follow-up of those cases with FRS only. On analysis of all eyes with FRS, there was a decline in VA measured from 0.19 (±0.21) to 0.23 (±0.3) that did not reach significance ($p=0.170$). Final VA was not significantly associated with disease duration in any pathology subgroup, nor on whole group analysis.

However, there was significant variation in anatomical metrics between baseline and follow-up; all FRS subgroups demonstrated a significant reduction in CRT over time, while ODP-M and IFRS showed additional significant reduction in CSH. On whole group analysis, a significant improvement was found for CRT, CSH and SA (all $p<0.022$), but not AvRT ($p=0.056$).

The relationship between anatomical and functional changes varied between pathologies. For example, in MFS, there was a significant association found between final VA and final absolute AvRT, CSH and SA (although with small effect sizes), but not with relative changes in these parameters. With the exception of SA, final absolute OCT metrics were not associated with VA in cases with ODP-M, although *relative* decreases in CRT, AvRT, CSH and SA *were* all associated with significantly greater improvement in VA. IFRS did not demonstrate any associations between VA and OCT parameters at baseline or final follow-up.

Table 7-3: Baseline and final characteristics of eyes with fovea-involving FRS only

	MFS			ODP-M			IFRS			All FRS Eyes		
Clinical characteristics	**Baseline**	**Final**	***p-value***	**Baseline**	**Final**	**p-value**	**Baseline**	**Final**	***p-value***	**Baseline**	**Final**	***p-value***
Number of eyes	68		-	11		-	20		-	99		-
F/up duration (years)	4.7 ±2.6		-	3.2 ±2.3		-	4.3 ±3.3		-	4.5 ±2.7		-
VA (logMAR)	0.23 ±0.20	0.26 ±0.31	*0.543*	0.12 ±0.17	0.11 ±0.11	*0.158*	0.13 ±0.24	0.17 ±0.33	*0.271*	0.19 ±0.21	0.23 ±0.30	*0.170*
OCT parameters	**Baseline**	**Final**	***p-value***	**Baseline**	**Final**	**p-value**	**Baseline**	**Final**	***p-value***	**Baseline**	**Final**	***p-value***
Number of eyes	44			11		-	14		-	69		**-**
CRT (µm)	268 ±111	229 ±90	***0.019***	430 ±151	336 ±119	***0.014***	300 ±92	232 ±47	***0.012***	300 ±127	247 ±96	***<0.001***
AvRT (µm)	312 ±72	309 ±79	*0.631*	334 ±66	310 ±62	*0.631*	306 ±35	286 ±37	*0.070*	314 ±65	305 ±69	*0.056*
CSH (µm)	186 ±110	186 ±142	*0.913*	264 ±157	171 ±128	***0.015***	177 ±86	110 ±71	***0.025***	197 ±117	167 ±129	***0.019***
SA (mm^2)	8.8 ±8.5	8.1 ±8.1	*0.127*	11.2 ±8.1	7.6 ±8.4	*0.483*	7.7 ±7.1	3.4 ±6.5	*0.058*	9.0 ±8.1	6.9 ±8.0	***0.022***

These findings support the assertion that, although the presence and duration of FRS does not appear to have a significant longitudinal affect on VA, there is both within- and between-group variation, which may be related to morphological characteristics of the schisis. The fact that this correlation was only demonstrated in cases of MFS and ODP-M, which have greater mean values for all parameters, as well as larger variances, than IFRS, indicates that this anatomico-functional relationship in FRS may be non-linear. Considering the abovementioned relationship between magnitude of retinal deformation and progression to OLH/FD, as well as the work by Govetto et al, modelling the association between MC stretch and VA, it is plausible that there is a threshold at which schisis begins to cause microstructural changes, sufficient to affect visual function (100).

I explored this concept further in Chapter 6, using a novel approach to segment and estimate the schisis cavity parameters and measure associations with microperimetric macular sensitivity and fixation indices. Using this methodology, I was able to stratify the anatomico-functional relationship according to both eccentricity from the fovea and schisis height. I demonstrated that, not only was there an association between local schisis height and pointwise macular sensitivity, but that this correlation was most evident in the centremost 4.2˚ of the macula and only became significant at schisis heights beyond 100µm. This supports the notion of a threshold relationship between schisis height and macular function, wherein functional decline may be observed earliest at the centremost retina, likely due to the variable properties of MC subpopulations at the fovea, leading to disproportionate deformation in this region. While FRS serves as an effective system to protect central function during biomechanical stretch of the retina, there is a threshold of deformation at which measurable visual dysfunction occurs, which appears to precede evidence of gross anatomical progression. The potential clinical relevance of psychovisual testing is discussed further in 7.4.

Overall, these results support the hypothesis that FRS does not, in itself, manifest in loss of visual function, regardless of the underlying aetiology or disease duration. However, despite this, FRS *may* result in loss of function, initially due to excessive

retinal deformation and, subsequently, via development of outer retinal defects or foveal detachment. The probability of progression to these anatomical end-points appears, in turn, to be related to the underlying pathology in question, since the pathomechanics and, therefore, the natural histories vary considerably. Armed with an understanding of the foveal ultrastructure and evidence of disease behaviour through a series of observational experiments, I have demonstrated that we can use various multimodal approaches to study, and possibly even predict, anatomico-functional behaviour in different forms of acquired FRS. It is worth noting that it is not possible to apply the same anatomico-functional modelling in cases of FRS that are not purely biomechanical, as demonstrated in chapter 6 using X-linked retinoschisis, by means of a negative control.

7.4 Clinical relevance

The next challenge is the application of this knowledge to the clinical management of patients with FRS. Clearly, progression to FD carries the highest burden of visual morbidity and early identification of high-risk patients ought to be the clinician's priority. Practically speaking, there are several qualitative and quantitative metrics that are readily available for consideration in the clinical setting, through inspection of OCT images and interpretation of automated OCT output metrics. For example, as outlined above, horizontal schisis extent and AvRT may be useful interval markers in MFS; in Chapter 3, using automated calculations from the Topcon 3D OCT-1000, I demonstrated that all eyes that went on to develop FD had an AvRT >450µm. Such patients may benefit from closer monitoring for the functional deterioration or microstructural outer retinal changes that precede FD. On the other hand, AvRT was not a useful predictive marker in ODP-M, but instead, all those in whom progression was observed in Chapter 4, there was a CRT >650µm and a CSH >400 in 80%. Considering the high rate of early progression in ODP-M, as well as the good surgical outcomes, it may be prudent to observe those with large central retinal deformation closely and intervene promptly at the point of visual and/or anatomical

deterioration. Finally, SNIFR appears to be a very stable condition, with minimal anatomical or functional effects and can reasonably be observed with reduced vigilance. This is caveated with the knowledge that there is an association with peripheral retinoschisis and absolute scotoma in this cohort, which may carry implications for patients' day-to-day activities, as well as a separate subgroup of eyes with IFRS (herein termed SPLIFR), which may carry an increased risk of progression. However, in all cases, the precise role for intervention remains unclear.

I have identified a series of potential anatomical biomarkers that may be used in the risk stratification of patients with MFS and ODP-M, to optimise surveillance intervals and facilitate early identification of anatomical and visual decline, in order to permit timely surgical intervention (Table 7-4). Given the potential for observer bias (as discussed in Chapters 3 and 4), both internal and external validation of this guidance is warranted before routine use in clinical practice.

Table 7-4: Proposed monitoring scoring systems for early detection of progression in MFS and ODP-M

MFS Monitoring Scoring System			**ODP-M Monitoring Scoring System**		
Characteristic	**Threshold**	**Score**	**Characteristic**	**Threshold**	**Score**
Schisis extent	S0-2	0	Central retinal thickness (µm)	<400	0
	S3-4	1		400-600	1
Average retinal thickness (µm)	<450	0		>600	2
	≥450	1			
Total score					
0 = low risk 1 = moderate risk 2 = high risk					
Suggested Monitoring Frequency					
Low risk			12 monthly		
Moderate risk			6 monthly		
High risk			≤3 monthly		

Of those cases detailed in Table 7-3, only 19 eyes (27%) had internal control data from an unaffected fellow eye. When direct comparison of VA is made between these affected eyes and healthy fellow eyes at final follow-up, a significant difference is noted (logMAR 0.13 vs 0.00, p=0.0015). This disparity varied by pathology; in the case of IFRS and MFS, the final VA was non-significantly different between eyes affected by FRS and healthy fellow eyes. However, due to the high proportion of concurrent disease affecting fellow eyes in MFS, there were insufficient healthy control eyes to draw a meaningful comparison. Moreover, fellow eyes of those with MFS had significantly smaller refractive errors and lower incidence of pre-macular

structures (as compared at baseline), somewhat confounding any comparison of in subgroup, based on presence of FRS alone. Those with ODP-M retained a significant difference in VA between affected and healthy fellow eyes (0.11 vs -0.04, p=0.008).

In a clinical setting, however, it is important to determine the absolute visual morbidity in addition to that which is relative to the healthy fellow eye. For example, of the 70 eyes with stable FRS during follow-up, only 12 had a final measured logMAR VA ≥0.30. That is to say, that 83% of eyes with FRS retain driving standard VA in the affected eye. With the exception of one eye with IFRS and unexplained visual loss, all those eyes with VA >0.30 were myopic eyes with concurrent contractile ERM and/or ILH.

Furthermore, in Chapter 6, in which I collected MP sensitivity and fixation data, only 3/21 (14%) eyes with FRS had average threshold sensitivity (ATS) outside of the reported normal range (i.e. <25dB), while all eyes had fixation indices (P1 and P2) that would be considered indicative of 'stable' fixation. There was no significant measureable difference in ATS and fixation indices between affected subjects and healthy controls. It ought to be noted that average MP sensitivity metrics may be misleading in the context of focal macular disease, and in chapter 6, the use of loci-specific comparisons did, in fact, reveal significant differences between normal and affected eyes. As such, serial MP may represent a more useful auxiliary test (in addition to the anatomical criteria detailed in Table 7-4) to confirm early, focal functional decline and aid surgical decision-making. External, case-controlled validation of this technique is warranted to clarify its role as a routine monitoring tool.

Therefore, while it is arguable that, from a functional perspective, the visual morbidity associated with FRS is not clinically significant in the majority of cases, it appears that it does convey a degree of functional loss, compared to unaffected fellow or healthy control eyes. Considering the demonstrated long-term stability of FRS and inherent risk of surgery, there is not currently a strong argument in favour of early intervention in such cases. The data from this thesis support a conservative approach to FRS, with frequency of observation being guided by the degree of

retinal deformation and associated visual function, on a case-by-case approach. The merit of such an individualised management approach is that progression may be detected earlier, or even pre-empted, through vigilant serial assessment and awareness of clinically relevant biomarkers.

Finally, I have demonstrated the feasibility of automated segmentation algorithms, using a deep learning approach, in the characterisation of schisis morphology. This indicates that there is scope for remote screening to provide quantification of anatomical biomarkers, which can plausibly be combined with functional testing, to enable unsupervised, semi-virtual surveillance in the future. Longitudinal data collection would shed light on the predictive value of these biomarkers, while also refining the prognostic precision of existing parameters and identifying novel metrics. Based on these findings, subsequent research can be focused on the anatomico-functional benefit of intervention, relative to observation, in those cases that are considered at high-risk of progression, in order to clarify the optimal timing of surgery.

7.5 Limitations

As discussed throughout the thesis, there are several limitations that affect our ability to apply these findings clinically. Firstly, the majority of data were acquired retrospectively, which introduces a potential for confounding. Although I have reported several significant findings relating to anatomical characteristics in FRS, these, for the most part, do not fully explain the observed variance in function. While I have attempted to control for many potentially confounding variables, this is not always practical in a clinical setting and extrapolation of the findings in this thesis might not carry sufficient external validity to be reasonably applied to individuals in a 'real-world' population. Moreover, some sample populations in this study were small with a high degree of inter-subject functional variability. While this type of research is important to introduce concepts and establish methodological feasibility, further large-scale investigation is merited to ensure validity.

Notwithstanding these limitations, Chapters 3, 4 and 5 each represent some of the largest observational cohorts of MFS, ODP-M and IFRS respectively to date, and ought to provide substantial novel contributions to the wider understanding of these disorders within the field of retinal research. Chapter 6 contains the unique application of both deep learning and psychovisual assessment to foveomacular retinoschisis; an approach that I believe reflects (and hope will contribute to) the increasing introduction of technology into the clinical environment, in which we can diagnose, monitor and treat our patients more effectively and efficiently than ever before.

7.6 Conclusion

In conclusion, this thesis sets about to investigate the anatomico-functional behaviour of foveomacular retinoschisis, through a series of observational and cross-sectional studies. Although not a common finding, FRS is far from rare and describes a morphology that retinal specialists will be familiar with. Despite this, it is often overlooked as an entity and, as such, the breadth of research into the field has been relatively limited.

This dissertation addresses some of these shortcomings through large natural history studies of common forms of acquired FRS, namely myopic foveoschisis, optic disc pit maculopathy and idiopathic foveomacular retinoschisis. I have demonstrated that both visual function and incidence of anatomical progression in different forms of FRS are associated with idiosyncratic and measurable structural parameters. In each of the unique pathomechanisms, the nature of foveomacular deformation can be modelled as a function of the biomechanical properties of the central Müller cell subpopulations.

Although FRS is a stable condition, with minimal clinical implications for the majority of eyes, there is a subset in which there is a high risk of progression and associated visual morbidity. My findings serve to establish a better understanding of the various

pathologies and their natural histories, the ways in which they are similar and in which they differ. Combined with the application of existing and emerging multimodal techniques and their respective metrics, in the evaluation of FRS, I have introduced several novel concepts, which can help to inform prognosis and guide the management of this interesting and unusual retinal pathological entity.

BIBLIOGRAPHY

“When I left you, I was but the learner. Now, I am the master”

– Darth Vader

1. Wilczek M. Ein Fall der Netzhautspaltung (Retinoschisis) mit einer Öffnung. Z Augenheilkd. 1935;85:108.

2. Byer NE. Clinical Study of Senile Retinoschisis. Arch Ophthalmol. 1968 Jan 1;79(1):36–44.

3. Lincoff H, Lopez R, Kreissig I, Yannuzzi L, Cox M, Burton T. Retinoschisis associated with optic nerve pits. Arch Ophthamol. 1988 Jan;106(1):61–7.

4. Imamura Y, Zweifel SA, Fujiwara T, Freund KB, Spaide RF. High-resolution optical coherence tomography findings in optic pit maculopathy. Retina Phila Pa. 2010 Jul;30(7):1104–12.

5. Reh T. Chapter 13: The development of the retina. In: Schachat A, editor. Retina. 6th ed. Elsevier; 2017. p. 330–41.

6. Gregg R, Singer J, Kamermans M, McCall M, Massey S. Function and Anatomy of the Mammalian Retina. In: Schachat AP, editor. Ryan's Retina. Sixth. Edinburgh: Elsevier; 2018. p. 1201–324.

7. Drexler W, Sattmann H, Hermann B, Ko TH, Stur M, Unterhuber A, et al. Enhanced visualization of macular pathology with the use of ultrahigh-resolution optical coherence tomography. Arch Ophthalmol Chic Ill 1960. 2003 May;121(5):695–706.

8. Spaide R, Curcio C. Anatomical correlates to the bands seen in the outer retina by optical coherence tomography. Retina Phila Pa. 2011 Sep;31(8):1609–19.

9. Bringmann A, Syrbe S, Görner K, Kacza J, Francke M, Wiedemann P, et al. The primate fovea: Structure, function and development. Prog Retin Eye Res. 2018 Sep;66:49–84.

10. Burris C, Klug K, Ngo IT, Sterling P, Schein S. How Müller glial cells in macaque fovea coat and isolate the synaptic terminals of cone photoreceptors. J Comp Neurol. 2002;453(1):100–11.

11. Lujan BJ, Roorda A, Knighton RW, Carroll J. Revealing Henle's fiber layer using spectral domain optical coherence tomography. Invest Ophthalmol Vis Sci. 2011 Mar;52(3):1486–92.

12. Mrejen S, Gallego-Pinazo R, Freund KB, Paques M. Recognition of Henle's Fiber Layer on OCT Images. Ophthalmology. 2013 Jun 1;120(6):e32-e33.e1.

13. Otani T, Yamaguchi Y, Kishi S. Improved visualization of Henle fiber layer by changing the measurement beam angle on optical coherence tomography. Retina Phila Pa. 2011 Mar;31(3):497–501.

14. Jonnal RS, Kocaoglu OP, Zawadzki RJ, Lee SH, Werner JS, Miller DT. The Cellular Origins of the Outer Retinal Bands in Optical Coherence Tomography Images. Invest Ophthalmol Vis Sci. 2014 Dec;55(12):7904–18.

15. Staurenghi G, Sadda S, Chakravarthy U, Spaide RF, International Nomenclature for Optical Coherence Tomography (IN•OCT) Panel. Proposed lexicon for anatomic landmarks in normal posterior segment spectral-domain optical coherence tomography: the IN•OCT consensus. Ophthalmology. 2014 Aug;121(8):1572–8.

16. Srinivasan VJ, Monson BK, Wojtkowski M, Bilonick RA, Gorczynska I, Chen R, et al. Characterization of outer retinal morphology with high-speed, ultrahigh-resolution optical coherence tomography. Invest Ophthalmol Vis Sci. 2008 Apr;49(4):1571–9.

17. Toth CA, Narayan DG, Boppart SA, Hee MR, Fujimoto JG, Birngruber R, et al. A comparison of retinal morphology viewed by optical coherence tomography and by light microscopy. Arch Ophthalmol Chic Ill 1960. 1997 Nov;115(11):1425–8.

18. Curcio CA, Sloan KR, Kalina RE, Hendrickson AE. Human photoreceptor topography. J Comp Neurol. 1990;292(4):497–523.

19. Distler C, Dreher Z. Glia Cells of the Monkey Retina—II. Müller Cells. Vision Res. 1996 Aug 1;36(16):2381–94.

20. Dubis AM, Hansen BR, Cooper RF, Beringer J, Dubra A, Carroll J. Relationship between the Foveal Avascular Zone and Foveal Pit Morphology. Invest Ophthalmol Vis Sci. 2012 Mar;53(3):1628–36.

21. Hendrickson A. Organization of the Adult Primate Fovea. In: Penfold PL, Provis JM, editors. Macular Degeneration [Internet]. Berlin/Heidelberg: Springer-Verlag; 2005 [cited 2021 Jan 20]. p. 1–23. Available from: http://link.springer.com/10.1007/3-540-26977-0_1

22. Syrbe S, Kuhrt H, Gärtner U, Habermann G, Wiedemann P, Bringmann A, et al. Müller glial cells of the primate foveola: An electron microscopical study. Exp Eye Res. 2018 Feb 1;167:110–7.

23. Yamada E. Some structural features of the fovea centralis in the human retina. Arch Ophthalmol Chic Ill 1960. 1969 Aug;82(2):151–9.

24. Curcio CA, Allen KA. Topography of ganglion cells in human retina. J Comp Neurol. 1990 Oct 1;300(1):5–25.

25. Kolb H, Marshak D. The midget pathways of the primate retina. Doc Ophthalmol Adv Ophthalmol. 2003 Jan;106(1):67–81.

26. Sjöstrand J, Conradi N, Klarén L. How many ganglion cells are there to a foveal cone? Graefes Arch Clin Exp Ophthalmol. 1994 Jul 1;232(7):432–7.

27. Kolb H, Nelson RF, Ahnelt PK, Ortuño-Lizarán I, Cuenca N. The Architecture of the Human Fovea. In: Kolb H, Fernandez E, Nelson R, editors. Webvision: The

Organization of the Retina and Visual System [Internet]. Salt Lake City (UT): University of Utah Health Sciences Center; 1995 [cited 2021 Jan 20]. Available from: http://www.ncbi.nlm.nih.gov/books/NBK554706/

28. Adhi M, Aziz S, Muhammad K, Adhi MI. Macular Thickness by Age and Gender in Healthy Eyes Using Spectral Domain Optical Coherence Tomography. PLoS ONE [Internet]. 2012 May 21 [cited 2021 Jan 20];7(5). Available from: https://www.ncbi.nlm.nih.gov/pmc/articles/PMC3357395/

29. Duke-Elder S. The Eye in Evolution. 1st ed. Kimpton, London; 1958.

30. Reardon A, Heinegård D, McLeod D, Sheehan JK, Bishop PN. The large chondroitin sulphate proteoglycan versican in mammalian vitreous. Matrix Biol J Int Soc Matrix Biol. 1998 Oct;17(5):325–33.

31. Bishop PN. Structural macromolecules and supramolecular organisation of the vitreous gel. Prog Retin Eye Res. 2000 May;19(3):323–44.

32. Reardon AJ, Le Goff M, Briggs MD, McLeod D, Sheehan JK, Thornton DJ, et al. Identification in vitreous and molecular cloning of opticin, a novel member of the family of leucine-rich repeat proteins of the extracellular matrix. J Biol Chem. 2000 Jan 21;275(3):2123–9.

33. Cain SA, Morgan A, Sherratt MJ, Ball SG, Shuttleworth CA, Kielty CM. Proteomic analysis of fibrillin-rich microfibrils. Proteomics. 2006 Jan;6(1):111–22.

34. Crafoord S, Ghosh F, Sebag J. Vitreous Biochemistry and Artificial Vitreous. In: Sebag J, editor. Vitreous: in Health and Disease [Internet]. New York, NY: Springer; 2014 [cited 2021 Jun 15]. p. 81–92. Available from: https://doi.org/10.1007/978-1-4939-1086-1_6

35. Sebag J, editor. Vitreous: in Health and Disease [Internet]. New York: Springer-Verlag; 2014 [cited 2021 Jun 15]. Available from: https://www.springer.com/gp/book/9781493910854

36. Sebag J. Vitreous and Vitreoretinal Interface. In: Schachat AP, editor. Ryan's Retina. Sixth. Edinburgh: Elsevier; 2018. p. 1613–707.

37. Sebag J, Balazs EA. Human vitreous fibres and vitreoretinal disease. Trans Ophthalmol Soc U K. 1985;104 (Pt 2):123–8.

38. Sebag J, Balazs EA. Morphology and ultrastructure of human vitreous fibers. Invest Ophthalmol Vis Sci. 1989 Aug;30(8):1867–71.

39. Worst JG. Cisternal systems of the fully developed vitreous body in the young adult. Trans Ophthalmol Soc UK. 1977;97(4):550–4.

40. Jongebloed WL, Worst JF. The cisternal anatomy of the vitreous body. Doc Ophthalmol Adv Ophthalmol. 1987 Oct;67(1–2):183–96.

41. J.G. Worst. The bursa intravitrealis premacularis: New developments in ophthalmology. Doc Ophth Proc Ser. 1976;275–9.

42. Sebag J. The Vitreous: Structure, Function, and Pathobiology [Internet]. New York: Springer-Verlag; 1989 [cited 2021 Jun 15]. Available from: https://www.springer.com/gp/book/9781461389101

43. Kishi S, Shimizu K. Posterior precortical vitreous pocket. Arch Ophthamol. 1990 Jul;108(7):979–82.

44. Balazs E. Molecular morphology of the vitreous body. In: Smelser G, editor. The Structure of the Eye. New York and London: Academic Press; 1961. p. 293–310.

45. Boltz-Nitulescu G, Grabner G, Förster O. Macrophage-like properties of human hyalocytes. Adv Exp Med Biol. 1979;121B:223–8.

46. Sebag J. Anatomy and pathology of the vitreo-retinal interface. Eye. 1992 Nov;6(6):541–52.

47. Sakamoto T, Ishibashi T. Hyalocytes: essential cells of the vitreous cavity in vitreoretinal pathophysiology? Retina Phila Pa. 2011 Feb;31(2):222–8.

48. Cohen AI. Electron microscopic observations of the internal limiting membrane and optic fiber layer of the retina of the Rhesus monkey (M. mulatta). Am J Anat. 1961 Mar;108:179–97.

49. Russell SR, Shepherd JD, Hageman GS. Distribution of glycoconjugates in the human retinal internal limiting membrane. Invest Ophthalmol Vis Sci. 1991 Jun 1;32(7):1986–95.

50. Reichenbach A, Bringmann A. Müller cells in the healthy and diseased retina. Springer, New York; 2010.

51. Foos RY. Vitreoretinal juncture; topographical variations. Invest Ophthalmol. 1972;11(10):801–8.

52. Henrich PB, Monnier CA, Halfter W, Haritoglou C, Strauss RW, Lim RYH, et al. Nanoscale Topographic and Biomechanical Studies of the Human Internal Limiting Membrane. Invest Ophthalmol Vis Sci. 2012 May 1;53(6):2561–70.

53. Kim Y, Wilson D. Pathophysiology of the Vitreoretinal Interface. In: Quiroz-Mercado H, Kerrison J, Alfaro D, Mieler W, Liggett P, editors. Macular surgery. 2nd ed. Lippincott Williams & Wilkins (LWW); 2011.

54. Gandorfer A, Rohleder M, Sethi C, Eckle D, Welge-Lüssen U, Kampik A, et al. Posterior vitreous detachment induced by microplasmin. Invest Ophthalmol Vis Sci. 2004 Feb;45(2):641–7.

55. Wolter JR. Pores in the internal limiting membrane of the human retina. Acta Ophthalmol (Copenh). 1964;42:971–4.

56. Kuwabara T. Studies of Retinal Vascular Patterns: Part I. Normal Architecture. Arch Ophthalmol. 1960 Dec 1;64(6):904.

57. Almeida DRP, Chin EK, Tarantola RM, Folk JC, Boldt HC, Skeie JM, et al. Effect of Internal Limiting Membrane Abrasion on Retinal Tissues in Macular Holes. Invest Ophthalmol Vis Sci. 2015 May;56(5):2783–9.

58. Kugler EC, Greenwood J, MacDonald RB. The "Neuro-Glial-Vascular" Unit: The Role of Glia in Neurovascular Unit Formation and Dysfunction. Front Cell Dev Biol [Internet]. 2021 [cited 2022 Dec 8];9. Available from: https://www.frontiersin.org/articles/10.3389/fcell.2021.732820

59. Ponsioen TL, van Luyn MJA, van der Worp RJ, Pas HH, Hooymans JMM, Los LI. Human retinal Müller cells synthesize collagens of the vitreous and vitreoretinal interface in vitro. Mol Vis. 2008;14:652–60.

60. Reichenbach A, Hagen E, Schippel K, Eberhardt W. Quantitative electron microscopy of rabbit Müller (glial) cells in dependence on retinal topography. Z Mikrosk Anat Forsch. 1988;102(5):721–55.

61. Uga S, Smelser GK. Comparative Study of the Fine Structure of Retinal MÜller Cells in Various Vertebrates. Invest Ophthalmol Vis Sci. 1973 Jun 1;12(6):434–48.

62. Yang B, Brown D, Verkman AS. The mercurial insensitive water channel (AQP-4) forms orthogonal arrays in stably transfected Chinese hamster ovary cells. J Biol Chem. 1996 Mar 1;271(9):4577–80.

63. Reid SNM, Farber DB. Glial transcytosis of a photoreceptor-secreted signaling protein, retinoschisin. Glia. 2005 Feb;49(3):397–406.

64. Roesch K, Jadhav AP, Trimarchi JM, Stadler MB, Roska B, Sun BB, et al. The transcriptome of retinal Müller glial cells. J Comp Neurol. 2008 Jul 10;509(2):225–38.

65. Bunt-Milam AH, Saari JC, Klock IB, Garwin GG. Zonulae adherentes pore size in the external limiting membrane of the rabbit retina. Invest Ophthalmol Vis Sci. 1985 Oct;26(10):1377–80.

66. Priore LVD, Lewis A, Tan S, Carley WW, Webb WW. Fluorescence light microscopy of F-actin in retinal rods and glial cells. Invest Ophthalmol Vis Sci. 1987 Apr 1;28(4):633–9.

67. Vaughan DK, Fisher SK. The distribution of F-actin in cells isolated from vertebrate retinas. Exp Eye Res. 1987 Mar;44(3):393–406.

68. Bringmann A, Reichenbach A, Wiedemann P. Pathomechanisms of Cystoid Macular Edema. Ophthalmic Res. 2004;36(5):241–9.

69. Karwoski CJ, Lu HK, Newman EA. Spatial Buffering of Light-Evoked Potassium Increases by Retinal Müller (Glial) Cells. Science. 1989 May 5;244(4904):578–80.

70. Newman EA. Voltage-dependent calcium and potassium channels in retinal glial cells. Nature. 1985 Oct 31;317(6040):809–11.

71. Newman EA, Frambach DA, Odette LL. Control of extracellular potassium levels by retinal glial cell K+ siphoning. Science. 1984 Sep 14;225(4667):1174–5.

72. Reichelt W, Stabel-Burow J, Pannicke T, Weichert H, Heinemann U. The glutathione level of retinal Müller glial cells is dependent on the high-affinity sodium-dependent uptake of glutamate. Neuroscience. 1997 Apr;77(4):1213–24.

73. Reichenbach A, Henke A, Eberhardt W, Reichelt W, Dettmer D. K+ ion regulation in retina. Can J Physiol Pharmacol. 1992;70 Suppl:S239-247.

74. Wolburg H, Berg K. Distribution of orthogonal arrays of particles in the Müller cell membrane of the mouse retina. Glia. 1988;1(4):246–52.

75. Agte S, Junek S, Matthias S, Ulbricht E, Erdmann I, Wurm A, et al. Müller Glial Cell-Provided Cellular Light Guidance through the Vital Guinea-Pig Retina. Biophys J. 2011 Dec 7;101(11):2611–9.

76. Franze K, Grosche J, Skatchkov SN, Schinkinger S, Foja C, Schild D, et al. Müller cells are living optical fibers in the vertebrate retina. Proc Natl Acad Sci. 2007 May 15;104(20):8287–92.

77. Bringmann A, Pannicke T, Grosche J, Francke M, Wiedemann P, Skatchkov SN, et al. Müller cells in the healthy and diseased retina. Prog Retin Eye Res. 2006 Jul;25(4):397–424.

78. Bignami A, Dahl D. The radial glia of Müller in the rat retina and their response to injury. An immunofluorescence study with antibodies to the glial fibrillary acidic (GFA) protein. Exp Eye Res. 1979 Jan 1;28(1):63–9.

79. Bringmann A, Iandiev I, Pannicke T, Wurm A, Hollborn M, Wiedemann P, et al. Cellular signaling and factors involved in Müller cell gliosis: Neuroprotective and detrimental effects. Prog Retin Eye Res. 2009 Nov 1;28(6):423–51.

80. Lewis GP, Fisher SK. Up-regulation of glial fibrillary acidic protein in response to retinal injury: its potential role in glial remodeling and a comparison to vimentin expression. Int Rev Cytol. 2003;230:263–90.

81. Lu YB, Iandiev I, Hollborn M, Körber N, Ulbricht E, Hirrlinger PG, et al. Reactive glial cells: increased stiffness correlates with increased intermediate filament expression. FASEB J. 2011;25(2):624–31.

82. Akiyama H, Nakazawa T, Shimura M, Tomita H, Tamai M. Presence of mitogen-activated protein kinase in retinal Müller cells and its neuroprotective effect ischemia-reperfusion injury. Neuroreport. 2002 Nov 15;13(16):2103–7.

83. Bringmann A, Reichenbach A. Role of Muller cells in retinal degenerations. Front Biosci J Virtual Libr. 2001 Oct 1;6:E72-92.

84. Reichenbach A, Fuchs U, Kasper M, el-Hifnawi E, Eckstein AK. Hepatic retinopathy: morphological features of retinal glial (Müller) cells accompanying hepatic failure. Acta Neuropathol (Berl). 1995;90(3):273–81.

85. Fischer AJ, Reh TA. Potential of Müller glia to become neurogenic retinal progenitor cells. Glia. 2003 Jul;43(1):70–6.

86. Ooto S, Akagi T, Kageyama R, Akita J, Mandai M, Honda Y, et al. Potential for neural regeneration after neurotoxic injury in the adult mammalian retina. Proc Natl Acad Sci U S A. 2004 Sep 14;101(37):13654–9.

87. Takeda M, Takamiya A, Jiao J wei, Cho KS, Trevino SG, Matsuda T, et al. α-Aminoadipate Induces Progenitor Cell Properties of Müller Glia in Adult Mice. Invest Ophthalmol Vis Sci. 2008 Mar 1;49(3):1142–50.

88. Cuthbertson RA, Lang RA, Coghlan JP. Macrophage products IL-1 alpha, TNF alpha and bFGF may mediate multiple cytopathic effects in the developing eyes of GM-CSF transgenic mice. Exp Eye Res. 1990 Sep;51(3):335–44.

89. Drescher KM, Whittum-Hudson JA. Modulation of immune-associated surface markers and cytokine production by murine retinal glial cells. J Neuroimmunol. 1996 Jan;64(1):71–81.

90. Kashiwagi K, Iizuka Y, Mochizuki S, Tsumamoto Y, Mishima HK, Araie M, et al. Differences in nitric oxide production: a comparison of retinal ganglion cells and retinal glial cells cultured under hypoxic conditions. Brain Res Mol Brain Res. 2003 Apr 10;112(1–2):126–34.

91. Nakazawa T, Hisatomi T, Nakazawa C, Noda K, Maruyama K, She H, et al. Monocyte chemoattractant protein 1 mediates retinal detachment-induced photoreceptor apoptosis. Proc Natl Acad Sci. 2007 Feb 13;104(7):2425–30.

92. Tezel G, Wax MB. Increased Production of Tumor Necrosis Factor-α by Glial Cells Exposed to Simulated Ischemia or Elevated Hydrostatic Pressure Induces Apoptosis in Cocultured Retinal Ganglion Cells. J Neurosci. 2000 Dec 1;20(23):8693–700.

93. Yuan L, Neufeld AH. Tumor necrosis factor-alpha: a potentially neurodestructive cytokine produced by glia in the human glaucomatous optic nerve head. Glia. 2000 Oct;32(1):42–50.

94. Rochon-Duvigneaud M. Déformation et lésions de lœil myope: in Mawas J, introduction à létude de la myopie et des choriorétinites myopiques. Bull Société Ophtalmol Paris. 1938;(1):1–10.

95. Gass JD. Müller cell cone, an overlooked part of the anatomy of the fovea centralis: hypotheses concerning its role in the pathogenesis of macular hole and foveomacualr retinoschisis. Arch Ophthalmol Chic Ill 1960. 1999 Jun;117(6):821–3.

96. Hogan MJ. Histology of the Human Eye: An Atlas and Textbook [by] Michael J. Hogan, Jorge A. Alvarado [and] Joan Esperson Weddell. Saunders; 1971. 712 p.

97. Govetto A, Bhavsar KV, Virgili G, Gerber MJ, Freund KB, Curcio CA, et al. Tractional Abnormalities of the Central Foveal Bouquet in Epiretinal Membranes: Clinical Spectrum and Pathophysiological Perspectives. Am J Ophthalmol. 2017 Dec 1;184:167–80.

98. Bringmann A, Unterlauft JD, Wiedemann R, Rehak M, Wiedemann P. Morphology of partial-thickness macular defects: presumed roles of Müller cells and tissue layer interfaces of low mechanical stability. Int J Retina Vitr [Internet]. 2020 Jul 6 [cited 2021 Jan 11];6. Available from: https://www.ncbi.nlm.nih.gov/pmc/articles/PMC7339408/

99. Bringmann A, Unterlauft JD, Wiedemann R, Barth T, Rehak M, Wiedemann P. Two different populations of Müller cells stabilize the structure of the fovea: an optical coherence tomography study. Int Ophthalmol. 2020 Nov;40(11):2931–48.

100. Govetto A, Hubschman JP, Sarraf D, Figueroa MS, Bottoni F, dell'Omo R, et al. The role of Müller cells in tractional macular disorders: an optical coherence tomography study and physical model of mechanical force transmission. Br J Ophthalmol. 2019 Jul 20;bjophthalmol-2019-314245.

101. Ahnelt PK. The photoreceptor mosaic. Eye Lond Engl. 1998;12 (Pt 3b):531–40.

102. Bringmann A, Grosche A, Pannicke T, Reichenbach A. GABA and Glutamate Uptake and Metabolism in Retinal Glial (Müller) Cells. Front Endocrinol. 2013;4:48.

103. Nishikawa S, Tamai M. Müller cells in the human foveal region. Curr Eye Res. 2001 Jan;22(1):34–41.

104. Packer O, Hendrickson AE, Curcio CA. Developmental redistribution of photoreceptors across the Macaca nemestrina (pigtail macaque) retina. J Comp Neurol. 1990;298(4):472–93.

105. Balaratnasingam C, Chae B, Remmer MH, Gomez E, Suzuki M, Engelbert M, et al. The Spatial Profile of Macular Pigments Is Related to the Topological

Characteristics of the Foveal Avascular Zone. Invest Ophthalmol Vis Sci. 2015 Dec 1;56(13):7859–65.

106. Reading VM, Weale RA. Macular pigment and chromatic aberration. JOSA. 1974 Feb 1;64(2):231–4.

107. Snodderly DM, Auran JD, Delori FC. The macular pigment. II. Spatial distribution in primate retinas. Invest Ophthalmol Vis Sci. 1984;25(6):674–85.

108. Ramón Y Cajal S. Histologie du Système Nerveux de l'Homme et des Vertébrés. Paris; 1909.

109. Drasdo N, Millican CL, Katholi CR, Curcio CA. The length of Henle fibers in the human retina and a model of ganglion receptive field density in the visual field. Vision Res. 2007 Oct 1;47(22):2901–11.

110. Schein SJ. Anatomy of macaque fovea and spatial densities of neurons in foveal representation. J Comp Neurol. 1988;269(4):479–505.

111. Sjöstrand J, Popovic Z, Conradi N, Marshall J. Morphometric study of the displacement of retinal ganglion cells subserving cones within the human fovea. Graefes Arch Clin Exp Ophthalmol. 1999 Dec 1;237(12):1014–23.

112. Curcio CA, Messinger JD, Sloan KR, Mitra A, McGwin G, Spaide RF. Human Chorioretinal Layer Thicknesses Measured in Macula-wide, High-Resolution Histologic Sections. Invest Ophthalmol Vis Sci. 2011 Jun 1;52(7):3943–54.

113. Diaz-Araya C, Provis JM. Evidence of photoreceptor migration during early foveal development: A quantitative analysis of human fetal retinae. Vis Neurosci. 1992;8(6):505–14.

114. Hendrickson A, Possin D, Vajzovic L, Toth C. Histological Development of the Human Fovea From Midgestation to Maturity. Am J Ophthalmol. 2012 Nov;154(5):767-778.e2.

115. Hendrickson AE, Yuodelis C. The morphological development of the human fovea. Ophthalmology. 1984 Jun;91(6):603–12.

116. Yuodelis C, Hendrickson A. A qualitative and quantitative analysis of the human fovea during development. Vision Res. 1986 Jan 1;26(6):847–55.

117. Provis JM, Diaz CM, Dreher B. Ontogeny of the primate fovea: A central issue in retinal development. Prog Neurobiol. 1998;54(5):549–81.

118. Springer AD, Troilo D, Possin D, Hendrickson AE. Foveal cone density shows a rapid postnatal maturation in the marmoset monkey. Vis Neurosci. 2011;28(6):473–84.

119. Distler C, Kopatz K, Telkes I. Developmental changes in astrocyte density in the macaque perifoveal region. Eur J Neurosci. 2000;12(4):1331–41.

120. Distler C, Kirby MA. Transience of Astrocytes In the Newborn Macaque Monkey Retina. Eur J Neurosci. 1996;8(4):847–51.

121. Provis JM, Sandercoe T, Hendrickson AE. Astrocytes and blood vessels define the foveal rim during primate retinal development. Invest Ophthalmol Vis Sci. 2000;41(10):2827–36.

122. Thomas MG, Kumar A, Mohammad S, Proudlock FA, Engle EC, Andrews C, et al. Structural grading of foveal hypoplasia using spectral-domain optical coherence tomography a predictor of visual acuity? Ophthalmology. 2011 Aug;118(8):1653–60.

123. Lee DJ, Woertz EN, Visotcky A, Wilk MA, Heitkotter H, Linderman RE, et al. The Henle Fiber Layer in Albinism: Comparison to Normal and Relationship to Outer Nuclear Layer Thickness and Foveal Cone Density. Invest Ophthalmol Vis Sci. 2018 Nov;59(13):5336–48.

124. Ramtohul P, Comet A, Denis D. Multimodal Imaging Correlation of the Concentric Macular Rings Sign in Foveal Hypoplasia: A Distinctive Henle Fiber Layer Geometry. Ophthalmol Retina. 2020 Sep 1;4(9):946–53.

125. Puro DG. Stretch-activated channels in human retinal muller cells. Glia. 1991;4(5):456–60.

126. Foster WJ, Davis JT, Lam PK, Otteson DC, Janmey PA. Substrate Elastic Modulus Regulates Müller Cell Expression of Extracellular Matrix Genes Known To Play a Role in Proliferative Vitreoretinopathy. Invest Ophthalmol Vis Sci. 2011 Apr 22;52(14):5341–5341.

127. Davis JT, Wen Q, Janmey PA, Otteson DC, Foster WJ. Müller Cell Expression of Genes Implicated in Proliferative Vitreoretinopathy Is Influenced by Substrate Elastic Modulus. Invest Ophthalmol Vis Sci. 2012 May 1;53(6):3014–9.

128. Bu SC, Kuijer R, Worp RJ van der, Putten SM van, Wouters O, Li XR, et al. Substrate Elastic Modulus Regulates the Morphology, Focal Adhesions, and α-Smooth Muscle Actin Expression of Retinal Müller Cells. Invest Ophthalmol Vis Sci. 2015 Sep 1;56(10):5974–82.

129. Foulds WS. The vitreous in retinal detachment. Trans Ophthalmol Soc U K. 1975;95(3):412–6.

130. Cantrill HL, Pederson JE. Experimental Retinal Detachment: VI. The Permeability of the Blood-Retinal Barrier. Arch Ophthalmol. 1984 May 1;102(5):747–51.

131. Anderson DH, Guérin CJ, Erickson PA, Stern WH, Fisher SK. Morphological recovery in the reattached retina. Invest Ophthalmol Vis Sci. 1986 Feb;27(2):168–83.

132. Hollyfield JG, Varner HH, Rayborn ME, Osterfeld AM. Retinal attachment to the pigment epithelium. Linkage through an extracellular sheath surrounding cone photoreceptors. Retina Phila Pa. 1989;9(1):59–68.

133. Marmor MF. Chapter 8 Mechanisms of retinal adhesion. Prog Retin Res. 1993 Jan;12:179–204.

134. Hageman GS, Marmor MF, Yao XY, Johnson LV. The interphotoreceptor matrix mediates primate retinal adhesion. Arch Ophthalmol Chic Ill 1960. 1995 May;113(5):655–60.

135. Ghazi NG, Green WR. Pathology and pathogenesis of retinal detachment. Eye. 2002 Jul;16(4):411–21.

136. Franze K, Francke M, Günter K, Christ AF, Körber N, Reichenbach A, et al. Spatial mapping of the mechanical properties of the living retina using scanning force microscopy. Soft Matter. 2011 Mar 22;7(7):3147–54.

137. Kuhn F, Aylward B. Rhegmatogenous Retinal Detachment: A Reappraisal of Its Pathophysiology and Treatment. Ophthalmic Res. 2014;51(1):15–31.

138. Romano MR, Comune C, Ferrara M, Cennamo G, De Cillà S, Toto L, et al. Retinal Changes Induced by Epiretinal Tangential Forces. J Ophthalmol [Internet]. 2015 [cited 2020 Jan 10];2015. Available from: https://www.ncbi.nlm.nih.gov/pmc/articles/PMC4573429/

139. Moisseiev E, Yiu G. Role of Tractional Forces and Internal Limiting Membrane in Macular Hole Formation: Insights from Intraoperative Optical Coherence Tomography. Case Rep Ophthalmol. 2016 Jul 21;7(2):372–6.

140. Parolini B, Palmieri M, Finzi A, Besozzi G, Lucente A, Nava U, et al. The new Myopic Traction Maculopathy Staging System. Eur J Ophthalmol. 2020 Jun 8;1120672120930590.

141. Bringmann A, Unterlauft JD, Barth T, Wiedemann R, Rehak M, Wiedemann P. Different modes of full-thickness macular hole formation. Exp Eye Res. 2021 Jan;202:108393.

142. Foos RY, Wheeler NC. Vitreoretinal juncture. Synchysis senilis and posterior vitreous detachment. Ophthalmology. 1982 Dec;89(12):1502–12.

143. Sebag J. Ageing of the vitreous. Eye. 1987 Mar;1(2):254–62.

144. Sebag J. Anomalous posterior vitreous detachment: a unifying concept in vitreo-retinal disease. Graefes Arch Clin Exp Ophthalmol Albrecht Von Graefes Arch Klin Exp Ophthalmol. 2004 Aug;242(8):690–8.

145. Kishi S, Demaria C, Shimizu K. Vitreous cortex remnants at the fovea after spontaneous vitreous detachment. Int Ophthalmol. 1986 Dec;9(4):253–60.

146. Gupta P, Yee KMP, Garcia P, Rosen RB, Parikh J, Hageman GS, et al. Vitreoschisis in macular diseases. Br J Ophthalmol. 2011 Mar;95(3):376–80.

147. Johnson MW. Posterior vitreous detachment: Evolution and Role in Macular Disease. Retina. 2012 Sep;32:S174–8.

148. Gass JDM. Reappraisal of Biomicroscopic Classification of Stages of Development of a Macular Hole. Am J Ophthalmol. 1995 Jun 1;119(6):752–9.

149. Gaudric A, Haouchine B, Massin P, Paques M, Blain P, Erginay A. Macular Hole Formation: New Data Provided by Optical Coherence Tomography. Arch Ophthalmol. 1999 Jun 1;117(6):744–51.

150. Uchino E, Uemura A, Ohba N. Initial Stages of Posterior Vitreous Detachment in Healthy Eyes of Older Persons Evaluated by Optical Coherence Tomography. Arch Ophthalmol. 2001 Oct 1;119(10):1475–9.

151. Johnson MW. Posterior Vitreous Detachment: Evolution and Complications of Its Early Stages. Am J Ophthalmol. 2010 Mar;149(3):371-382.e1.

152. Duker JS, Kaiser PK, Binder S, de Smet MD, Gaudric A, Reichel E, et al. The International Vitreomacular Traction Study Group Classification of Vitreomacular Adhesion, Traction, and Macular Hole. Ophthalmology. 2013 Dec 1;120(12):2611–9.

153. Spaide RF, Wong D, Fisher Y, Goldbaum M. Correlation of vitreous attachment and foveal deformation in early macular hole states. Am J Ophthalmol. 2002 Feb;133(2):226–9.

154. Koizumi H, Spaide RF, Fisher YL, Freund KB, Klancnik JM, Yannuzzi LA. Three-dimensional evaluation of vitreomacular traction and epiretinal membrane using spectral-domain optical coherence tomography. Am J Ophthalmol. 2008 Mar;145(3):509–17.

155. Haouchine B, Massin P, Gaudric A. Foveal pseudocyst as the first step in macular hole formation: A prospective study by optical coherence tomography. Ophthalmology. 2001 Jan 1;108(1):15–22.

156. Sonmez K, Capone A, Trese MT, Williams GA. Vitreomacular traction syndrome: Impact of anatomical configuration on anatomical and visual outcomes. Retina. 2008;28(9):1207–14.

157. Theodossiadis G, Petrou P, Eleftheriadou M, Moustakas AL, Datseris I, Theodossiadis P. Focal vitreomacular traction: a prospective study of the evolution to macular hole: the mathematical approach. Eye. 2014 Dec;28(12):1452–60.

158. Kozak I, Barteselli G, Sepah YJ, Sadiq MA, High R, Do DV, et al. Correlation of Vitreomacular Traction with Foveal Thickness, Subfoveal Choroidal Thickness, and Vitreomacular/Foveal Angle. Curr Eye Res. 2017 Feb;42(2):297–301.

159. Uzel MM, Citirik M, Ilhan C, Tekin K. Correlation between central foveal thickness and visual acuity in patients with idiopathic vitreomacular traction. Retina. 2018 May;38(5):907–12.

160. Petrou P, Chalkiadaki E, Errera MH, Liyanage S, Wickham L, Papakonstantinou E, et al. Factors Associated with the Clinical Course of Vitreomacular Traction. J Ophthalmol. 2020 Dec 21;2020:9457670.

161. Grover S, Murthy RK, Brar VS, Chalam KV. Normative data for macular thickness by high-definition spectral-domain optical coherence tomography (spectralis). Am J Ophthalmol. 2009 Aug;148(2):266–71.

162. Grover S, Murthy RK, Brar VS, Chalam KV. Comparison of retinal thickness in normal eyes using Stratus and Spectralis optical coherence tomography. Invest Ophthalmol Vis Sci. 2010 May;51(5):2644–7.

163. Mitchell P, Smith W, Chey T, Wang JJ, Chang A. Prevalence and associations of epiretinal membranes. The Blue Mountains Eye Study, Australia. Ophthalmology. 1997 Jun;104(6):1033–40.

164. McCarty DJ, Mukesh BN, Chikani V, Wang JJ, Mitchell P, Taylor HR, et al. Prevalence and associations of epiretinal membranes in the visual impairment project. Am J Ophthalmol. 2005 Aug;140(2):288–94.

165. Duan XR, Liang YB, Friedman DS, Sun LP, Wei WB, Wang JJ, et al. Prevalence and associations of epiretinal membranes in a rural Chinese adult population: the Handan Eye Study. Invest Ophthalmol Vis Sci. 2009 May;50(5):2018–23.

166. Ng CH, Cheung N, Wang JJ, Islam AFM, Kawasaki R, Meuer SM, et al. Prevalence and risk factors for epiretinal membranes in a multi-ethnic United States population. Ophthalmology. 2011 Apr;118(4):694–9.

167. Koh V, Cheung CY, Wong WL, Cheung CM, Wang JJ, Mitchell P, et al. Prevalence and risk factors of epiretinal membrane in Asian Indians. Invest Ophthalmol Vis Sci. 2012 Feb 27;53(2):1018–22.

168. Ye H, Zhang Q, Liu X, Cai X, Yu W, Yu S, et al. Prevalence and associations of epiretinal membrane in an elderly urban Chinese population in China: the Jiangning Eye Study. Br J Ophthalmol. 2015 Dec;99(12):1594–7.

169. Cheung N, Tan SP, Lee SY, Cheung GCM, Tan G, Kumar N, et al. Prevalence and risk factors for epiretinal membrane: the Singapore Epidemiology of Eye Disease study. Br J Ophthalmol. 2017 Mar;101(3):371–6.

170. Foos RY. Vitreoretinal juncture; epiretinal membranes and vitreous. Invest Ophthalmol Vis Sci. 1977 May;16(5):416–22.

171. Gass JDM. Stereoscopic Atlas of Macular Diseases: Diagnosis and Treatment. Mosby; 1997. 520 p.

172. McLeod D, Hiscott PS, Grierson I. Age-related cellular proliferation at the vitreoretinal juncture. Eye Lond Engl. 1987;1 (Pt 2):263–81.

173. Foos RY. Vitreoretinal juncture--simple epiretinal membranes. Albrecht Von Graefes Arch Klin Exp Ophthalmol Albrecht Von Graefes Arch Clin Exp Ophthalmol. 1974 Jan 28;189(4):231–50.

174. Hikichi T, Takahashi M, Trempe CL, Schepens CL. Relationship between premacular cortical vitreous defects and idiopathic premacular fibrosis. Retina Phila Pa. 1995;15(5):413–6.

175. Johnson MW. Perifoveal vitreous detachment and its macular complications. Trans Am Ophthalmol Soc. 2005;103:537–67.

176. Schumann RG, Hagenau F, Guenther SR, Wolf A, Priglinger SG, Vogt D. Premacular Cell Proliferation Profiles in Tangential Traction Vitreo-Maculopathies Suggest a Key Role for Hyalocytes. Ophthalmologica. 2019;242(2):106–12.

177. Snead DRJ, James S, Snead MP. Pathological changes in the vitreoretinal junction 1: epiretinal membrane formation. Eye Lond. 2008 Oct;22(10):1310–7.

178. Joshi M, Agrawal S, Christoforidis JB. Inflammatory mechanisms of idiopathic epiretinal membrane formation. Mediators Inflamm. 2013;2013:192582.

179. Fincham GS, James S, Spickett C, Hollingshead M, Thrasivoulou C, Poulson AV, et al. Posterior Vitreous Detachment and the Posterior Hyaloid Membrane. Ophthalmology. 2018 Feb;125(2):227–36.

180. Snead MP, Snead DRJ, Richards AJ, Harrison JB, Poulson AV, Morris AHC, et al. Clinical, histological and ultrastructural studies of the posterior hyaloid membrane. Eye Lond Engl. 2002 Jul;16(4):447–53.

181. Snead DRJ, Cullen N, James S, Poulson AV, Morris AHC, Lukaris A, et al. Hyperconvolution of the inner limiting membrane in vitreomaculopathies. Graefes Arch Clin Exp Ophthalmol Albrecht Von Graefes Arch Klin Exp Ophthalmol. 2004 Oct;242(10):853–62.

182. Kritzenberger M, Junglas B, Framme C, Helbig H, Gabel VP, Fuchshofer R, et al. Different collagen types define two types of idiopathic epiretinal membranes. Histopathology. 2011 May;58(6):953–65.

183. Kohno R i, Hata Y, Kawahara S, Kita T, Arita R, Mochizuki Y, et al. Possible contribution of hyalocytes to idiopathic epiretinal membrane formation and its contraction. Br J Ophthalmol. 2009 Aug;93(8):1020–6.

184. Okada M, Ogino N, Matsumura M, Honda Y, Nagai Y. Histological and immunohistochemical study of idiopathic epiretinal membrane. Ophthalmic Res. 1995 Apr;27(2):118–28.

185. Michels RG. A clinical and histopathologic study of epiretinal membranes affecting the macula and removed by vitreous surgery. Trans Am Ophthalmol Soc. 1982;80:580–656.

186. Smiddy WE, Maguire AM, Green WR, Michels RG, de la Cruz Z, Enger C, et al. Idiopathic epiretinal membranes. Ultrastructural characteristics and clinicopathologic correlation. Ophthalmology. 1989 Jun;96(6):811–20; discussion 821.

187. Kase S, Saito W, Yokoi M, Yoshida K, Furudate N, Muramatsu M, et al. Expression of glutamine synthetase and cell proliferation in human idiopathic epiretinal membrane. Br J Ophthalmol. 2006 Jan;90(1):96–8.

188. Bringmann A, Wiedemann P. Involvement of Müller glial cells in epiretinal membrane formation. Graefes Arch Clin Exp Ophthalmol Albrecht Von Graefes Arch Klin Exp Ophthalmol. 2009 Jul;247(7):865–83.

189. Stevenson W, Prospero Ponce CM, Agarwal DR, Gelman R, Christoforidis JB. Epiretinal membrane: optical coherence tomography-based diagnosis and classification. Clin Ophthalmol Auckl NZ. 2016 Mar 29;10:527–34.

190. George B, Chen S, Chaudhary V, Gonder J, Chakrabarti S. Extracellular matrix proteins in epiretinal membranes and in diabetic retinopathy. Curr Eye Res. 2009 Feb;34(2):134–44.

191. Sramek SJ, Wallow IH, Stevens TS, Nork TM. Immunostaining of preretinal membranes for actin, fibronectin, and glial fibrillary acidic protein. Ophthalmology. 1989 Jun;96(6):835–41.

192. Arora PD, McCulloch CA. Dependence of collagen remodelling on alpha-smooth muscle actin expression by fibroblasts. J Cell Physiol. 1994 Apr;159(1):161–75.

193. Guidry C. The role of Müller cells in fibrocontractive retinal disorders. Prog Retin Eye Res. 2005 Jan 1;24(1):75–86.

194. Govetto A, Lalane RA, Sarraf D, Figueroa MS, Hubschman JP. Insights Into Epiretinal Membranes: Presence of Ectopic Inner Foveal Layers and a New Optical Coherence Tomography Staging Scheme. Am J Ophthalmol. 2017 Mar;175:99–113.

195. Govetto A, Dacquay Y, Farajzadeh M, Platner E, Hirabayashi K, Hosseini H, et al. Lamellar Macular Hole: Two Distinct Clinical Entities? Am J Ophthalmol. 2016 Apr;164:99–109.

196. Govetto A, Hubschman JP, Sarraf D, Figueroa MS, Bottoni F, dell'Omo R, et al. The role of Müller cells in tractional macular disorders: an optical coherence tomography study and physical model of mechanical force transmission. Br J Ophthalmol. 2020 Apr 1;104(4):466–72.

197. Govetto A, Virgili G, Rodriguez FJ, Figueroa MS, Sarraf D, Hubschman JP. Functional and anatomical significance of the ectopic inner foveal layers in eyes with idiopathic epiretinal membranes: Surgical Results at 12 Months. Retina. 2019 Feb;39(2):347–57.

198. Hussnain SA, Sharma T, Hood DC, Chang S. Schisis of the Retinal Nerve Fiber Layer in Epiretinal Membranes. Am J Ophthalmol. 2019 Nov 1;207:304–12.

199. Luu KY, Koenigsaecker T, Yazdanyar A, Mukkamala L, Durbin-Johnson BP, Morse LS, et al. Long-term natural history of idiopathic epiretinal membranes with good visual acuity. Eye. 2019 May;33(5):714–23.

200. Doguizi S, Sekeroglu MA, Ozkoyuncu D, Omay AE, Yilmazbas P. Clinical significance of ectopic inner foveal layers in patients with idiopathic epiretinal membranes. Eye. 2018 Oct;32(10):1652–60.

201. Koerner F, Garweg J. Vitrectomy for macular pucker and vitreomacular traction syndrome. Doc Ophthalmol. 1999 Jan 1;97(3):449–58.

202. Spaide RF. Vitreomacular traction syndrome. Retina. 2012 Sep;32:S187.

203. Gass JD. Lamellar macular hole: a complication of cystoid macular edema after cataract extraction: a clinicopathologic case report. Trans Am Ophthalmol Soc. 1975;73:230–50.

204. Takahashi H, Kishi S. Tomographic features of a lamellar macular hole formation and a lamellar hole that progressed to a full-thickness macular hole. Am J Ophthalmol. 2000 Nov;130(5):677–9.

205. Haouchine B, Massin P, Tadayoni R, Erginay A, Gaudric A. Diagnosis of macular pseudoholes and lamellar macular holes by optical coherence tomography. Am J Ophthalmol. 2004 Nov;138(5):732–9.

206. Witkin AJ, Ko TH, Fujimoto JG, Schuman JS, Baumal CR, Rogers AH, et al. Redefining lamellar holes and the vitreomacular interface: an ultrahigh-resolution optical coherence tomography study. Ophthalmology. 2006 Mar;113(3):388–97.

207. Gaudric A, Aloulou Y, Tadayoni R, Massin P. Macular pseudoholes with lamellar cleavage of their edge remain pseudoholes. Am J Ophthalmol. 2013 Apr;155(4):733–42, 742.e1-4.

208. Hubschman JP, Govetto A, Spaide RF, Schumann R, Steel D, Figueroa MS, et al. Optical coherence tomography-based consensus definition for lamellar macular hole. Br J Ophthalmol. 2020 Feb 27;bjophthalmol-2019-315432.

209. Bottoni F, Carmassi L, Cigada M, Moschini S, Bergamini F. Diagnosis of macular pseudoholes and lamellar macular holes: is optical coherence tomography the 'gold standard'? Br J Ophthalmol. 2008 May;92(5):635–9.

210. Bottoni F, Deiro AP, Giani A, Orini C, Cigada M, Staurenghi G. The natural history of lamellar macular holes: a spectral domain optical coherence tomography study. Graefes Arch Clin Exp Ophthalmol Albrecht Von Graefes Arch Klin Exp Ophthalmol. 2013 Feb;251(2):467–75.

211. Pang CE, Spaide RF, Freund KB. Comparing functional and morphologic characteristics of lamellar macular holes with and without lamellar hole-associated epiretinal proliferation. Retina Phila Pa. 2015 Apr;35(4):720–6.

212. Donati S, Della Valle P, Premi E, Mazzola M, Lo Presti L, Azzolini C. Lamellar Macular Holes: The Role of Microperimetry in Functional Assessment. J Ophthalmol. 2019 Apr 14;2019:e9035837.

213. Pang CE, Spaide RF, Freund KB. Epiretinal proliferation seen in association with lamellar macular holes: a distinct clinical entity. Retina Phila Pa. 2014 Aug;34(8):1513–23.

214. Itoh Y, Levison AL, Kaiser PK, Srivastava SK, Singh RP, Ehlers JP. Prevalence and characteristics of hyporeflective preretinal tissue in vitreomacular interface disorders. Br J Ophthalmol. 2016 Mar;100(3):399–404.

215. Compera D, Entchev E, Haritoglou C, Scheler R, Mayer WJ, Wolf A, et al. Lamellar Hole-Associated Epiretinal Proliferation in Comparison to Epiretinal Membranes of Macular Pseudoholes. Am J Ophthalmol. 2015 Aug;160(2):373-384.e1.

216. Parolini B, Schumann RG, Cereda MG, Haritoglou C, Pertile G. Lamellar macular hole: a clinicopathologic correlation of surgically excised epiretinal membranes. Invest Ophthalmol Vis Sci. 2011 Nov 25;52(12):9074–83.

217. Yang YS, Lee JS, Son G, Sohn J. Epiretinal Proliferation Associated with Lamellar Hole or Macular Hole: Origin and Surgical Prognosis. Korean J Ophthalmol KJO. 2019 Apr;33(2):142–9.

218. Haas J. Über das zusammenvorkommen von veranderungen der retina und choroidea. Arch Augenheilkd. 1898;37:343–8.

219. Jager G. A hereditary retinal disease. Trans Ophthalmol Soc UK. 1953;73:617–9.

220. Tang S, Ding X, Luo Y. Hereditary Vitreoretinal Degenerations. In: Retina [Internet]. Elsevier; 2013 [cited 2020 Jan 10]. p. 836–51. Available from: https://linkinghub.elsevier.com/retrieve/pii/B9781455707379000412

221. George ND, Yates JR, Bradshaw K, Moore AT. Infantile presentation of X linked retinoschisis. Br J Ophthalmol. 1995 Jul;79(7):653–7.

222. Kirsch LS, Brownstein S, de Wolff-Rouendaal D. A histopathological, ultrastructural and immunohistochemical study of congenital hereditary retinoschisis. Can J Ophthalmol J Can Ophtalmol. 1996 Oct;31(6):301–10.

223. Yanoff M, Kertesz Rahn E, Zimmerman LE. Histopathology of juvenile retinoschisis. Arch Ophthalmol Chic Ill 1960. 1968 Jan;79(1):49–53.

224. Condon GP, Brownstein S, Wang NS, Kearns JAF, Ewing CC. Congenital Hereditary (Juvenile X-linked) Retinoschisis: Histopathologic and Ultrastructural Findings in Three Eyes. Arch Ophthalmol. 1986 Apr 1;104(4):576–83.

225. Miller RF, Dowling JE. Intracellular responses of the Müller (glial) cells of mudpuppy retina: their relation to b-wave of the electroretinogram. J Neurophysiol. 1970 May;33(3):323–41.

226. Sauer CG, Gehrig A, Warneke-Wittstock R, Marquardt A, Ewing CC, Gibson A, et al. Positional cloning of the gene associated with X-linked juvenile retinoschisis. Nat Genet. 1997 Oct;17(2):164–70.

227. Molday RS, Kellner U, Weber BHF. X-linked juvenile retinoschisis: clinical diagnosis, genetic analysis, and molecular mechanisms. Prog Retin Eye Res. 2012 May;31(3):195–212.

228. Mooy CM, Born LI van den, Baarsma S, Paridaens DA, Kraaijenbrink T, Bergen A, et al. Hereditary X-Linked Juvenile Retinoschisis: A Review of the Role of Müller Cells. Arch Ophthalmol. 2002 Jul 1;120(7):979–84.

229. Grayson C, Reid SNM, Ellis JA, Rutherford A, Sowden JC, Yates JRW, et al. Retinoschisin, the X-linked retinoschisis protein, is a secreted photoreceptor protein, and is expressed and released by Weri–Rb1 cells. Hum Mol Genet. 2000 Jul 22;9(12):1873–9.

230. Molday LL, Hicks D, Sauer CG, Weber BHF, Molday RS. Expression of X-Linked Retinoschisis Protein RS1 in Photoreceptor and Bipolar Cells. Invest Ophthalmol Vis Sci. 2001 Mar 1;42(3):816–25.

231. Gehrig AE, Warneke-Wittstock R, Sauer CG, Weber BH. Isolation and characterization of the murine X-linked juvenile retinoschisis (Rs1h) gene. Mamm Genome Off J Int Mamm Genome Soc. 1999 Mar;10(3):303–7.

232. Reid SN, Akhmedov NB, Piriev NI, Kozak CA, Danciger M, Farber DB. The mouse X-linked juvenile retinoschisis cDNA: expression in photoreceptors. Gene. 1999 Feb 18;227(2):257–66.

233. Takada Y, Fariss RN, Muller M, Bush RA, Rushing EJ, Sieving PA. Retinoschisin expression and localization in rodent and human pineal and consequences of mouse RS1 gene knockout. Mol Vis. 2006 Sep 28;12:1108–16.

234. Reid SNM, Yamashita C, Farber DB. Retinoschisin, a Photoreceptor-Secreted Protein, and Its Interaction with Bipolar and Müller Cells. J Neurosci. 2003 Jul 9;23(14):6030–40.

235. Takada Y, Fariss RN, Tanikawa A, Zeng Y, Carper D, Bush R, et al. A Retinal Neuronal Developmental Wave of Retinoschisin Expression Begins in Ganglion Cells during Layer Formation. Invest Ophthalmol Vis Sci. 2004 Sep 1;45(9):3302–12.

236. Wang T, Zhou A, Waters CT, O'Connor E, Read RJ, Trump D. Molecular pathology of X linked retinoschisis: mutations interfere with retinoschisin secretion and oligomerisation. Br J Ophthalmol. 2006 Jan;90(1):81–6.

237. Tolun G, Vijayasarathy C, Huang R, Zeng Y, Li Y, Steven AC, et al. Paired octamer rings of retinoschisin suggest a junctional model for cell-cell adhesion in the retina. Proc Natl Acad Sci U S A. 2016 May 10;113(19):5287–92.

238. Weber BHF, Schrewe H, Molday LL, Gehrig A, White KL, Seeliger MW, et al. Inactivation of the murine X-linked juvenile retinoschisis gene, Rs1h, suggests a role of retinoschisin in retinal cell layer organization and synaptic structure. Proc Natl Acad Sci U S A. 2002 Apr 30;99(9):6222–7.

239. Kotova S, Vijayasarathy C, Dimitriadis EK, Ikonomou L, Jaffe H, Sieving PA. Retinoschisin (RS1) interacts with negatively charged lipid bilayers in the presence of Ca2+: an atomic force microscopy study. Biochemistry. 2010 Aug 24;49(33):7023–32.

240. Steiner-Champliaud MF, Sahel J, Hicks D. Retinoschisin forms a multimolecular complex with extracellular matrix and cytoplasmic proteins: interactions with β2 laminin and αB-crystallin. Mol Vis. 2006;10.

241. Shi L, Ko ML, Ko GYP. Retinoschisin Facilitates the Function of L-Type Voltage-Gated Calcium Channels. Front Cell Neurosci Lausanne [Internet]. 2017 Aug 8 [cited 2020 Jan 9]; Available from: http://search.proquest.com/docview/2282038308/abstract/6A2B25206818431DPQ/1

242. Molday LL, Wu WWH, Molday RS. Retinoschisin (RS1), the protein encoded by the X-linked retinoschisis gene, is anchored to the surface of retinal photoreceptor and bipolar cells through its interactions with a Na/K ATPase-SARM1 complex. J Biol Chem. 2007 Nov 9;282(45):32792–801.

243. Plössl K, Schmid V, Straub K, Schmid C, Ammon M, Merkl R, et al. Pathomechanism of mutated and secreted retinoschisin in X-linked juvenile retinoschisis. Exp Eye Res. 2018 Dec;177:23–34.

244. Plössl K, Straub K, Schmid V, Strunz F, Wild J, Merkl R, et al. Identification of the retinoschisin-binding site on the retinal Na/K-ATPase. PLoS One San Franc. 2019 May;14(5):e0216320.

245. Plössl K, Royer M, Bernklau S, Tavraz NN, Friedrich T, Wild J, et al. Retinoschisin is linked to retinal Na/K-ATPase signaling and localization. Mol Biol Cell. 2017 Aug 1;28(16):2178–89.

246. Friedrich U, Stöhr H, Hilfinger D, Loenhardt T, Schachner M, Langmann T, et al. The Na/K-ATPase is obligatory for membrane anchorage of retinoschisin, the protein involved in the pathogenesis of X-linked juvenile retinoschisis. Hum Mol Genet. 2011 Mar 15;20(6):1132–42.

247. George NDL, Yates JRW, Moore AT. Clinical Features in Affected Males With X-Linked Retinoschisis. Arch Ophthalmol. 1996 Mar 1;114(3):274–80.

248. Roesch MT, Ewing CC, Gibson AE, Weber BH. The natural history of X-linked retinoschisis. Can J Ophthalmol J Can Ophtalmol. 1998 Apr;33(3):149–58.

249. Apushkin MA, Fishman GA, Rajagopalan AS. Fundus findings and longitudinal study of visual acuity loss in patients with x-linked retinoschisis: Retina. 2005 Jul;25(5):612–8.

250. Pimenides D, George NDL, Yates JRW, Bradshaw K, Roberts SA, Moore AT, et al. X-linked retinoschisis: clinical phenotype and RS1 genotype in 86 UK patients. J Med Genet. 2005 Jun;42(6):e35–e35.

251. Ando A, Takahashi K, Sho K, Matsushima M, Okamura A, Uyama M. Histopathological findings of X-linked retinoschisis with neovascular glaucoma. Graefes Arch Clin Exp Ophthalmol Albrecht Von Graefes Arch Klin Exp Ophthalmol. 2000 Jan;238(1):1–7.

252. Ozdemir H, Karacorlu S, Karacorlu M. Optical coherence tomography findings in familial foveal retinoschisis. Am J Ophthalmol. 2004 Jan;137(1):179–81.

253. Manschot WA. Pathology of Hereditary Juvenile Retinoschisis. Arch Ophthalmol. 1972 Aug 1;88(2):131–8.

254. Minami Y, Ishiko S, Takai Y, Kato Y, Kagokawa H, Takamiya A, et al. Retinal changes in juvenile X linked retinoschisis using three dimensional optical coherence tomography. Br J Ophthalmol. 2005 Dec;89(12):1663–4.

255. Gerth C, Zawadzki RJ, Werner JS, Heon E. Retinal morphological changes of patients with X-linked retinoschisis evaluated by Fourier-domain optical coherence tomography. Arch Ophthamol. 2008 Jun;126(6):807–11.

256. Yu J, Ni Y, Keane PA, Jiang C, Wang W, Xu G. Foveomacular schisis in juvenile X-linked retinoschisis: an optical coherence tomography study. Am J Ophthalmol. 2010 Jun;149(6):973-978.e2.

257. Gregori NZ, Lam BL, Gregori G, Ranganathan S, Stone EM, Morante A, et al. Wide-field spectral-domain optical coherence tomography in patients and carriers of X-linked retinoschisis. Ophthalmology. 2013 Jan;120(1):169–74.

258. Yoshida-Uemura T, Katagiri S, Yokoi T, Nishina S, Azuma N. Different foveal schisis patterns in each retinal layer in eyes with hereditary juvenile retinoschisis evaluated by en-face optical coherence tomography. Graefes Arch Clin Exp Ophthalmol Albrecht Von Graefes Arch Klin Exp Ophthalmol. 2017 Apr;255(4):719–23.

259. Padrón-Pérez N, Català-Mora J, Díaz J, Arias L, Prat J, Caminal JM. Swept-source and optical coherence tomography angiography in patients with X-linked retinoschisis. Eye Lond Engl. 2018 Apr;32(4):707–15.

260. Hu QR, Huang LZ, Chen XL, Xia HK, Li TQ, Li XX. X-Linked Retinoschisis in Juveniles: Follow-Up by Optical Coherence Tomography. BioMed Res Int. 2017;2017:1704623.

261. Eksandh LC, Ponjavic V, Ayyagari R, Bingham EL, Hiriyanna KT, Andréasson S, et al. Phenotypic Expression of Juvenile X-linked Retinoschisis in Swedish Families With Different Mutations in the XLRS1 Gene. Arch Ophthalmol. 2000 Aug 1;118(8):1098–104.

262. Sieving PA, MacDonald IM, Chan S. X-Linked Juvenile Retinoschisis. In: Adam MP, Ardinger HH, Pagon RA, Wallace SE, Bean LJ, Stephens K, et al., editors. GeneReviews® [Internet]. Seattle (WA): University of Washington, Seattle; 1993 [cited 2020 Jan 10]. Available from: http://www.ncbi.nlm.nih.gov/books/NBK1222/

263. Kim DY, Mukai S. X-linked Juvenile Retinoschisis (XLRS): A Review of Genotype-Phenotype Relationships. Semin Ophthalmol. 2013 Sep 1;28(5–6):392–6.

264. Andreoli MT, Lim JI. Optical Coherence Tomography Retinal Thickness and Volume Measurements in X-Linked Retinoschisis. Am J Ophthalmol. 2014 Sep 1;158(3):567-573.e2.

265. Menke MN, Feke GT, Hirose T. EFFECT OF AGING ON MACULAR FEATURES OF X-LINKED RETINOSCHISIS ASSESSED WITH OPTICAL COHERENCE TOMOGRAPHY: Retina. 2011 Jun;31(6):1186–92.

266. Cukras CA, Huryn LA, Jeffrey BG, Turriff A, Sieving PA. Analysis of anatomic and functional measures in x-linked retinoschisis. Invest Ophthalmol Vis Sci. 2018 Jun;59(7):2841–7.

267. Kellner U, Brümmer S, Foerster MH, Wessing A. X-linked congenital retinoschisis. Graefes Arch Clin Exp Ophthalmol Albrecht Von Graefes Arch Klin Exp Ophthalmol. 1990;228(5):432–7.

268. Kjellström S, Vijayasarathy C, Ponjavic V, Sieving PA, Andréasson S. Long-term 12 year follow-up of X-linked congenital retinoschisis. Ophthalmic Genet. 2010 Sep;31(3):114–25.

269. Wood EH, Lertjirachai I, Ghiam BK, Koulisis N, Moysidis SN, Dirani A, et al. The Natural History of Congenital X-Linked Retinoschisis and Conversion between Phenotypes over Time. Ophthalmol Retina. 2019 Jan 1;3(1):77–82.

270. Lee JJ, Kim JH, Kim SY, Park SS, Yu YS. Infantile Vitreous Hemorrhage as the Initial Presentation of X-linked Juvenile Retinoschisis. Korean J Ophthalmol KJO. 2009 Jun;23(2):118–20.

271. Bradshaw K, George N, Moore A. Mutations of the XLRS1 gene cause abnormalities of photoreceptor as well as inner retinal responses of the ERG. 1999;21.

272. Renner AB, Kellner U, Fiebig B, Cropp E, Foerster MH, Weber BHF. ERG variability in X-linked congenital retinoschisis patients with mutations in the RS1 gene and the diagnostic importance of fundus autofluorescence and OCT. Doc Ophthalmol. 2008 Mar 1;116(2):97–109.

273. Bowles K, Cukras C, Turriff A, Sergeev Y, Vitale S, Bush RA, et al. X-Linked Retinoschisis: RS1 Mutation Severity and Age Affect the ERG Phenotype in a Cohort of 68 Affected Male Subjects. Invest Ophthalmol Vis Sci. 2011 Nov 1;52(12):9250–6.

274. Lesch B, Szabó V, Kánya M, Somfai GM, Vámos R, Varsányi B, et al. Clinical and genetic findings in Hungarian patients with X-linked juvenile retinoschisis. Mol Vis. 2008 Dec 12;14:2321–32.

275. Matet A, Savastano MC, Rispoli M, Bergin C, Moulin A, Crisanti P, et al. En Face Optical Coherence Tomography of Foveal Microstructure in Full-Thickness Macular Hole: A Model to Study Perifoveal Müller Cells. Am J Ophthalmol. 2015 Jun 1;159(6):1142-1151.e3.

276. Daruich A, Matet A, Moulin A, Kowalczuk L, Nicolas M, Sellam A, et al. Mechanisms of macular edema: Beyond the surface. Prog Retin Eye Res. 2018 Mar;63:20–68.

277. Lewis RA, Lee GB, Martonyi CL, Barnett JM, Falls HF. Familial foveal retinoschisis. Arch Ophthamol. 1977 Jul;95(7):1190–6.

278. Kabanarou SA, Holder GE, Bird AC, Webster AR, Stanga PE, Vickers S, et al. Isolated foveal retinoschisis as a cause of visual loss in young females. Br J Ophthalmol. 2003 Jun;87(6):801–3.

279. Han DP, Sieving PA, Johnson MW, Martonyi CL. Foveal retinoschisis associated with senile retinoschisis in a woman. Am J Ophthalmol. 1988 Jul;106(1):107–9.

280. Tsang SH, Burke T, Oll M, Yzer S, Lee W, Xie Y (Angela), et al. Whole Exome Sequencing Identifies CRB1 Defect in an Unusual Maculopathy Phenotype. Ophthalmology. 2014 Sep;121(9):1773–82.

281. Vincent A, Ng J, Gerth-Kahlert C, Tavares E, Maynes JT, Wright T, et al. Biallelic Mutations in CRB1 Underlie Autosomal Recessive Familial Foveal Retinoschisis. Invest Ophthalmol Vis Sci. 2016 May 1;57(6):2637–46.

282. Shah N, Damani MR, Zhu XS, Bedoukian EC, Bennett J, Maguire AM, et al. Isolated maculopathy associated with biallelic CRB1 mutations. Ophthalmic Genet. 2017 Apr;38(2):190–3.

283. Wolfson Y, Applegate CD, Strauss RW, Han IC, Scholl HP. *CRB1* -Related Maculopathy With Cystoid Macular Edema. JAMA Ophthalmol. 2015 Nov 1;133(11):1357.

284. Mucciolo DP, Murro V, Giorgio D, Passerini I, Sodi A, Virgili G, et al. Long-term follow-up of a CRB1-associated maculopathy. Ophthalmic Genet. 2018 Jul 4;39(4):522–5.

285. Oh DJ, Sheth V, Fishman GA, Grassi MA. Simplex Crumbs Homologue 1 Maculopathy Masquerading as Juvenile X-Linked Retinoschisis in Male Patients. J Vitreoretin Dis. 2020 Oct 1;4(5):437–40.

286. Oh DJ, Daily MJ, Grassi MA. CRB1 maculopathy presenting as fenestrated sheen macular dystrophy with 15-year follow-up. Doc Ophthalmol. 2021 Jun 1;142(3):381–8.

287. Paun CC, Pijl BJ, Siemiatkowska AM, Collin RWJ, Cremers FPM, Hoyng CB, et al. A novel crumbs homolog 1 mutation in a family with retinitis pigmentosa, nanophthalmos, and optic disc drusen. Mol Vis. 2012;18:2447–53.

288. Khan KN, Robson A, Mahroo OAR, Gavin A, Inglehearn CF, Armengol M, et al. A clinical and molecular characterisation of CRB1-associated maculopathy. Eur J Hum Genet EJHG Leiden. 2018 May;26(5):687–94.

289. Tepass U, Theres C, Knust E. crumbs encodes an EGF-like protein expressed on apical membranes of Drosophila epithelial cells and required for organization of epithelia. Cell. 1990 Jun 1;61(5):787–99.

290. Pellikka M, Tanentzapf G, Pinto M, Smith C, McGlade CJ, Ready DF, et al. Crumbs, the Drosophila homologue of human CRB1/RP12, is essential for photoreceptor morphogenesis. Nature. 2002 Mar 14;416(6877):143–9.

291. van de Pavert SA, Kantardzhieva A, Malysheva A, Meuleman J, Versteeg I, Levelt C, et al. Crumbs homologue 1 is required for maintenance of photoreceptor cell

polarization and adhesion during light exposure. J Cell Sci. 2004 Aug 15;117(Pt 18):4169–77.

292. van Rossum AGSH, Aartsen WM, Meuleman J, Klooster J, Malysheva A, Versteeg I, et al. Pals1/Mpp5 is required for correct localization of Crb1 at the subapical region in polarized Muller glia cells. Hum Mol Genet. 2006 Sep 15;15(18):2659–72.

293. Alves CH, Pellissier LP, Wijnholds J. The CRB1 and adherens junction complex proteins in retinal development and maintenance. Prog Retin Eye Res. 2014 May;40:35–52.

294. Quinn PM, Pellissier LP, Wijnholds J. The CRB1 Complex: Following the Trail of Crumbs to a Feasible Gene Therapy Strategy. Front Neurosci [Internet]. 2017 [cited 2021 Jun 12];11. Available from: https://www.frontiersin.org/articles/10.3389/fnins.2017.00175/full

295. Fitzgerald JR, McCARTHY JL. Hereditary retinoschisis. Report of two cases occurring in a mother and son. Trans - Am Acad Ophthalmol Otolaryngol Am Acad Ophthalmol Otolaryngol. 1962 Dec;66:765–75.

296. Yassur Y, Nissenkorn I, Ben-Sira I, Kaffe S, Goodman RM. Autosomal Dominant Inheritance of Retinoschisis. Am J Ophthalmol. 1982 Sep 1;94(3):338–43.

297. Shimazaki J, Matsuhashi M. Familial retinoschisis in female patients. Doc Ophthalmol Adv Ophthalmol. 1987 Mar;65(3):393–400.

298. Chen FK, McAllister IL, Chelva ES. Thirteen-year follow up of isolated foveal retinoschisis in a 24-year-old woman: 13-year follow up of isolated foveal retinoschisis. Clin Experiment Ophthalmol. 2006 Aug 17;34(6):600–5.

299. Favre M. [Two cases of hyaloid-retinal degeneration]. Ophthalmol J Int Ophtalmol Int J Ophthalmol Z Augenheilkd. 1958 Jun;135(5–6):604–9.

300. Fishman GA, Jampol LM, Goldberg MF. Diagnostic features of the Favre-Goldmann syndrome. Br J Ophthalmol. 1976 May 1;60(5):345–53.

301. Peyman GA, Fishman GA, Sanders DR, Vlchek J. Histopathology of Goldmann-Favre syndrome obtained by full-thickness eye-wall biopsy. Ann Ophthalmol. 1977 Apr;9(4):479–84.

302. Haider NB, Jacobson SG, Cideciyan AV, Swiderski R, Streb LM, Searby C, et al. Mutation of a nuclear receptor gene, NR2E3, causes enhanced S cone syndrome, a disorder of retinal cell fate. Nat Genet. 2000 Feb;24(2):127–31.

303. Sharon D, Sandberg MA, Caruso RC, Berson EL, Dryja TP. Shared mutations in NR2E3 in enhanced S-cone syndrome, Goldmann-Favre syndrome, and many cases of clumped pigmentary retinal degeneration. Arch Ophthalmol Chic Ill 1960. 2003 Sep;121(9):1316–23.

304. Bechet L, Atia R, Zeitz C, Mohand-Saïd S, Sahel JA, Barale PO, et al. Management of a case of Enhanced S-cone syndrome with massive foveoschisis treated with pars plana vitrectomy with silicone oil tamponade. Ophthalmic Genet. 2021 May 10;0(0):1–4.

305. Özateş S, Tekin K, Teke MY. Goldmann-Favre Syndrome: Case Series. Turk J Ophthalmol. 2018 Feb;48(1):47–51.

306. Batioğlu F. Goldmann-Favre vitreoretinal degeneration. Eur J Ophthalmol. 2003 Apr;13(3):307–10.

307. Bhandari M, Rajan R, Krishnan PT, Pal SS, Raman R, Sharma T. Morphological and functional correlates in Goldmann-Favre syndrome: a case series. Korean J Ophthalmol. 2012 Apr;26(2):143–6.

308. Audo I, Michaelides M, Robson AG, Hawlina M, Vaclavik V, Sandbach JM, et al. Phenotypic variation in enhanced S-cone syndrome. Invest Ophthalmol Vis Sci. 2008 May;49(5):2082–93.

309. Rinaldi C, Vitale L, Pachydaki S, Yannuzzi LA. Spontaneous resolution of macular schisis in goldmann favre syndrome. Retin Cases Brief Rep. 2011 Winter;5(1):84–6.

310. Naik A, Ratra D, Banerjee A, Dalan D, Jandyal S, Rao G, et al. Enhanced S-cone syndrome: Clinical spectrum in Indian population. Indian J Ophthalmol. 2019 Apr;67(4):523–9.

311. Chawla R, Banerjee M. Bilateral giant macular schisis in a case of Goldmann-Favre syndrome. BMJ Case Rep CP. 2019 Sep 1;12(9):e230351.

312. Parida H, Kannan NB, Rathinam SR. Imaging of Muller cell sheen dystrophy. Indian J Ophthalmol. 2020 Mar;68(3):533–5.

313. Kellner U, Kraus H, Heimann H, Helbig H, Bornfeld N, Foerster M. Electrophysiological evaluation of visual loss in Müller cell sheen dystrophy. Br J Ophthalmol. 1998 Jun;82(6):650–4.

314. Renner AB, Radeck V, Kellner U, Jägle H, Helbig H. Ten-year follow-up of two unrelated patients with Müller cell sheen dystrophy and first report of successful vitrectomy. Doc Ophthalmol. 2014 Dec 1;129(3):191–202.

315. Kishk. Internal limiting membrane dsytrophy: a case series study of a rarely reported retinal dystrophy [Internet]. [cited 2021 Jun 11]. Available from: https://www.jeos.eg.net/article.asp?issn=2090-0686;year=2017;volume=110;issue=4;spage=118;epage=126;aulast=Kishk

316. Chertkof J, Hufnagel RB, Blain D, Gropman AL, Brooks BP. Retinoschisis associated with Kearns-Sayre syndrome. Ophthalmic Genet. 2020 Sep 2;41(5):497–500.

317. Phadke SR, Sharda S, Urquhart J, Jenkinson E, Chawala S, Trump D. Report of two brothers with short stature, microcephaly, mental retardation, and retinoschisis-A new mental retardation syndrome? Am J Med Genet A. 2011 Jan;155A(1):9–13.

318. Ayala-Ramirez R, Graue-Wiechers F, Robredo V, Amato-Almanza M, Horta-Diez I, Zenteno JC. A new autosomal recessive syndrome consisting of posterior microphthalmos, retinitis pigmentosa, foveoschisis, and optic disc drusen is caused by a MFRP gene mutation. Mol Vis. 2006 Dec 4;12:1483–9.

319. Weng CY, Barnett D. Nanophthalmos-Retinitis Pigmentosa-Foveoschisis-Optic Disc Drusen Syndrome (MFRP). Ophthalmol Retina. 2018 Nov 1;2(11):1162.

320. Marques João Pedro. MFRP-Related Nanophthalmos-Retinitis Pigmentosa-Foveoschisis-Optic Disc Drusen Syndrome. Ophthalmic Surg Lasers Imaging Retina. 2021 Feb 1;52(2):110–110.

321. Arno G, Carss KJ, Hull S, Zihni C, Robson AG, Fiorentino A, et al. Biallelic Mutation of ARHGEF18, Involved in the Determination of Epithelial Apicobasal Polarity, Causes Adult-Onset Retinal Degeneration. Am J Hum Genet. 2017 Feb 2;100(2):334–42.

322. Spaide RF. Retinal vascular cystoid macular edema: Review and New Theory. Retina Phila Pa. 2016 Oct;36(10):1823–42.

323. Reichenbach A, Wurm A, Pannicke T, Iandiev I, Wiedemann P, Bringmann A. Müller cells as players in retinal degeneration and edema. Graefes Arch Clin Exp Ophthalmol Albrecht Von Graefes Arch Klin Exp Ophthalmol. 2007 May;245(5):627–36.

324. Nagelhus EA, Mathiisen TM, Ottersen OP. Aquaporin-4 in the central nervous system: cellular and subcellular distribution and coexpression with KIR4.1. Neuroscience. 2004;129(4):905–13.

325. Verkman AS. Role of aquaporin water channels in eye function. Exp Eye Res. 2003 Feb;76(2):137–43.

326. Amann B, Kleinwort KJH, Hirmer S, Sekundo W, Kremmer E, Hauck SM, et al. Expression and Distribution Pattern of Aquaporin 4, 5 and 11 in Retinas of 15 Different Species. Int J Mol Sci [Internet]. 2016 Jul 16 [cited 2021 Jun 10];17(7). Available from: https://www.ncbi.nlm.nih.gov/pmc/articles/PMC4964518/

327. Chung YR, Kim YH, Lee SY, Byeon HE, Lee K. Insights into the pathogenesis of cystoid macular edema: leukostasis and related cytokines. Int J Ophthalmol. 2019 Jul 18;12(7):1202–8.

328. Yanoff M, Fine BS, Brucker AJ, Eagle RC. Pathology of human cystoid macular edema. Surv Ophthalmol. 1984 May;28 Suppl:505–11.

329. Gass JD, Anderson DR, Davis EB. A clinical, fluorescein angiographic, and electron microscopic correlation of cystoid macular edema. Am J Ophthalmol. 1985 Jul 15;100(1):82–6.

330. Johnson MW. Etiology and treatment of macular edema. Am J Ophthalmol. 2009 Jan;147(1):11-21.e1.

331. Haller JA, Bandello F, Belfort R, Blumenkranz MS, Gillies M, Heier J, et al. Randomized, sham-controlled trial of dexamethasone intravitreal implant in patients with macular edema due to retinal vein occlusion. Ophthalmology. 2010 Jun;117(6):1134-1146.e3.

332. Pielen A, Clark WL, Boyer DS, Ogura Y, Holz FG, Korobelnik JF, et al. Integrated results from the COPERNICUS and GALILEO studies. Clin Ophthalmol Auckl NZ. 2017 Aug 23;11:1533–40.

333. Heier JS, Korobelnik JF, Brown DM, Schmidt-Erfurth U, Do DV, Midena E, et al. Intravitreal Aflibercept for Diabetic Macular Edema: 148-Week Results from the VISTA and VIVID Studies. Ophthalmology. 2016 Nov;123(11):2376–85.

334. Rosenblatt A, Udaondo P, Cunha-Vaz J, Sivaprasad S, Bandello F, Lanzetta P, et al. A Collaborative Retrospective Study on the Efficacy and Safety of Intravitreal Dexamethasone Implant (Ozurdex) in Patients with Diabetic Macular Edema: The European DME Registry Study. Ophthalmology. 2020 Mar;127(3):377–93.

335. Govetto A, Sarraf D, Hubschman JP, Tadayoni R, Couturier A, Chehaibou I, et al. Distinctive mechanisms and patterns of exudative versus tractional intraretinal cystoid spaces as seen with multimodal imaging. Am J Ophthalmol [Internet]. 2019 Dec; Available from: https://linkinghub.elsevier.com/retrieve/pii/S0002939419306117

336. dell'Omo R, Filippelli M, De Turris S, Cimino L, Steel DH, Pavesio CE, et al. Fluorescein Angiography Findings in Eyes With Lamellar Macular Hole and Epiretinal Membrane Foveoschisis. Invest Ophthalmol Vis Sci. 2021 Jan 29;62(1):34.

337. Johnson MW. Tractional Cystoid Macular Edema: A Subtle Variant of the Vitreomacular Traction Syndrome. Am J Ophthalmol. 2005 Aug 1;140(2):184.e1-184.e10.

338. Casalino G, Upendran M, Bandello F, Chakravarthy U. Stellate nonhereditary idiopathic foveomacular retinoschisis concomitant to exudative maculopathies. Eye Lond Engl. 2016 May;30(5):754–7.

339. Falb T, Malle EM, Haas A, Weger M, Wedrich A. STellate nonhereditary idiopathic foveomacular retinoschisis in a patient with macular telangiectasia type 2. Retin Cases Brief Rep. 2018 Jul;Publish Ahead of Print:1.

340. Ziada J, Hagenau F, Compera D, Wolf A, Scheler R, Schaumberger MM, et al. Vitrectomy for intermediate age-related macular degeneration associated with tangential vitreomacular traction: a clinicopathologic correlation. Retina. 2018 Mar;38(3):531–40.

341. Moorfields Eye Hospital annual report 2018-19.pdf [Internet]. [cited 2020 Apr 6]. Available from: https://www.moorfields.nhs.uk/sites/default/files/Moorfields%20Eye%20Hospital%20annual%20report%202018-19.pdf

342. Elm E von, Altman DG, Egger M, Pocock SJ, Gøtzsche PC, Vandenbroucke JP. Strengthening the reporting of observational studies in epidemiology (STROBE) statement: guidelines for reporting observational studies. BMJ. 2007 Oct 18;335(7624):806.

343. Ferris FL, Kassoff A, Bresnick GH, Bailey I. New visual acuity charts for clinical research. Am J Ophthalmol. 1982 Jul;94(1):91–6.

344. Bailey IL, Lovie-Kitchin JE. Visual acuity testing. From the laboratory to the clinic. Vision Res. 2013 Sep 20;90:2–9.

345. Early Treatment Diabetic Retinopathy Study design and baseline patient characteristics. ETDRS report number 7. Ophthalmology. 1991 May;98(5 Suppl):741–56.

346. Schulze-Bonsel K, Feltgen N, Burau H, Hansen L, Bach M. Visual Acuities "Hand Motion" and "Counting Fingers" Can Be Quantified with the Freiburg Visual Acuity Test. Invest Ophthalmol Vis Sci. 2006 Mar 1;47(3):1236–40.

347. Jaycock P, Johnston RL, Taylor H, Adams M, Tole DM, Galloway P, et al. The Cataract National Dataset electronic multi-centre audit of 55 567 operations: updating benchmark standards of care in the United Kingdom and internationally. Eye. 2009 Jan;23(1):38–49.

348. Dimopoulos IS, Tseng C, MacDonald IM. Microperimetry as an Outcome Measure in Choroideremia Trials: Reproducibility and Beyond. Invest Ophthalmol Vis Sci. 2016 Aug 1;57(10):4151–61.

349. da Cruz L, Fynes K, Georgiadis O, Kerby J, Luo YH, Ahmado A, et al. Phase 1 clinical study of an embryonic stem cell–derived retinal pigment epithelium patch in age-related macular degeneration. Nat Biotechnol. 2018 Apr;36(4):328–37.

350. Yang Y, Dunbar H. Clinical Perspectives and Trends: Microperimetry as a Trial Endpoint in Retinal Disease. Ophthalmologica [Internet]. 2021 Feb 10 [cited 2021 Aug 28]; Available from: https://www.karger.com/Article/FullText/515148

351. Han RC, Jolly JK, Xue K, MacLaren RE. Effects of pupil dilation on MAIA microperimetry. Clin Experiment Ophthalmol. 2017;45(5):489–95.

352. Charng J, Sanfilippo PG, Attia MS, Dolliver M, Arunachalam S, Chew AL, et al. Interpreting MAIA Microperimetry Using Age- and Retinal Loci-Specific Reference Thresholds. Transl Vis Sci Technol. 2020 Jun 3;9(7):19–19.

353. Molina-Martín A, Piñero DP, Pérez-Cambrodí RJ. Normal Values for Microperimetry with the MAIA Microperimeter: Sensitivity and Fixation Analysis in Healthy Adults and Children. Eur J Ophthalmol. 2017 Sep 1;27(5):607–13.

354. Schindelin J, Arganda-Carreras I, Frise E, Kaynig V, Longair M, Pietzsch T, et al. Fiji: an open-source platform for biological-image analysis. Nat Methods. 2012 Jul;9(7):676–82.

355. Rueden CT, Schindelin J, Hiner MC, DeZonia BE, Walter AE, Arena ET, et al. ImageJ2: ImageJ for the next generation of scientific image data. BMC Bioinformatics. 2017 Nov 29;18(1):529.

356. Holden BA, Fricke TR, Wilson DA, Jong M, Naidoo KS, Sankaridurg P, et al. Global prevalence of myopia and high myopia and temporal trends from 2000 through 2050. Ophthalmology. 2016 May;123(5):1036–42.

357. Katz J, Tielsch JM, Sommer A. Prevalence and risk factors for refractive errors in an adult inner city population. Invest Ophthalmol Vis Sci. 1997 Feb;38(2):334–40.

358. Iwase A, Araie M, Tomidokoro A, Yamamoto T, Shimizu H, Kitazawa Y, et al. Prevalence and causes of low vision and blindness in a Japanese adult population: the Tajimi Study. Ophthalmology. 2006 Aug;113(8):1354–62.

359. Xu L, Li J, Cui T, Hu A, Fan G, Zhang R, et al. Refractive error in urban and rural adult Chinese in Beijing. Ophthalmology. 2005 Oct;112(10):1676–83.

360. Sun J, Zhou J, Zhao P, Lian J, Zhu H, Zhou Y, et al. High prevalence of myopia and high myopia in 5060 Chinese university students in Shanghai. Invest Ophthalmol Vis Sci. 2012 Nov;53(12):7504–9.

361. Williams KM, Verhoeven VJM, Cumberland P, Bertelsen G, Wolfram C, Buitendijk GHS, et al. Prevalence of refractive error in europe: the european eye epidemiology (E(3)) consortium. Eur J Epidemiol. 2015 Apr;30(4):305–15.

362. Vitale S, Sperduto RD, Ferris FL. Increased prevalence of myopia in the United States between 1971-1972 and 1999-2004. Arch Ophthalmol Chic Ill 1960. 2009 Dec;127(12):1632–9.

363. Ohno-Matsui K, Kawasaki R, Jonas JB, Cheung CMG, Saw SM, Verhoeven VJM, et al. International photographic classification and grading system for myopic maculopathy. Am J Ophthalmol. 2015 May;159(5):877-83.e7.

364. Tideman JWL, Snabel MCC, Tedja MS, van Rijn GA, Wong KT, Kuijpers RWAM, et al. Association of axial length with risk of uncorrectable visual impairment for europeans with myopia. JAMA Ophthalmol. 2016 Dec;134(12):1355–63.

365. Saka N, Ohno-Matsui K, Shimada N, Sueyoshi SI, Nagaoka N, Hayashi W, et al. Long-term changes in axial length in adult eyes with pathologic myopia. Am J Ophthalmol. 2010 Oct;150(4):562-568.e1.

366. Hayashi K, Ohno-Matsui K, Shimada N, Moriyama M, Kojima A, Hayashi W, et al. Long-term pattern of progression of myopic maculopathy: a natural history study. Ophthalmology. 2010 Aug;117(8):1595-611-1611.e1-4.

367. Hsiang HW, Ohno-Matsui K, Shimada N, Hayashi K, Moriyama M, Yoshida T, et al. Clinical characteristics of posterior staphyloma in eyes with pathologic myopia. Am J Ophthalmol. 2008 Jul;146(1):102–10.

368. Wang NK, Wu YM, Wang JP, Liu L, Yeung L, Chen YP, et al. Clinical characteristics of posterior staphylomas in myopic eyes with axial length shorter than 26.5 millimeters. Am J Ophthalmol. 2016 Feb;162:180-190.e1.

369. Steidl SM, Pruett RC. Macular complications associated with posterior staphyloma. Am J Ophthalmol. 1997 Feb;123(2):181–7.

370. Chang L, Pan CW, Ohno-Matsui K, Lin X, Cheung GCM, Gazzard G, et al. Myopia-related fundus changes in Singapore adults with high myopia. Am J Ophthalmol. 2013 Jun;155(6):991-999.e1.

371. Ohno-Matsui K. Proposed classification of posterior staphylomas based on analyses of eye shape by three-dimensional magnetic resonance imaging and wide-field fundus imaging. Ophthalmology. 2014 Sep;121(9):1798–809.

372. Shinohara K, Tanaka N, Jonas JB, Shimada N, Moriyama M, Yoshida T, et al. Ultrawide-field OCT to investigate relationships between myopic macular retinoschisis and posterior staphyloma. Ophthalmology. 2018 Oct;125(10):1575–86.

373. Von Graefe A. Zwei Sektionsbefunde bei Sclerotico-choroiditis posterior und Bemerkunger uber diese Kramkheit. Arch Ophthamol. 1854;1:390–401.

374. Curtin BJ, Karlin DB. Axial length measurements and fundus changes of the myopic eye. I. The posterior fundus. Trans Am Ophthalmol Soc. 1970;68:312–34.

375. Curtin BJ, Karlin DB. Axial length measurements and fundus changes of the myopic eye. Am J Ophthalmol. 1971 Jan;71(1 Pt 1):42–53.

376. Curtin BJ. The posterior staphyloma of pathologic myopia. Trans Am Ophthalmol Soc. 1977;75:67–86.

377. Panozzo G, Mercanti A. Optical coherence tomography findings in myopic traction maculopathy. Arch Ophthamol. 2004 Oct;122(10):1455–60.

378. Henaine-Berra A, Zand-Hadas IM, Fromow-Guerra J, García-Aguirre G. Prevalence of macular anatomic abnormalities in high myopia. Ophthalmic Surg Lasers Imaging Retina. 2013 Mar;44(2):140–4.

379. Elnahry AG, Khafagy MM, Esmat SM, Mortada HA. Prevalence and associations of posterior segment manifestations in a cohort of egyptian patients with pathological myopia. Curr Eye Res. 2019 Apr;69:1–8.

380. Gaucher D, Erginay A, Lecleire-Collet A, Haouchine B, Puech M, Cohen SY, et al. Dome-shaped macula in eyes with myopic posterior staphyloma. Am J Ophthalmol. 2008 May;145(5):909–14.

381. Zhao X, Ding X, Lyu C, Li S, Lian Y, Chen X, et al. Observational study of clinical characteristics of dome-shaped macula in Chinese Han with high myopia at Zhongshan Ophthalmic Centre. BMJ Open. 2018 Dec;8(12):e021887.

382. PHILLIPS CI. Retinal detachment at the posterior pole. Br J Ophthalmol. 1958 Dec;42(12):749–53.

383. Takano M, Kishi S. Foveal retinoschisis and retinal detachment in severely myopic eyes with posterior staphyloma. Am J Ophthalmol. 1999 Oct;128(4):472–6.

384. Wu Q, Li S wei, Lu B, Wang W qing, Fang J, Yu J yi, et al. [Clinical observation of highly myopic eyes with retinoschisis after phacoemulsification]. Zhonghua Yan Ke Za Zhi Chin J Ophthalmol. 2011 Apr;47(4):303–9.

385. Shimada N, Tanaka Y, Tokoro T, Ohno-Matsui K. Natural course of myopic traction maculopathy and factors associated with progression or resolution. Am J Ophthalmol. 2013 Nov;156(5):948-957.e1.

386. Cheng C, Teo K, Tan CS, Lee SY, Loh BK, Wong E, et al. MYOPIC RETINOSCHISIS IN ASIANS: Structural features and determinants of visual acuity and prognostic factors for progression. Retina Phila Pa. 2016 Apr;36(4):717–26.

387. Rey A, Jürgens I, Maseras X, Carbajal M. Natural course and surgical management of high myopic foveoschisis. Ophthalmol J Int Ophtalmol Int J Ophthalmol Z Augenheilkd. 2014;231(1):45–50.

388. Panozzo G, Mercanti A. Vitrectomy for myopic traction maculopathy. Arch Ophthamol. 2007 Jun;125(6):767–72.

389. Gaucher D, Haouchine B, Tadayoni R, Massin P, Erginay A, Benhamou N, et al. Long-term follow-up of high myopic foveoschisis: natural course and surgical outcome. Am J Ophthalmol. 2007 Mar;143(3):455–62.

390. Wu PC, Chen YJ, Chen YH, Chen CH, Shin SJ, Tsai CL, et al. Factors associated with foveoschisis and foveal detachment without macular hole in high myopia. Eye Lond Engl. 2009 Feb;23(2):356–61.

391. Matsumura S, Sabanayagam C, Wong CW, Tan CS, Kuo A, Wong YL, et al. Characteristics of myopic traction maculopathy in myopic Singaporean adults. Br J Ophthalmol [Internet]. 2020 May 23 [cited 2020 May 28]; Available from: https://bjo.bmj.com/content/early/2020/05/23/bjophthalmol-2020-316182

392. Baba T, Ohno-Matsui K, Futagami S, Yoshida T, Yasuzumi K, Kojima A, et al. Prevalence and characteristics of foveal retinal detachment without macular hole in high myopia. Am J Ophthalmol. 2003 Mar;135(3):338–42.

393. Benhamou N, Massin P, Haouchine B, Erginay A, Gaudric A. Macular retinoschisis in highly myopic eyes. Am J Ophthalmol. 2002 Jun;133(6):794–800.

394. Fujimoto M, Hangai M, Suda K, Yoshimura N. Features associated with foveal retinal detachment in myopic macular retinoschisis. Am J Ophthalmol. 2010 Dec;150(6):863–70.

395. Larsen JS. The sagittal growth of the eye. IV. Ultrasonic measurement of the axial length of the eye from birth to puberty. Acta Ophthalmol (Copenh). 1971;49(6):873–86.

396. Gohil R, Sivaprasad S, Han LT, Mathew R, Kiousis G, Yang Y. Myopic foveoschisis: a clinical review. Eye Lond Engl. 2015 May;29(5):593–601.

397. Akiba J. Prevalence of posterior vitreous detachment in high myopia. OPHTHA. 1993 Sep;100(9):1384–8.

398. Yonemoto J, Ideta H, Sasaki K, Tanaka S, Hirose A, Oka C. The age of oneset of posterior vitreous detachment. Graefes Arch Clin Exp Ophthalmol. 1994 Feb 1;232(2):67–70.

399. Bond-Taylor M, Jakobsson G, Zetterberg M. Posterior vitreous detachment - prevalence of and risk factors for retinal tears. Clin Ophthalmol Auckl NZ. 2017;11:1689–95.

400. Hayashi K, Manabe S ichi, Hirata A, Yoshimura K. Posterior Vitreous Detachment in Highly Myopic Patients. Invest Ophthalmol Vis Sci. 2020 Apr 25;61(4):33.

401. Larsson L, Osterlin S. Posterior vitreous detachment. A combined clinical and physiochemical study. Graefes Arch Clin Exp Ophthalmol. 1985;223(2):92–5.

402. Kobayashi K, Mandai M, Suzuma I, Kobayashi H, Okinami S. Expression of estrogen receptor in the choroidal neovascular membranes in highly myopic eyes. Retina Phila Pa. 2002 Aug;22(4):418–22.

403. Ouyang PB, Duan XC, Zhu XH. Diagnosis and treatment of myopic traction maculopathy. Int J Ophthalmol. 2012;5(6):754–8.

404. VanderBeek BL, Johnson MW. The diversity of traction mechanisms in myopic traction maculopathy. Am J Ophthalmol. 2012 Jan;153(1):93–102.

405. Grossniklaus HE, Green WR. Pathologic findings in pathologic myopia. Retina Phila Pa. 1992;12(2):127–33.

406. Tang J, Rivers MB, Moshfeghi AA, Flynn HW, Chan CC. Pathology of macular foveoschisis associated with degenerative myopia. J Ophthalmol. 2010;2010(3):1–4.

407. AttaAllah HR, Omar IAN, Abdelhalim AS. Assessment of posterior segment using spectral domain OCT in highly myopic eyes. Open Ophthalmol J. 2017;11(1):334–45.

408. Ripandelli G, Rossi T, Scarinci F, Scassa C, Parisi V, Stirpe M. Macular vitreoretinal interface abnormalities in highly myopic eyes with posterior staphyloma: 5-year follow-up. Retina Phila Pa. 2012 Sep;32(8):1531–8.

409. Kobayashi H, Kishi S. Vitreous surgery for highly myopic eyes with foveal detachment and retinoschisis. OPHTHA. 2003 Sep;110(9):1702–7.

410. Kishi S. Vitreous Changes in Myopia. In: Spaide RF, Ohno-Matsui K, Yannuzzi LA, editors. Pathologic Myopia [Internet]. New York, NY: Springer; 2014 [cited 2020 Jan 12]. p. 143–66. Available from: https://doi.org/10.1007/978-1-4614-8338-0_11

411. Morita H, Funata M, Tokoro T. A clinical study of the development of posterior vitreous detachment in high myopia. Retina Phila Pa. 1995;15(2):117–24.

412. Itakura H, Kishi S, Li D, Akiyama H. Observation of posterior precortical vitreous pocket using swept-source optical coherence tomography. Invest Ophthalmol Vis Sci. 2013 May 3;54(5):3102–7.

413. Ishida S, Yamazaki K, Shinoda K, Kawashima S, Oguchi Y. Macular hole retinal detachment in highly myopic eyes: ultrastructure of surgically removed epiretinal membrane and clinicopathologic correlation. Retina Phila Pa. 2000;20(2):176–83.

414. Itakura H, Kishi S, Li D, Nitta K, Akiyama H. Vitreous changes in high myopia observed by swept-source optical coherence tomography. Invest Ophthalmol Vis Sci. 2014 Mar;55(3):1447–52.

415. Ikuno Y, Gomi F, Tano Y. Potent retinal arteriolar traction as a possible cause of myopic foveoschisis. Am J Ophthalmol. 2005 Mar;139(3):462–7.

416. Sayanagi K, Ikuno Y, Gomi F, Tano Y. Retinal vascular microfolds in highly myopic eyes. Am J Ophthalmol. 2005 Apr;139(4):658–63.

417. Shimada N, Ohno-Matsui K, Nishimuta A, Moriyama M, Yoshida T, Tokoro T, et al. Detection of Paravascular Lamellar Holes and Other Paravascular

Abnormalities by Optical Coherence Tomography in Eyes with High Myopia. Ophthalmology. 2008 Apr 1;115(4):708–17.

418. Forte R, Cennamo G, Pascotto F, de Crecchio G. En face optical coherence tomography of the posterior pole in high myopia. Am J Ophthalmol. 2008 Feb;145(2):281–8.

419. Johnson MW. Myopic traction maculopathy: pathogenic mechanisms and surgical treatment. Retina Phila Pa. 2012 Sep;32 Suppl 2:S205-10.

420. Sayanagi K, Morimoto Y, Ikuno Y, Tano Y. Spectral-domain optical coherence tomographic findings in myopic foveoschisis. Retina Phila Pa. 2010 Apr;30(4):623–8.

421. Li T, Wang X, Zhou Y, Feng T, Xiao M, Wang F, et al. Paravascular abnormalities observed by spectral domain optical coherence tomography are risk factors for retinoschisis in eyes with high myopia. Acta Ophthalmol (Copenh). 2018 Jun;96(4):e515–23.

422. Yang Y, Wang J, Jiang H, Yang X, Feng L, Hu L, et al. Retinal Microvasculature Alteration in High Myopia. Invest Ophthalmol Vis Sci. 2016 Nov 7;57(14):6020–30.

423. Wang T, Li H, Zhang R, Yu Y, Xiao X, Wu C. Evaluation of retinal vascular density and related factors in youth myopia without maculopathy using OCTA. Sci Rep. 2021 Jul 28;11(1):15361.

424. Mao J, Deng X, Ye Y, Liu H, Fang Y, Zhang Z, et al. Morphological characteristics of retinal vessels in eyes with high myopia: Ultra-wide field images analyzed by artificial intelligence using a transfer learning system. Front Med [Internet]. 2023 [cited 2023 Jun 20];9. Available from: https://www.frontiersin.org/articles/10.3389/fmed.2022.956179

425. Harrell CR, Simovic Markovic B, Fellabaum C, Arsenijevic A, Djonov V, Volarevic V. Molecular mechanisms underlying therapeutic potential of pericytes. J Biomed Sci. 2018 Mar 9;25(1):21.

426. Little K, Ma JH, Yang N, Chen M, Xu H. Myofibroblasts in macular fibrosis secondary to neovascular age-related macular degeneration - the potential sources and molecular cues for their recruitment and activation. eBioMedicine. 2018 Dec 1;38:283–91.

427. Bando H, Ikuno Y, Choi JS, Tano Y, Yamanaka I, Ishibashi T. Ultrastructure of internal limiting membrane in myopic foveoschisis. Am J Ophthalmol. 2005 Jan;139(1):197–9.

428. Fang X, Weng Y, Xu S, Chen Z, Liu J, Chen B, et al. Optical coherence tomographic characteristics and surgical outcome of eyes with myopic foveoschisis. Eye Lond Engl. 2009 Jun;23(6):1336–42.

429. Yokota R, Hirakata A, Hayashi N, Hirota K, Rii T, Itoh Y, et al. Ultrastructural analyses of internal limiting membrane excised from highly myopic eyes with myopic traction maculopathy. Jpn J Ophthalmol. 2018 Jan;62(1):84–91.

430. Chen L, Wei Y, Zhou X, Zhang Z, Chi W, Gong L, et al. Morphologic, Biomechanical, and Compositional Features of the Internal Limiting Membrane in Pathologic Myopic Foveoschisis. Invest Ophthalmol Vis Sci. 2018 Nov 1;59(13):5569–78.

431. Russell JF, Naranjo A, Dubovy SR, Smiddy WE. Clinicopathologic correlation of preretinal tissues in myopic traction maculopathy. Retina Phila Pa. 2021 Jul 1;41(7):1512–7.

432. Wang S, Peng Q, Zhao P. SD-OCT use in myopic retinoschisis pre- and post-vitrectomy. Optom Vis Sci Off Publ Am Acad Optom. 2012 May;89(5):678–83.

433. Sayanagi K, Ikuno Y, Tano Y. Tractional Internal Limiting Membrane Detachment in Highly Myopic Eyes. Am J Ophthalmol. 2006 Nov 1;142(5):850–2.

434. Spaide RF, Fisher Y. Removal of adherent cortical vitreous plaques without removing the internal limiting membrane in the repair of macular detachments in highly myopic eyes. Retina Phila Pa. 2005 Apr;25(3):290–5.

435. Alkabes M, Burés-Jelstrup A, Salinas C, Medeiros MD, Rios J, Corcóstegui B, et al. Macular buckling for previously untreated and recurrent retinal detachment due to high myopic macular hole: a 12-month comparative study. Graefes Arch Clin Exp Ophthalmol Albrecht Von Graefes Arch Klin Exp Ophthalmol. 2014 Apr;252(4):571–81.

436. Shimada N, Ohno-Matsui K, Yoshida T, Sugamoto Y, Tokoro T, Mochizuki M. Progression from macular retinoschisis to retinal detachment in highly myopic eyes is associated with outer lamellar hole formation. Br J Ophthalmol. 2008 Jun;92(6):762–4.

437. Sun CB, Liu Z, Xue AQ, Yao K. Natural evolution from macular retinoschisis to full-thickness macular hole in highly myopic eyes. Eye Lond Engl. 2010 Dec;24(12):1787–91.

438. Tanaka Y, Shimada N, Moriyama M, Hayashi K, Yoshida T, Tokoro T, et al. Natural history of lamellar macular holes in highly myopic eyes. Am J Ophthalmol. 2011 Jul;152(1):96-99.e1.

439. Lim LS, Ng WY, Wong D, Wong E, Yeo I, Ang CL, et al. Prognostic factor analysis of vitrectomy for myopic foveoschisis. Br J Ophthalmol. 2015 Dec;99(12):1639–43.

440. Lee DH, Moon I, Kang HG, Choi EY, Kim SS, Byeon SH, et al. Surgical outcome and prognostic factors influencing visual acuity in myopic foveoschisis patients. Eye Lond Engl. 2019 Oct;33(10):1642–8.

441. Ichibe M, Baba E, Funaki S, Yoshizawa T, Abe H. Retinoschisis in a highly myopic eye without vision impairment. Retina Phila Pa. 2004 Apr;24(2):331–3.

442. Ruiz-Medrano J, Montero JA, Flores-Moreno I, Arias L, García-Layana A, Ruiz-Moreno JM. Myopic maculopathy: Current status and proposal for a new classification and grading system (ATN). Prog Retin Eye Res. 2019 Mar 1;69:80–115.

443. Ruiz-Medrano J, Flores-Moreno I, Ohno-Matsui K, Cheung CMG, Silva R, Ruiz-Moreno JM. Validation of the recently developed atn classification and grading system for myopic maculopathy. Retina. 2020 Nov;40(11):2113–8.

444. Li J, Liu B, Li Y, Zhao X, Chen S, Huang X, et al. Clinical characteristics of eyes with different grades of myopic traction maculopathy – based on the atn classification system. Retina [Internet]. 2020 Nov 20 [cited 2020 Nov 27];Publish Ahead of Print. Available from: https://journals.lww.com/10.1097/IAE.0000000000003043

445. Zhang RR, Yu Y, Hou YF, Wu CF. Intra- and interobserver concordance of a new classification system for myopic maculopathy. BMC Ophthalmol. 2021 Apr 23;21(1):187.

446. MILLER WW, BORLEY WE. Surgical treatment of degenerative myopia. Scleral reinforcement. Am J Ophthalmol. 1964 May;57(5):796–804.

447. Ripandelli G, Coppé AM, Fedeli R, Parisi V, D'Amico DJ, Stirpe M. Evaluation of primary surgical procedures for retinal detachment with macular hole in highly myopic eyes: a comparison [corrected] of vitrectomy versus posterior episcleral buckling surgery. OPHTHA. 2001 Dec;108(12):2258-64-discussion 2265.

448. Kuhn F. Internal limiting membrane removal for macular detachment in highly myopic eyes. Am J Ophthalmol. 2003 Apr;135(4):547–9.

449. Ikuno Y, Sayanagi K, Ohji M, Kamei M, Gomi F, Harino S, et al. Vitrectomy and internal limiting membrane peeling for myopic foveoschisis. Am J Ophthalmol. 2004 Apr;137(4):719–24.

450. Ikuno Y, Sayanagi K, Soga K, Oshima Y, Ohji M, Tano Y. Foveal anatomical status and surgical results in vitrectomy for myopic foveoschisis. Jpn J Ophthalmol. 2008 Jul;52(4):269–76.

451. Hirakata A, Hida T. Vitrectomy for myopic posterior retinoschisis or foveal detachment. Jpn J Ophthalmol. 2006 Jan;50(1):53–61.

452. Kumagai K, Furukawa M, Ogino N, Larson E. Factors correlated with postoperative visual acuity after vitrectomy and internal limiting membrane peeling for myopic foveoschisis. Retina Phila Pa. 2010 Jun;30(6):874–80.

453. Kim KS, Lee SB, Lee WK. Vitrectomy and internal limiting membrane peeling with and without gas tamponade for myopic foveoschisis. Am J Ophthalmol. 2012 Feb;153(2):320-326.e1.

454. Lim SJ, Kwon YH, Kim SH, You YS, Kwon OW. Vitrectomy and internal limiting membrane peeling without gas tamponade for myopic foveoschisis. Graefes Arch Clin Exp Ophthalmol Albrecht Von Graefes Arch Klin Exp Ophthalmol. 2012 Nov;250(11):1573–7.

455. Yun LN, Xing YQ. Long-term outcome of highly myopic foveoschisis treated by vitrectomy with or without gas tamponade. Int J Ophthalmol. 2017;10(9):1392–5.

456. Sborgia G, Recchimurzo N, Sborgia L, Niro A, Sborgia A, Piepoli M, et al. Inverted internal limiting membrane-flap technique for optic disk pit maculopathy: morphologic and functional analysis. Retin Cases Brief Rep. 2018 Feb;1.

457. Rizzo S, Giansanti F, Finocchio L, Caporossi T, Barca F, Bacherini D, et al. Vitrectomy with internal limiting membrane peeling and air tamponade for myopic foveoschisis. Retina Phila Pa. 2019 Nov;39(11):2125–31.

458. Peng KL, Kung YH, Hsu CM, Chang SP, Tseng PL, Wu TT. Surgical outcomes of centripetal non-fovea-sparing internal limiting membrane peeling for myopic foveoschisis with and without foveal detachment: a follow-up of at least 3 years. Br J Ophthalmol. 2019 Dec;bjophthalmol-2019-314972.

459. Kwok AKH, Lai TYY, Yip WWK. Vitrectomy and gas tamponade without internal limiting membrane peeling for myopic foveoschisis. Br J Ophthalmol. 2005 Sep;89(9):1180–3.

460. Shimada N, Sugamoto Y, Ogawa M, Takase H, Ohno-Matsui K. Fovea-sparing internal limiting membrane peeling for myopic traction maculopathy. Am J Ophthalmol. 2012 Oct;154(4):693–701.

461. Ho TC, Chen MS, Huang JS, Shih YF, Ho H, Huang YH. Foveola nonpeeling technique in internal limiting membrane peeling of myopic foveoschisis surgery. Retina Phila Pa. 2012 Mar;32(3):631–4.

462. Jin H, Zhang Q, Zhao P. Fovea sparing internal limiting membrane peeling using multiple parafoveal curvilinear peels for myopic foveoschisis: technique and outcome. BMC Ophthalmol. 2016 Oct;16(1):180.

463. Tian T, Jin H, Zhang Q, Zhang X, Zhang H, Zhao P. Long-term surgical outcomes of multiple parfoveolar curvilinear internal limiting membrane peeling for myopic foveoschisis. Eye Lond Engl. 2018 Nov;32(11):1783–9.

464. Iwasaki M, Miyamoto H, Okushiba U, Imaizumi H. Fovea-sparing internal limiting membrane peeling versus complete internal limiting membrane peeling for myopic traction maculopathy. Jpn J Ophthalmol. 2019 Nov;122:1455–9.

465. Meng B, Zhao L, Yin Y, Li H, Wang X, Yang X, et al. Internal limiting membrane peeling and gas tamponade for myopic foveoschisis: a systematic review and meta-analysis. BMC Ophthalmol. 2017 Sep;17(1):166.

466. Wu J, Xu Q, Luan J. Vitrectomy with fovea-sparing ILM peeling versus total ILM peeling for myopic traction maculopathy: A meta-analysis. Eur J Ophthalmol. 2020 Nov 3;1120672120970111.

467. Wang Y, Zhao X, Zhang W, Yang J, Chen Y. Fovea-sparing versus complete internal limiting membrane peeling in vitrectomy for vitreomacular interface diseaseS: A Systematic Review and Meta-Analysis. Retina Phila Pa. 2021 Jun 1;41(6):1143–52.

468. El Rayes EN, Elborgy E. Suprachoroidal buckling: technique and indications. J Ophthalmic Vis Res. 2013 Oct;8(4):393–9.

469. Ghoraba HH, Mansour HO, Elgouhary SM. Effect of 360° episcleral band as adjunctive to pars plana vitrectomy and silicone oil tamponade in the management of myopic macular hole retinal detachment. Retina Phila Pa. 2014 Apr;34(4):670–8.

470. Li XJ, Yang XP, Li QM, Wang YY, Wang J, Lyu XB, et al. Posterior scleral reinforcement combined with vitrectomy for myopic foveoschisis. Int J Ophthalmol. 2016;9(2):258–61.

471. Ando Y, Hirakata A, Ohara A, Yokota R, Orihara T, Hirota K, et al. Vitrectomy and scleral imbrication in patients with myopic traction maculopathy and macular hole retinal detachment. Graefes Arch Clin Exp Ophthalmol Albrecht Von Graefes Arch Klin Exp Ophthalmol. 2017 Apr;255(4):673–80.

472. Ma J, Li H, Ding X, Tanumiharjo S, Lu L. Effectiveness of combined macular buckle under direct vision and vitrectomy with ILM peeling in refractory macular hole retinal detachment with extreme high axial myopia: a 24-month comparative study. Br J Ophthalmol. 2017 Oct;101(10):1386–94.

473. Cao K, Wang J, Zhang J, Yusufu M, Jin S, Zhu G, et al. The effectiveness and safety of posterior scleral reinforcement with vitrectomy for myopic foveoschisis treatment: a systematic review and meta-analysis. Graefes Arch Clin Exp Ophthalmol Albrecht Von Graefes Arch Klin Exp Ophthalmol. 2019 Dec;37(12):2347–15.

474. Zhao X, Ma W, Lian P, Tanumiharjo S, Lin Y, Ding X, et al. Three-year outcomes of macular buckling for macular holes and foveoschisis in highly myopic eyes. Acta Ophthalmol (Copenh). 2020 Jun;98(4):e470–8.

475. Hattori K, Kataoka K, Takeuchi J, Ito Y, Terasaki H. Predictive factors of surgical outcomes in vitrectomy for myopic traction maculopathy. Retina Phila Pa. 2018 Sep;38 Suppl 1:S23–30.

476. Panozzo G, Mercanti A. Optical coherence tomography findings in myopic traction maculopathy. Arch Ophthamol. 2004 Oct;122(10):1455–60.

477. Wu PC, Chen YJ, Chen YH, Chen CH, Shin SJ, Tsai CL, et al. Factors associated with foveoschisis and foveal detachment without macular hole in high myopia. Eye Lond Engl. 2009 Feb;23(2):356–61.

478. Feng J, Wang R, Yu J, Chen Q, He J, Zhou H, et al. Association between Different Grades of Myopic Tractional Maculopathy and OCT-Based Macular Scleral Deformation. J Clin Med. 2022 Mar 14;11(6):1599.

479. Bringmann A, Unterlauft JD, Barth T, Wiedemann R, Rehak M, Wiedemann P. Müller cells and astrocytes in tractional macular disorders. Prog Retin Eye Res. 2022 Jan;86:100977.

480. Fang D, Wang L, Chen L, Liang J, Li K, Mao X, et al. Vitreomacular Interface Abnormalities in Myopic Foveoschisis: Correlation With Morphological Features and Outcome of Vitrectomy. Front Med. 2021;8:796127.

481. Vogt D, Stefanov S, Guenther SR, Hagenau F, Wolf A, Priglinger SG, et al. Comparison of Vitreomacular Interface Changes in Myopic Foveoschisis and Idiopathic Epiretinal Membrane Foveoschisis. Am J Ophthalmol. 2020 Sep;217:152–61.

482. Baptista PM, Silva N, Coelho J, José D, Almeida D, Meireles A. Microperimetry as Part of Multimodal Assessment to Evaluate and Monitor Myopic Traction Maculopathy. Clin Ophthalmol Auckl NZ. 2021;15:235–42.

483. Figueroa MS, Ruiz-Moreno JM, Gonzalez del Valle F, Govetto A, de la Vega C, Plascencia RN, et al. Long-term outcomes of 23-gauge pars plana vitrectomy with internal limiting membrane peeling and gas tamponade for myopic traction maculopathy: A Prospective Study. RETINA. 2015 Sep;35(9):1836–43.

484. Kumagai K, Furukawa M, Ogino N, Larson E. Factors correlated with postoperative visual acuity after vitrectomy and internal limiting membrane peeling for myopic foveoschisis. Retina Phila Pa. 2010 Jun;30(6):874–80.

485. Sborgia G, Boscia F, Niro A, Giancipoli E, D'Amico Ricci G, Sborgia A, et al. Morphologic and functional outcomes of different optical coherence tomography patterns of myopic foveoschisis after vitrectomy and inner limiting membrane peeling. Eye Lond Engl. 2019 Nov;33(11):1768–75.

486. Gao X, Ikuno Y, Fujimoto S, Nishida K. Risk factors for development of full-thickness macular holes after pars plana vitrectomy for myopic foveoschisis. Am J Ophthalmol. 2013 Jun;155(6):1021-1027.e1.

487. Shiraki N, Wakabayashi T, Ikuno Y, Matsumura N, Sato S, Sakaguchi H, et al. Fovea-Sparing Versus Standard Internal Limiting Membrane Peeling for Myopic Traction Maculopathy: A Study of 102 Consecutive Cases. Ophthalmol Retina

[Internet]. 2020 May 26 [cited 2020 May 31]; Available from: http://www.sciencedirect.com/science/article/pii/S2468653020302086

488. Chen G, Mao S, Tong Y, Jiang F, Yang J, Li W. Fovea sparing versus complete internal limiting membrane peeling for myopic traction maculopathy: a meta-analysis. Int Ophthalmol. 2022 Mar;42(3):765–73.

489. Lehmann M, Devin F, Rothschild P, Massin P, Couturier A, Tadayoni R. Preoperative factors influencing visual recovery after vitrectomy for myopic foveoschisis. Retina. 2017;1–9.

490. Flores-Moreno I, Lugo F, Duker JS, Ruiz-Moreno JM. The Relationship Between Axial Length and Choroidal Thickness in Eyes With High Myopia. Am J Ophthalmol. 2013 Feb 1;155(2):314-319.e1.

491. Wei WB, Xu L, Jonas JB, Shao L, Du KF, Wang S, et al. Subfoveal choroidal thickness: the Beijing Eye Study. Ophthalmology. 2013 Jan;120(1):175–80.

492. Weithe T. Ein Fall von angeborener Diformitat der Sehnervpapille. (A case of inborn defect of the optic nerve head.). Arch Augenheilkd. 1882;11:14–9.

493. Reis W. I. Eine wenig bekannte typische missbildung am sehnerveneintritt: Umschriebene grubenbildung auf der papilla n. optici. Ophthalmol J Int Ophtalmol Int J Ophthalmol Z Augenheilkd. 1908;19(6):505–28.

494. Kranenburg EW. Crater-like holes in the optic disc and central serous retinopathy. Arch Ophthamol. 1960 Dec;64:912–24.

495. Healey PR, Mitchell P. The prevalence of optic disc pits and their relationship to glaucoma. J Glaucoma. 2008 Feb;17(1):11–4.

496. Wang Y, Xu L, Jonas JB. Prevalence of congenital optic disc pits in adult Chinese: The Beijing Eye Study. Eur J Ophthalmol. 2006 Dec;16(6):863–4.

497. Steel DHW, Suleman J, Murphy DC, Song A, Dodds S, Rees J. Optic disc pit maculopathy: A two-year nationwide prospective population-based study. Ophthalmology. 2018 Nov;125(11):1757–64.

498. Kalogeropoulos D, Ch'ng SW, Lee R, Elaraoud I, Purohit M, Felicida V, et al. Optic Disc Pit Maculopathy: A Review. Asia-Pac J Ophthalmol Phila Pa. 2019 Jun;8(3):247–55.

499. Uzel MM, Karacorlu M. Optic disc pit and optic disc pit maculopathy: a review. Surv Ophthalmol [Internet]. 2019 Feb; Available from: https://linkinghub.elsevier.com/retrieve/pii/S0039625718302042

500. Moisseiev E, Moisseiev J, Loewenstein A. Optic disc pit maculopathy: when and how to treat? A review of the pathogenesis and treatment options. Int J Retina Vitr. 2015 Dec;1(1):13.

501. Brown G, Shields J, Goldberg R. Congenital pits of the optic nerve head: II. Clinical studies in humans. OPHTHA. 1980 Jan;87(1):51–65.

502. Sugar HS. Congenital pits in the optic disc with acquired macular pathology. Am J Ophthalmol. 1962 Feb;53(2):307–11.

503. Brown GC, Augsburger JJ. Congenital pits of the optic nerve head and retinochoroidal colobomas. Can J Ophthalmol J Can Ophtalmol. 1980 Jul;15(3):144–6.

504. Sugar HS. Congenital pits in the optic disc. Am J Ophthalmol. 1967 Feb;63(2):298–307.

505. Sobol WM, Blodi CF, Folk JC, Weingeist TA. Long-term visual outcome in patients with optic nerve pit and serous retinal detachment of the macula. OPHTHA. 1990 Nov;97(11):1539–42.

506. Theodossiadis GP, Panopoulos M, Kollia AK, Georgopoulos G. Long-term study of patients with congenital pit of the optic nerve and persistent macular detachment. Acta Ophthalmol (Copenh). 1992 Aug;70(4):495–505.

507. Roy R, Waanbah AD, Mathur G, Raman R, Sharma T. Optical coherence tomography characteristics in eyes with optic pit maculopathy. Retina Phila Pa. 2013 Apr;33(4):771–5.

508. Steel DHW, Williamson TH, Laidlaw DAH, Sharma P, Matthews C, Rees J, et al. Extent and location of intraretinal and subretinal fluid as prognostic factors for the outcome of patients with optic disk pit maculopathy. Retina Phila Pa. 2016 Jan;36(1):110–8.

509. Rii T, Hirakata A, Inoue M. Comparative findings in childhood-onset versus adult-onset optic disc pit maculopathy. Acta Ophthalmol (Copenh). 2013 Aug;91(5):429–33.

510. Meyer CH, Rodrigues EB. Optic disc pit maculopathy after blunt ocular trauma. Eur J Ophthalmol. 2004 Feb;14(1):71–3.

511. Akça Bayar S, Sarıgül Sezenöz A, Yaman Pınarcı E, Yılmaz G. Spontaneous regression of optic disc pit maculopathy in a six-year-old child. Turk J Ophthalmol. 2017 Jan;47(1):56–8.

512. Benatti E, Garoli E, Viola F. Spontaneous resolution of optic disk pit maculopathy in a child after a six-year follow-up. Retin Cases Brief Rep. 2018 Aug 6;

513. Brodsky MC. Congenital optic pit with serous maculopathy in childhood. J Am Assoc Pediatr Ophthalmol Strabismus. 2003 Apr;7(2):150.

514. Yuen CHW, Kaye SB. Spontaneous resolution of serous maculopathy associated with optic disc pit in a child: a case report. J AAPOS Off Publ Am Assoc Pediatr Ophthalmol Strabismus. 2002 Oct;6(5):330–1.

515. Gass JDM. Serous detachment of the macula: Secondary to congenital pit of the optic nervehead. Am J Ophthalmol. 1969 Jun;67(6):821–41.

516. Ferry AP. Macular detachment associated with congenital pit of the optic nerve head. Pathologic findings in two cases simulating malignant melanoma of the choroid. Arch Ophthamol. 1963 Sep;70:346–57.

517. Christoforidis JB, Terrell W, Davidorf FH. Histopathology of optic nerve pit-associated maculopathy. Clin Ophthalmol Auckl NZ. 2012;6:1169–74.

518. Postel EA, Pulido JS, McNamara JA, Johnson MW. The etiology and treatment of macular detachment associated with optic nerve pits and related anomalies. Trans Am Ophthalmol Soc. 1998;96:73-88-discussion 88-93.

519. Karacorlu SA, Karacorlu M, Ozdemir H, Burumcek E, Esgin H. Optical coherence tomography in optic pit maculopathy. Int Ophthalmol. 2007 Oct;27(5):293–7.

520. Johnson TM, Johnson MW. Pathogenic implications of subretinal gas migration through pits and atypical colobomas of the optic nerve. Arch Ophthalmol Chic Ill 1960. 2004 Dec;122(12):1793–800.

521. Yannuzzi NA, Zhou XY, Monsalve P, Dubovy SR, Smiddy WE. Clinicopathologic Correlation of the Optic Pit Glial Plug in Optic Disc Pit Maculopathy. Ophthalmic Surg Lasers Imaging Retina Thorofare. 2018 Dec;49(12):287–91.

522. Theodossiadis PG, Grigoropoulos VG, Emfietzoglou J, Theodossiadis GP. Vitreous findings in optic disc pit maculopathy based on optical coherence tomography. Graefes Arch Clin Exp Ophthalmol. 2007 Sep;245(9):1311–8.

523. Hirakata A, Hida T, Wakabayashi T, Fukuda M. Unusual Posterior Hyaloid Strand in a Young Child with Optic Disc Pit Maculopathy: Intraoperative and Histopathological Findings. Jpn J Ophthalmol. 2005 Jun 6;49(3):264–6.

524. Doyle E, Trivedi D, Good P, Scott RA, Kirkby GR. High-resolution optical coherence tomography demonstration of membranes spanning optic disc pits and colobomas. Br J Ophthalmol. 2009 Mar;93(3):360–5.

525. Bonnet M. Serous macular detachment associated with optic nerve pits. Graefes Arch Clin Exp Ophthalmol. 1991;229(6):526–32.

526. Brockhurst RJ. Optic pits and posterior retinal detachment. Trans Am Ophthalmol Soc. 1975;73:264–91.

527. Sugar HS. An explanation for the acquired macular pathology associated with congenital pits of the optic disc. Am J Ophthalmol. 1964 May;57:833–5.

528. Brown GC, Shields JA, Patty BE, Goldberg RE. Congenital pits of the optic nerve head. I. Experimental studies in collie dogs. Arch Ophthamol. 1979 Jul;97(7):1341–4.

529. Dithmar S, Schuett F, Voelcker HE, Holz FG. Delayed sequential occurrence of perfluorodecalin and silicone oil in the subretinal space following retinal detachment surgery in the presence of an optic disc pit. Arch Ophthamol. 2004 Mar;122(3):409–11.

530. Salam A, Khan-Lim D, Luff AJ. Superior retinal detachment in an oil-filled eye with a colobomatous optic disc. Retin Cases Brief Rep. 2008;2(2):124–5.

531. Bartz-Schmidt KU, Heimann K. Pathogenesis of retinal detachment associated with morning glory disc. Int Ophthalmol. 1995;19(1):35–8.

532. Coll GE, Chang S, Flynn TE, Brown GC. Communication between the subretinal space and the vitreous cavity in the morning glory syndrome. Graefes Arch Clin Exp Ophthalmol. 1995 Jul;233(7):441–3.

533. Irvine AR, Crawford JB, Sullivan JH. The pathogenesis of retinal detachment with morning glory disc and optic pit. Retina Phila Pa. 1986;6(3):146–50.

534. Kuhn F, Kover F, Szabo I, Mester V. Intracranial migration of silicone oil from an eye with optic pit. Graefes Arch Clin Exp Ophthalmol. 2006 Oct;244(10):1360–2.

535. Regenbogen L, Stein R, Lazar M. Macular and juxtapapillar serous retinal detachment associated with pit of optic disc. Ophthalmol J Int Ophtalmol Int J Ophthalmol Z Augenheilkd. 1964;148:247–51.

536. Krivoy D, Gentile R, Liebmann JM, Stegman Z, Rosen R, Walsh JB, et al. Imaging congenital optic disc pits and associated maculopathy using optical coherence tomography. Arch Ophthamol. 1996 Feb;114(2):165–70.

537. Chang S, Haik BG, Ellsworth RM, St Louis L, Berrocal JA. Treatment of total retinal detachment in morning glory syndrome. Am J Ophthalmol. 1984 May;97(5):596–600.

538. Michalewski J, Michalewska Z, Nawrocki J. Spectral domain optical coherence tomography morphology in optic disc pit associated maculopathy. Indian J Ophthalmol. 2014 Jul;62(7):777–81.

539. Türkçüoğlu P, Taskapan C. The origin of subretinal fluid in optic disc pit maculopathy. Ophthalmic Surg Lasers Imaging Retina. 2016 Mar;47(3):294–8.

540. Ohno-Matsui K, Hirakata A, Inoue M, Akiba M, Ishibashi T. Evaluation of congenital optic disc pits and optic disc colobomas by swept-source optical coherence tomography. Invest Ophthalmol Vis Sci. 2013 Nov;54(12):7769–78.

541. Makdoumi K, Nilsson TK, Crafoord S. Levels of beta-trace protein in optic disc pit with macular detachment. Acta Ophthalmol (Copenh). 2017 Dec;95(8):815–9.

542. Gordon R, Chatfield RK. Pits in the optic disc associated with macular degeneration. Br J Ophthalmol. 1969 Jul;53(7):481–9.

543. Theodossiadis GP, Ladas ID, Panagiotidis DN, Kollia AC, Voudouri AN, Theodossiadis PG. Fluorescein and indocyanine green angiographic findings in congenital optic disk pit associated with macular detachment. Retina Phila Pa. 1999;19(1):6–11.

544. Gupta RR, Choudhry N. Spontaneous resolution of optic disc pit maculopathy after posterior vitreous detachment. Can J Ophthalmol J Can Ophtalmol. 2016 Feb;51(1):e24-7.

545. Gandorfer A, Kampik A. [Role of vitreoretinal interface in the pathogenesis and therapy of macular disease associated with optic pits]. Ophthalmol Z Dtsch Ophthalmol Ges. 2000 Apr;97(4):276–9.

546. Hirakata A, Okada AA, Hida T. Long-term results of vitrectomy without laser treatment for macular detachment associated with an optic disc pit. Ophthalmology. 2005 Aug;112(8):1430–5.

547. Hirakata A, Inoue M, Hiraoka T, McCuen BW. Vitrectomy without laser treatment or gas tamponade for macular detachment associated with an optic disc pit. Ophthalmology. 2012 Apr;119(4):810–8.

548. Rayat JS, Rudnisky CJ, Waite C, Huang P, Sheidow TG, Kherani A, et al. LONG-TERM OUTCOMES FOR OPTIC DISK PIT MACULOPATHY AFTER VITRECTOMY. Retina Phila Pa. 2015 Oct;35(10):2011–7.

549. Abouammoh MA, Alsulaiman SM, Gupta VS, Mousa A, Hirakata A, Berrocal MH, et al. Pars plana vitrectomy with juxtapapillary laser photocoagulation versus vitrectomy without juxtapapillary laser photocoagulation for the treatment of optic disc pit maculopathy: the results of the KKESH International Collaborative Retina Study Group. Br J Ophthalmol. 2016 Apr;100(4):478–83.

550. Bottoni F, Cereda M, Secondi R, Bochicchio S, Staurenghi G. Vitrectomy for optic disc pit maculopathy: a long-term follow-up study. Graefes Arch Clin Exp Ophthalmol Albrecht Von Graefes Arch Klin Exp Ophthalmol. 2018 Apr;256(4):675–82.

551. Theodossiadis GP. Treatment of maculopathy associated with optic disk pit by sponge explant. Am J Ophthalmol. 1996 Jun;121(6):630–7.

552. Theodossiadis GP, Theodossiadis PG. Optical coherence tomography in optic disk pit maculopathy treated by the macular buckling procedure. Am J Ophthalmol. 2001 Aug 1;132(2):184–90.

553. Joko T, Kusaka S. Tangential vitreous traction observed in optic disc pit maculopathy without apparent serous detachment. Ophthalmic Surg Lasers. 1998 Aug;29(8):677–9.

554. Inoue M. Retinal complications associated with congenital optic disc anomalies determined by swept source optical coherence tomography. Taiwan J Ophthalmol. 2016;6(1):8–14.

555. Akiba J, Kakehashi A, Hikichi T, Trempe CL. Vitreous findings in cases of optic nerve pits and serous macular detachment. Am J Ophthalmol. 1993 Jul 15;116(1):38–41.

556. Hasegawa T, Akiba J, Ishiko S, Hikichi T, Kakehashi A, Hirokawa H, et al. Abnormal vitreous structure in optic nerve pit. Jpn J Ophthalmol. 1997 Sep 1;41(5):324–7.

557. Gregory-Roberts EM, Mateo C, Corcóstegui B, Schiff WM, Chang LK, Quiroz-Mercado H, et al. Optic disk pit morphology and retinal detachment: optical coherence tomography with intraoperative correlation. Retina Phila Pa. 2013 Feb;33(2):363–70.

558. Imamura Y, Iida T, Maruko I, Zweifel SA, Spaide RF. Enhanced depth imaging optical coherence tomography of the sclera in dome-shaped macula. Am J Ophthalmol. 2011 Feb;151(2):297–302.

559. Polunina AA, Todorova MG, Palmowski-Wolfe AM. Function and morphology in macular retinoschisis associated with optic disc pit in a child before and after its spontaneous resolution. Doc Ophthalmol Adv Ophthalmol. 2012 Apr;124(2):149–55.

560. Georgalas I, Kouri A, Ladas I, Gotzaridis E. Optic disc pit maculopathy treated with vitrectomy, internal limiting membrane peeling, and air in a 5-year-old boy. Can J Ophthalmol J Can Ophtalmol. 2010 Apr;45(2):189–91.

561. Kalogeropoulos D, Ch'ng SW, Lee R, Elaraoud I, Felicida V, Purohit M, et al. Optic Disc Pit Maculopathy - Case Series, Clinical Approach, and Management. Middle East Afr J Ophthalmol. 2020 Mar;27(1):34–9.

562. Lorusso M, Zito R, Micelli Ferrari L, Nikolopoulou E, Cicinelli MV, Borrelli E, et al. Spontaneous resolution of optic pit maculopathy: an OCT report. Ther Adv Ophthalmol. 2020 Dec;12:2515841420950843.

563. Jain N, Johnson MW. Pathogenesis and treatment of maculopathy associated with cavitary optic disc anomalies. Am J Ophthalmol. 2014 Sep;158(3):423–35.

564. Friberg TR, McLellan TG. Vitreous pulsations, relative hypotony, and retrobulbar cyst associated with a congenital optic pit. Am J Ophthalmol. 1992 Dec 15;114(6):767–9.

565. Maertz J, Kolb JP, Klein T, Mohler KJ, Eibl M, Wieser W, et al. Combined in-depth, 3D, en face imaging of the optic disc, optic disc pits and optic disc pit maculopathy using swept-source megahertz OCT at 1050 nm. Graefes Arch Clin Exp Ophthalmol Albrecht Von Graefes Arch Klin Exp Ophthalmol. 2018 Feb;256(2):289–98.

566. Cañete Campos C, Gili Manzanaro P, Yangüela Rodilla J, Martín Rodrigo JC. Retinal detachment associated with Morning Glory syndrome. Arch Soc Esp Oftalmol Engl Ed. 2011 Sep 1;86(9):295–9.

567. Chang S, Gregory-Roberts E, Chen R. Retinal detachment associated with optic disc colobomas and morning glory syndrome. Eye. 2012 Apr;26(4):494–500.

568. Halbertsma KTA. Crater-Like Hole and Coloboma of the Disc Associated with Changes at the Macula. Br J Ophthalmol. 1927 Jan 1;11(1):11–7.

569. Ho TC, Tsai PC, Chen MS, Lin LLK. Optical coherence tomography in the detection of retinal break and management of retinal detachment in morning glory syndrome. Acta Ophthalmol Scand. 2006 Apr;84(2):225–7.

570. Pandita A, Guest SJ. Sectorial retinoschisis associated with field defect in a patient with tilted discs. Clin Experiment Ophthalmol. 2010;38(3):317–20.

571. Ruiz-Medrano J, Flores-Moreno I, Montero JA, Ruiz-Moreno JM. Intercalary membrane as the inner wall overlying optic and chorio-retinal colobomas. Deep penetration Swept Source-OCT study. Indian J Ophthalmol. 2018 Jul;66(7):1027–30.

572. Abe RY, Iguma CI, Wen LC. A hybrid coloboma and optic disc pit associated with macular retinoschisis. BMC Ophthalmol. 2019 Nov 4;19(1):212.

573. Jain S, Kumar V, Salunkhe N, Tewari R, Chandra P, Kumar A. Swept-Source OCT Analysis of the Margin of Choroidal Coloboma: New Insights. Ophthalmol Retina. 2020 Jan 1;4(1):92–9.

574. Kindler P. Morning glory syndrome: unusual congenital optic disk anomaly. Am J Ophthalmol. 1970 Mar;69(3):376–84.

575. Traboulsi EI. Morning glory disk anomaly—more than meets the eye. J Am Assoc Pediatr Ophthalmol Strabismus JAAPOS. 2009 Aug 1;13(4):333–4.

576. Traboulsi EI, O'Neill JF. The spectrum in the morphology of the so-called 'morning glory disc anomaly'. J Pediatr Ophthalmol Strabismus. 1988 Apr;25(2):93–8.

577. Hubschman JP, Reddy S, Kaines A, Law S. Nasal Retinoschisis Associated with Glaucoma. Ophthalmic Surg Lasers Imaging Off J Int Soc Imaging Eye. 2010 Mar 9;1–4.

578. Zhao M, Li X. Macular retinoschisis associated with normal tension glaucoma. Graefes Arch Clin Exp Ophthalmol Albrecht Von Graefes Arch Klin Exp Ophthalmol. 2011 Aug;249(8):1255–8.

579. Lee EJ, Kim TW, Kim M, Choi YJ. Peripapillary Retinoschisis in Glaucomatous Eyes. PLoS ONE [Internet]. 2014 Feb 28 [cited 2020 Jun 10];9(2). Available from: https://www.ncbi.nlm.nih.gov/pmc/articles/PMC3938601/

580. van der Schoot J, Vermeer KA, Lemij HG. Transient Peripapillary Retinoschisis in Glaucomatous Eyes. J Ophthalmol. 2017 Jan 12;2017:e1536030.

581. Govetto A, Su D, Farajzadeh M, Megerdichian A, Platner E, Ducournau Y, et al. Microcystoid Macular Changes in Association With Idiopathic Epiretinal Membranes in Eyes With and Without Glaucoma: Clinical Insights. Am J Ophthalmol. 2017 Sep;181:156–65.

582. Fortune B, Ma KN, Gardiner SK, Demirel S, Mansberger SL. Peripapillary Retinoschisis in Glaucoma: Association With Progression and OCT Signs of Müller Cell Involvement. Invest Ophthalmol Vis Sci. 2018 Jun;59(7):2818–27.

583. Kahook MY, Noecker RJ, Ishikawa H, Wollstein G, Kagemann L, Wojtkowski M, et al. Peripapillary schisis in glaucoma patients with narrow angles and increased intraocular pressure. Am J Ophthalmol. 2007 Apr;143(4):697–9.

584. Moreno-López M, González-López JJ, Jarrín E, Bertrand J. Retinoschisis and macular detachment associated with acquired enlarged optic disc cup. Clin Ophthalmol Auckl NZ. 2012;6:433–6.

585. Grewal DS, Merlau DJ, Giri P, Munk MR, Fawzi AA, Jampol LM, et al. Peripapillary retinal splitting visualized on OCT in glaucoma and glaucoma suspect patients. PLoS ONE [Internet]. 2017 Aug 23 [cited 2021 Jun 4];12(8). Available from: https://www.ncbi.nlm.nih.gov/pmc/articles/PMC5568282/

586. Lee JH, Park HYL, Baek J, Lee WK. Alterations of the Lamina Cribrosa Are Associated with Peripapillary Retinoschisis in Glaucoma and Pachychoroid Spectrum Disease. Ophthalmology. 2016 Oct;123(10):2066–76.

587. Nagesha CK, Ganne P. Occult Optic Disc Pit Maculopathy in a Glaucomatous Disc. Middle East Afr J Ophthalmol. 2017;24(3):165–6.

588. Nishijima R, Ogawa S, Nishijima E, Itoh Y, Yoshikawa K, Nakano T. Factors Determining the Morphology of Peripapillary Retinoschisis. Clin Ophthalmol Auckl NZ. 2021;15:1293–300.

589. Yoshitake T, Nakanishi H, Setoguchi Y, Kuroda K, Amemiya K, Taniguchi M, et al. Bilateral papillomacular retinoschisis and macular detachment accompanied by focal lamina cribrosa defect in glaucomatous eyes. Jpn J Ophthalmol. 2014 Sep 1;58(5):435–42.

590. Ornek N, Büyüktortop N, Ornek K. Peripapillary and macular retinoschisis in a patient with pseudoexfoliation glaucoma. BMJ Case Rep. 2013 May;2013(may31 1):bcr2013009469–bcr2013009469.

591. Park SC, De Moraes CGV, Teng CC, Tello C, Liebmann JM, Ritch R. Enhanced depth imaging optical coherence tomography of deep optic nerve complex structures in glaucoma. Ophthalmology. 2012 Jan;119(1):3–9.

592. You JY, Park SC, Su D, Teng CC, Liebmann JM, Ritch R. Focal lamina cribrosa defects associated with glaucomatous rim thinning and acquired pits. JAMA Ophthalmol. 2013 Mar;131(3):314–20.

593. Dhingra N, Manoharan R, Gill S, Nagar M. Peripapillary schisis in open-angle glaucoma. Eye Lond Engl. 2017 Mar;31(3):499–502.

594. Farjad H, Besada E, Frauens BJ. Peripapillary Schisis with Serous Detachment in Advanced Glaucoma. Optom Vis Sci. 2010 Mar;87(3):E205.

595. Inoue M, Itoh Y, Rii T, Kita Y, Hirota K, Kunita D, et al. Spontaneous resolution of peripapillary retinoschisis associated with glaucomatous optic neuropathy. Acta Ophthalmol (Copenh). 2015 Jun;93(4):e317-318.

596. Mavrikakis E, Lam WC. Macular schisis and detachment secondary to large optic nerve head cup: a newly recognized syndrome amenable to vitrectomy. Acta Ophthalmol (Copenh). 2011;89(1):95–6.

597. Takashina S, Saito W, Noda K, Katai M, Ishida S. Membrane tissue on the optic disc may cause macular schisis associated with a glaucomatous optic disc without optic disc pits. Clin Ophthalmol Auckl NZ. 2013;7:883–7.

598. Zumbro DS, Jampol LM, Folk JC, Olivier MMG, Anderson-Nelson S. Macular schisis and detachment associated with presumed acquired enlarged optic nerve head cups. Am J Ophthalmol. 2007 Jul;144(1):70–4.

599. Orazbekov L, Yasukawa T, Hirano Y, Ogura S, Usui H, Nozaki M, et al. Vitrectomy without gas tamponade for macular retinoschisis associated with normal-tension glaucoma. Ophthalmic Surg Lasers Imaging Retina. 2015 Jan;46(1):107–10.

600. Patel S, Ling J, Kim SJ, Schey KL, Rose K, Kuchtey RW. Proteomic Analysis of Macular Fluid Associated With Advanced Glaucomatous Excavation. JAMA Ophthalmol. 2016 Jan;134(1):108–10.

601. Hollander DA. Macular Schisis Detachment Associated With Angle-closure Glaucoma. Arch Ophthalmol. 2005 Feb 1;123(2):270.

602. Woo R, Akil H, Koulisis N, Olmos de Koo LC, Tan JCH. Sustained Resolution of Macular Retinoschisis After Trabeculectomy in a Patient With Progressive Glaucoma. J Glaucoma. 2017 Jun 1;26(6):e180–6.

603. Zimmerman LE, De Venecia G, Hamasaki DI. Pathology of the optic nerve in experimental acute glaucoma. Invest Ophthalmol. 1967 Apr;6(2):109–25.

604. Chen FK, Acheson JF, Franks WA, Da Cruz L. Microperimetry evidence of functional improvement after vitrectomy for optic disc pit-related intraretinal fluid without serous detachment. Clin Experiment Ophthalmol. 2011 Oct;39(7):707–10.

605. Song IS, Shin JW, Shin YW, Uhm KB. Optic disc pit with peripapillary retinoschisis presenting as a localized retinal nerve fiber layer defect. Korean J Ophthalmol KJO. 2011 Dec;25(6):455–8.

606. Iglicki M, Busch C, Loewenstein A, Fung AT, Invernizzi A, Mariussi M, et al. Underdiagnosed optic disk pit maculopathy: Spectral Domain Optical Coherence Tomography Features For Accurate Diagnosis. Retina Phila Pa. 2019 Nov;39(11):2161–6.

607. Phasukkijwatana N, Freund KB, Dolz-Marco R, Al-Sheikh M, Keane PA, Egan CA, et al. Peripapillary pachychoroid syndrome. Retina. 2018 Sep;38(9):1652–67.

608. Yzer S, Pothof A, Martinez J. Treatment of Peripapillary Pachychoroid Syndrome. Invest Ophthalmol Vis Sci. 2020 Jun 10;61(7):5255.

609. Govetto A, Sarraf D, Scialdone A. “hide and seek” neurosensory retinal detachments in peripapillary pachychoroid syndrome associated with pulmonary arterial hypertension. Retin Cases Brief Rep [Internet]. 2021 Sep 19 [cited 2021 Sep 23]; Available from: http://journals.lww.com/retinalcases/Abstract/9000/_HIDE_AND_SEEK__NEUROSENSORY_RETINAL_DETACHMENTS.98635.aspx

610. Brown GC. Congenital pits of the optic nerve head. Arch Ophthamol. 1979 Jul;97(7):1341–4.

611. Theodossiadis GP. Visual acuity in patients with optic nerve pit. Ophthalmology. 1991 May;98(5):563.

612. Brown GC. Congenital anomalies of the optic disc [Internet]. Grune & Stratton, Incorporated; 1983. Available from: http://books.google.co.uk/books?id=s6lsAAAAMAAJ&q=intitle:Congenital+Anomalies+of+the+Optic+Disc&dq=intitle:Congenital+Anomalies+of+the+Optic+Disc&hl=&cd=1&source=gbs_api

613. Theodossiadis G. Evolution of congenital pit of the optic disk with macular detachment in photocoagulated and nonphotocoagulated eyes. Am J Ophthalmol. 1977 Nov;84(5):620–31.

614. Garcia-Arumi J, Corcóstegui IA, Navarro R, Zapata MA, Berrocal MH. Vitreoretinal surgery without schisis cavity excision for the management of juvenile X linked retinoschisis. Br J Ophthalmol Lond. 2008 Nov;92(11):1558.

615. Hirakata A, Hida T, Ogasawara A, Iizuka N. Multilayered retinoschisis associated with optic disc pit. Jpn J Ophthalmol. 2005 Sep;49(5):414–6.

616. Lalwani GA, Punjabi OS, Flynn HW, Knighton RW, Puliafito CA. Documentation of optic nerve pit with macular schisis-like cavity by spectral domain OCT. Ophthalmic Surg Lasers Imaging Off J Int Soc Imaging Eye. 2007 May;38(3):262–4.

617. Teke MY, Elgin U, Ozdal P, Ozturk F. Autofluorescence and optical coherence tomography findings in optic disc pit-associated maculopathy: case series. Int Ophthalmol. 2011 Dec;31(6):485–91.

618. Rutledge BK, Puliafito CA, Duker JS, Hee MR, Cox MS. Optical coherence tomography of macular lesions associated with optic nerve head pits. Ophthalmology. 1996 Jul;103(7):1047–53.

619. Lincoff H, Schiff W, Krivoy D, Ritch R. Optic coherence tomography of optic disk pit maculopathy. Am J Ophthalmol. 1996 Aug;122(2):264–6.

620. Skaat A, Moroz I, Moisseiev J. Macular detachment associated with an optic pit: optical coherence tomography patterns and surgical outcomes. Eur J Ophthalmol. 2013 May;23(3):385–93.

621. Schneider M, Geitzenauer W, Ahlers C, Golbaz I, Schmidt-Erfurth U. Three-dimensional imaging of an optic disk pit using high resolution optical coherence tomography. Eur J Ophthalmol. 2009 Apr;19(2):321–3.

622. Moon SJ, Kim JE, Spaide RF. Optic pit maculopathy without inner retinal schisis cavity. Retina Phila Pa. 2006 Jan;26(1):113–6.

623. Annesley W, Brown G, Bolling J, Goldberg R, Fischer D. Treatment of retinal detachment with congenital optic pit by krypton laser photocoagulation. Graefes Arch Clin Exp Ophthalmol Albrecht Von Graefes Arch Klin Exp Ophthalmol. 1987;225(5):311–4.

624. Cox MS, Witherspoon CD, Morris RE, Flynn HW. Evolving techniques in the treatment of macular detachment caused by optic nerve pits. OPHTHA. 1988 Jul;95(7):889–96.

625. Theodossiadis G. Treatment of retinal detachment with congenital optic pit by krypton laser photocoagulation. Graefes Arch Clin Exp Ophthalmol Albrecht Von Graefes Arch Klin Exp Ophthalmol. 1988;226(3):299.

626. Akiyama H, Shimoda Y, Fukuchi M, Kashima T, Mayuzumi H, Shinohara Y, et al. Intravitreal gas injection without vitrectomy for macular detachment associated with an optic disk pit: Retina. 2014 Feb;34(2):222–7.

627. Lei L, Li T, Ding X, Ma W, Zhu X, Atik A, et al. Gas tamponade combined with laser photocoagulation therapy for congenital optic disc pit maculopathy. Eye Lond Engl. 2015 Jan;29(1):106–14.

628. Lincoff H, Kreissig I. Optical coherence tomography of pneumatic displacement of optic disc pit maculopathy. Br J Ophthalmol. 1998 Apr;82(4):367–72.

629. Georgopoulos GT, Theodossiadis PG, Kollia AC, Vergados J, Patsea EE, Theodossiadis GP. Visual field improvement after treatment of optic disk pit maculopathy with the macular buckling procedure. Retina Phila Pa. 1999;19(5):370–7.

630. Theodossiadis GP, Theodossiadis PG. The macular buckling technique in the treatment of optic disk pit maculopathy. Semin Ophthalmol. 2000 Jun;15(2):108–15.

631. Theodossiadis GP, Grigoropoulos VG, Liarakos VS, Rouvas A, Emfietzoglou I, Theodossiadis PG. Restoration of the photoreceptor layer and improvement of visual acuity in successfully treated optic disc pit maculopathy: a long follow-up study by optical coherence tomography. Graefes Arch Clin Exp Ophthalmol. 2012 Jan;250(7):971–9.

632. Theodossiadis GP, Chatziralli IP, Theodossiadis PG. Macular buckling in optic disc pit maculopathy in association with the origin of macular elevation: 13-year mean postoperative results. Eur J Ophthalmol. 2015 Jun;25(3):241–8.

633. Rizzo S, Belting C, Genovesi-Ebert F, di Bartolo E, Cresti F, Cinelli L, et al. Optic disc pit maculopathy: the value of small-gauge vitrectomy, peeling, laser treatment, and gas tamponade. Eur J Ophthalmol. 2012 Jul;22(4):620–5.

634. Shukla D, Kalliath J, Tandon M, Vijayakumar B. Vitrectomy for optic disk pit with macular schisis and outer retinal dehiscence. Retina Phila Pa. 2012 Jul;32(7):1337–42.

635. Avci R, Yilmaz S, Inan UU, Kaderli B, Kurt M, Yalcinbayir O, et al. Long-term outcomes of pars plana vitrectomy without internal limiting membrane peeling for optic disc pit maculopathy. Eye Lond Engl. 2013 Dec;27(12):1359–67.

636. Georgalas I, Papaconstantinou D, Koutsandrea C. Optic disc pit maculopathy: the value of small-gauge vitrectomy, peeling, laser treatment, and gas tamponade. Eur J Ophthalmol. 2013 Mar;23(2):275–275.

637. Sanghi G, Padhi TR, Warkad VU, Vazirani J, Gupta V, Dogra MR, et al. Optical coherence tomography findings and retinal changes after vitrectomy for optic disc pit maculopathy. Indian J Ophthalmol. 2014 Mar;62(3):287–90.

638. Teke MY, Citirik M. 23 gauge vitrectomy, endolaser, and gas tamponade versus vitrectomy alone for serous macular detachment associated with optic disc pit. Am J Ophthalmol. 2015 Oct;160(4):779-85.e2.

639. Talli PM, Fantaguzzi PM, Bendo E, Pazzaglia A. Vitrectomy without laser treatment for macular serous detachment associated with optic disc pit: long-term outcomes. Eur J Ophthalmol. 2016 Mar;26(2):182–7.

640. Avci R, Kapran Z, Ozdek Ş, Teke MY, Oz O, Guven D, et al. Multicenter study of pars plana vitrectomy for optic disc pit maculopathy: MACPIT study. Eye Lond Engl. 2017 Sep;31(9):1266–73.

641. Chatziralli I, Theodossiadis G, Brouzas D, Theodossiadis P. Incidence and evolution of subretinal precipitates in optic disc pit maculopathy. Eur J Ophthalmol. 2017 Jun;27(6):0–773.

642. Chatziralli I, Theodossiadis P, Theodossiadis GP. Optic disk pit maculopathy: current management strategies. Clin Ophthalmol Auckl. 2018;12:1417–22.

643. Spaide RF, Fisher Y, Ober M, Stoller G. Surgical hypothesis: inner retinal fenestration as a treatment for optic disc pit maculopathy. Retina Phila Pa. 2006 Jan;26(1):89–91.

644. Ooto S, Mittra RA, Ridley ME, Spaide RF. Vitrectomy with inner retinal fenestration for optic disc pit maculopathy. Ophthalmology. 2014 Sep;121(9):1727–33.

645. Karacorlu M, Sayman Muslubas I, Hocaoglu M, Ozdemir H, Arf S, Uysal O. Long-term outcomes of radial optic neurotomy for management of optic disk pit maculopathy. Retina Phila Pa. 2016 Dec;36(12):2419–27.

646. Ravani R, Kumar A, Karthikeya R, Kumar P, Gupta Y, Mutha V, et al. Comparison of inverted ILM-Stuffing technique and ILM peeling alone for optic disc pit-associated maculopathy: Long-term results. Ophthalmic Surg Lasers Imaging Retina. 2018 Dec;49(12):e226–32.

647. Zacharias LC, Nascimento MVD do, Ghosn NB, Ciongoli MR, Preti RC, Monteiro MLR. Inverted internal limiting membrane flap for the management of optic disc pit maculopathy. Arq Bras Oftalmol. 2019 Oct 31;

648. de Oliveira PRC, Berger AR, Chow DR. Use of Evicel Fibrin Sealant in Optic Disc Pit-Associated Macular Detachment. Ophthalmic Surg Lasers Imaging Retina. 2017 Apr 1;48(4):358–63.

649. Ozdek S, Ozdemir HB. A new technique with autologous fibrin for the treatment of persistent optic pit maculopathy. Retin Cases Brief Rep. 2017 Winter;11(1):75–8.

650. Almeida DRP, Chin EK, Arjmand P, Velez G, Evans LP, Mahajan VB. Fibrin Glue and Internal Limiting Membrane Abrasion for Optic Disc Pit Maculopathy. Ophthalmic Surg Lasers Imaging Retina. 2018 01;49(12):e271–7.

651. Babu N, Baliga G, Kohli P, Ramasamy K. Management of double optic disc pit complicated by maculopathy. Indian J Ophthalmol. 2020 Apr;68(4):663–5.

652. Muftuoglu IK, Tokuc EO, Karabas VL. Management of optic disc pit-associated maculopathy: A case series from a tertiary referral center. Eur J Ophthalmol. 2021 Jun 16;11206721211023728.

653. D'souza P, Verghese S, Ranjan R, Kumarswamy K, Saravanan VR, Manayath GJ, et al. Optic Disc Pit Maculopathy: One-Year Outcomes of Pars Plana Vitrectomy with Foveal Sparing Inverted Internal Limiting Membrane Flap. Cureus. 2021 Mar 23;13(3):e14057.

654. Kohli GM, Shenoy P, Khanna A, Bhatia P, Tripathi S, Thacker A, et al. Resolution Pattern and Predictors of Outcome for Optic Disc Pit - Maculopathy Following Vitrectomy: An Optical Coherence Tomography Based Morphometric Analysis. Semin Ophthalmol. 2021 Mar 30;1–6.

655. Rubinstein K, Ali M. Complications of optic disc pits. Trans Ophthalmol Soc U K. 1978;98(2):195–200.

656. Brown GC, Shields JA. Cilioretinal arteries and retinal arterial occlusion. Arch Ophthamol. 1979 Jan;97(1):84–92.

657. Justice J, Lehmann RP. Cilioretinal arteries. A study based on review of stereo fundus photographs and fluorescein angiographic findings. Arch Ophthamol. 1976 Aug;94(8):1355–8.

658. Lorentzen SE. Incidence of cilioretinal arteries. Acta Ophthalmol (Copenh). 1970;48(3):518–24.

659. Meng L, Zhao X, Zhang W, Wang D, Chen Y. The characteristics of optic disc pit maculopathy and the efficacy of vitrectomy: a systematic review and meta-analysis. Acta Ophthalmol (Copenh) [Internet]. 2021 [cited 2021 Jul 4];n/a(n/a). Available from: http://onlinelibrary.wiley.com/doi/abs/10.1111/aos.14730

660. Babu N, Kohli P, Ramasamy K. Comparison of various surgical techniques for optic disc pit maculopathy: vitrectomy with internal limiting membrane (ILM) peeling alone versus inverted ILM flap 'plug' versus autologous scleral 'plug'. Br J Ophthalmol. 2020 Nov 1;104(11):1567–73.

661. Li D, Kishi S, Itakura H, Ikeda F, Akiyama H. Posterior Precortical Vitreous Pockets and Connecting Channels in Children on Swept-Source Optical Coherence Tomography. Invest Ophthalmol Vis Sci. 2014 Apr 15;55(4):2412–6.

662. Uzel AGT, Gelisken F, Bartz-Schmidt KU, Neubauer J. Natural Course of Optic Disc Pit Maculopathy: An Optical Coherence Tomography Study. Ophthalmologica. 2022;245(6):563–9.

663. Vedantham V, Ramasamy K. Spontaneous improvement of serous maculopathy associated with congenital optic disc pit: an OCT study. Eye Lond Engl. 2004 Sep;19(5):596–9.

664. Tripathy K. Spontaneous resolution of optic disc pit maculopathy. Turk J Ophthalmol. 2017 Jun;47(3):184–5.

665. Patton N, Aslam SA, Aylward GW. Visual improvement after long-standing central serous macular detachment associated with an optic disc pit. Graefes Arch Clin Exp Ophthalmol. 2008 Aug;246(8):1083–5.

666. Parikakis EA, Chatziralli IP, Peponis VG, Karagiannis D, Stratos A, Tsiotra VA, et al. Spontaneous resolution of long-standing macular detachment due to optic disc pit with significant visual improvement. Case Rep Ophthalmol. 2014 Jan;5(1):104–10.

667. Chatziralli I, Theodossiadis G, Panagiotidis D, Emfietzoglou I, Grigoropoulos V, Theodossiadis P. Long-term changes of macular thickness after pars plana vitrectomy in optic disc pit maculopathy: A spectral-domain optical coherence tomography study. Semin Ophthalmol. 2017;32(3):302–8.

668. Shukla D, Leila M. Surgical management of optic pit maculopathy: controversies and caveats. Expert Rev Ophthalmol. 2017 Jan 2;12(1):3–9.

669. Makdoumi K, Crafoord S. A prospective long-term follow-up study of optic disc pit maculopathy treated with pars plana vitrectomy, drainage of subretinal fluid and peeling of internal limiting membrane. Acta Ophthalmol (Copenh). 2020;98(8):822–7.

670. Oli A, Balakrishnan D. Treatment outcomes of optic disc pit maculopathy over two decades. Ther Adv Ophthalmol. 2021 Jan 1;13:25158414211027716.

671. Ober MD, Freund KB, Shah M, Ahmed S, Mahmoud TH, Aaberg TM, et al. Stellate nonhereditary idiopathic foveomacular retinoschisis. Ophthalmology. 2014 Jul;121(7):1406–13.

672. Weiss SJ, Adam MK, Hsu J. En face optical coherence tomography of stellate nonhereditary idiopathic foveomacular retinoschisis. JAMA Ophthalmol. 2017 Nov;135(11):e174280–e174280.

673. Fragiotta S, Leong BCS, Kaden TR, Bass SJ, Sherman J, Yannuzzi LA, et al. A proposed mechanism influencing structural patterns in X-linked retinoschisis and stellate nonhereditary idiopathic foveomacular retinoschisis. Eye Lond Engl. 2019 May;33(5):724–8.

674. Ahmed D, Stattin M, Glittenberg C, Krebs I, Ansari-Shahrezaei S. Stellate nonhereditary idiopathic foveomacular retinoschisis accompanied by contralateral peripheral retinoschisis. Retin Cases Brief Rep. 2019;13(2):135–40.

675. Mandell JB, Kim AY, Shahidzadeh A, Ameri H, Puliafito CA, Moshfeghi AA. Widefield OCT findings of a patient with stellate nonhereditary idiopathic foveomacular retinoschisis. Ophthalmic Surg Lasers Imaging Retina. 2016 Aug;47(8):774–7.

676. Valikodath NG, Scripsema NK, Lim JI. Bilateral Macular Schisis in a Woman. JAMA Ophthalmol. 2021 Aug 1;139(8):906–7.

677. Montano M, Alfaro DVI, Quiroz-Reyes MA, Lima-Gómez V, Bonilla LA, Chew-Bonilla A, et al. Stellate unilateral nonhereditary idiopathic foveomacular retinoschisis: a multimodal imaging analysis and case report. Retin Cases Brief Rep [Internet]. 2020 Jul 17 [cited 2020 Aug 1];Publish Ahead of Print. Available from: http://journals.lww.com/retinalcases/Abstract/9000/stellate_unilateral_nonhereditary_idiopathic.98571.aspx

678. Panos GD, Zambarakji H, McKechnie CJ, Dadoukis P. Stellate Nonhereditary Idiopathic Foveomacular Retinoschisis in a Female Patient: Case Report and Brief Literature Review. Klin Monatsblätter Für Augenheilkd. 2020 Apr;237(04):474–6.

679. Javaheri M, Sadda SR. ATYPICAL peripapillary inner retinoschisis in stellate nonhereditary idiopathic foveomacular retinoschisis. Retin Cases Brief Rep. 2018;12 Suppl 1:S92–7.

680. Machado Nogueira T, de Souza Costa D, Isenberg J, Rezende FA. Stellate nonhereditary idiopathic foveomacular retinoschisis resolution after vitreomacular adhesion release. Am J Ophthalmol Case Rep. 2021 Jun 19;23:101153.

681. Dolz-Marco R, Kato K, Freund KB, Yannuzzi LA. Unusual case of stellate nonhereditary idiopathic foveomacular retinoschisis. Retin Cases Brief Rep. 2017;11 Suppl 1:S49–53.

682. Haruta M, Yamakawa R. Vitrectomy for macular retinoschisis without a detectable optic disk pit. Retina. 2017 May;37(5):915–20.

683. Maruko I, Morizane Y, Kimura S, Shiode Y, Hosokawa M, Sekiryu T, et al. Clinical characteristics of idiopathic foveomacular retinoschisis. Retina Phila Pa. 2016 Aug;36(8):1486–92.

684. Moraes BRM, A. Ferreira BF, Nogueira TM, Nakashima Y, Júnior HPP, C. Souza E. Vitrectomy for stellate nonhereditary idiopathic foveomacular retinoschisis associated with outer retinal layer defect. Retin Cases Brief Rep [Internet]. 2020 Jul 17 [cited 2020 Aug 1];Publish Ahead of Print. Available from: http://journals.lww.com/retinalcases/Abstract/9000/VITRECTOMY_FOR_STELLATE_NONHEREDITARY_IDIOPATHIC.98608.aspx

685. Ajlan RS, Hammamji KS. Stellate nonhereditary idiopathic foveomacular retinoschisis: response to topical dorzolamide therapy. Retin Cases Brief Rep. 2017 Jun;Publish Ahead of Print:1.

686. Schildroth KR, Mititelu M, Etheridge T, Holman I, Chang JS. Stellate Nonhereditary Idiopathic Foveomacular Retinoschisis: Novel Findings and OCT-Angiography Analysis. Retin Cases Brief Rep [Internet]. 2022 Mar 2 [cited 2022 May 16]; Available from: http://journals.lww.com/retinalcases/Abstract/9000/Stellate_Nonhereditary_Idiopathic_Foveomacular.98455.aspx

687. Lavia C, Mecê P, Nassisi M, Bonnin S, Marie-Louise J, Couturier A, et al. Retinal Capillary Plexus Pattern and Density from Fovea to Periphery Measured in Healthy Eyes with Swept-Source Optical Coherence Tomography Angiography. Sci Rep. 2020 Jan 30;10(1):1474.

688. Campbell JP, Zhang M, Hwang TS, Bailey ST, Wilson DJ, Jia Y, et al. Detailed Vascular Anatomy of the Human Retina by Projection-Resolved Optical Coherence Tomography Angiography. Sci Rep. 2017 Feb 10;7(1):42201.

689. Au A, Sarraf D. Vascular anatomy and its relationship to pathology in retinoschisis. Eye. 2019 May;33(5):693–4.

690. Bartels M. Über die entstehung von netzhautablösungen. Klin Monatsbl Augenheilkd. 1933;(91):437–50.

691. Samuels B, Fuchs A. Clinical Pathology of the Eye: A Practical Treatise of Histopathology. New York: Paul B. Hoeber; 1952.

692. Straatsma BR. Typical and reticular degenerative retinoschisis. Ber Uber Zusammenkunft Dtsch Ophthalmol Ges. 1977;74:123–30.

693. Byer NE. Long-term natural history study of senile retinoschisis with implications for management. Ophtha. 1986 Sep;93(9):1127–37.

694. Straatsma BR, Foss RY. Typical and reticular degenerative retinoschisis. Am J Ophthalmol. 1973 Apr;75(4):551–75.

695. Buch H, Vinding T, Nielsen NV. Prevalence and long-term natural course of retinoschisis among elderly individuals: the Copenhagen City Eye Study. Ophthalmology. 2007 Apr;114(4):751–5.

696. Straatsma BR. Clinical features of degenerative retinoschisis. Aust J Ophthalmol. 1980 Aug;8(3):201–6.

697. Shea M, Schepens CL, Von Pirquet SR. Retionoschisis. I. Senile type: a clinical report of one hundred seven cases. Arch Ophthalmol Chic Ill 1960. 1960 Jan;63:1–9.

698. Engstrom R, Glasgow BJ, Foos R, Straatsma B. Chapter 26: Degenerative Diseases of the Peripheral Retina. In: Duane's Ophthalmology. 2006.

699. Yanoff M, Sassani, Joseph William. Chapter 11: Neural (Sensory) Retina. In: Ocular Pathology. 7th ed. Edinburgh: Mosby,Elsevier; 2009. p. 393–480.

700. O'Malley PF, Allen RA. Peripheral cystoid degeneration of the retina. Incidence and distribution in 1,000 autopsy eyes. Arch Ophthalmol Chic Ill 1960. 1967 Jun;77(6):769–76.

701. Foos R, Spencer L, Straatsma B. Trophic degenerations of the peripheral retina. In: Transactions of the New Orleans Academy of Ophthalmology: Symposium on Retina and Retinal Surgery. St Louis: CV Mosby; 1969. p. 90–102.

702. Foos RY, Allen RA. Retinal tears and lesser lesions of the peripheral retina in autopsy eyes. Am J Ophthalmol. 1967 Sep;64(3):Suppl:643-655.

703. Foos RY, Feman SS. Reticular Cystoid Degeneration of the Peripheral Retina. Am J Ophthalmol. 1970 Mar 1;69(3):392–403.

704. Clinical Atlas of Peripheral Retinal Disorders | Keith M. Zinn | Springer [Internet]. [cited 2020 Jan 11]. Available from: https://www.springer.com/gb/book/9781461237204#otherversion=9781461283195

705. Foos RY. Senile retinoschisis. Relationship to cystoid degeneration. Trans - Am Acad Ophthalmol Otolaryngol Am Acad Ophthalmol Otolaryngol. 1970 Jan;74(1):33–51.

706. Kamppeter BA, Jonas JB. Optical coherence tomography of a peripheral retinal schisis with an outer retinal layer break. Acta Ophthalmol Scand. 2004 Oct;82(5):574–5.

707. Landa G, Shirkey BL, Garcia PMT, Milman T, Garcia JPS, Rosen RB. Acquired Senile Retinoschisis of the Peripheral Retina Imaged by Spectral Domain Optical Coherence Tomography: A Case Report. Eur J Ophthalmol. 2010 Nov 1;20(6):1079–81.

708. Yeoh J, Rahman W, Chen FK, da Cruz L. Use of spectral-domain optical coherence tomography to differentiate acquired retinoschisis from retinal detachment in difficult cases. Retina Phila Pa. 2012 Sep;32(8):1574–80.

709. Stehouwer M, Tan SH, Leeuwen TG van, Verbraak FD. Senile retinoschisis versus retinal detachment, the additional value of peripheral retinal OCT scans (SL SCAN-1, Topcon). Acta Ophthalmol (Copenh). 2014;92(3):221–7.

710. Choudhry N, Golding J, Manry MW, Rao RC. Ultra-Widefield Steering-Based Spectral-Domain Optical Coherence Tomography Imaging of the Retinal Periphery. Ophthalmology. 2016 Jun 1;123(6):1368–74.

711. Eibenberger K, Sacu S, Rezar-Dreindl S, Pöcksteiner J, Georgopoulos M, Schmidt-Erfurth U. Monitoring retinoschisis and non-acute retinal detachment by optical coherence tomography: morphologic aspects and clinical impact. Acta Ophthalmol (Copenh). 2017 Nov;95(7):710–6.

712. Thanos A, Todorich B, Pasadhika S, Khundkar T, Xu D, Jain A, et al. Degenerative Peripheral Retinoschisis: Observations From Ultra-Widefield Fundus Imaging. Ophthalmic Surg Lasers Imaging Retina. 2019 Sep 1;50(9):557–64.

713. Joshi MM, Drenser K, Hartzer M, Dailey W, Capone A, Trese MT. Intraschisis cavity fluid composition in congenital X-linked retinoschisis. Retina Phila Pa. 2006 Sep;26(7 Suppl):S57-60.

714. Rao P, Robinson J, Yonekawa Y, Thomas BJ, Drenser KA, Trese MT, et al. WIDE-FIELD IMAGING OF NONEXUDATIVE AND EXUDATIVE CONGENITAL X-LINKED RETINOSCHISIS: Retina. 2016 Jun;36(6):1093–100.

715. Yassur Y, Feldberg R, Axer-Siegel R, Silverston B, Manor R, Ben-Sira I. Argon laser treatment of senile retinoschisis. Br J Ophthalmol. 1983 Jun;67(6):381–4.

716. Dhrami-Gavazi E, Schiff WM, Barile GR. Nanophthalmos and Acquired Retinoschisis. Am J Ophthalmol. 2009 Jan 1;147(1):108-110.e1.

717. Byer NE. The natural history of senile retinoschisis. Mod Probl Ophthalmol. 1977;18:304–11.

718. Dobbie JG. Cryotherapy in the management of senile retinoschisis. Trans - Am Acad Ophthalmol Otolaryngol Am Acad Ophthalmol Otolaryngol. 1969 Nov;73(6):1047–60.

719. Lincoff H, Kreissig I. The misdiagnosis of retinoschisis. Acta Ophthalmol (Copenh). 2012 Aug;90(5):492–4.

720. Chapman-Davies A, Kiel J. Degenerative retinoschisis threatening central vision. Clin Exp Optom. 2000 Mar;83(2):65–70.

721. Weng CY, Flynn HW. Retinal imaging in perimacular degenerative retinoschisis. Ophthalmic Surg Lasers Imaging Retina. 2014 Jan;45(1):79–82.

722. Ambler JS, Gass JD, Gutman FA. Symptomatic retinoschisis-detachment involving the macula. Am J Ophthalmol. 1991 Jul;112(1):8–14.

723. Brockhurst R. Discussion of: Dobbie JG. Cryotherapy in the management of senile retinoschisis. Trans Am Acad Ophthalmol Otolaryngol. 1969;73:1060.

724. Hagler W, Woldoff H. Retinal detachment in relation to senile retinoschisis. Trans Am Acad Ophthalmol Otolaryngol. 1973;77:99–113.

725. Bloch E, Flores-Sánchez B, Georgiadis O, Sundaram V, Saihan Z, Mahroo OA, et al. An association between stellate nonhereditary idiopathic foveomacular

retinoschisis, peripheral retinoschisis, and posterior hyaloid attachment. Retina. 2021 Nov;41(11):2361–9.

726. Hayashi K, Sato T, Manabe SI, Hirata A. Sex-Related Differences in the Progression of Posterior Vitreous Detachment with Age. Ophthalmol Retina. 2019;3(3):237–43.

727. Engstrom R, Glasgow B, Foos R, Straatsma B. Chapter 26. Degenerative Diseases of the Peripheral Retina. In: Tasman W, Jaeger E, editors. Duane's Ophthalmology [Internet]. Philadelphia, PA: Lippincott Williams & Wilkins; 2001 [cited 2021 Jul 6]. Available from: http://www.oculist.net/downaton502/prof/ebook/duanes/pages/v3/v3c026.html

728. Sun Z, Gao H, Wang M, Chang Q, Xu G. Rapid progression of foveomacular retinoschisis in young myopics. Retina Phila Pa. 2019 Jul;39(7):1278–88.

729. Yang J, Chen Y. Vitreoretinal Traction with Vitreoschisis Using OCT. Ophthalmol Retina. 2019 Nov;3(11):961.

730. Hwang ES, Kraker JA, Griffin KJ, Sebag J, Weinberg DV, Kim JE. Accuracy of Spectral-Domain OCT of the Macula for Detection of Complete Posterior Vitreous Detachment. Ophthalmol Retina. 2020 Feb 1;4(2):148–53.

731. Grewal PS, Oloumi F, Rubin U, Tennant MTS. Deep learning in ophthalmology: a review. Can J Ophthalmol J Can Ophtalmol. 2018 Aug;53(4):309–13.

732. Ting DSW, Pasquale LR, Peng L, Campbell JP, Lee AY, Raman R, et al. Artificial intelligence and deep learning in ophthalmology. Br J Ophthalmol. 2019 Feb 1;103(2):167–75.

733. Schmidt-Erfurth U, Reiter GS, Riedl S, Seeböck P, Vogl WD, Blodi BA, et al. AI-based monitoring of retinal fluid in disease activity and under therapy. Prog Retin Eye Res. 2021 Jun 22;100972.

734. Ajaz A, Kumar H, Kumar D. A review of methods for automatic detection of macular edema. Biomed Signal Process Control. 2021 Aug 1;69:102858.

735. Rohrschneider K, Bültmann S, Springer C. Use of fundus perimetry (microperimetry) to quantify macular sensitivity. Prog Retin Eye Res. 2008 Sep 1;27(5):536–48.

736. Bagdonaite-Bejarano L, Hansen RM, Fulton AB. Microperimetry in Three Inherited Retinal Disorders. Semin Ophthalmol. 2019;34(4):334–9.

737. What is Machine Learning? - United Kingdom | IBM [Internet]. 2020 [cited 2021 Aug 28]. Available from: https://www.ibm.com/uk-en/cloud/learn/machine-learning

738. Supervised vs. Unsupervised Learning: What's the Difference? | IBM [Internet]. 2021 [cited 2021 Aug 28]. Available from: https://www.ibm.com/cloud/blog/supervised-vs-unsupervised-learning

739. Hecht-Nielsen. Theory of the backpropagation neural network. In: International 1989 Joint Conference on Neural Networks. 1989. p. 593–605 vol.1.

740. Kawaguchi K. A multithreaded software model for backpropagation neural network applications. ETD Collect Univ Tex El Paso. 2000 Jan 1;1–92.

741. What are Neural Networks? | IBM [Internet]. 2021 [cited 2021 Aug 28]. Available from: https://www.ibm.com/cloud/learn/neural-networks

742. What is Deep Learning? | IBM [Internet]. 2021 [cited 2021 Aug 28]. Available from: https://www.ibm.com/cloud/learn/deep-learning

743. What is Overfitting? [Internet]. 2021 [cited 2021 Aug 28]. Available from: https://www.ibm.com/cloud/learn/overfitting

744. Lecun Y, Bottou L, Bengio Y, Haffner P. Gradient-based learning applied to document recognition. Proc IEEE. 1998 Nov;86(11):2278–324.

745. Shafkat I. Medium. 2018 [cited 2021 Sep 9]. Intuitively Understanding Convolutions for Deep Learning. Available from: https://towardsdatascience.com/intuitively-understanding-convolutions-for-deep-learning-1f6f42faee1

746. Dumoulin V, Visin F. A guide to convolution arithmetic for deep learning [Internet]. arXiv; 2018 [cited 2022 Oct 1]. Available from: http://arxiv.org/abs/1603.07285

747. Krizhevsky A, Sutskever I, Hinton GE. ImageNet Classification with Deep Convolutional Neural Networks. In: Advances in Neural Information Processing Systems [Internet]. Curran Associates, Inc.; 2012 [cited 2021 Aug 26]. Available from: https://papers.nips.cc/paper/2012/hash/c399862d3b9d6b76c8436e924a68c45b-Abstract.html

748. Russakovsky O, Deng J, Su H, Krause J, Satheesh S, Ma S, et al. ImageNet Large Scale Visual Recognition Challenge. Int J Comput Vis. 2015 Dec 1;115(3):211–52.

749. He K, Zhang X, Ren S, Sun J. Deep Residual Learning for Image Recognition. ArXiv151203385 Cs [Internet]. 2015 Dec 10 [cited 2021 Aug 26]; Available from: http://arxiv.org/abs/1512.03385

750. What are Convolutional Neural Networks? [Internet]. 2021 [cited 2021 Aug 28]. Available from: https://www.ibm.com/cloud/learn/convolutional-neural-networks

751. Biswal A. Simplilearn.com. [cited 2021 Aug 26]. Convolutional Neural Network Tutorial. Available from: https://www.simplilearn.com/tutorials/deep-learning-tutorial/convolutional-neural-network

752. Long J, Shelhamer E, Darrell T. Fully Convolutional Networks for Semantic Segmentation. ArXiv14114038 Cs [Internet]. 2015 Mar 8 [cited 2021 Aug 26]; Available from: http://arxiv.org/abs/1411.4038

753. Rawlani H. Medium. 2020 [cited 2021 Aug 28]. Implementing a fully convolutional network (FCN) in TensorFlow 2. Available from: https://towardsdatascience.com/implementing-a-fully-convolutional-network-fcn-in-tensorflow-2-3c46fb61de3b

754. Le T, Li Y, Duan Y. RED-NET: A Recursive Encoder-Decoder Network for Edge Detection. ArXiv191202914 Cs [Internet]. 2019 Dec 5 [cited 2021 Aug 26]; Available from: http://arxiv.org/abs/1912.02914

755. Ronneberger O, Fischer P, Brox T. U-Net: Convolutional Networks for Biomedical Image Segmentation. ArXiv150504597 Cs [Internet]. 2015 May 18 [cited 2021 Aug 19]; Available from: http://arxiv.org/abs/1505.04597

756. He K, Zhang X, Ren S, Sun J. Spatial Pyramid Pooling in Deep Convolutional Networks for Visual Recognition. ArXiv14064729 Cs. 2014;8691:346–61.

757. Chen LC, Papandreou G, Kokkinos I, Murphy K, Yuille AL. DeepLab: Semantic Image Segmentation with Deep Convolutional Nets, Atrous Convolution, and Fully Connected CRFs. ArXiv160600915 Cs [Internet]. 2017 May 11 [cited 2021 Aug 26]; Available from: http://arxiv.org/abs/1606.00915

758. Chen LC, Zhu Y, Papandreou G, Schroff F, Adam H. Encoder-Decoder with Atrous Separable Convolution for Semantic Image Segmentation. ArXiv180202611 Cs [Internet]. 2018 Aug 22 [cited 2021 Aug 26]; Available from: http://arxiv.org/abs/1802.02611

759. Gulshan V, Peng L, Coram M, Stumpe MC, Wu D, Narayanaswamy A, et al. Development and Validation of a Deep Learning Algorithm for Detection of Diabetic Retinopathy in Retinal Fundus Photographs. JAMA. 2016 Dec 13;316(22):2402–10.

760. Kermany DS, Goldbaum M, Cai W, Valentim CCS, Liang H, Baxter SL, et al. Identifying Medical Diagnoses and Treatable Diseases by Image-Based Deep Learning. Cell. 2018 Feb 22;172(5):1122-1131.e9.

761. De Fauw J, Ledsam JR, Romera-Paredes B, Nikolov S, Tomasev N, Blackwell S, et al. Clinically applicable deep learning for diagnosis and referral in retinal disease. Nat Med. 2018 Sep;24(9):1342–50.

762. Roy AG, Conjeti S, Karri SPK, Sheet D, Katouzian A, Wachinger C, et al. ReLayNet: Retinal Layer and Fluid Segmentation of Macular Optical Coherence

Tomography using Fully Convolutional Network. ArXiv170402161 Cs [Internet]. 2017 Jul 7 [cited 2021 Aug 19]; Available from: http://arxiv.org/abs/1704.02161

763. Lee CS, Tyring AJ, Deruyter NP, Wu Y, Rokem A, Lee AY. Deep-learning based, automated segmentation of macular edema in optical coherence tomography. Biomed Opt Express. 2017 Jun 23;8(7):3440–8.

764. Venhuizen FG, van Ginneken B, Liefers B, van Asten F, Schreur V, Fauser S, et al. Deep learning approach for the detection and quantification of intraretinal cystoid fluid in multivendor optical coherence tomography. Biomed Opt Express. 2018 Mar 7;9(4):1545–69.

765. Lu D, Heisler M, Lee S, Ding GW, Navajas E, Sarunic MV, et al. Deep-learning based multiclass retinal fluid segmentation and detection in optical coherence tomography images using a fully convolutional neural network. Med Image Anal. 2019 May 1;54:100–10.

766. Bogunovic H, Venhuizen F, Klimscha S, Apostolopoulos S, Bab-Hadiashar A, Bagci U, et al. RETOUCH: The Retinal OCT Fluid Detection and Segmentation Benchmark and Challenge. IEEE Trans Med Imaging. 2019;38(8):1858–74.

767. Schlegl T, Waldstein SM, Bogunovic H, Endstraßer F, Sadeghipour A, Philip AM, et al. Fully Automated Detection and Quantification of Macular Fluid in OCT Using Deep Learning. Ophthalmology. 2018 Apr 1;125(4):549–58.

768. Hassan B, Hassan T, Li B, Ahmed R, Hassan O. Deep Ensemble Learning Based Objective Grading of Macular Edema by Extracting Clinically Significant Findings from Fused Retinal Imaging Modalities. Sensors. 2019 Jul 5;19(13):2970.

769. Hu J, Chen Y, Yi Z. Automated segmentation of macular edema in OCT using deep neural networks. Med Image Anal. 2019 Jul 1;55:216–27.

770. Hassan B, Qin S, Ahmed R. SEADNet: Deep learning driven segmentation and extraction of macular fluids in 3D retinal OCT scans. In: 2020 IEEE International Symposium on Signal Processing and Information Technology (ISSPIT). 2020. p. 1–6.

771. Alsaih K, Yusoff MZ, Faye I, Tang TB, Meriaudeau F. Retinal Fluid Segmentation Using Ensembled 2-Dimensionally and 2.5-Dimensionally Deep Learning Networks. IEEE Access. 2020;8:152452–64.

772. Kingma DP, Ba J. Adam: A Method for Stochastic Optimization. ArXiv14126980 Cs [Internet]. 2017 Jan 29 [cited 2021 Aug 26]; Available from: http://arxiv.org/abs/1412.6980

773. Berman M, Triki AR, Blaschko MB. The Lov\'asz-Softmax loss: A tractable surrogate for the optimization of the intersection-over-union measure in neural networks. ArXiv170508790 Cs [Internet]. 2018 Apr 9 [cited 2021 Aug 26]; Available from: http://arxiv.org/abs/1705.08790

774. Dong L, He W, Zhang R, Ge Z, Wang YX, Zhou J, et al. Artificial Intelligence for Screening of Multiple Retinal and Optic Nerve Diseases. JAMA Netw Open. 2022 May 3;5(5):e229960.

775. Prahs P, Radeck V, Mayer C, Cvetkov Y, Cvetkova N, Helbig H, et al. OCT-based deep learning algorithm for the evaluation of treatment indication with anti-vascular endothelial growth factor medications. Graefes Arch Clin Exp Ophthalmol Albrecht Von Graefes Arch Klin Exp Ophthalmol. 2018 Jan;256(1):91–8.

776. Ipp E, Liljenquist D, Bode B, Shah VN, Silverstein S, Regillo CD, et al. Pivotal Evaluation of an Artificial Intelligence System for Autonomous Detection of Referrable and Vision-Threatening Diabetic Retinopathy. JAMA Netw Open. 2021 Nov 15;4(11):e2134254.

777. Abràmoff MD, Lavin PT, Birch M, Shah N, Folk JC. Pivotal trial of an autonomous AI-based diagnostic system for detection of diabetic retinopathy in primary care offices. Npj Digit Med. 2018 Aug 28;1(1):1–8.

778. Verbraak FD, Abramoff MD, Bausch GCF, Klaver C, Nijpels G, Schlingemann RO, et al. Diagnostic Accuracy of a Device for the Automated Detection of Diabetic Retinopathy in a Primary Care Setting. Diabetes Care. 2019 Feb 14;42(4):651–6.

779. Tufail A, Rudisill C, Egan C, Kapetanakis VV, Salas-Vega S, Owen CG, et al. Automated Diabetic Retinopathy Image Assessment Software: Diagnostic Accuracy and Cost-Effectiveness Compared with Human Graders. Ophthalmology. 2017 Mar;124(3):343–51.

780. Ruamviboonsuk P, Chantra S, Seresirikachorn K, Ruamviboonsuk V, Sangroongruangsri S. Economic Evaluations of Artificial Intelligence in Ophthalmology. Asia-Pac J Ophthalmol. 2021 Jun;10(3):307–16.

781. Dong L, Yang Q, Zhang RH, Wei WB. Artificial intelligence for the detection of age-related macular degeneration in color fundus photographs: A systematic review and meta-analysis. eClinicalMedicine [Internet]. 2021 May 1 [cited 2022 Jun 9];35. Available from: https://www.thelancet.com/journals/eclinm/article/PIIS2589-5370(21)00155-3/fulltext

782. Cavarretta S, Salvatore S, Vingolo EM. Use of MP-1 microperimetry in optic disc pit and secondary retinoschisis. Int Ophthalmol. 2009 Oct 1;29(5):423–5.

783. Brar VS, Murthy RK, Chalam KV. Functional microperimetry and SD-OCT confirm consecutive retinal atrophy from optic nerve pit. Clin Ophthalmol Auckl NZ. 2009;3:625–8.

APPENDIX

“Sorry sweetheart, I haven’t got time for anything else.”

– Han Solo

UCL Research Paper Declaration Form
referencing the doctoral candidate's own published work(s)

Please use this form to declare if parts of your thesis are already available in another format, e.g. if data, text, or figures:

- *have been uploaded to a preprint server*
- *are in submission to a peer-reviewed publication*
- *have been published in a peer-reviewed publication, e.g. journal, textbook.*

This form should be completed as many times as necessary. For instance, if you have seven thesis chapters, two of which containing material that has already been published, you would complete this form twice.

1. For a research manuscript that has already been published (if not yet published, please skip to section 2)

a) **What is the title of the manuscript?**

Optic disc pit maculopathy: New perspectives on the natural history

b) **Please include a link to or doi for the work**

10.1016/j.ajo.2019.05.010

c) **Where was the work published?**

American Journal of Ophthalmology

d) **Who published the work?** (e.g. OUP)

Elsever

e) **When was the work published?**

2019

f) **List the manuscript's authors in the order they appear on the publication**

Bloch E, Georgiadis O, Lukic M, da Cruz L

g) **Was the work peer reviewed?**

Yes

h) **Have you retained the copyright?**

No

i) **Was an earlier form of the manuscript uploaded to a preprint server?** (e.g. medRxiv). If 'Yes', please give a link or doi)

No

If 'No', please seek permission from the relevant publisher and check the box next to the below statement:

☒

*I acknowledge permission of the publisher named under **1d** to include in this thesis portions of the publication named as included in **1c**.*

2. **For a research manuscript prepared for publication but that has not yet been published** (if already published, please skip to section 3)

- a) **What is the current title of the manuscript?**

  Click or tap here to enter text.

  b) **Has the manuscript been uploaded to a preprint server?** (e.g. medRxiv; if 'Yes', please give a link or doi)

  Click or tap here to enter text.

  c) **Where is the work intended to be published?** (e.g. journal names)

  Click or tap here to enter text.

  d) **List the manuscript's authors in the intended authorship order**

  Click or tap here to enter text.

  e) **Stage of publication** (e.g. in submission)

  Click or tap here to enter text.

3. **For multi-authored work, please give a statement of contribution covering all authors** (if single-author, please skip to section 4)

   EB – conception, design, data collection, analysis, development of manuscript

   OG, ML – data collection, review of manuscript

   LdC – design, approval of final version of manuscript

4. **In which chapter(s) of your thesis can this material be found?**

   Chapter 4

5. **e-Signatures confirming that the information above is accurate** (this form should be co-signed by the supervisor/ senior author unless this is not appropriate, e.g. if the paper was a single-author work)

   Candidate

   Date: 04/02/2023

   Supervisor/ Senior Author (where appropriate)

   Date: 04/02/2023

UCL Research Paper Declaration Form
referencing the doctoral candidate's own published work(s)

Please use this form to declare if parts of your thesis are already available in another format, e.g. if data, text, or figures:

- *have been uploaded to a preprint server*
- *are in submission to a peer-reviewed publication*
- *have been published in a peer-reviewed publication, e.g. journal, textbook.*

This form should be completed as many times as necessary. For instance, if you have seven thesis chapters, two of which containing material that has already been published, you would complete this form twice.

1. For a research manuscript that has already been published (if not yet published, please skip to section 2)

j) **What is the title of the manuscript?**

An association between stellate nonhereditary foveomacular retinoschisis, peripheral retinoschisis, and posterior hyaloid attachment

k) **Please include a link to or doi for the work**

10.1097/IAE.0000000000003191

l) **Where was the work published?**

Retina

m) **Who published the work?** (e.g. OUP)

Wolters Kluwer

n) **When was the work published?**

2021

o) **List the manuscript's authors in the order they appear on the publication**

Bloch E, Flores-Sánchez B, Georgiadis O, Sundaram V, Saihan Z, Mahroo O, Webster A, Da Cruz L

p) **Was the work peer reviewed?**

Yes

q) **Have you retained the copyright?**

No

r) **Was an earlier form of the manuscript uploaded to a preprint server?** (e.g. medRxiv). If 'Yes', please give a link or doi)

No

If 'No', please seek permission from the relevant publisher and check the box next to the below statement:

☒

*I acknowledge permission of the publisher named under **1d** to include in this thesis portions of the publication named as included in **1c**.*

2. **For a research manuscript prepared for publication but that has not yet been published** (if already published, please skip to section 3)

- f) **What is the current title of the manuscript?**

  Click or tap here to enter text.

  g) **Has the manuscript been uploaded to a preprint server?** (e.g. medRxiv; if 'Yes', please give a link or doi)

  Click or tap here to enter text.

  h) **Where is the work intended to be published?** (e.g. journal names)

  Click or tap here to enter text.

  i) **List the manuscript's authors in the intended authorship order**

  Click or tap here to enter text.

  j) **Stage of publication** (e.g. in submission)

  Click or tap here to enter text.

3. **For multi-authored work, please give a statement of contribution covering all authors** (if single-author, please skip to section 4)

   EB – conception, design, data collection, analysis, development of manuscript

   BFS, OG, VS, ZS – data collection, review of manuscript

   OM, AW, LdC – design, approval of final version of manuscript

4. **In which chapter(s) of your thesis can this material be found?**

   Chapter 5

5. **e-Signatures confirming that the information above is accurate** (this form should be co-signed by the supervisor/ senior author unless this is not appropriate, e.g. if the paper was a single-author work)

   Candidate

   Date: 04/02/2023

   Supervisor/ Senior Author (where appropriate)

   Date: 04/02/2023

UCL Research Paper Declaration Form

referencing the doctoral candidate's own published work(s)

Please use this form to declare if parts of your thesis are already available in another format, e.g. if data, text, or figures:

- *have been uploaded to a preprint server*
- *are in submission to a peer-reviewed publication*
- *have been published in a peer-reviewed publication, e.g. journal, textbook.*

This form should be completed as many times as necessary. For instance, if you have seven thesis chapters, two of which containing material that has already been published, you would complete this form twice.

1. For a research manuscript that has already been published (if not yet published, please skip to section 2)

s) **What is the title of the manuscript?**

Click or tap here to enter text.

t) **Please include a link to or doi for the work**

Click or tap here to enter text.

u) **Where was the work published?**

Click or tap here to enter text.

v) **Who published the work?** (e.g. OUP)

Click or tap here to enter text.

w) **When was the work published?**

Click or tap here to enter text.

x) **List the manuscript's authors in the order they appear on the publication**

Click or tap here to enter text.

y) **Was the work peer reviewed?**

Click or tap here to enter text.

z) **Have you retained the copyright?**

Click or tap here to enter text.

aa) **Was an earlier form of the manuscript uploaded to a preprint server?** (e.g. medRxiv). If 'Yes', please give a link or doi)

Click or tap here to enter text.

If 'No', please seek permission from the relevant publisher and check the box next to the below statement:

☐

*I acknowledge permission of the publisher named under **1d** to include in this thesis portions of the publication named as included in **1c**.*

2. **For a research manuscript prepared for publication but that has not yet been published** (if already published, please skip to section 3)

- k) **What is the current title of the manuscript?**

  Associations between optical coherence tomographic biomarkers and anatomico-functional changes in myopic foveoschisis

  l) **Has the manuscript been uploaded to a preprint server?** (e.g. medRxiv; if 'Yes', please give a link or doi)

  No

  m) **Where is the work intended to be published?** (e.g. journal names)

  Eye (Lond)

  n) **List the manuscript's authors in the intended authorship order**

  Bloch E, Flores-Sánchez B, Georgiadis O, Whiteman A, da Cruz L

  o) **Stage of publication** (e.g. in submission)

  In submission

3. **For multi-authored work, please give a statement of contribution covering all authors** (if single-author, please skip to section 4)

   EB – conception, design, data collection, analysis, development of manuscript

   BFS, OG, AW – data collection, review of manuscript

   LdC – design, approval of final version of manuscript

4. **In which chapter(s) of your thesis can this material be found?**

   Chapter 3

5. **e-Signatures confirming that the information above is accurate** (this form should be co-signed by the supervisor/ senior author unless this is not appropriate, e.g. if the paper was a single-author work)

   Candidate

   Date: 04/02/2023

   Supervisor/ Senior Author (where appropriate)

   Date: 04/02/2023

Ymchwil Iechyd a Gofal Cymru
Health and Care Research Wales

NHS
Health Research Authority

Professor Lyndon da Cruz
Consultant Retinal Surgeon Moorfields Eye Hospital
Moorfields Eye Hospital, NHS Foundation Trust
162 City Rd, London
EC1V 2PD

Email: hra.approval@nhs.net
Research-permissions@wales.nhs.uk

12 November 2018

Dear Professor da Cruz

HRA and Health and Care Research Wales (HCRW) Approval Letter

Study title:	**Optic disc pit maculopathy: a single-site retrospective, observational study of the natural history of the disease in a clinical cohort**
IRAS project ID:	**216619**
Protocol number:	**v1.2**
Sponsor	**Moorfields Eye Hospital NHS Foundation Trust**

I am pleased to confirm that **HRA and Health and Care Research Wales (HCRW) Approval** has been given for the above referenced study, on the basis described in the application form, protocol, supporting documentation and any clarifications received. You should not expect to receive anything further relating to this application.

How should I continue to work with participating NHS organisations in England and Wales?
You should now provide a copy of this letter to all participating NHS organisations in England and Wales, as well as any documentation that has been updated as a result of the assessment.

This is a single site study sponsored by the site. The sponsor R&D office will confirm to you when the study can start following issue of HRA and HCRW Approval.

It is important that you involve both the research management function (e.g. R&D office) supporting each organisation and the local research team (where there is one) in setting up your study. Contact details of the research management function for each organisation can be accessed here.

How should I work with participating NHS/HSC organisations in Northern Ireland and Scotland?
HRA and HCRW Approval does not apply to NHS/HSC organisations within the devolved administrations of Northern Ireland and Scotland.

Ymchwil Iechyd a Gofal Cymru
Health and Care Research Wales

NHS
Health Research Authority

Professor Lyndon da Cruz
Consultant Retinal Surgeon, Moorfields Eye Hospital
Moorfields Eye Hospital
162 City Road
London
EC1V 2PD

Email: hra.approval@nhs.net
HCRW.approvals@wales.nhs.uk

16 January 2020

Dear Professor da Cruz

HRA and Health and Care Research Wales (HCRW) Approval Letter

Study title:	**A single-site, retrospective, observational study of the anatomico-functional characteristics of conditions manifesting with foveomacular retinoschisis**
IRAS project ID:	**272332**
Protocol number:	**v1.2**
REC reference:	**20/HRA/0083**
Sponsor	**Moorfields Eye Hospital**

I am pleased to confirm that **HRA and Health and Care Research Wales (HCRW) Approval** has been given for the above referenced study, on the basis described in the application form, protocol, supporting documentation and any clarifications received. You should not expect to receive anything further relating to this application.

Please now work with participating NHS organisations to confirm capacity and capability, in line with the instructions provided in the "Information to support study set up" section towards the end of this letter.

How should I work with participating NHS/HSC organisations in Northern Ireland and Scotland?
HRA and HCRW Approval does not apply to NHS/HSC organisations within Northern Ireland and Scotland.

If you indicated in your IRAS form that you do have participating organisations in either of these devolved administrations, the final document set and the study wide governance report (including this letter) have been sent to the coordinating centre of each participating nation. The relevant national coordinating function/s will contact you as appropriate.

APPENDIX: STROBE Statement—checklist of items that should be included in reports of observational studies

Item	No	Recommendation
Title and abstract	1	(a) Indicate the study's design with a commonly used term in the title or the abstract (b) Provide in the abstract an informative and balanced summary of what was done and what was found
Introduction	2	Explain the scientific background and rationale for the investigation being reported
Background/rationale	3	State specific objectives, including any prespecified hypotheses
Study design	4	Present key elements of study design early in the paper
Setting	5	Describe the setting, locations, and relevant dates, including periods of recruitment, exposure, follow-up, and data collection
Participants	6	(a) *Cohort study*—Give the eligibility criteria, and the sources and methods of selection of participants. Describe methods of follow-up *Case-control study*—Give the eligibility criteria, and the sources and methods of case ascertainment and control selection. Give the rationale for the choice of cases and controls

		Cross-sectional study—Give the eligibility criteria, and the sources and methods of selection of participants (b) *Cohort study*—For matched studies, give matching criteria and number of exposed and unexposed *Case-control study*—For matched studies, give matching criteria and the number of controls per case
Variables	7	Clearly define all outcomes, exposures, predictors, potential confounders, and effect modifiers. Give diagnostic criteria, if applicable
Data sources/measurements	8*	For each variable of interest, give sources of data and details of methods of assessment (measurement). Describe comparability of assessment methods if there is more than one group
Bias	9	Describe any efforts to address potential sources of bias
Study size	10	Explain how the study size was arrived at
Quantitative variables	11	Explain how quantitative variables were handled in the analyses. If applicable, describe which groupings were chosen and why
Statistical methods	12	(a) Describe all statistical methods, including those used to control for confounding

		(b) Describe any methods used to examine subgroups and interactions (c) Explain how missing data were addressed (d) *Cohort study*—If applicable, explain how loss to follow-up was addressed Case-control study—If applicable, explain how matching of cases and controls was addressed *Cross-sectional study*—If applicable, describe analytical methods taking account of sampling strategy (e) Describe any sensitivity analyses
Results		
Participants	13*	(a) Report numbers of individuals at each stage of study—eg numbers potentially eligible, examined for eligibility, confirmed eligible, included in the study, completing follow-up, and analysed (b) Give reasons for non-participation at each stage (c) Consider use of a flow diagram

Descriptive data	14*	(a) Give characteristics of study participants (eg demographic, clinical, social) and information on exposures and potential confounders (b) Indicate number of participants with missing data for each variable of interest (c) Cohort study—Summarise follow-up time (eg, average and total amount)
Outcome data	15*	*Cohort study*—Report numbers of outcome events or summary measures over time *Case-control study*—Report numbers in each exposure category, or summary measures of exposure *Cross-sectional study*—Report numbers of outcome events or summary measures
Main results	16	(a) Give unadjusted estimates and, if applicable, confounder-adjusted estimates and their precision (eg, 95% confidence interval). Make clear which confounders were adjusted for and why they were included (b) Report category boundaries when continuous variables were categorized

		(c) If relevant, consider translating estimates of relative risk into absolute risk for a meaningful time period
Other analyses	17	Report other analyses done—eg analyses of subgroups and interactions, and sensitivity analyses
Discussion		
Key results	18	Summarise key results with reference to study objectives
Limitations	19	Discuss limitations of the study, taking into account sources of potential bias or imprecision. Discuss both direction and magnitude of any potential bias
Interpretation	20	Give a cautious overall interpretation of results considering objectives, limitations, multiplicity of analyses, results from similar studies, and other relevant evidence
Generalisability	21	Discuss the generalisability (external validity) of the study results
Other information		
Funding	22	Give the source of funding and the role of the funders for the present study and, if applicable, for the original study on which the present article is based

*Give information separately for cases and controls in case-control studies and, if applicable, for exposed and unexposed groups in cohort and cross-sectional studies.

Note: An Explanation and Elaboration article discusses each checklist item and gives methodological background and published examples of transparent reporting. The STROBE checklist is best used in conjunction with this article (freely

available on the Web sites of PLoS Medicine at http://www.plosmedicine.org/, Annals of Internal Medicine at http://www.annals.org/, and Epidemiology at http://www.epidem.com/). Information on the STROBE Initiative is available at www.strobe-statement.org.

Appendix: MFS Study SOP

DESIGN:

- Images acquired on Spectralis/Topcon/Zeiss (see 'acquisition device' column)
- 2 ophthalmologists review all OCT slices (EB and BF)
- 3rd ophthalmologist to review cases of disagreement (OG)
- Record following qualitative features:
    - Foveal status
        - 'Normal'
        - Inner LMH
        - FTMH
    - Premacular features
        - Vitreomacular traction
        - Epiretinal proliferation
        - Epiretinal membrane
        - ILM-detachment
    - Schisis morphology
        - Predominantly inner/outer schisis (or both)
            - Which layers are involved (sub-ILM, NFL, IPL, INL, OPL)
        - Intraretinal microcystoid spaces only (i.e. not foveoschisis)
        - Outer LMH
        - Schisis + foveal detachment
        - Foveal detachment only
        - Shimada classification (S0-S4)
    - Presence of staphyloma
    - Presence of dome-shaped maculopathy

1. SCHISIS MORPHOLOGY (ATN)

1: Inner retinoschisis

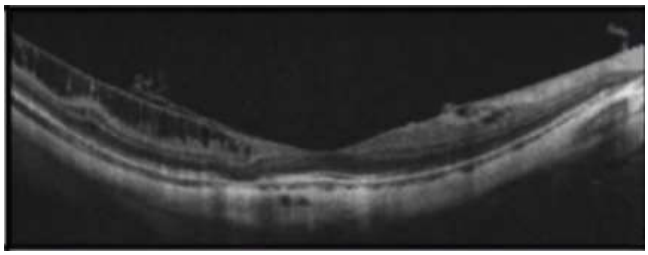

2: outer ± inner retinoschisis

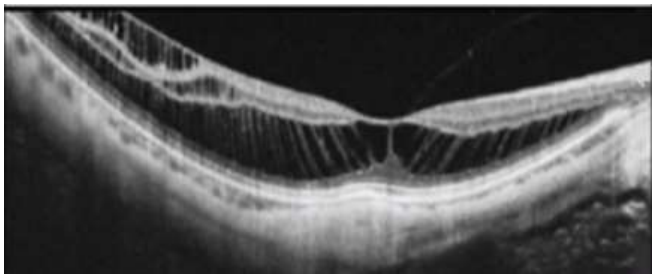

3: schisis + foveal detachment (note also OLH here)

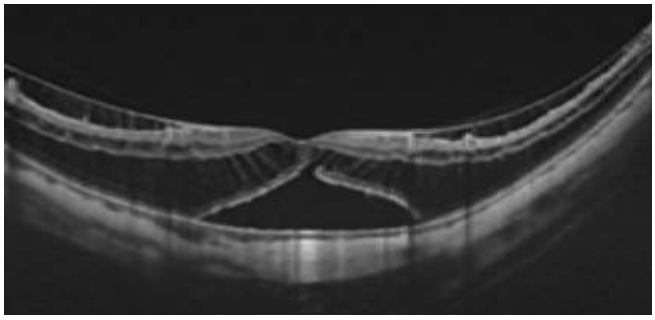

4: Foveal detachment only (note no OLH here)

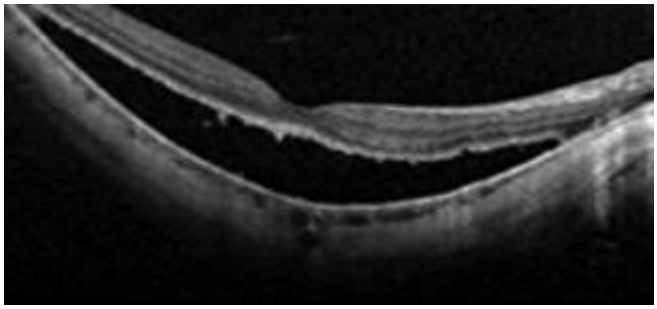

2. FOVEAL STATUS

a.) normal foveal contour (i.e. no inner lamellar hole)

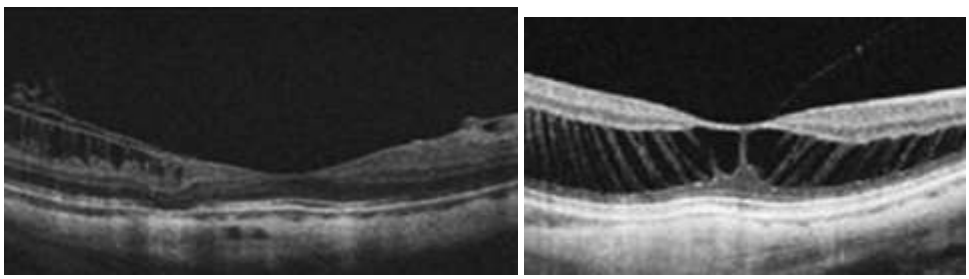

b.) Inner lamellar hole (degenerative or tractional)

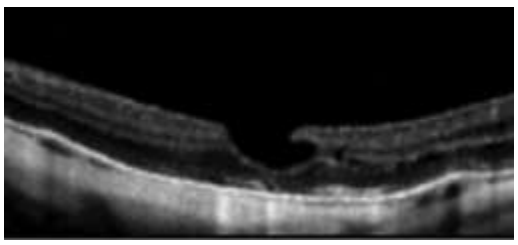

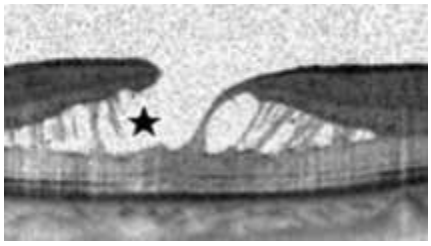

c.) FTMH/full-thickness defect

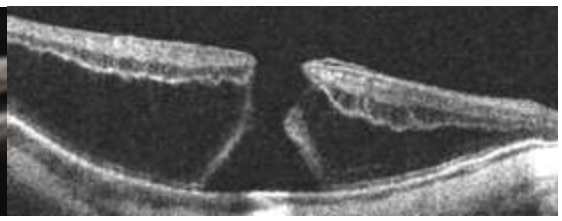

3. OUTER LAMELLAR HOLE

Simply the disruption of the outer layers, with no inner retinal defect – often associated with foveal detachment. Specifically look for **EZ AND ELM** discontinuity

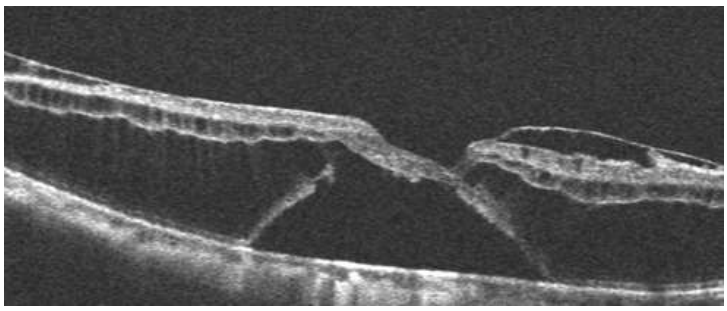

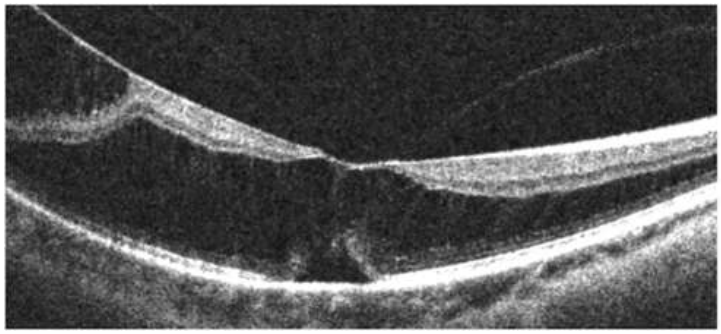

4. VITREOMACULAR TRACTION

This may be co-existent with ERM/FTMH or occur independently

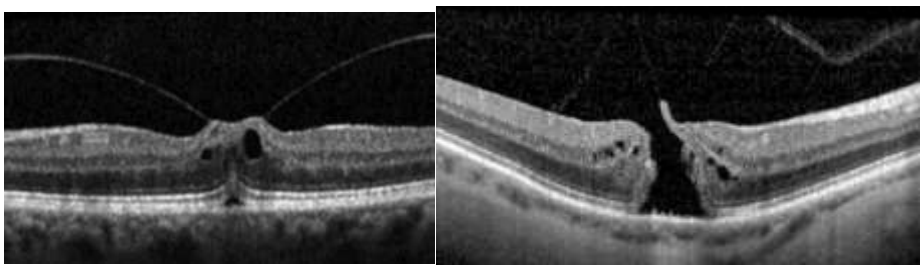

Rarely you may see traction from a posterior hyaloid band – this can be characteristed as VMT or ERM, depending on what you think it most resembles…

5. EPIRETINAL PROLIFERATION (ERP)

Thick, homogenous, isoreflective material over ILM. Typically (but not always) associated with degenerative LMH formation

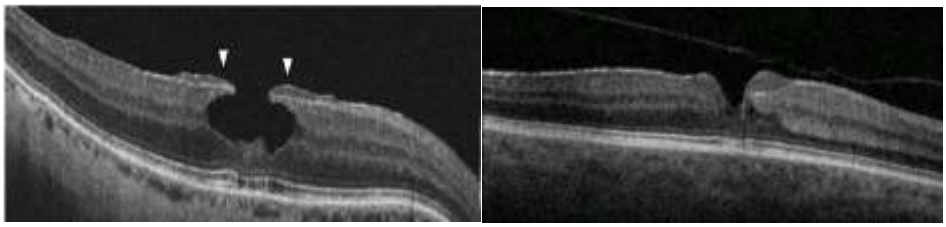

6. EPIRETINAL MEMBRANE (ERM)

ERM is defined as presence of irregular and hyperreflective layer over ILM. This will tend to have contractile properties – needs to be distinguished from ERP.

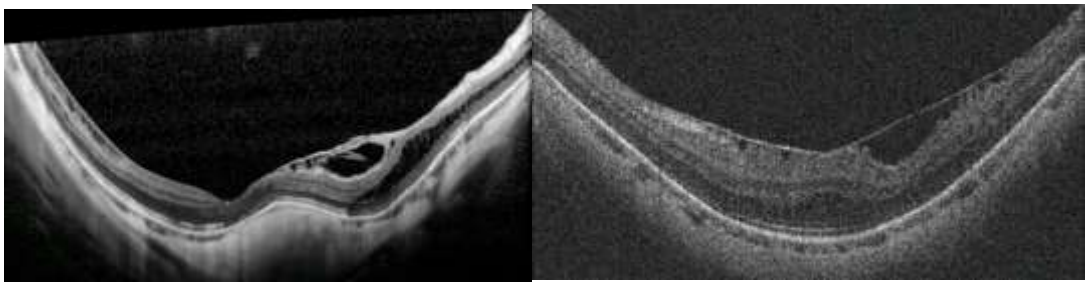

NB: ERM/ERP/VMT may be associated with intraretinal microcystoid spaces (IMCS) or foveoschisis (or neither)

7. ILM DETACHMENT

ILM detachment needs to be differentiated from ERM traction. If is a continuous line with the inner retinal layer and is parafoveal only. It will usually be associated with inner schisis ± outer schisis ± FD/OLH (see later)

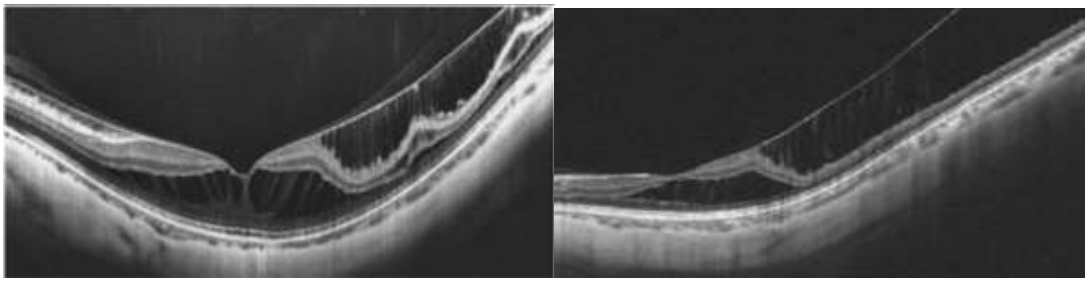

8. IMCS

Presence of IR microcystoid spaces defined as small, usually non-confluent and hyporeflective spaces in the inner nuclear layer. This may be with or without and ILD (inner lamellar defect). This will generally mean exclusion if there is no foveoschisis.

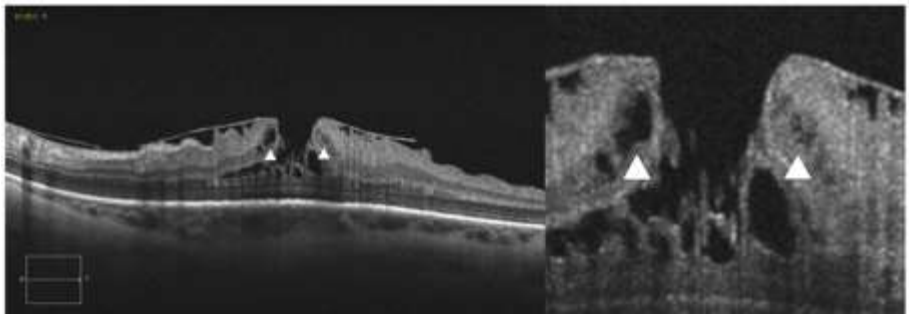

9. STAPHYLOMA

Can be tricky to see – defined as posterior outpouching of the sclera or a focal change in the radial curvature of the retina. Look at both OCT and CFP/*en face* imaging where possible. See Curtin classification for commonest distributions.

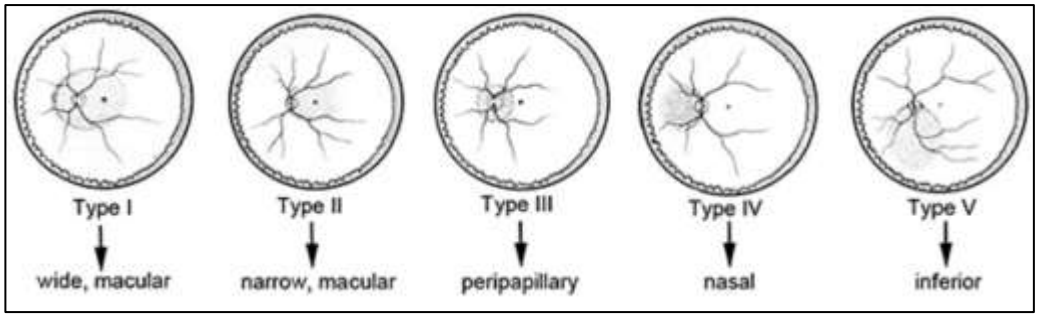

These have staphyloma on OCT/CFP:

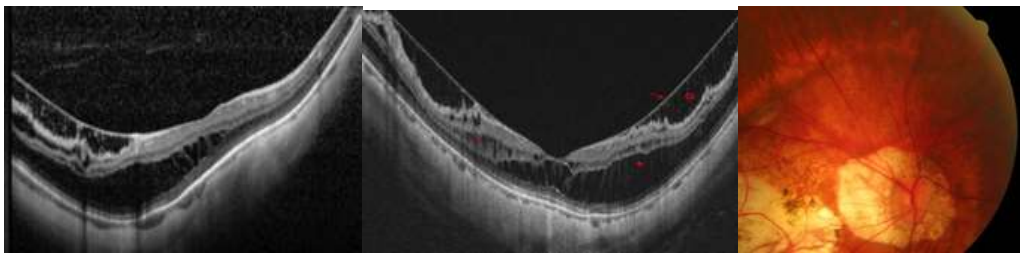

These do not have evidence of staphyloma on OCT:

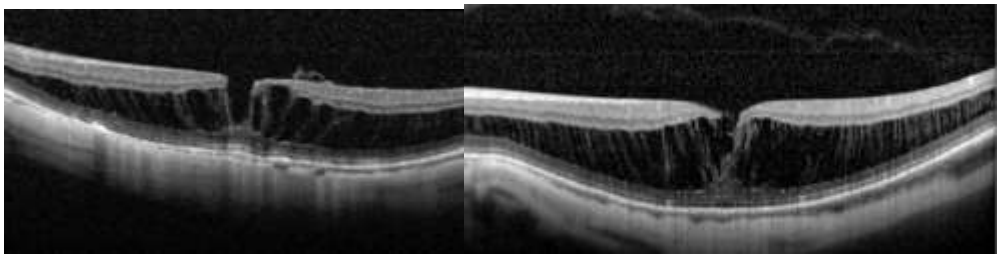

If it is ambiguous, maybe like these – make a decision and mark for discussion/agreement later:

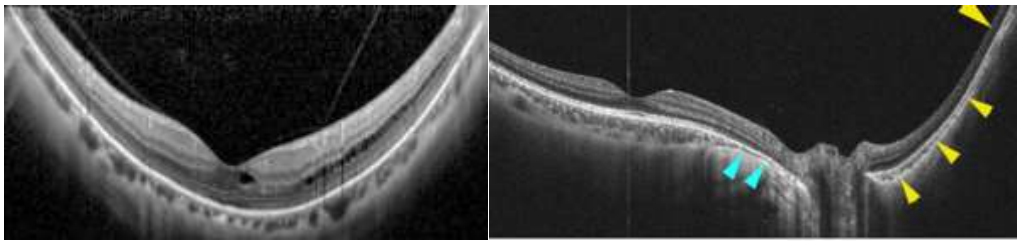

10. DOME-SHAPED MACULA

Just needs noting if there is submacular dome-shaped thickening (may well be missed if only vertical/horizontal orientated scans)

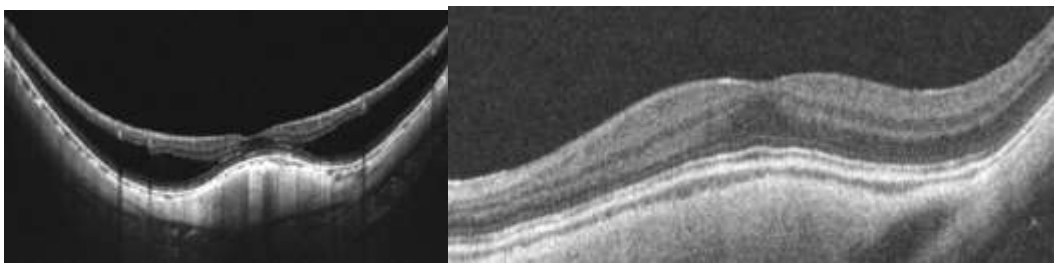

EXAMPLES

For each case, you will need to fill out a spreadsheet for all these features.

No	Stage	Fovea	O-LMH	ERP	ERM	VMT	ILMD	IMCS	PS	DSM
12345										

Stage = Retinal stages 1-4
Fovea = foveal stages a-c
O-LMH = outer lamellar macular hole
VMT = vitreomacular traction
ERP = epiretinal proliferation
ERM = epiretinal membrane
ILMD = ILM detachment
IMCS = intraretinal microcystoid spaces (inner nuclear layer cysts)
PS = posterior staphyloma
DSM = dome-shaped maculopathy

Example 1:

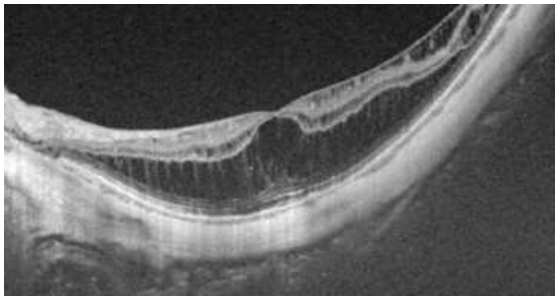

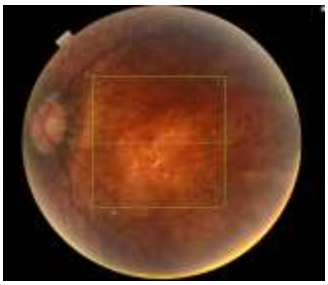

No	Stage	Fovea	O-LMH	ERP	ERM	VMT	ILMD	IMCS	PS	DSM
Ex. 1	2	a					✓		✓	

Example 2:

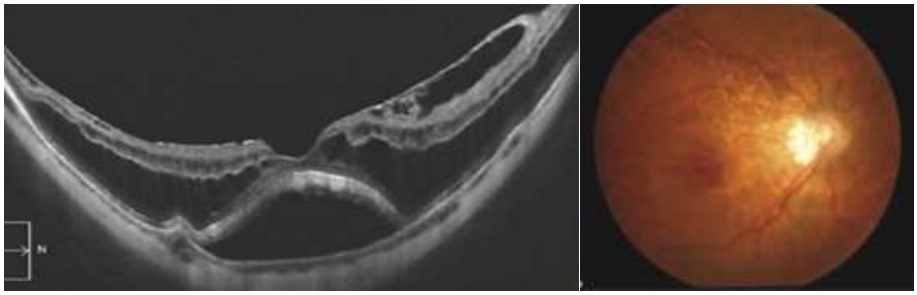

No	Stage	Fovea	O-LMH	ERP	ERM	VMT	ILMD	IMCS	PS	DSM
Ex. 2	3	a	✓		✓		✓			

Example 3:

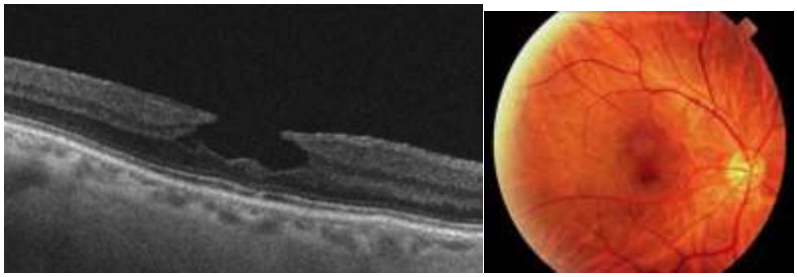

No	Stage	Fovea	O-LMH	ERP	ERM	VMT	ILMD	IMCS	PS	DSM
Ex. 3	1	b		✓						

Example 4:

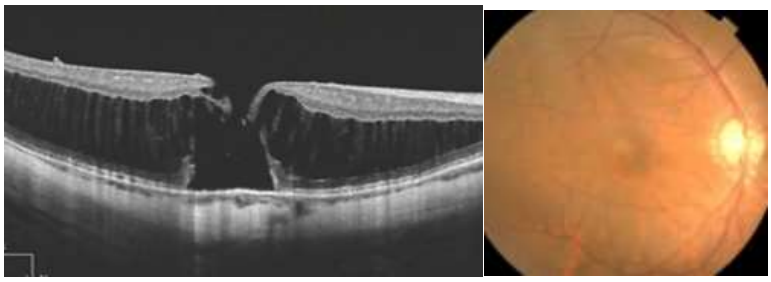

No	Stage	Fovea	O-LMH	ERP	ERM	VMT	ILMD	IMCS	PS	DSM
Ex. 4	3	c	✓						✓	

Example 5:

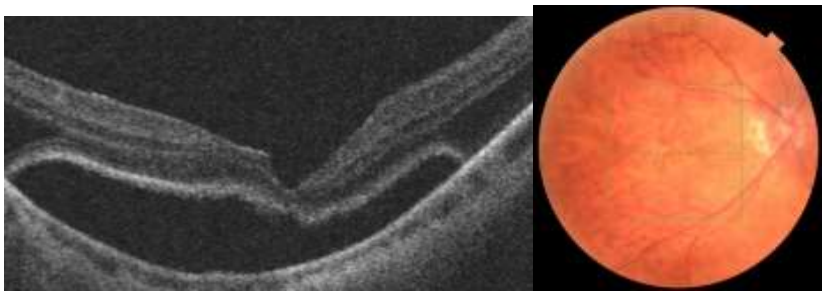

No	Stage	Fovea	O-LMH	ERP	ERM	VMT	ILMD	IMCS	PS	DSM
Ex. 5	4	a							✓	

Example 6:

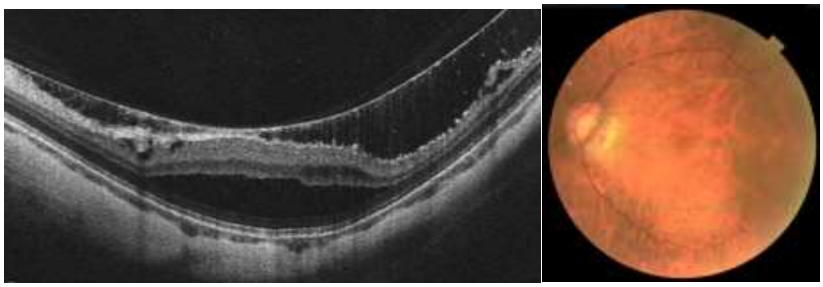

No	Stage	Fovea	O-LMH	ERP	ERM	VMT	ILMD	IMCS	PS	DSM
Ex. 6	1	a					✓		✓	